Bulging of Fatigue Cracks in a Pressurized Aircraft Fuselage

October 1990   D. Chen

TUDelft   **Faculty of Aerospace Engineering**

Delft University of Technology
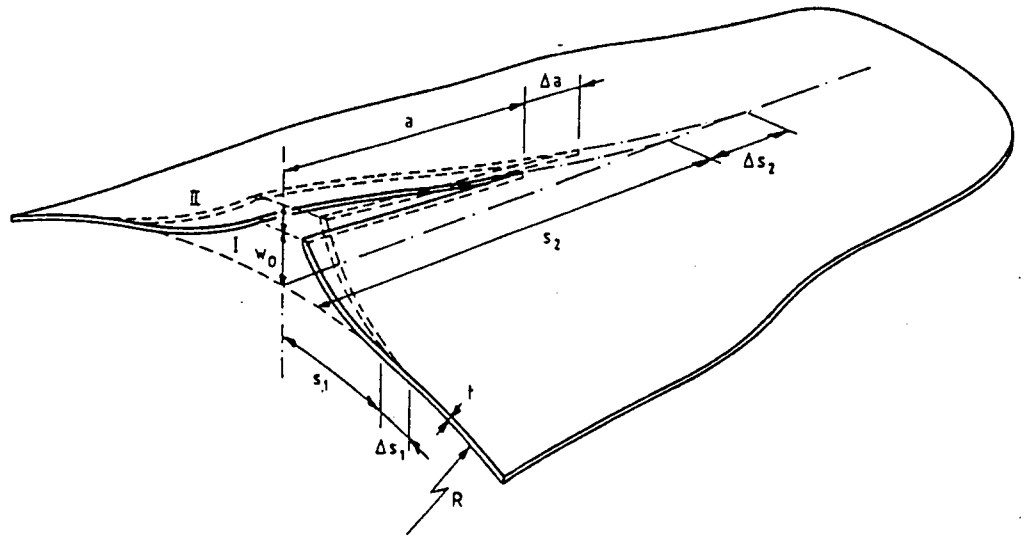
Bulging of Fatigue Cracks in a Pressurized Aircraft Fuselage

D. Chen

To my wife Hong, for her understanding and support,

and to our lovely daughter Iris.

Abstract

Three new set-ups have been developed for testing of sheet specimens under biaxial tensile loading, for tensile loading of sheet specimens with a curvature, and for sheet specimens with a large radius of curvature loaded by an internal air pressure and hoop stress. Studies have been carried out on the fatigue crack growth behaviour of thin aluminium alloy sheets and ARALL laminates under various aircraft fuselage loading conditions, including stress biaxiality, combined bending and extension and crack edge bulge-out conditions. Some residual tensile strength tests have also been conducted. Theories for the effect of combined bending and extension as well for the effect of bulging have been developed. The theories agree well with the present test results and results from the literature.

Key words:

Contents

iii

List of symbols

		Unit:
A	coefficient	
a	half-crack-length	m
B	coefficient	
C	correction factor	
E	Young's modulus	MPa
f	dimensionless coefficient	
F	work performed by external force	Nm
G	energy release rate	N
K	stress intensity factor	MPa$\sqrt{m}$
K_b	bending stress intensity factor	MPa$\sqrt{m}$
K_c	critical stress intensity factor	MPa$\sqrt{m}$
K_e	extension (tensile) stress intensity factor	MPa$\sqrt{m}$
K_I	mode I stress intensity factor	MPa$\sqrt{m}$
L	frame spacing	m
M_0	uniform bending moment	Nm
P	potential energy	Nm
	point force	N/m
p	internal pressure	MPa
U	elastic strain energy	Nm
u	displacement	m
r	distance from crack tip	m
r_p	plastic correction factor	
R	radius	m
	minimum stress to maximum stress ratio	
S	longeron spacing	m
s_1, s_2	characteristic lengths in the out-of-plane	
	deformation field around a crack	m
t	thickness	m
W	width	m
w	out-of-plane displacement	m
w_0	out-of-plane displacement of the center of a crack	m
z	coordinate in thickness direction	m
$\Delta a, da$	crack extension	m

α	dimensionless exponent	
β_b	bulge factor	
λ	dimensionless factor for cracked cylindrical shell	
ε	deformation	
χ	stress biaxiality	
Φ	load efficiency factor	
$\phi(1)$	solution of a Fredholm integral equation	
ν	Poisson constant	
σ	stress	MPa
σ_h	hoop stress	MPa
σ_l	longitudinal stress	MPa
φ	plasticity correction factor	
θ	angle	rad.

SUBSCRIPT

e	extension
b	bending
	bulge
c	critical
h	hoop
x	x-direction
y	y-direction

ABBREVIATIONS

CA	Constant Amplitude
CETS	Curvature Effect Test System
FEM	Finite Element Method
LEFM	Linear Elastic Fracture Mechanics
PFSTS	Pressurized Fuselage Skin Test System
SUPERBAT	Specimen Using Poisson Ratio Effect for Bi-Axial Testing

CHAPTER 1 INTRODUCTION

Three years before the first powered flight, Wilbur Wright wrote to reassure his father[1]:

'I am constructing my machine to sustain about five times my weight and am testing every piece. I think there is no possible chance of its breaking while in the air.... My machine will be trussed like a bridge...'

At that time, the Wright brothers already realized the value of full scale testing. Only two weeks before the historical first flight, Wilbur wrote to his friend George Spratt:

'We hung it on its wing tips some days ago, loaded the front set of trussing to more than six times its regular strain in the air. We also hung it by the tips and ran the engine screws with the man also on board. The strength of the machine seems "OK".'

The machine did fly and landed safely.

Some thirty years later, Orville Wright wrote to Willard A. Driggers:

'In answer to your inquiry on to whether there was any stress analysis of the original Wright aeroplane, and whether early aircraft constructors attempted strength calculations, will say that there was a stress analysis made of our first powered machine as well as the gliders which preceded it. These analyses, however, were not so complete as those made today.'

So the story of structural airworthiness precedes the story of powered flight.

Since the founding of the Wright's aircraft, the speed of aircraft has considerably increased, operators have demanded longer service lives, new materials have been introduced with their own susceptibilities. The developments have demanded more comprehensive design requirements and better design techniques to ensure that each new aircraft maintains the existing standards of airworthiness.

After the second world war, the phenomenon of fatigue has become a dominant aspect of structural airworthiness. Its effect on the choice of material, on the geometry and arrangement of structures, on the choice of stress levels and therefore on the airframe mass, has been little short of revolutionary.

Nevertheless, the history of fatigue failures goes back to more than 150 years ago. A number of engineers in Europe recognized that fractures of some mechanical components were due to repeated loadings. 130 years later, Professor Schijve stated in a lecture in 1969[2]:

'Fatigue in aircraft structures is a problem for which quantitative and generally accepted solutions are not available as yet.'

As a direct consequence of considering fatigue problems the 'fail-safe' design philosophy has been introduced to the aircraft designer by the 1950's. It is amazing to note that Leonardo da Vinci (1452-1519) wrote[3]:

'In constructing wings one should make one cord to bear the strain and a loose one in the same position so that if the one breaks under the strain the other is in position to serve the same function.'

It took 500 years (!) to accept this philosophy.

Professor Gassner made a perceptive observation in 1973[4]:

'Increasing demands for economy and safety in highly utilized structures under random loading necessitate a fatigue life to failure only slightly in excess of service life. This presupposes reliable calculation and experimental procedures for both fatigue life prediction and fatigue life substantiation.'

There are two important aspects to these statements. The first is the balance between economics and safety and the second is the necessity of providing a fatigue life only slightly in excess of service life in order to achieve a balance between economy and safety. However, as stated by Swift[5] 'Fatigue is a random variable. Even though service life goals are initially specified and the best analytical methods, backed by full-scale testing, are employed, fatigue may still occur to some extent in a fleet of aircraft. Safety in these cases is being maintained by the diligently combined efforts of the manufacturers, regulatory authorities, and the operators through inspection programs that depend upon the degree of damage tolerance inherent in the structure in the case of the ageing fleet and designed into the structure for future aircraft.'. Inspection of aircraft is also an essential aspect to maintain the safety.

The rapid development of Fracture Mechanics in recent years has led to a new design concept, that of damage tolerance design. This new design philosophy was officially introduced by the USAF first (Mil.-A-83444)[6] in 1974. Four years later, the Federal Aviation Administration (FAA) published a new Federal Aviation Regulations (FAR) Part 25.571[7] containing the damage tolerance and fatigue evaluation certification requirements of transport category aircraft structures. The FAA has also outlined an acceptable means of compliance of the FAR 25.571[8]. The European aviation authority has also accepted this new

design philosophy and has issued it in JAR 25.571[9].

Because of the large number of areas to be considered in the damage tolerance evaluation a high degree of reliance must be placed on analysis. It is obvious that to test every principal structural element for damage tolerance characteristics would generally be economically unfeasible. Thus, the evaluation is considered to be an analytical evaluation. However, sufficient testing must be performed to ensure that analysis methods are not un-conservative.

According to Swift[10] there are several major tasks for the damage tolerance evaluation. Some of them are:

* develop crack growth rate data for each location;

* validate basic crack growth analysis methods;

* obtain fracture toughness data for each material and geometry;

* determine the maximum extent of damage for each location under limit load conditions;

* validate residual strength analysis methods.

To fulfill these tasks, advanced testing and analysis methods must be developed.

During the last decade much attention is paid to the damage tolerance evaluation of the aircraft fuselage structure, particularly in pressurized fuselage shell structures. Since the design of the first jet transport aircraft, the load in the fuselage skin material has more than doubled due to the increase of the fuselage diameter and higher cabin pressures. Design of a modern pressurized fuselage shell structure demands more refined techniques and improved materials.

One of the most important aspects of designing an aircraft fuselage shell structure is to consider skin cracks resulting from fatigue and to choose material and stress level in such a way that the cracks will be discovered within a certain inspection period (interval) prior to reaching a critical crack length.

Different critical areas of an aircraft fuselage can be selected according to the damage tolerance requirements and the expected stress distribution of the shell structure. An example of the selection is given in Fig.1.1. Further detailed static and dynamic test programs are necessary to qualify these structures according to the requirements. These test programs must cover all

the primary and secondary effects induced by the specific geometry of the structure and loading conditions, if it is possible. Tests covered by such a program are indicated in Fig.1.2 as an example.

Since the introduction of the damage tolerance design principle, aircraft fuselage design goals have been defined more specifically. The two-bay crack design criterion has become a major design goal for the transport aircraft fuselage skin structures (Fig.1.3). Experience has shown that longitudinal cracks in a fuselage skin structure are more difficult to handle than circumferential ones, partly because the hoop stress is larger than the longitudinal stress, but also because of geometrical complexities and the secondary effects. In the first place, curvature of the structure, combined with the internal pressurization introduces both geometrical and stress non-linearity, leading to a more complicated fracture mechanics analysis procedure. Secondly, the biaxial loading condition, which is characteristic for the fuselage skin structure, may also have an influence on the crack growth behaviour.

Three important aspects concerning the fracture mechanics behaviour of a longitudinal crack in the fuselage skin structure can be recognized:

(1) bending effect of the skin sheet introduced by bending the skin sheets to the radius of the fuselage;

(2) biaxial loading conditions and

(3) the so-called "bulge-out" effects (see Fig.1.4). Very limited studies, both theoretical and experimental, have been done in this field.

Since the introduction of ARALL Laminate materials at about 1980, ARALL Laminates (ARamid ALuminium Laminate) have been widely regarded as a family of highly damage tolerant materials with a high weight saving potential. Damage tolerance design of full scale ARALL aircraft lower wing structures has been achieved with weight savings of more than 30%[11]. Attention is now focused on the application of ARALL Laminates as an aircraft fuselage skin material. Yet, several questions concerning the basic design principles and material properties have to be answered. As mentioned above, fatigue properties of the material under realistic fuselage loading conditions, such as, the effects of biaxiality, internal pressurization, curvature, frequency effects, etc, have to be investigated. And the last and certainly not the least question is how

to certificate an ARALL fuselage skin structure according to the airworthiness regulations.

Unfortunately, very limited theoretical analysis methods and experimental experience are available for the damage tolerance design evaluation of aircraft fuselage skin structures. It is thus essential to study both the static and dynamic behaviour of the fuselage skin sheets on a laboratory scale in order to get a better understanding of the problems.

The present study consists of the following parts:

(1) Bi-axial fatigue testing on flat sheets;

A new test setup for biaxial fatigue test of thin sheet materials, the so-called "SUPERBAT" (Specimen Using Poisson's Effect Ratio for Bi-Axial Testing) has been designed and evaluated. Biaxial stress ratio of $0 < \lambda < \nu$ (Poisson's ratio of the material) can be obtained with this technique.

(2) Combined extension and bending of thin sheets with a central crack;

Again, a new test setup has been developed, the so-called "CETS" (Curvature Effect Test System). This test setup can be used for investigating the bending effect of the skin sheet introduced by bending the skin sheets to the radius of the fuselage. It has been observed that the so-called "Bulge-out" does occur in this test condition. A theory on the combined extension and bending of thin sheets with a central crack has been developed which suggests that "bulge-out" is caused by the interaction between the tensile and bending stress fields.

(3) Test on pressurized fuselage skin sheets;

An unique test system for both static and dynamic tests on pressurized fuselage skin sheets has been developed where air is used for the pressurization and very realistic test conditions have been achieved. Sectional tests can be carried out with both uniaxial and biaxial stress fields. A wide range of test data have been obtained for both monolithic aluminium alloy sheets and ARALL sheets. A better understanding of the "bulge-out" phenomenon has been achieved.

In chapter 2 of this report, the occurrence of dangerous fatigue cracks in fuselage structures under service conditions and laboratory conditions are summarized. The basic principals of the damage tolerance design philosophy are also briefly discussed. Chapter 3 deals with the analysis of longitudinal cracks in pressurized unstiffened thin-walled cylinders. The existing theories, both empirical and theoretical, are recorded and evaluated. A new theory for analyzing the bulge-out phenomenon, an approximate energy balance approach, is developed. Three different test set-ups for studying the effects of stress biaxiality, bending stress and bulge-out effect are discussed respectively in chapter 4. Test results obtained in these test set-ups are presented and evaluated in chapter 5. The results are compared to predictions by the theory of an approximate energy balance approach developed in chapter 3. The results are also compared to test results and non-linear FEM results found in the literature. Results of tests on ARALL specimens are discussed in chapter 6. The application of the damage tolerance design philosophy to ARALL fuselage structures is also presented in chapter 6. Finally, the main results and conclusions are summarized in chapter 7.

REFERENCES

1. McFarland, M.W., (Editor), *The paper of Wilbur and Orville Wright.* McGraw Hill, 1953.

2. Schijve, J. "Cumulative Damage Problems in Aircraft Structures and Materials" *The Aeronautical Journal* Vol.74, 1970. P.517. *The Third Plantema Memorial Lecture.*

3. Hart, I.B. *The World of Leonardo da Vinci,* Macdonald, London, 1961.

4. Gassner, E. "Fatigue life of Structural Components under Random Loading", *The Fourth Plantema Memorial Lecture,* Presented to ICAF, London, England, July, 1973.

5. Swift, T. "Damage Tolerance in Pressurized Fuselage", *The 11th Plantema Memorial Lecture.* Paper in New Materials and Fatigue Resistant Aircraft Design. Proc. 14th ICAF Symposium, June 1987, Ottawa. EMAS, UK 1987, pp.1-77.

6. Military Specification, Airplane Damage Tolerance Requirements, *Mil-A-83444 (USAF),* July 1974.

7. Code of Federal Regulations, Aeronautics and Space, FAR-Part-25.571. 1984.

8. Advisory Circular, Damage-Tolerance and Fatigue Evaluation of. Structure, AC No. 25.571-1A.-1A.

9. Joint Airworthiness Requirements, JAR-25.571.

10. Swift, T., *"Verification of Methods for Damage Tolerance Evaluation of Aircraft Structures to FAA Requirements".* Paper 1.1 in Industrial Applications of Damage Tolerance Concepts. Proc. 12th ICAF Symposium, May 1983, Toulouse. Issued by Centre d'Essais Aéronautique de Toulouse.

11. Vogelesang, L.B., J.W. Gunnink, D. Chen, G.H.J.J. Roebroeks, A. Vlot, *"New Developments in ARALL laminates",* Specialists Conference on ARALL laminates, 25-26 Oct. 1988, Delft, The Netherlands.

CHAPTER 2 CRACKS IN FUSELAGE

2.1 CRACKS IN SERVICE

In this chapter, the occurrence of dangerous fatigue cracks in fuselage structures is summarized. It includes several examples from service experience as well as results from full-scale fatigue tests. The meaning of damage tolerance requirements for fatigue cracks in aircraft structures will then be summarized.

The continued efforts of the entire fatigue and fracture community to develop analytical means and test procedures have considerably increased the level of safety. However, it appears that inadvertent incidents have been responsible for the greatest loss of life in structurally related accidents in the past 35 years.

On April 28, 1988, a Boeing 737-200's fuselage blew off at 7300 m (24,000ft) (see Fig.2.1 a). This airplane, Aloha N73711 was on its 89,681st flight and in its 35,496th flight hour. It was the second-oldest jet in the world, measured in flight-cycles or landings. The possible cause of this most massive structural failure was a longitudinal fatigue crack in the upper fuselage structure between sta 360 and sta 540 (see Figs.2.1 b and c) due to repeated internal pressurization.

Initial checks of the accident aircraft revealed cracks at rivets, measuring 0.2-0.6 in. (5-15 mm), on the S10L stringer. In the aft fuselage section, there were 14 indications of additional cracks. Seven of these 14 cracks were in one row. Inspection of the S4L stringer revealed 15 cracks which were also believed to be a result of fatigue[1]. Different suggestions have been made for the starting location of the rupture[1,2], but it appears to be sure that fatigue cracks in the stringers and the fuselage skin were the cause of the fracture.

The Aloha accident is not of remote concern. As reported in Ref.3, three 45,000-flights-plus low-corrosion 737s were found with multiple cracks between stations 360 and 540 along stringers S4R and S4L (see Fig.2.2) before the Aloha accident. The same 45,000 flights-plus aircraft had multiple cracks of

8

similar length in the aft fuselage S4 lap joints. The total length of these cracks was found to be 6m (20ft). Little corrosion was found.

The history of fatigue of fuselage structures can be recorded as early as 1954 when on January 10, 1954, a Comet I aircraft (registration number G-ALYP) known as Yoke Peter (Fig.2.3) disintegrated in the air at approximately 9000 m (30,000 ft) and crashed into the Mediterranean Sea of the island of Elba. At the time of the accident, the aircraft had experienced 1,286 pressurized flights and had flown 3,680 hours. Yoke Peter was the first high-altitude jet-propelled passenger aircraft in the world to enter scheduled service. It was advancing the state-of-the-art in a number of areas, not the least of which was that its cabin pressure was almost double that of any other pressurized transport aircraft in operation at that time.

The day after the Elba accident, on January 11, 1954, the Comets were removed from service. A number of modifications were made to the fleet to rectify some of the items that might have caused the accident. Two months later, on March 23, 1954, service was resumed. Only 16 days later, another disaster happened to the Comet fleet. Yoke Yoke disintegrated in the air at approximately 10,000 m (35,000 ft) and crashed into the sea of Naples. At the time of the crash, the aircraft had experienced 903 pressurized flights and had flown 2,703 hours.

After the loss of Yoke Yoke, it was immediately thought that a repeated loading (fatigue) test of the pressurized fuselage was needed. The tests were conducted under water to minimize damage in the event of failure. Yoke Uncle, a Comet I aircraft removed from service which had already experienced 1,231 pressurized flights during its service, was tested. After 1,826 more test pressurizations, for a total of 3,057, a failure occurred in the pressure cabin. Examination of the failure provided evidence of fatigue. The failure origin on Yoke Uncle was found at the aft lower corner of the forward escape hatch, as shown in Fig.2.4. The cracks emanated from the corners into the fuselage skin structure causing rupture of the entire structure. Further investigation of Yoke Peter structure recovered from the sea near Elba confirmed that the primary cause of failure was pressure cabin rupture due to fatigue. The origin in this case was at the right-hand aft corner of the rear automatic direction finding (ADF) window on top of the aircraft, as shown in Fig.2.5.

The role of cabin pressure, which can vary between 0.29 bar (4.16 psi) for early pressurized aircraft and 0.61 bar (8.90 psi) for modern wide-body transport aircraft, as the primary damage driver in the fracture mechanism of pressurized fuselage structures, was clearly demonstrated by the following incidents.

On August 22, 1950, a propeller blade from the No.3 engine failed on a DC-6 aircraft flying at 6400 m (21,000 ft). The cabin differential pressure was 0.29 bar (4.16 psi). The blade struck the fuselage edgewise and left the other side flat wise. The resulting damage was a hole about 23 m^2 (250 feet^2) in size. A similar incident occurred on March 5, 1957, when an entire propeller assembly left No.1 engine of a DC-7 flying at 4300 m (14,000 ft). The propeller assembly sawed its way through the cabin. All three blades made separate, long cuts at distinct, longitudinally spaced intervals. The final damage amounted to an opening of about 7.4 m^2 (80 feet^2). The cabin was pressurized with a differential pressure of 0.35 bar (5.1 psi). A propeller failure of this type had occurred on the ground with the cabin unpressurized. In this case, the damage was confined to a narrow sawcut-like slot in the lower fuselage.

Recently, cracks in fuselage structures of ageing pressurized transport aircraft, mostly a result of structural fatigue, have become a serious threat to the safety of air transport. Many fatigue cracks in fuselage structures are fortunately found prior to reaching a critical length.

On February 17, 1976, a telex was sent by Boeing Company to all 747 customers alerting for cracks in 747 fuselage skin structures[4].An unknown 747 operator reported a loud noise followed by a pressurization loss after leveling off at 9400m (31,000 ft). After the aircraft had landed, a crack was found in the left-hand lower body, running along the upper-outboard-fastener row of the outboard skin at the stringer 44 lap splice between sta 836 and 900. The crack had a length of 1m (40 in.). It was not found during the routine inspections because the crack was covered by the fairing and thus invisible from the outside of the airplane. The airplane had experienced 7100 landings and 21,500 flight hours. The cause of the crack was believed to be severe corrosion and repeated fuselage pressurization.

This incident was not an isolated case. In 1985, a Boeing 747 operator reported a large number of fatigue cracks in the forward fuselage (section 41-S41) of several high time 747 aircraft. One aircraft was found to have 11 frames cracked, three adjacent frames of which were completely severed. In early 1986, FAA issued an urgent Airworthiness Directive calling for external skin inspections around the problem areas for aircraft which had achieved more than 10,000 flights. Boeing subsequently developed internal visual inspection procedures for the fuselage frames. The inspections discovered serious fatigue problems in the Section 41 of the 747s with around 10,500 flight cycles. The inspection threshold was then lowered to 8,000 flight cycles and again to 7,000 flight cycles. In December 1986, three Australian 747 aircraft had completed the 7,000 cycle inspection resulting in the discovery of a 46 mm frame web crack. Two aircraft have also completed the 10,000 cycle inspection resulting in 14 frame cracks being discovered, with one crack extending 20 mm. Investigations carried out by Boeing confirmed that cracking in section S41 was related to fatigue (pressurization) only.

As a result of the previously mentioned Aloha 737 accident, extra inspections were ordered by FAA for inspecting ageing aircraft, especially Boeing 737's and DC-9's. According to Ref.6 and Ref.7, cracks were found on the skin at four locations near stringer 1 on an US AIR DC-9-30 which had accumulated 69,000 flight cycles (Fig.2.6). Cracks in skin fasteners and 14 stringer cracks were noted in a second US AIR DC-9 aircraft which had completed 65,000 landings. The longest crack had reached a length of 1 in. (25.4 mm). Further inspections on the DC-9 fleet had found similar cracks in 24 aircraft. Fuselage skin cracks had been found in 5 aircraft [5].
Similar problems were met in both ageing Boeing 737 and 727 aircraft which led to the proposals by FAA for replacing rivets in the problem areas of those aircraft[7].

The Boeing- and the DC-aircraft are not the only aircraft suffering from the cracks in their pressurized fuselage structures. Cracks in the pressurized fuselage structure of other types of aircraft have also been found. It was reported in Ref.9 that cracks occurred in the upper fuselage skin of a British

11

Airways' Concorde. It has also been reported that a cabin decompression of an Airbus A310 occurred in January 1988 while the aircraft was in flight above Cyprus. It is believed that fatigue of the fuselage structure was the main cause of the incident.

A summary of aircraft accidents involving fuselage fatigue in the last 35 years is given in Table 2.1. The table is probably not complete, but the cases listed reached the headlines of the news papers. The latter does not apply to the many more incidents of fatigue cracks which were discovered in time.

2.2 CRACKS IN FULL-SCALE FATIGUE TEST

The introduction of the so-called "Damage Tolerance" design philosophy has resulted in a change of aircraft design criteria, which now require additional consideration of structural integrity, assuming certain damage to exist in the structure. The overall effect of the damage tolerance design philosophy is to require additional tests to establish not only the locations of likely fatigue crack initiation and the duration of these crack initiation lives, but also the growth rate of such cracks under spectrum loading and the resulting critical crack length within the complex full scale structure, considering all load redistributions within the cracked structure. This can only be satisfactorily accomplished with full scale tests of aircraft sections.

The first full scale test on a fuselage was conducted as early as in 1954 on a Comet I aircraft after the loss of two aircraft discussed before. In 1954, the RAE (Royal Aircraft Establishment) decided that a repeated loading test of the pressurized cabin was needed. The test was conducted in a tank under water to minimize damage in the event of failure. After 1,826 test pressurization cycles, a failure occurred in the pressure cabin. Examination of the failure provided evidence of fatigue[10]. The aircraft was repaired and strain gauge measurements were carried out at the various locations on the outer skin of the fuselage (Figs.2.4 and 2.5). It turned out that the skin material in the corners of the cutouts was extremely highly loaded. Combined with the bending effects described in Ref.10, the structure should indeed fail within a very short service life. The investigation further showed that the most likely

12

cracking configuration was a crack adjacent in the frame because of the high stress concentration caused by the notch. In that case, either a one- or a two-bay crack would result in failure of the entire structure because of a low skin fracture toughness, a high stress level, and the specific frame geometry of the aircraft.

An investigation on fatigue damage occurring in aircraft both in service and during a full-scale test[11] has shown, that despite the experience gathered in aircraft constructions and world wide research, many fatigue problems remained unsolved. A full-scale test on DC-10/30, which was designed about 20 years later than the Comet I, showed a similar design error made in Comet I. During the large-scale fatigue test on the DC-10 fuselage, a crack appeared in the skin and doubler at a corner of a door frame after 30800 simulated flights (Fig.2.7). Strain gauge measurements at that area revealed that the stresses in the entire area of the door frame were far in excess of the calculated nominal stresses. Damage of the same type also occurred in other fuselage openings in earlier DC-10's. This type of cracks has been found in several types of aircraft. Passengers entering the aircraft can easily observe the repairs.

The Bristol Britannia type 100 was a pressurized passenger aircraft designed in the late fifties. Although the damage tolerance design philosophy was not yet developed at that time, large-scale fatigue tests were carried out on the fuselage of the aircraft. In those tests fatigue cracks were found along the longitudinal fuselage joints after 30,000 simulated flights. Due to the detail design of the aircraft, the fatigue cracks were not visible from the outside of the fuselage, at least not in the early stages. The cracks had reached a length of 70 to 300 mm when they were discovered[12] (Fig.2.8). In two cases these cracks led to a catastrophic failure causing bursting of the fuselage skin over a length of several meters. The cracks which ran along the longitudinal joints through the rivet holes, emanated from almost every rivet hole. It was a typical case of the now so-called "multiple site damage", which is still a weak link in the damage tolerance design philosophy.

These fuselage skin cracks were not the only fatigue cracks found during large scale fatigue tests of the Bristol Britannia type 100 aircraft. Only after

6616 simulated flights several frame fractures or cracks were also discovered in the fuselage. The cracks originated from the last rivet holes of the frame reinforcement running toward the skin sheet. Fresh cracks were discovered even after modifications were applied to that area. Due to early discovery of the cracks, no resulting skin cracks were found, which otherwise might lead to catastrophic failure of the fuselage.

The fact that fatigue is still a matter of great concern for the aircraft industry even in the 80s, is once again demonstrated by the full-scale tests carried out by Airbus Industry on its A310 in 1984. Four major full-scale fatigue and damage tolerance tests were conducted (Fig.2.9). After 37,000 simulated flights frame 51 in the center fuselage section was found to be completely failed at the location of stringer 25 (Fig.2.10). Inspection in the surrounding area of the crack did not show resulting damage in the skin structure[13]. However, the fatigue damage was located in an area, which is very difficult to inspect in service. Cracks in the neighbouring skin structure might be generated as a result of the loss of local stiffness in the frame. A similar crack of 80 mm was found at frame 46/stringer 22 after 56,000 simulated flights (Fig.2.11). Further damage tolerance tests with artificial damages showed significant crack growth in a mid bay area between frames 54.2 and 54.3 (Fig.2.12). A crack growth rate of about 0.01 mm/cycle was observed.

Full-scale testing of aircraft structures is regarded as the best method to verify the design philosophy, including stress analyses, production methods and inspection programs of an aircraft. Short comings and even errors in the structure can be exposed in an early stage. Inspection programs can be adjusted according to the test results. Unfortunately, catastrophic accidents of those carefully designed and tested aircraft still occur in service. It is very difficult to indicate the main causes of those failures. Anyhow, it is certain that new generation transport aircraft can be and must be designed to fly more safely and economically.

2.3 DAMAGE TOLERANCE DESIGN PHILOSOPHY

Since the introduction of pressurized fuselage, aircraft speeds have been increased, operators have demanded longer service lives, and new materials have been introduced with their own characteristic properties. The developments have demanded more comprehensive design requirements and better design techniques to ensure that each new aircraft maintains the existing standards of airworthiness.

The first document in this field probably is the British Handbook of Strength Calculation, referred to as AP 970[14], SP 970 and later AvP 970[15]. This book was considered as a recommendation document rather than a requirement. The book was solely concerned with strength calculations, that is to say with the derivation of loads and their applications to the structure. Little attention was paid to stiffness, fatigue and temperature in the first issue of the handbook. As a 'Bible' of the British structural designer and analyst, the handbook has been used for a long period.

At that time, the aircraft structure was regarded as a rigid body. The so-called 'load-factor' n which included a factor of safety of 2.0, had been widely used. The term 'proof load' was not introduced to the aircraft structure designers. Components were designed to withstand the ultimate load resulting from the factor n, and no account was taken of possible distortion, permanent or otherwise. However, deflections must have been small in the braced truss structures at that time.

During the 1930's, the ultimate factor of safety was reduced from 2.0 to 1.5. This reduction has been regarded as a large progress in the design philosophy of aircraft structures. However, in several discussions on this safety factor [16,17,18] it was said that the value of 1.5 did not account for the compression members which failed by buckling, and for most tensile members, like joints, which were severely loaded. For those reasons, U.S. commercial aircraft designers have applied two supplementary factors of safety, the 1.15 extra factor for fittings and an 1.33 extra factor for pressurized fuselages [19]. The extra factor of safety for pressurized fuselage was meant to cover any uncertainty in the stress calculations of the pressurized fuselage, and to compensate the lack of fatigue knowledge at that time.

After the second world war, the phenomenon fatigue became a dominant aspect of structural airworthiness. Its effect on the choice of material, on the geometry and arrangement of structures, on the choice of stress levels and therefore on the air frame mass, has been little short of revolutionary. As a direct consequence of considering fatigue problems the 'fail-safe' design philosophy was introduced to aircraft design by the 1950's.

The rapid development of Fracture Mechanics in later years has led to a new design concept, that of damage tolerance design. This new design philosophy was officially introduced by the USAF (Mil.-A-83444)[20] in 1974. Four years later, the Federal Aviation Administration (FAA) published a new Federal Aviation Regulations (FAR) Part 25.571 containing the damage tolerance and fatigue evaluation certification requirements for transport category aircraft structures. The FAA has also outlined an Acceptable Means of Compliance of the FAR 25.571 [21]. The European aviation authorities have also accepted this new design philosophy in the JAR 25.571 document[22] which is almost identical to the FAR 25.571.

A definition of damage tolerance given by Boeing states[23]:
Damage tolerance structure is able to sustain regulatory fail-safe loads in the presence of damage, such as fatigue cracks, until the damage is detected through inspection or malfunction, and repaired.
Through the discussion in reference 23, it is clear that the damage tolerance philosophy contains the following aspects:
A.   Structures always contain damages, such as initial flaws, fatigue cracks, corrosion and incidental damage. The last two kinds of damage should not be ignored, but more attention has to be paid to fatigue cracks;
B.   Residual strength of the remaining structure should be sufficient to sustain the regulatory fail-safe loads or the design limit loads;
C.   Damage should be detected in time through inspection or malfunction. As stated by Swift[24]:
The objective of the damage tolerance evaluation, is simply to provide an inspection program for each principal structural element (PSE) such that cracking, initiated by fatigue, accident or corrosion will never propagate to

16

failure prior to detection. Inspection programs are essential for the aircraft structure to be damage tolerant. However, malfunctioning of the structure should be prevented. When it does occur, it should be noticed;

D. Repair or replacement of the damaged structure or element must be possible in order to ensure the continuity of the airworthiness of the aircraft.

According to the current FAR and JAR damage tolerance requirements all flight structures must be damage tolerant, unless it can be shown that damage tolerance design of certain structures is not practical. In the latter case, the safe-life approach should be used (FAR and JAR 25.571). In practice, only the landing gear and its attachments are considered to be not feasible for damage tolerance design, because potential cracking in such structures could lead to catastrophic failure before reaching detectable limits using current in-service inspection methods.

There are three main damage tolerance design concepts (terminology of Ref.20):

      Multiple-Load-Path (MLP)

      Crack-Arrest Fail-Safe (CAFS) and

      Slow-Crack-Growth (SCG)

Typical examples of these structures are shown in Fig.2.13.

All damage tolerance design concepts are acceptable according to the current requirements. None of them has been made mandatory by the authorities. However, damage tolerance can be achieved more easily by incorporating such fail-safe features as redundancy, multiple load paths and crack arresters. The so-called fail- safe structure can sustain large damage (e.g. a failed load path), but if unattended such damage will grow and eventually cause a catastrophic failure. Hence, fail-safety features by themselves do not prevent loss of the aircraft. The partial failure (e.g. the failed load path) must be detected and repaired. Even if the structure is fail-safe, inspection and detection are essential to achieve safety.

As shown by the ageing Boeing aircraft, the problem of multiple damage is still of great concern for the aircraft designer.In the AC 25.571-1A, section 5, the following sentences can be found:

Design features which should be considered in attaching a damage-tolerant structure include the following:

17

(iv)Provisions to limit the probability of concurrent multiple damage, particularly after long service, which could conceivably contribute to a common fracture path. Examples of such multiple damage are:

(A) *A number of small cracks which might coalesce to form a single long crack.*

(B) *Failures, or partial failures, in adjacent areas due to the redistribution of loading following a failure of a single element; and*

(C) *Simultaneous failure, or partial failure, of multiple load path discrete elements, working at similar stress levels.*

Swift[24] and Stone[25] believe that this problem can be solved satisfactorily with the two bay crack criterion. However, a particularly difficult problem to rationalize is multiple cracking along a row of fastener holes where a number of small cracks, each of less than detectable size, which may coalesce to form a single long crack (case Aloha Boeing 737-200). This condition, which is more likely to occur in aircraft operating beyond their original design service life, can present a difficult inspection problem, because the visible length of the cracks on each side of the fastener hole will be of the same order as the critical crack length of the structure (see Fig.2.14). In this case, Swift suggested that a stress level should be chosen to make sure that cracks of initial quality flaw size will not grow in the life of the aircraft[24].

For most aircraft structures, inspection programs must be matched to the structural characteristics for timely damage detection. There are three distinct elements of equal importance for achieving the desired level of safety[26]:

A. Allowable damage: the maximum damage, including multiple secondary cracks, that the structure can sustain under limit load conditions.

B. Damage growth: the interval of damage progression from detection threshold to maximum allowable based on proper recognition of operating loads, sequence effects, and environmental influences.

C. Inspection program: a sequence of inspections in a fleet of aircraft with methods and frequencies selected to achieve timely damage detection.

18

A structure containing features, such as large allowable damage and long damage growth period, is better damage tolerant than the structure which wholly depends on the inspection programs.

The allowable damage, or the residual strength of a structure depends mainly on two factors: the structure design concept and the fracture toughness properties of the material. The rate of damage propagation is a function of material properties, structural configuration, environment, crack length of primary and secondary cracks, and operating stress exposure. Since inspection is the key factor for safety of the aircraft structure, crack growth from detection threshold lengths to the allowable damage determined by residual strength analyses is critical. This can only be achieved by intensive testing on structures under realistic condition or by incorporating advanced fracture mechanics analyses.

During the last 10 years, progress has been made in developing fiber reinforced plastics as a high performance structural material. Increasing numbers of secondary aircraft structures are being made of composite materials. Nevertheless, application of composite material in the primary aircraft structures has not yet been generally accepted by the authorities. However, exceptions exist, such as the full-composite Beechcraft Starship, which has recently been certified under the existing damage tolerance requirements.

Originally the damage tolerance concept was developed for metallic structures. Some difficulties were recognized when composite structures also had to be certified under the damage tolerance requirements.

Important differences between metallic materials and composite materials are:

1. Composite materials generally have a small strain to failure. They do not exhibit yielding and plastic deformations.

2. Composite materials have properties which can be highly anisotropic.

3. Composite components can exhibit a significant strength variation (scatter) when compared to their metallic counterparts.

4. Large readily detectable flaws in composite components can have good residual strength capabilities and can be demonstrated not to grow under cyclic loading. This "no-growth" phenomenon of composites is in contrast to metallic materials.

19

5. Large changes in properties of composite materials after impact.

6. Erosion damage can lead to moisture ingress and delamination of the composite.

7. Inspection of composite materials in service can be complicated by the lack of commonly accepted rules for visual inspections such as observation on surface deformation and reflections.

8. Repair of composite components can also be very complicated even impossible.

Experience has learned that fatigue of composite structures is not of great importance. This is strongly in contrast to metal structures. On the other hand, impact and durability of a composite structure are the major concerns with respect to the damage tolerance certification.

In general, application of composite materials in aircraft structures should achieve a safety level equivalent to that of the current conventionally constructed aircraft with the underlying principles that the structure should be designed to retain ultimate load capability at any time during its service life, including the effect of repeated load and environmental exposure.

Damage tolerance design exercises are thus in fact a process of finding the acceptable balance between safety and economy by looking for an optimal combination of material, structural configuration, operating stress level and inspection procedures. The allowable damage, or the residual strength of a structure, depends mainly on two factors: the design features and the fracture toughness properties of the material. The crack growth behaviour of the structure is the decisive factor for the establishment of inspection programs. As stated above, a structure containing features such as large allowable damage and long damage growth period is better damage tolerant than the one which wholly depends on the inspection programs. This has clearly been shown by the recent accidents with the ageing Boeing aircraft where catastrophic failures still occur in spite of intensive inspection programs ordered by the authorities. Besides, it is certainly incorrect to give full responsibility of safety to the maintenance teams of the operator where human error, qualification of the technicians and financial aspects can have important influence on the quality of inspection. This is especially true when ageing aircraft are concerned. It is thus the author's opinion that *emphasis must be*

put on the research and development of application of new materials in primary aircraft structures in order to achieve a larger allowable damage and longer damage growth periods. It is then also of vital importance that the crack growth behaviour of materials under realistic condition are known in order to get better damage tolerance design and more relevant inspection programs.

The damage tolerance design philosophy has undoubtedly enhanced safety of modern aircraft, but accidents have shown that short-comings exist in this design philosophy, especially when safety of the aircraft depends too much on the inspection programs. It is certainly true that with the conventional materials (aluminium alloys) damage tolerance of fuselage structures can only be achieved with very complicated design exercises and inspection procedures. The fact is that over 90% of the aircraft structures (both primary and secondary) are still made of these conventional aluminium alloys. It is thus important that profound knowledge of the fracture mechanics properties of these materials under realistic loading conditions are available in order to achieve better damage tolerance design of aircraft structures. With the introduction of the new generation of structural materials, such as ARALL and GLARE laminates, it is also important to develop new test techniques to study the fracture mechanics properties in order to produce basic design data for the damage tolerance design with these materials.

It should also be noted that the crack initiation in the fuselage structure occurs not always at the rivet holes. From the fracture mechanics point of view, a more severe situation can arise, which is a crack in the fuselage skin sheet between the stiffening elements (the so-called free-field), where the skin material is not supported by the surrounding stiffening elements and suffers more from secondary effects (such as the bulge-out effect). Crack initiation in the free-field will mainly be due to ground handling damage. Accidental damage of the skin sheet may be caused by ground service personnel, e.g. by falling of equipment on the upper fuselage skin structure and impact by service vehicles at the lower fuselage sections. These impact damages will cause fatigue crack initiation in flight if they are not reported and repaired properly.

It must thus be concluded that further research efforts on the fracture mechanics properties of both conventional and new materials are necessary in order to achieve better damage tolerance design of aircraft fuselage structures. Within this context, three new test techniques have been developed. Both conventional monolithic aluminium sheets and ARALL laminates have been tested using these new techniques. A detailed description of these test methods and evaluation of the test results are reported later on in this report.

REFERENCES

1. **Ramsden, J.M. and J. Marsden,** "Caring for the high-time jet", *Flight International,* 3 September 1988, and "The long-life structure", *Flight International,* 17 September 1988. p.153.

2. "Passengers on Board Aloha Flight Cite Fuselage 'Crack' Seen Prior to Accident", *Aviation Week & Space Technology,* July 25, 1988. p.61.

3. **Ott, J. and R.G. O'Lone,** "737 Fuselage Separation Spurs Review of Safeguards", *Aviation Week & Space Technology,* May 9, 1988. p.92.

4. *Boeing service letter number 747-sl-53-1,* February 17, 1976.

5. **Fotos, C.P.,** "Airline Officials Defend Safety of Fleets Following FAA Ruling", *Aviation Week & Space Technology,* November 7, 1988. p.68.

6. "DC-9 Operators Ordered to Conduct Upper Fuselage Fatigue Crack Inspections", *Aviation Week & Space Technology,* November 28, 1988 p.99.

7. "FAA proposes Checks for Cracks on 727s", *Aviation Week & Space Technology,* January 16, 1989. p.63.

8. "Cracks Found in Two Concorde Fuselages", *Aviation Week & Space Technology,* February 20, 1989 p.119.

9. **Campbell, G.S. and R.T.C. Lahey,** A Survey of Serious Aircraft Accidents Involving Fatigue Fracture, Vol.1 Fixed-Wing Aircraft. Aeronautical Note, NAE-AN-7, NRC NO.21276, National Aeronautical Establishment, Ottawa, Canada. April 1983.

10. **Swift, T.,** Damage Tolerance in Pressurized Fuselage, 11th Plantema Memorial Lecture, presented to 14th Symposium of the International Committee on Aeronautical Fatigue (ICAF), New Materials and Fatigue Resistant Aircraft Design, Ottawa, Canada, June 10-12, 1987.

11. **Huth, H. and D. Schütz,** The Collection and Analysis of Fatigue Damage Occurring in Aircraft in Service, Library Translation 1934, Royal Aircraft Establishment, Farnborough, Hants.ICAF Doc. No 1035 August 1977.

12. **Morgan, W.H.,** The Fatigue Test Failures of a Pressurized Fuselage (Britannia Type 100), Royal Aircraft Establishment, Farnborough, Hants, RAE TR 70241, ICAF Doc. No 538, December 1970.

13. Schmidt, H.-J., and C.L. Hammond, "A310 structural testing for certification philosophy and application to meet current durability and damage tolerance requirements", ICAS-84-3.6.1, 1984.

14. Handbook of strength calculations AP 970, HMSO, 1928.

15. Design Requirements for aircraft for the Royal Air Force and Royal Navy, AvP 970, HMSO, 1935.

16. Grinsted, F., Suggested changes in the design basis for structural airworthiness of military aircraft. REA Tech Noto Structures 38, June 1949.

17. Margurian, G.N., "Is the present aircraft structural factor of safety realistic ?" *Aeronautical Engineering Review,* Sept. 1954. p.63.

18. Montagnon, P.E., The case for factor of safety of 1.5 instead of 2.0, with special reference to the flight envelope, R&M 2578, Jan. 1944.

19. Shanley, F.R., "Historical note on the 1.5 factor of safety for aircraft structures", *J. Aero. Sci.* (AIAA) Vol.29, No.2. Feb. 1962, p.243.

20. Military Specification "Airplane Damage Tolerance Requirements", Mil-A-83444, 2 July 1974.

21. Advisory Circular AC 25.571-1, FAA, 1978.

22. JAR-25.571, Part 25, Section 1, Paragraph 25.571.

23. Hall, J. and Goranson, G., Structural Damage Tolerance of Commercial Jet Transporters, Boeing Airliners Articles, 1984.

24. Swift, T., "Verification of aircraft structures to FAA requirements", ICAF, Toulouse, May 25-27, 1983, p.1.1/1.

25. Stone, M. and T. Swift, "Future damage tolerance approach to airworthiness certification" 10th ICAF, Brussels, Belgium, May, 1979.

26. Goranson, U.G. and J.T. Rogers, "Elements of damage tolerance verification. ICAF, Toulouse, May 25-27, 1983, p.1.8/1.

CHAPTER 3 ANALYSIS OF LONGITUDINAL CRACKS IN PRESSURIZED
UNSTIFFENED THIN-WALLED CYLINDERS

3.1 PHENOMENA

As mentioned in the previous chapter, pressurization of the fuselage has a significant influence on the stress distribution in the fuselage skin structure. It does not only affect the overall stress level due to the hoop stress induced by the internal pressure, but it also creates complicated stress conditions caused by both geometrical and stress non-linearities. According to the damage tolerance requirements, analysis of cracks in fuselage must consider all the stress conditions in a realistic manner, including these secondary effects.

In the past 30 years, linear elastic fracture mechanics (LEFM) has been proven to be a useful analysis method in aircraft structural design. The stress intensity factor K is considered to be the major decisive parameter for fatigue crack growth and the residual strength behaviour of a cracked structure. The general equation for stiffened thin-walled structure of finite size (fuselage) with a longitudinal crack a and hoop stress σ_h is

$$K = \sigma_h \sqrt{\pi a}\, \beta_1 \beta_2 \beta_3 \ldots \beta_n$$

where the β_n terms are modification factors including the following, if applicable:

- finite size correction factors;
- factors accounting for the effect of stiffening on a cracked sheet;
- factors accounting for the effect of nonuniform stress distribution from the pressurized stiffened cylinder due to pillowing;
- factor accounting for the effect of a biaxial state of stresses;
- and last but not least, correction factors accounting for the effect of bulging of the crack edges due to pressure and local sheet bending.

The above equation assumes that the effects are not interrelated. If they do interfere the effect cannot simply be represented by a multiplication factor. The last correction factor is generally called the bulge factor β_b, which is defined as:

$$\beta_b = \frac{K_{curved}}{K_{flat}} \tag{3.1}$$

where K_{curved} = stress intensity factor of a curved panel with a crack

K_{flat} = stress intensity factor of a flat panel of the same material, thickness, crack length and in-plane remote tensile stress perpendicular to the crack

The biaxiality and the bulge correction factors are strongly associated with the pressurized thin-walled cylinders. They have been a topic of fracture mechanics research for about 30 years.

As early as in 1957, Peters and Kuhn conducted series of tests on the bursting strength of 2024-T3 and 7075-T6 aluminium-alloy unstiffened cylinders containing longitudinal slits to simulate cracks[1](Fig.3.1). It was recognized that the residual strength of the cylinders could not be described with the linear elastic fracture mechanics theory developed for cracked flat sheets. Significant residual strength reductions were found in comparison with flat sheets. This effect was later described as a result of deflection and rotation of the crack edges due to lateral pressurization. It was called the 'bulge-effect' [2](Fig.3.2). Much effort has been made to understand this 'bulge-effect' through both analytical and experimental research. Unfortunately, no satisfactory explanation, which is generally accepted, has emerged until now.

3.2 THEORIES (EMPIRICAL AND THEORETICAL)

The theories developed in the last thirty years can generally be divided into two major groups. Within each group, two methods can be distinguished:

(1)empirical formulas ——⌈— through tests on bursting strength
                                        of unstiffened cylinders

                                    └— through full-scale fatigue tests
                                        on fuselage structures

(2)theoretical considerations ——⌈— linear fracture mechanics analyses

                                        └— finite element calculations
                                        (both linear and non-linear)
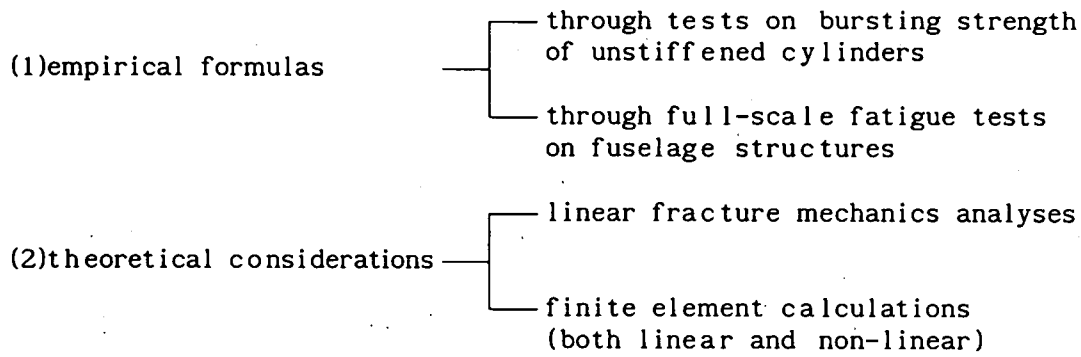
In this section a brief review of the theories will be given.

3.2.1 PETERS & KUHN[1] (TESTS ON BURSTING STRENGTH OF UNSTIFFENED CYLINDERS)

A series of unstiffened cylinders of 2024-T3 and 7075-T6 aluminium alloy containing slits of various lengths were tested by internal pressurization using air or oil. Two cylinder radii, 91.4 mm and 365.7 mm, and four nominal skin thicknesses, 0.15 mm, 0.30 mm, 0.40 mm and 0.635 mm, were the primary variables investigated. The cylinder length varied between 508 mm and 1892 mm and the slits (cracks) had a length (2a) between 6.1 mm and 202.4 mm. It was found that the bursting strength (nominal hoop stress at failure) was substantially reduced by increasing the slit length and decreasing the curvature (Fig.3.3). No effect of the pressure medium was found. The effect of slit length was in agreement with linear elastic fracture mechanics theory, but the strong effect of curvature could not be explained by known theories at that time. Because the curvature effect could not be calculated, it was taken into account by an empirical curvature correction factor to be applied to the stress intensity factor:

$$\beta_b = 1 + 9.2 \, \frac{a}{R} \qquad\qquad (3.2)$$

where   a = half slit (crack) length

              R = radius of cylinder

The hoop stress at failure then followed from:

$$K_c = \sigma_h \sqrt{\pi a} \, \beta_b$$

where K_c is the critical stress intensity factor of a centrally cracked flat sheet subjected to remote uniform tensile stress.

It is remarkable that the sheet thickness does not appear in Eq.(3.2). Apparently it was supposed not to affect the empirical correlation represented by this equation.
The curvature correction factor (bulge factor) was applied to both 2024-T3 and 7075-T6 aluminium alloy sheet with very satisfactory results. It was pointed out by the authors that the correction factor could not be applied to other materials.

3.2.2 ANDERSON & SULLIVAN[2] (TESTS ON BURSTING STRENGTH OF UNSTIFFENED CYLINDERS)

Bursting tests were carried out on cylinders of two different materials (an Al-alloy and a Ti-alloy) for various thicknesses, radii, crack lengths and temperature (room temperatures, $160°C$, and $217°C$). The 2014-T6 cylinders had a wall thickness of 1.52 mm and a radius of 71.4 mm. The initial half crack length varied between 1.32 mm and 25.40 mm. The titanium (5Al-2.5Sn-Ti) cylinders had a wall thickness of 0.51 mm and a radius of 76.2 mm. The initial half crack length varied between 1.18 mm and 20.32 mm.
The linear elastic fracture mechanics approach was followed. The stress intensity factor K_h due to hoop stress σ_h alone was assumed to be that of a centrally cracked wide sheet subjected to a remote uniform tensile stress

$$K_h = \sigma_h \sqrt{\pi a} \qquad (3.3)$$

The contribution of the longitudinal stress σ_l to the stress intensity (biaxiality effects) was ignored. The influence of lateral pressure on the stress intensity was considered to be the effect of pressure on the sheet material at both sides of the crack. Pressure against the material near the crack was assumed to be the main cause of the deflection and rotation of the crack edges. The bending moment associated with the deflection and rotation was considered to cause an increased stress intensity at the crack tip. The

surface bending stress $\sigma_{y,bending}$ ahead of the crack tip, but still close to the crack tip, was then related to a stress intensity factor associated with pressure bulging K_b by

$$\sigma_{y,bending} = \frac{K_b}{\sqrt{2\pi r}}$$ (3.4)

where r = distance from the crack tip.

On the other hand, the surface tensile bending stress ahead of the crack, $\sigma_{y,bending}$ was assumed to be a function of distance from the crack tip r, pressure p, shell thickness t, Young's modulus E, and crack length 2a. In the absence of an explicit relation between $\sigma_{y,bending}$ and this set of variable, it was assumed that $\sigma_{y,bending}$ can be expressed in the functional form

$$\sigma_{y,bending}(p,E,a,t,r) = f\ p^{\alpha 1}E^{\alpha 2}a^{\alpha 3}t^{\alpha 4}r^{\alpha 5}$$ (3.5)

where f is a dimensionless coefficient and α_n are dimensionless exponents. Correct dimensionality of equation (3.3) led to $\alpha_2 = 1 - \alpha_1$ and $\alpha_3 = -(\alpha_4 + \alpha_5)$ or

$$\sigma_b = f\ E\ (\frac{p}{E})^{\alpha_1}\ (\frac{a}{t})^{-\alpha_4}\ (\frac{r}{a})^{\alpha_5}$$ (3.6)

From the additional assumption that the problem is a linear elastic one, the bending stress had to be proportional to the pressure, (thus $\alpha_1 = 1$) and the stress near the crack tip had to vary inversely with the square root of the distance from the crack tip (thus $\alpha_5 = -\frac{1}{2}$). Replacing $-\alpha_4$ by α in equation (3.6) yields

$$\sigma_{y,bending} = f\ p\ \sqrt{\frac{a}{r}}(\frac{a}{t})^{\alpha}$$ (3.7)

From equations (3.4) and (3.7) the bulge stress intensity factor K_b was then related to pressure, crack length and shell thickness by

$$K_b = C\ p\sqrt{\pi a}\ (\frac{a}{t})^{\alpha}$$ (3.8)

where C is a dimensionless coefficient equal to $f\sqrt{2}$.

29

The total stress intensity factor K_{total} was then assumed to be the sum of the stress intensity due to the hoop membrane stress K_h and that due to bulging K_b:

$$K_{total} = \sigma_h \sqrt{\pi a} + Cp\sqrt{\pi a} \left(\frac{a}{t}\right)^{\alpha} \qquad (3.9)$$

Replacing p by $\sigma_h t/R$ for a cylinder of radius R, equation (3.9) becomes

$$K_{total} = \sigma_h \sqrt{\pi a} \left[1 + C\frac{t}{R}\left(\frac{a}{t}\right)^{\alpha}\right]$$

$$= \sigma_h \sqrt{\pi a}\ \beta_b \qquad (3.10)$$

It was found from the test results that the dimensionless coefficient α was equal to 1. The bulging correction factor β_b thus became

$$\beta_b = 1 + C\frac{a}{R} \qquad (3.11)$$

which is identical to the bulging correction factor suggested by Peters & Kuhn (equation 3.2).

Unfortunately, it was found empirically that the coefficient C was not a constant and could vary between 1.57 and 9.50 (Fig.3.4). Moreover, the coefficient C was also observed to depend on the temperature which is beyond the scope of this report. For room temperature it was found for 2014-T6 that C = 6.5 which should be compared to C = 9.2 as found by Peters and Kuhn. It then should be realized that Anderson and Sullivan used relatively thick sheet material, i.e. t/R = 0.0213, whereas the Peters and Kuhn values are in the range of 0.0004 to 0.0070.

3.2.3 SWIFT[3,4] (FATIGUE TEST ON FULL-SCALE DC-10 FUSELAGE AND BURSTING TEST ON UNSTIFFENED CYLINDERS)

After intensive testing on full-scale DC-10 fuselage panels, Swift found an empirical formula for the bulge factor β_b

$$\beta_b = 1 + 10\frac{a}{R} \qquad (3.12)$$

which is very close to the equation of Peters & Kuhn (eq.(3.2)).

Equation (3.12) was found by comparing the test results of the full-scale DC-10 fuselage panels and those of flat panels.

The bulge factor was found to be valid only when the crack tip was sufficiently remote from the stiffener. It was found that with a full two-bay crack, when the crack tips were in the vicinity of the stiffener, the bulging might be ignored and flat panel data could be used to determine the residual strength of the curved structure.

It should be noted that Swift also reported on bursting tests on a series of unstiffened 0.81 mm thick 2024-T3 aluminium alloy cylinders with a radius R = 305 mm. The tests were arranged in such a way that, in addition to the internal pressure, stresses (tension or compression) could be applied simultaneously in the longitudinal direction of the cylinder. The validity of equation (3.12) was not checked by Swift, because K_c was not available for t = 0.81 mm. However, adopting his K_c value for 2024-T3 for t = 0.81 mm (K_c = 125.3 MPa$\sqrt{m}$) and reducing this value by 8%[18] for the lower sheet thickness, the test results (2a from 100 mm to 216 mm) agreed rather well with Eq.(3.12). Further, it was found that a compression stress in the longitudinal direction of the cylinder did significantly reduce the critical hoop stress of the cylinder. Swift did not discuss this phenomenon in his report. A possible explanation is that due to the hoop stress, a compression stress occurs along the crack edge (from tip to tip) in the longitudinal direction. This stress is increased by the application of a compression load in the longitudinal direction. Bulge out will be enhanced which can be responsible for the reduced strength. Although this case is not practically relevant, because in pressurized cylinders a longitudinal tensile load does occur, the observations are instructive.

It should be noted that despite the very limited theoretical background of equation (3.12), it is the most frequently used bulge factor for calculating the bulge effect of pressurized fuselage structures.

3.2.4 FOLIAS[6,7] (LINEAR ELASTIC FRACTURE MECHANICS ANALYSIS)

Folias was the first scientist to find an approximate analytical solution of the problem[6,7]. In his theory, bending and stretching of thin shells were treated according to the traditional two-dimensional linear theory with an additional assumption of shallowness (large R/t). This theory is only valid for elastic cases.

For an axially cracked cylindrical shell loaded under boiler stresses $(\frac{\sigma_1}{\sigma_h} = \frac{1}{2})$, the following theoretical bulge factor for $\lambda < 1$ was found

$$\beta_b = 1 + \frac{5\pi\lambda^2}{64} \qquad \text{for } \lambda < 1 \qquad (3.13)$$

An approximation of the bulge factor for all λ was also given by Folias:

$$\beta_b \cong \sqrt{1 + 0.317\lambda^2} \qquad \text{for all } \lambda \qquad (3.14)$$

$$\text{where } \lambda = \sqrt[4]{12(1-\nu^2)} \ \frac{a}{\sqrt{Rt}}$$

It should be noted that equations (3.13) and (3.14) are strictly linear elastic solutions. The practical value of the formulas was proven to be rather limited [10,15,16] (see 3.2.8 and 3.2.9).

3.2.5 ERDOGAN[8,9] & KIBLER[9] (LINEAR ELASTIC FRACTURE MECHANICS ANALYSES)

In reference 8 Erdogan developed a linear elastic fracture mechanics analysis method for crack problems in cylindrical and spherical shells made of composite material. As in references 6 and 7, the theory was mainly based on the assumptions that the deformation and strains remained small and the system behaved purely linear elastic. The solutions for isotropic cylinders given by Erdogan and Kibler were numerical solutions, which were very close to the solutions given by Folias. The relationship between the bulge factor β_b and λ according to Erdogan and Kibler is almost linear. A linear curve fitting of the results was given by Barrois[10].

$$\beta_b = 0.64 + 0.49\lambda \qquad \text{for } 2 < \lambda < 6 \qquad (3.15)$$

where again $\lambda = \sqrt[4]{12(1-\nu^2)} \ \dfrac{a}{\sqrt{Rt}}$

Substitution of λ with $\nu = 0.33$ in Eq.(3.15) gives:

$$\beta_b = 0.64 + 0.886 \ \dfrac{a}{\sqrt{Rt}} \qquad (3.16)$$

Like the solution of Folias, the numerical solutions given by Erdogan and Kibler are linear elastic solutions and do not really have any practical value[10,15,16] (see 3.2.8 and 3.2.9).

It should be noted that Eq.(3.15a) as well as Eq.(3.14) indicate a $\dfrac{1}{\sqrt{R}}$ effect and also a sheet thickness (t) effect. These effects are not confirmed by the previously presented empirical results, which are more in agreement with a relation as shown in Eqs.(3.2) and (3.12).

3.2.6 HAHN, SARRATE & ROSENFIELD[11] (MODIFICATIONS TO [6,7,8,9])

In reference 11, three closely related criteria for the extension of through-cracks in pressure vessels (bursting of internal pressurized cylinders) were derived: (i) a fracture-toughness criterion mainly for low- and medium-toughness materials, (ii) a flow-stress (large section yielding) criterion for short cracks in tough materials, and (iii) a modification of (i) for very thin-walled vessels. The criteria were based on the Folias analysis for a pressurized cylindrical shell and a plasticity correction based on the crack-tip displacement of the Dugdale crack model. The bursting criterion for very thin-walled vessels reads

$$\sigma_h^* = \dfrac{K_c}{\sqrt{\pi a \varphi}} \cdot \dfrac{1}{\beta_b} \qquad \text{for } \dfrac{R}{t} > 50 \qquad (3.17)$$

where σ_h^* = bursting hoop stress

φ = plasticity correction

$$= \left(\frac{\pi\sigma_h^{*}\beta_b}{2\bar{\sigma}}\right)^{-2} \ln\left[\sec\frac{\pi\sigma_h^{*}\beta_b}{2\bar{\sigma}}\right]^2 \qquad (3.18)$$

$$\beta_b = \sqrt{1 + 1.61\frac{a^2}{R^2}\left(50\tanh\frac{R}{50t}\right)} \qquad (3.19)$$

$\bar{\sigma}$ is an average flow stress ($\sigma_{yield} < \bar{\sigma} < \sigma_{ultimate}$) which depends on the material

For the stress levels associated with fatigue crack growth in aluminium alloys, (substituting in Eq.3.18 the practical values of $\beta_b \cong 2$, $\sigma_h^{*} \cong 85$ MPa, $\bar{\sigma} \cong 400$ MPa and $\bar{\sigma} \cong 450$ MPa for Al2024-T3 and Al7075-T6 respectively) the plasticity correction is fairly close to 1, and it can thus be ignored. For practical values of R/t ($\cong 2000$) the value of $\tanh\frac{R}{50t}$ is very close to 1 and Eq.(3.19) becomes:

$$\beta_b = \sqrt{1 + 80.5\frac{a^2}{R^2}} \qquad (3.20)$$

which is significantly different from previously presented results. It should be noted that Eq.(3.17) is based on the evaluation of bursting strength results of thin-walled cylinders loaded by an internal pressure which is much higher than the internal pressure applied in the pressurized aircraft fuselage.

3.2.7 COPLEY & SANDERS[12], MURTHY, RAO & RAO[13] (LINEAR ELASTIC FRACTURE MECHANICS ANALYSES) AND EHLERS[14] (LINEAR FINITE ELEMENT CALCULATION)

In references 12 and 13, different numerical methods were used to calculate the bulge factor of thin walled cylindrical pressure vessel with a longitudinal crack. The basic concept adopted in those studies is again linear elastic fracture mechanics. Numerical solutions were found which were more or less identical to the Folias' solution.

In reference 14, a linear elastic finite element study was carried out to investigate the validity of the existing analytical solutions. The finite

element model employed shell elements which included transverse shear deformation. The calculations were made for thick walled cylinders ($5 \leq R/t \leq 40$) with a very large crack ($0.525 \leq a/R \leq 3$) which is clearly beyond the scope of this report.

3.2.8 RIKS[15] (NON-LINEAR FINITE ELEMENT CALCULATIONS)

The first non-linear approach of the problem was carried out by Riks[15] using a finite element code called STAGSC-1. Predictor-corrector methods were used, where information along the path obtained in the calculation of previous points was used to construct estimates for the computation of the next point. The tension stress intensity in the mid-plane of the shell material was calculated through the energy release rate G by

$$K = \sqrt{\frac{EG}{t}} \qquad (3.21)$$

The following formula was used for obtaining the G for certain crack length a:

$$G_{a_1 + \frac{1}{2}\Delta a_1} = \frac{P(\underset{\sim}{d}(a_1 + \Delta a_1); \ a_1 + \Delta a_1) - P(\underset{\sim}{d}(a_1); \ a_1)}{\Delta a_1} \qquad (3.22)$$

where $\underset{\sim}{d}(a_1)$ = deformation field describing the configuration of the structure with a crack length 2a under a given internal pressure and $P(...)$ = the total potential energy of the system.

The boiler stresses ($\frac{\sigma_1}{\sigma_h} = \frac{1}{2}$) were used in the calculations.

The bulge factor β_b was further calculated according to equation (3.1).

It was found that the out-of-plane deflection at the center of the crack (w_0) was a non-linear function of the internal pressure (Fig.3.5) and the bulge factor of a given crack length decreased with increasing internal pressure (Fig.3.7). Furthermore it was found that the non-linear bulge factor was smaller than the linear bulge factor and tended to vary linearly with the crack length for the range of the crack length considered in the calculations (Fig.3.6). It was pointed out by Riks that the non-linear character of the cracked fuselage problem could not be ignored in the fracture mechanics consideration.

The non-linear consideration of the problem is certainly a step forwards for understanding the phenomena of "bulge-out". However, the significance of the calculation results has still to be verified by experiments.

3.2.9 ANSELL[16] (NON-LINEAR FINITE ELEMENT CALCULATIONS)

A similar non-linear FEM study of the problem was carried out by Ansell[16] with the FEM program ABAQUS. The boiler stresses were also used in his calculations. The stress intensity factors were also calculated through the energy release rate of the system. The bending stress intensity factors were calculated using linear elastic theory developed by Folias and compared to the non-linear FEM results. It was found that the bending stress intensity factors were much smaller than the tension stress intensity factor and could be neglected in the fracture mechanics considerations.

The displacements obtained from non-linear calculations were found to be similar to the results of Riks[15], i.e. significantly smaller than the results from linear calculations (see Fig.3.8). Again, the bulge factor was found to be dependent on the load, similar to Riks' results (see Fig.3.9).

Constant amplitude fatigue tests were conducted both on flat specimens and curved panels. Measurements of the out-of-plane deformation of the crack edge and the stress intensity factors (which were found by using the similarity concept involving the fatigue test results) of both flat and curved panels, showed good agreement with the non-linear results (Fig.3.10 and 3.11). It is remarkable that Ansell gives predicted K-values for a large crack length only (crack approaching the stiffening element) and not for small values of a.

Based on the FEM results for fuselage structures containing stiffening elements, Ansell suggested the following empirical formula for the bulge factor β_b

$$\beta_b = (1 + f) \cdot g \qquad (3.23)$$

The functions f and g account for the influences of the crack length, the geometry and the effect of internal pressure. For the case of a longitudinal crack starting from a frame with a crack length of half of the frame spacing, the bulge factor was assumed to be identical to that of an unstiffened

cylinder[4]. Without any argumentation, Ansell suggested that the function f should take the following form

$$f = 0.337 \cdot \,^{10}\!\log\left[1 + 10^{\,3\left(0.2\lambda - 7.5 \cdot 10^{-5}\frac{R}{t} - 7.5 \cdot 10^{-6}\lambda\frac{R}{t} - 0.54\right)}\right] \tag{3.24}$$

where $\lambda = \sqrt[4]{12(1-\nu^2)}\dfrac{a}{\sqrt{Rt}}$

The function g in Eq.(3.23) was proposed to be

$$g = (1-g_1)\cos(\arctan(g_2 \cdot \Delta p)) + g_1$$

or, which is the same

$$g = \frac{1 - g_1}{\sqrt{1 + g_2^2 \Delta p^2}} + g_1 \tag{3.25}$$

where g_1 and g_2 are subfunctions depending on crack length and the λ-value.
The function g_1 defines the lower limit of function g when the internal pressure Δp approaches infinity. It was assumed that g_1 decreases with increasing λ-value. The function g_2 governs the rate of the function g when it approaches the value of g_1. It increases with increasing crack length a. The functions g_1 and g_2 were not given explicitly by Ansell. It was suggested that these functions must be determined experimentally.
For $\Delta p = 0$, the function g equals unity and equation (3.23) represents the linear bulge factor.

3.3 EVALUATION OF THE EXISTING THEORIES

The theories discussed so far were divided into the following groups:

a. purely empirical formulas which are found after extensive bursting tests on pressurized unstiffened thin-walled cylinders [1,2,11];

b. purely empirical formulas which are found after fatigue tests on full-scale aircraft fuselage structures [3,4];

c. linear elastic analytical considerations using various numerical calculation methods[6,7,8,9,12,13,14]; and

d. non-linear finite element calculations based on energy considerations (energy release rate calculations)[15,16].

In Fig.3.12 calculated bulge factors are shown as a function of the λ-value. Values of λ applicable to several aircraft fuselage configurations are given in Table 3.1 for half crack lengths of 20 mm, 100 mm and 250 mm respectively. In Fig.3.13 the bulge factors are shown as a function of the half crack length a, for R=2000 mm and t=1.2 mm.

It was shown by the non-linear finite element calculations that the linear elastic theories can be valid only if the internal pressure is very small (Δp close to zero). As found by Riks and Ansell, the bulge factor of a crack in an internal pressurized cylindrical shell depends not only strongly on the geometrical parameters, but also on the internal pressure itself. This is in contrast with the empirical formulas and the formulas based on linear elastic considerations. For these formulas the bulge factor for a crack in an internal pressurized cylindrical shell is assumed to be independent of the internal pressure. Rather high bulge factors are obtained for the linear elastic analytical formulas, but noteworthy the empirical relations of Swift and Peters & Kuhn show a much lower bulge effect (see Figures 3.12 and 3.13). At the same time, it should be realized that most empirical data were obtained from static tests (i.e. at failure loads) where the large plastic zones may have influenced the bulge behaviour of the crack considerably. It must be concluded that up till now the non-linear finite element calculation is the only relevant theoretical approach towards the problem. Although it is still an elastic solution, it should be expected to be the more realistic approach for fatigue problems.

As a consequence it is of great interest to consider the problem from the fracture mechanics point of view by taking into account the non-linear effects associated with the non-linear deformations of the shell in the neighbourhood of the crack.

3.4 APPROXIMATE ENERGY BALANCE APPROACH

As mentioned previously, bulging of a cracked unstiffened thin-walled cylinder is a nonlinear problem which can not be analyzed by classical linear elastic theory. In this section, a basic concept of an approximate energy balance approach of the problem is given based on the Griffith energy balance approach of a cracked pressurized cylinder. An approximation of the energy release rate G for a cracked unstiffened thin-walled cylinder is given. The approximation contains a factor which must be experimentally determined. A more detailed solution of the problem will be given in chapter 5.

Consider a longitudinal cracked cylindrical shell with a radius R, thickness t and half-crack length a loaded by a constant internal pressure p. Due to this internal pressure, both in-plane and out-of-plane deformations of the crack edges will occur (Fig.3.14). Let s_1 and s_2 be the lengths of the out-of-plane deformation field in the neighbourhood of the crack in the direction perpendicular to the crack and in the direction along the crack edges respectively (situation I in Fig.3.14). Consider the next situation when the crack has extended from a to a+Δa under the constant internal pressure p. Due to the pressure the out-of-plane deformation field will increase. The lengths s_1 and s_2 will increase to $s_1 + \Delta s_1$ and $s_2 + \Delta s_2$ respectively (see situation II in Fig.3.14).

According to the Griffith energy balance approach for a cracked plate, the energy release rate G is defined by:

$$G = \frac{d}{da} (F - U_a) \qquad (3.26)$$

where   F = work performed by external forces;

U = change in the elastic strain energy of the system associated with the crack extension.

An exact solution of these energies requires complicated mathematical considerations and costly finite element calculations. However, estimations can be made by considering the geometrical effects of the problem.

For a cracked cylinder loaded by internal pressure, the change in the elastic

39

strain energy dU is assumed to be the sum of the change in the elastic strain energy for a cracked cylinder without bulging, loaded by the hoop stress $(dU_{cylinder})$ and the change of strain energy in the bulge area (dU_{bulge}). Hence

$$G = \frac{d}{da} (F - U_{bulge} - U_{flat})$$ (3.27)

Consider further the situation when the crack extension occurs under the constant load condition. During the crack extension, the hoop stress can be supposed to do work F_{hoop}. At the same time, the internal pressure acting on the bulge area will do work $F_{bulge\ area}$.
Hence

$$G = \frac{d}{da} (F_{bulge\ area} - U_{bulge} + F_{hoop} - U_{flat})$$ (3.28)

It means that the work done by the internal pressure acting on the bulge area $F_{bulge\ area}$ is partly going to be used to introduce the change in the elastic strain energy in the bulge area U_{bulge}. The term $(F_{bulge\ area} - U_{bulge})$ is thus the additional energy available to the crack extension da, which is responsible for the increase of the stress intensity factor of the cracked cylinder loaded by internal pressure as compared to the unbulged situation.

The more problematic parts of Eq.(3.28) are F_{bulge} and U_{bulge}. Simple approximations will be adopted here. One half of the bulged area is sketched in Fig.3.15. It will be assumed that the bulge (out-of-plane) deformation can be approximated by the pyramidal shape ABCD in Fig.3.15, with the characteristic dimensions s_1, s_2 and w_0 (out-of-plane displacement of point A). It should be noted that s_2 is always larger than a due to lower bending stiffness in the neighbourhood of the crack. The assumption that BD is a straight line is a plausible approximation.

The increment ΔF_{bulge} is the work done by the internal pressure by moving the bulged skin from position I to position II (Fig.3.14). With the pyramidal shape approximation it implies that:

$$\Delta F_{bulge} \cong 4p \cdot \Delta(\text{volume of pyramid ABCD})$$

$$= \frac{2}{3} p \Delta (s_1 s_2 w_0)$$

Consider that $w_0 \ll s_1, s_2$ the result is:

$$dF_{bulge} = \frac{2}{3} \cdot p \cdot s_1 s_2 dw_0 \qquad (3.29)$$

where dw_0 is the increment of the out-of-plane displacement of point A.

The bulging strain energy increment can be estimated by adopting the analogy with the well known "fixed-load" problem of a flat panel. It implies that $\Delta U = \frac{1}{2} \Delta F$ (see Fig.3.16). As a consequence:

$$d(F_{bulge} - U_{bulge}) \cong \frac{1}{3} \cdot p \cdot (s_1 s_2) dw_0 \qquad (3.30)$$

For the cylindric part of Eq.(3.28) it is rather easy to arrive at:

$$\frac{d}{da} (F_{hoop} - U_{cylinder}) = t\sigma_{hoop}^2 \pi a / E = \frac{p^2 R^2 \pi a}{Et} \qquad (3.31)$$

Combining Eqs.(3.28), (3.30) and (3.31) gives:

$$G = \frac{1}{3} p s_1 s_2 \frac{dw_0}{da} + \frac{p^2 R^2 \pi a}{Et} \qquad (3.32)$$

Without bulging:

$$G = \frac{p^2 R^2 \pi a}{Et}$$

The bulge factor β_b can thus be expressed as

$$\beta_b = \frac{K_{curved}}{K_{flat}} = \sqrt{\frac{G_{with\ bulging}}{G_{without\ bulging}}}$$

$$= \sqrt{1 + \frac{Ets_1 s_2 dw_0 / da}{3\pi a R^2 p}} \qquad (3.33)$$

41

The energy release rate of a longitudinal cracked cylinder loaded by internal pressure can thus be approximately calculated through the deformation field around the crack (s_1, s_2 and dw_0/da).

Linear elastic case

In reference 17, Erdogan & Ratwani calculated the linear out-of-plane deformation around the bulge area for a cracked thin-walled cylinder loaded by boiler stresses. For $\lambda = \sqrt[4]{12(1-\nu^2)}\dfrac{a}{\sqrt{Rt}} = 2$, a numerical solution was given. The out-of-plane deformation at the center of the crack ($w_{0,\text{lin.}}$) and the lengths s_1 and s_2 were found to be:

$$w_{0,\text{lin.}} = 0.63 \cdot \frac{\lambda^2 R^2 p}{2Et}$$

$$= 0.63 \cdot \sqrt{12(1-\nu^2)} \frac{a^2 pR}{2Et^2} \qquad (3.34)$$

$$s_1 = 2a, \quad s_2 = 2.5a$$

Hence;

$$\frac{dw_{0,\text{lin.}}}{da} = 0.63 \cdot \sqrt{12(1-\nu^2)} \cdot \frac{pR}{Et^2} \cdot a \qquad (3.35)$$

Substitution in Eq.(3.33) gives:

$$\beta_{b,\text{lin.}} = \sqrt{1 + 0.334 \cdot \sqrt{12(1-\nu^2)} \cdot \frac{a^2}{Rt}} = \sqrt{1 + 0.334\lambda^2} \qquad (3.36)$$

which is very close to Folias' analytical solution:

$$\beta_{b,\text{Folias}} \cong \sqrt{1 + 0.317\lambda^2} \qquad \text{for all } \lambda \qquad (3.14)$$

For the linear elastic case, the above mentioned estimation of the bulge factor is thus a very good approximation of the analytical solution, at least for $\lambda=2$. The bulge factor is indeed found to be independent of the internal pressure p for the linear case.

Nonlinear elastic case

For the non-linear case, there are no analytical solutions for the factors s_1, s_2 and dw_0/da. The factors s_1, s_2 and dw_0/da are nonlinear functions of the geometry (R,t), half-crack-length (a), material constants (E,ν), biaxiality χ and internal pressure (p). The determination of these factors can be done by non-linear finite element calculations or by experimental measurements. A formula for the nonlinear bulge factor will be given later in this report.

3.5 SUMMARY

It has been clearly demonstrated by FEM calculations that the problem of a longitudinal cracked thin-walled cylinder loaded by internal pressure (aircraft fuselage) is a non-linear problem. The linear theories developed by Folias, Erdogan etc. are thus invalid. Non-linear finite element analyses carried out by Riks and Ansell give good indications of the solution of the problem. A more practical theoretical consideration of the problem can be given by considering the problem from the fracture mechanics point of view, taking account of the non-linear effects associated with the non-linear deformations of the cylinder in the neighbourhood of the crack. An approximate energy balance approach results in an expression of the elastic energy release rate for longitudinal cracked thin-walled cylinder loaded by internal pressure $G_{cylinder}$ which can be calculated through the deformation field around the crack. For the linear elastic case, the approximate energy balance approach gives an expression which is very close to the analytical solution of Folias. An expression for the nonlinear bulge factor can be given by considering the nonlinear effects of the pressure p on s_1, s_2 and dw_0/da, which can be determined by experimental measurements (chapter 5).

References

1. Peters, R.W. and P. Kuhn, Bursting strength of unstiffened pressure cylinders with slits, NACA Technical Note 3993, April 1957

2. Anderson, R.B. and T.L. Sullivan, Fracture mechanics of through-cracked cylindrical pressure vessels, NASA TN D-3252, Feb. 1966

3. Swift, T., "The application of fracture mechanics in the development of DC-10 fuselage", *Fracture Mechanics of Aircraft structures*, edited by H.Liebowitz, AGARD-AG-176, pp.227-287

4. Swift, T. "Damage Tolerance in Pressurized Fuselage", *The 11th Plantema Memorial Lecture*. Paper in New Materials and Fatigue Resistant Aircraft Design. Proc. 14th ICAF Symposium, June 1987, Ottawa. EMSA, UK 1987, pp.1-77.

5. Williams, D., "An Experimental Verification of the Theoretical Conclusions of RAE Technical Note No. Structures 156 (ARC CP No. 286)", ARC Technical CP No. 357, May 1957.

6. Folias, E.S., "An Axial crack in a pressurized cylindrical shell", *Int. J. of Fracture Mechanics*, Vol.1. 1965, pp.104-113

7. Folias, E.S., Mechanics of Fracture 3, "Plates and shells", edited by G.C.Sih, Noordhoff International Publishing, 1977, p.117

8. Erdogan, F. "Crack problems in cylindrical and spherical shells", Mechanics of Fracture 3, "Plates and shells", edited by G.C.Sih, Noordhoff International Publishing, 1977, p.2.

9. Erdogan, F. and J.J. Kibler, "Cylindrical and spherical shells with crack", *Int. J. of Fracture Mechanics*, 5. (1969), pp.229-237.

10. Barrois, W., "Practical use of the 'equivalent' measured stress intensity factor to control fatigue crack propagation rates in aircraft full-scale fatigue tests-first assessment of the method in testing of a pressurized aircraft fuselage", *Engineering Fracture Mechanics*, 1975, Vol.7. pp.673-688

11. Hahn, G.T., M. Sarrate and A.R. Rosenfield, "Criteria for crack extension in cylindrical pressure vessels", *Int. J. of Fracture Mechanics*, Vol.5, Sep. 1969.

12. Copley, L.G., and J.L. Sanders Jr, "A longitudinal crack in a cylindrical shell under internal pressure", *Int. J. of Fracture Mechanics*, Vol.5,

13. **Murthy, M.V.V., K.P. Rao and A.P. Rao,** "Stresses around an axial crack in a pressurized cylindrical shell", *Int. J. of Fracture Mechanics,* Vol.8, Sep. 1972

14. **Ehlers, R.** "Stress intensity factors and crack opening areas for axial through cracks in hollow cylinders under internal pressure loading", *Engineering Fracture Mechanics,* Vol.25, 1986, pp.63-77.

15. **Riks, E.,** Bulging cracks in pressurized fuselages: A numerical study, NLR-MP-87058 U, 1987

16. **Ansell, H.,** Bulging of cracked pressurized aircraft structure, LIU-TEK-LIC-1988:11, Institute of Technology, Dept. of Mech. Eng., S-581 83 Linköping, Sweden.

17. **Erdogan, F. and M. Ratwani,** "Plasticity and crack opening displacement in shells", *Int. J. of Fracture Mechanics,* Vol.8, Dec. 1972, p.413.

18. **Schijve, J.,** The effect of low sheet thickness on the fracture toughness of an Al-alloy (7075-T6), Report LR-425, April 1984, Faculty of Aerospace Engineering, Delft University of Technology, Delft, The Netherlands.

CHAPTER 4 THREE NEW TEST SET-UPS AND THEIR THEORETICAL BACKGROUND

4.1 INTRODUCTION

As mentioned in the previous chapters, fracture mechanics analysis of cracks in aircraft fuselage skin structures is very complicated due to the complexity of the problem. The stress intensity of a longitudinal crack in an aircraft fuselage skin structure is affected, not only by the internal pressurization, but also by the various secondary effects associated with this internal pressurization, such as the biaxial state of stress and the local bending stresses around the crack tips. In this chapter, the design and the evaluation of three new test set-ups concerning these effects are discussed. The acronyms of the test set-ups are: (i) SUPERBAT (Specimen Using Poisson Ratio Effect for Bi-Axial Testing) (ii) CETS (Curvature Effect Test System) and (iii) PFSTS (Pressurized Fuselage Skin Test System).

4.2 SUPERBAT (Specimen Using Poisson Ratio Effect for Bi-Axial Testing)

4.2.1 EXISTING BIAXIAL FATIGUE TESTING TECHNIQUES

The biaxial stress ratio is defined as:

$$\chi = \frac{\sigma_y}{\sigma_x}.$$

Several authors have reviewed the existing biaxial testing techniques[1,2,3]. These techniques include:

(1) Cruciform specimens (Fig.4.1). Cross-shaped specimens are loaded in two perpendicular directions. The complete range of biaxial stress ratios ($1 \geq \chi \geq -1$) can be obtained with this technique.

(2) Thin-walled tubes (Fig.4.2) subjected to axial tension-compression plus (a) torsion loading where the range of stress states available is limited to $0 \geq \chi \geq -1$, or (b) internal-external pressure which increases the stress states available to $1 \geq \chi \geq -1$.

(3) Bulge-testing on round or oval-shaped specimens, which are clamped along the periphery of the specimen. A pressure is applied to one or both sides of the specimen. An equibiaxial stress state ($\chi = 1$) can be produced in the central area of the round specimen, whereas an oval shape will produce a biaxial stress ratio of $1 > \chi > \nu$.

46

(4) Reversed bending of wide cantilever specimens. A biaxial stress ratio of $\nu \geq \chi \geq 0$ can be produced by varying the width-to-thickness ratio. The maximum χ to be obtained is equal to ν, i.e. if anticlastic bending is fully prevented.

Two methods are used most frequently: (1) the cruciform specimen techniques, and (2) combined tension-torsion of thin-walled tubular specimens.

Both advantages and disadvantages of these techniques are summarized by Beaver in his review[1].

The cruciform specimen is excellent for static biaxial loading studies. However, for fatigue tests the corners of the specimen give problems due to high stress concentrations. The thickness of the test area has to be reduced, which is a problem in the case of testing sheet materials. Besides, a special biaxial testing rig is needed and the specimens are expensive. The combined tension-torsion of thin-walled tubular specimen is obviously unsuitable for aircraft fuselage skin studies because of the geometry of the specimen.

To overcome these problems, a new biaxial testing technique, has been developed which is suitable for aircraft fuselage skin tests and which does not need a special test rig. The idea of this technique is to create a biaxial test area by restraining the lateral Poisson contraction in a sheet specimen.

4.2.2 Design of the specimen: SUPERBAT

The Poisson ratio effect is a well known phenomenon in material science. For a biaxial state of stress, according to Hooke's law:

$$\varepsilon_x = \frac{\sigma_x}{E_x} - \nu_{xy} \cdot \frac{\sigma_y}{E_y} \qquad (4.1)$$

When the Poisson contraction in the x-direction is prevented ($\varepsilon_x = 0$), Eq.(4.1) becomes:

$$\frac{\sigma_x}{\sigma_y} = \chi = \nu_{xy} \cdot \frac{E_x}{E_y} \qquad (4.2)$$

where χ is the biaxial stress ratio.

47

For isotropic material where $\nu_{xy} = \nu$ and $E_x = E_y$ Eq.(4.2) reduces to:

$$\chi = \nu \qquad\qquad\qquad (4.3)$$

A complete restraining of the Poisson contraction in a sheet material will thus create a biaxial stress field with a biaxial stress ratio, $\chi = \nu$, for an isotropic material.

After various considerations, a method for local restraining of the Poisson ratio effect has been chosen, which is obtained by fastening steel strips onto a sheet specimen, see Fig.4.3. Because of the high stiffness of the steel strips and the low stiffness of the aluminium sheet material, a local biaxial stress field can be created. This type of test specimen is further called: SUPERBAT (Specimen Using Poisson Ratio Effect for Bi-Axial Testing). If the lateral contraction is completely prevented the biaxial stress ratio is equal to ν (0.33 for Al-alloys). That is the absolute maximum to be reached by this method. It is lower than $\chi = 0.5$ in an unstiffened pressure vessel. However, an aircraft fuselage has longitudinal stiffeners, which carry load in the longitudinal direction, but not in the hoop stress direction. With a stiffeness ratio $\varphi = 25\%$ (= cross section stiffener /(stiffener pitch * skin thickness)) the stress biaxiality in the fuselage is: $\chi = \frac{1}{2(1+\varphi)} = 0.4$ which is rather close to the maximum stress biaxiality obtained by the SUPERBAT technique.

4.2.3 STRESS ANALYSIS

The steel strips (2x4 strips) are fastened symmetrically with respect to the test area (Fig.4.3). As required by equilibrium, the bolt forces act in opposite directions on the sheet and the strips. All forces acting on the sheet and strips were assumed to act at the mid-thickness planes.

The equations necessary to determine the unknown bolt forces P_i were obtained by equating the displacements at the bolt locations in the sheet and the strips. The displacements were written in terms of the following influence coefficients: A_{ij} and B_i, which represent the displacements in the sheet at bolt No.i, because of unit values of the bolt forces P_j and the remote stress in the sheet material $\sigma_{appl.}$, respectively; and C_i, which represents the displacements in the strips at bolt No.i because of unit value of the bolt forces P_i.

48

Thus the displacement at bolt No.i in the sheet and strips can be written as:

$$u_i = \sum_j A_{ij} P_j + B_i \qquad (4.4)$$

$$u_i^s = C_i P_i \qquad (4.5)$$

For symmetry reasons i and j can be restricted to the bolts in one quadrant of the sheet. Equating these displacements and collecting terms gives:

$$\sum_j A_{ij} P_j - C_i P_i = -B_i \sigma_{appl.} \qquad (4.6)$$

or

$$\sum_j A_{ij} P_j - C_i P_i + B_i \sigma_{appl.} = 0 \qquad (i = 1,2; \ j = 1,2) \qquad (4.7)$$

These simultaneous equations can be solved when the influence coefficients are known.

The analytical solutions for the influence coefficients are given in Appendix A (based on solutions by Love[4]).

4.2.4 CALCULATIONS AND EXPERIMENTAL VERIFICATIONS WITH STATIC LOADS

Calculations have been made for a SUPERBAT specimen (Fig.4.3). In this specimen, steel strips of 1.5 mm in thickness and 15 mm in width were used. The other dimensions of the specimen are given in Fig.4.3. The Al 7075-T6 bare sheet material used in the specimens has a thickness of 1.55 mm. Strain-gauge measurements have been conducted at 4 locations on the specimen.

The results of the strain-gauge measurements in the middle of the test area along the X-axis (Y=0) before and after introducing the strips, are given in Fig.4.4. The specimen appears to behave slightly more stiff in the loading direction after the strips are fastened onto the sheet (lower ε_y). This trend had to be expected in view of the constraint on lateral contraction.

An excellent linearity was found for the deformations in both directions.

The biaxial stress ratio χ can then be calculated from the deformations according to the following formula:

$$\chi = \frac{\sigma_x^b}{\sigma_y^b} = \frac{(\varepsilon_x^b + \nu\varepsilon_y^b)}{(\varepsilon_y^b + \nu\varepsilon_x^b)} \qquad (4.8)$$

where b stands for biaxial stress state.

As mentioned before, the specimen behaves slightly more stiff in the loading direction after restraining of the contraction. The stresses σ_y in the test area differ slightly from the remote loading stress $\sigma_{appl.}$. For practical reasons, a load-efficiency-factor Φ can be defined as follows:

$$\Phi = \frac{\sigma_y^b}{\sigma_{appl.}}$$

which leads to

$$\Phi = \frac{1}{\sigma_{appl.}} \cdot \frac{E}{(1 - \nu^2)} (\varepsilon_y^b + \nu\varepsilon_x^b) \qquad (4.9)$$

In the case of uniaxial loading $(\varepsilon_x = -\nu\varepsilon_y)$, the load-efficiency-factor Φ equals 1.

Based on the experimental data, the biaxial stress ratio χ and the load-efficiency-factors Φ are calculated for all strain-gauge locations (specimen without center crack). In Fig.4.5 and Fig.4.6, the test results are compared to the values obtained by the theoretical calculations. A good agreement between the measurements and the theoretical calculations has been found. It should be noted that the load-efficiency-factors Φ shown in Fig.4.6 are all smaller than 1. This is because of the infinite width of the model used in the calculations. Theoretically, the average of the loading-efficiency- factors Φ must be equal to 1.

Strain-gauge measurements on the strips were also carried out at various half-crack-lengths a. Two strain gauges were applied to one strip of each pair, one at each side to eliminate possible bending effects. The bolt forces P_1 can then be calculated from these strain-gauge measurements. It can be seen from Fig.4.7 that the bolt forces remain constant throughout the full range of crack lengths measured during the test. The biaxial stress ratio χ remains

thus constant.

Constant-amplitude fatigue test results using SUPERBAT technique are presented in chapter 5 (see section 5.1).

4.2.5 CONCLUSIONS

A new biaxial testing method for sheet material called: SUPERBAT (Specimen Using Poisson Ratio Effect for Bi-Axial Testing) has been developed. With this technique, a biaxial test area can be obtained in a simple sheet specimen. Biaxial tests of sheet material can be carried out in a conventional uniaxial test arrangement. Excellent agreement has been found between the test results and the theoretical calculations. The biaxial stress ratio χ in the test area is found to be constant for a range of half crack length a in the specimen.

There is one obvious limitation. The stress biaxiality χ can never exceed the Poisson ratio ν. In general it will be slightly smaller (approximately 0.25).

4.3 CETS (CURVATURE EFFECT TESTING SYSTEM)

In this paragraph, an engineering method for predicting the fracture behaviour of thin metal sheets under combined extension and bending stress condition will be discussed. For that problem a new testing method called "CETS" (Curvature Effect Testing System) was developed. The main goal is to study the contribution of the bending stress to the fracture mechanics behaviour of thin sheet loaded under combined bending and extension. An improved fracture criterion for combined extension and bending of thin sheet will be outlined.

4.3.1 LEFM ANALYSIS

LEFM has been successfully used in predicting fracture and fatigue behaviour of metal sheets containing cracks. Much work has been done concerning fracture mechanic problems of flat sheets loaded in tension and some mathematical models for local stresses in cracked plates under bending fields have also been developed[5-11].

Extension

The well-known elastic solution for the stress field around the tips of a through crack in an infinite flat plate loaded in tension (crack opening mode I) is given below:

$$\sigma_{xx} = \frac{K_I}{\sqrt{2\pi r}} \cos\frac{\theta}{2}\left[1 - \sin\frac{\theta}{2} \sin\frac{3\theta}{2} \right]$$

$$\sigma_{yy} = \frac{K_I}{\sqrt{2\pi r}} \cos\frac{\theta}{2}\left[1 + \sin\frac{\theta}{2} \sin\frac{3\theta}{2} \right] \qquad (4.10)$$

$$\sigma_{xy} = \frac{K_I}{\sqrt{2\pi r}} \cos\frac{\theta}{2} \sin\frac{\theta}{2} \cos\frac{3\theta}{2}$$

$$\sigma_{xz} = \sigma_{yz} = 0;$$

$$\sigma_{zz} = 0 \text{ (plane stress for thin sheets)};$$

$$K_I = \bar{\sigma}_e \sqrt{\pi a}$$

where $\bar{\sigma}_e$ = remote tensile stress.

In the equations, r and θ are polar coordinates (Fig.4.8). The equations are the singular terms of more general equations. As a consequence they characterize the crack tip stress field only in the neighbourhood of a crack tip. It should be noted that

1. A state of biaxial tension ($\frac{\sigma_{xx}}{\sigma_{yy}} = 1$) exists in the crack plane (θ=0) just ahead of the crack tip.

2. The field strength of the stress singularity is of the type $\sqrt{r}$.

Bending

The first successful theoretical analysis of a cracked plate in bending was made by Williams[5,6,10]. In his theory, based on a classical fourth-order thin plate theory, stresses and deflections in bent, cracked plates were calculated, but, as a consequence of the eigenfunction method used in the

analysis, an unspecified constant in the local stresses was present, which was not evaluated until a later paper by Ang and Williams[11]. The theory was modified by Sih, Paris, and Erdogan[7] to introduce a bending stress intensity factor. However, the Williams equations did provide the $\sqrt{r}$ type stress singularity, but a different state of biaxial stress was found just ahead of the crack tip in the crack plane, namely:

$$\frac{\sigma_{xx}}{\sigma_{yy}} = - \frac{(1-\nu)}{(3+\nu)}$$

It was noted later by Williams[11] that this discrepancy was due to the boundary layer effect inherent in the use of Kirchhoff-type boundary conditions.

Reissner's sixth-order theory was used by Knowles and Wang[8] to find a refined solution of the problem. A vanishingly thin infinite plate with a through crack loaded by bending moments (Fig.4.9) was studied. The solution was found by superimposing a system of bending moments at the crack site which negated the stress resultants at the crack site in a solid plate due to the uniform bending moment (Fig.4.10). Near a crack tip, the following stresses were found:

$$\sigma_{xx} = \frac{1+\nu}{3+\nu} \frac{K_b}{\sqrt{2\pi r}} \cos\frac{\theta}{2}\left[1 - \sin\frac{\theta}{2} \sin\frac{3\theta}{2} \right]$$

$$\sigma_{yy} = \frac{1+\nu}{3+\nu} \frac{K_b}{\sqrt{2\pi r}} \cos\frac{\theta}{2}\left[1 + \sin\frac{\theta}{2} \sin\frac{3\theta}{2} \right] \qquad (4.11)$$

$$\sigma_{xy} = \frac{1+\nu}{3+\nu} \frac{K_b}{\sqrt{2\pi r}} \cos\frac{\theta}{2} \sin\frac{\theta}{2} \cos\frac{3\theta}{2}$$

where

$$K_b = \bar{\sigma}_b\sqrt{\pi a} = \frac{6M_0\sqrt{\pi a}}{t^2}$$

In this solution, both the $\sqrt{r}$ type singularity and the state of biaxial tension $\left(\frac{\sigma_{xx}}{\sigma_{yy}} = 1\right)$ in the crack plane ahead of the crack tip are present, as was the case for Eq.(4.10).

Hartranft and Sih[9] modified the theory of Knowles and Wang by taking into account the variation of the value of the bending stress-intensity factor along the crack front due to plate thickness. The singular stresses near the crack tip were found to be:

$$\sigma_{xx} = \frac{K_b}{\sqrt{2\pi r}} \; \frac{12z}{t^3} \; \cos\frac{\theta}{2}\left[\; 1 - \sin\frac{\theta}{2}\;\sin\frac{3\theta}{2}\; \right]$$

$$\sigma_{yy} = \frac{K_b}{\sqrt{2\pi r}} \; \frac{12z}{t^3} \; \cos\frac{\theta}{2}\left[\; 1 + \sin\frac{\theta}{2}\;\sin\frac{3\theta}{2}\; \right] \qquad (4.12)$$

$$\sigma_{xy} = \frac{K_b}{\sqrt{2\pi r}} \; \frac{12z}{t^3} \; \cos\frac{\theta}{2}\;\sin\frac{\theta}{2}\;\cos\frac{3\theta}{2}$$

where z is coordinate in the thickness direction measured from the neutral plane of the plate, $K_b = \phi(1)\cdot M_0\sqrt{\pi a}$ and $\phi(1)$ represents the solution of a Fredholm integral equation, which is a function of the plate thickness t. For vanishingly plate thickness, the dimensionless factor $\phi(1)$ approaches $\frac{1+\nu}{3+\nu}$. Replacing M_0 by $\frac{t^2\bar{\sigma}_b}{6}$ and z by $\frac{t}{2}$, the theory reduces to the Knowles-Wang theory.

Combined Extension and Bending

In the solutions discussed above, the stresses in the vicinity of the crack tip are found by imposing a free-surface boundary condition to the solution satisfying either the Kirchhoff or the Reissner boundary conditions. Thus all these bending theories for cracked plates imply that bending loads must be accompanied by sufficient extension perpendicular to the crack plane to prevent closure of the crack on the compression side of the plate.

It is often assumed that such an extension field may be superimposed; which means that plate deflections are small enough to ignore crack closure on the compression side of the plate.

a. point-type and energy-type fracture criteria

For the fracture criterion of a plate under a combined bending and extension load, Ang and Williams[11] postulated the following formula:

$$\bar{\sigma}_e + \frac{1+\nu}{3+\nu}\ \bar{\sigma}_b = \bar{\sigma}_{crit} \qquad (4.13)$$

where $\bar{\sigma}_e$ = remote tensile stress

$\bar{\sigma}_b$ = remote bending stress at $z = \frac{t}{2}$

$\bar{\sigma}_{crit}$ = critical remote tensile stress if bending is absent

The equation is obtained by combining Eqs.(4.10) and (4.11), i.e. by superposition of two mode I cases. A fracture criterion based upon the Sih-Hartranft theory can also be postulated by combining Eqs.(4.10) and (4.12):

$$\bar{\sigma}_e + \phi(1)\ \bar{\sigma}_b = \bar{\sigma}_{crit} \qquad (4.14)$$

The basic assumption of these two criteria is that fracture of the plate occurs when the sum of the stress intensity factors at the tensile side of the crack tip (i.e. in one point) reaches a critical value, or

$$K_e + K_{b,tensile\ side} = K_{crit}.$$

After substitution of $K = \bar{\sigma}\sqrt{\pi a}$, Eqs.(4.13) and (4.14) are obtained. These criteria may thus be designated as point-type criteria.

When considering the variation in stress along the crack front trough the thickness of the plate, it may be attempted to account for the fact that all lamina of the plate are not stressed to the maximum level of the surface layer on the tensile side of the plate. Swedlow and Williams[13] suggested a fracture criterion based upon equating the strain energy through the thickness to that associated with the critical extensional case. This strain energy was obtained by integrating the Folias[14] solution through the thickness. The fracture criterion then reads:

$$\bar{\sigma}_e^2 + \frac{(33+6\nu-7\nu^2)(1+\nu)}{3(9-7\nu)(3+\nu)^2}\ \bar{\sigma}_b^2 = \bar{\sigma}_{crit}^2 \qquad (4.15)$$

Wynn and Smith[15] suggested that fracture of the plate will occur when the strain-energy-release rate for combined extension and bending reaches the

value at which fracture occurs due to extension alone. Thus

$$\mathcal{G}_{e+b} = \mathcal{G}_{crit} \qquad (4.16)$$

where $\mathcal{G}_{e+b}$ is found by first superimposing the stress and the deformation fields of Eqs.(4.10) and (4.12) and then integrating through the thickness of the plate. The final result of the calculation gives the following fracture criterion:

$$\left(\bar{\sigma}_e^2 + \frac{\phi^2(1)}{3} \bar{\sigma}_b^2 \right) \cdot a_{b+e} = \bar{\sigma}_{crit}^2 \cdot a_{crit} \qquad (4.17)$$

where a_{b+e} = half-crack length in the surface layer on the tensile side of the plate (see Fig.4.11)

a_{crit} = critical half-crack length when extension only is present.

For a thin sheet Eq.(4.17) reduces to

$$\left(\bar{\sigma}_e^2 + \frac{1}{3} \frac{(1+\nu)^2}{(3+\nu)^2} \bar{\sigma}_b^2 \right) \cdot a_{b+e} = \bar{\sigma}_{crit}^2 \cdot a_{crit} \qquad (4.18)$$

It is remarkable that in Eq.(4.17) and (4.18) the half-crack-length in the surface layer on the tensile side of the plate is used, which implies that the shape of the crack front does not influence the fracture behaviour of the plate. No explanation of this consideration was given in reference 15.

Equations (4.17) and (4.18) can be designated as energy-type fracture criteria. In fact, Eqs.(4.17) and (4.18) are energy-release-rate type criteria.

b. average stress-intensity-type criterion

As mentioned previously, the bending stress intensity factor varies through the thickness of the plate (Eq.(4.12)). To account for the total contribution of the bending stress intensity factors acting in different layers of the plate, an equivalent bending stress intensity factor K_{I_b} can be defined as:

$$K^2_{I_b} = \frac{E \cdot \mathcal{G}_b}{t} \qquad\qquad (4.19)$$

where $\mathcal{G}_b$ = bending strain-energy-release-rate.

For a "fixed grip" situation, with sufficient extension to keep the crack open on the compression side of the plate, the bending strain-energy-release- rate can be determined by calculating the work done by the forces which are applied to the crack edges to close the crack over a distance α (Fig.4.12, Irwin's method):

$$\mathcal{G}_b = \lim_{\alpha \to 0} \frac{2}{\alpha} \int_{-\frac{t}{2}}^{+\frac{t}{2}} \int_0^\alpha \left[\frac{\sigma_{yy} u_y}{2} \right] dx\ dz \qquad\qquad (4.20)$$

where $\sigma_{yy} = \phi(1) \cdot \bar{\sigma}_b \frac{2z}{t} \sqrt{\frac{a}{2r}} \cos\frac{\theta}{2} \left[1 + \sin\frac{\theta}{2} \sin\frac{3\theta}{2} \right]$

$$u_y = \frac{1}{G} \cdot \phi(1) \bar{\sigma}_b \frac{2z}{t} \sqrt{\frac{ar}{2}} \left[\sin\frac{\theta}{2} \left(\frac{2}{1+\nu} - \cos^2\frac{\theta}{2} \right) \right]$$

Substituting $r = x$, $\theta = 0$ in the stress terms and $r = \alpha-x$, $\theta = \pi$ in the displacement terms, yields

$$\mathcal{G}_b = \lim_{\alpha \to 0} \frac{1}{\alpha G} \int_{-\frac{t}{2}}^{+\frac{t}{2}} \int_0^\alpha \left(\phi(1) \bar{\sigma}_b \frac{2z}{t} \right)^2 \frac{a}{2} \sqrt{\frac{\alpha-x}{x}} \frac{2}{1+\nu} dx\ dz$$

$$= \lim_{\alpha \to 0} \frac{2t}{\alpha E} \int_0^\alpha \frac{1}{3} \left(\phi(1)\ \bar{\sigma}_b \right)^2 \cdot a \cdot \sqrt{\frac{\alpha-x}{x}} dx$$

$$= \frac{\phi^2(1)\ \bar{\sigma}_b^2 \pi a t}{3E} \qquad\qquad (4.21)$$

Substitution of this result in Eq.(4.19) gives the equivalent bending stress intensity factor relation:

$$K^2_{I_b} = \frac{1}{3}\,\phi^2(1)\,\bar{\sigma}^2_b\pi a \qquad\qquad (4.22)$$

For a thin sheet, Eq.(4.22) becomes

$$K^2_{I_b} = \frac{1}{3}\,\frac{(1+\nu)^2}{(3+\nu)^2}\,\bar{\sigma}^2_b\pi a \qquad\qquad (4.23)$$

For the tensile situation, the well-known solution reads

$$K^2_{I_e} = \bar{\sigma}^2_e\pi a \qquad\qquad (4.24)$$

The following fracture criterion for combined extension and bending of an infinite thin sheet containing a through crack can then be postulated as:

$$K_{I_e} + K_{I_b} = K_{I_c} \qquad\qquad (4.25)$$

or

$$\bar{\sigma}_e + \frac{1}{\sqrt{3}}\,\frac{1+\nu}{3+\nu}\,\bar{\sigma}_b = \bar{\sigma}_c \qquad\qquad (4.26)$$

If this equation is compared to Eq.(4.13) it obviously gives less weight to the bending contribution. An essential difference between Eq.(4.26) and Eqs.(4.13) and (4.14) is that variation of the stress-intensity-factor in the thickness of the plate is accounted for in Eq.(4.26), whereas Eqs.(4.13) and (4.14) are based upon a critical value of the local stress at one point (crack tip at tension side of the plate).

4.3.2 TEST SET-UP

An experimental set-up has been designed to investigate the fracture behaviour of thin Al-alloy sheets loaded under combined extension and bending loading conditions. An originally flat sheet is forced to take a predetermined curvature by placing the sheet between a curved block and two press rolls. A sketch and two photographs of the set-up (CETS: Curvature Effect Testing System) are given in Fig.4.13 and Fig.4.14. To reduce the friction force, thin flexible teflon films are fixed between the rolls and the block. The width of

the blocks is 180 mm, which allows the standard specimens of 160 mm in width to be tested.

Four blocks were made. The radii of the form blocks are 130 mm, 375 mm, 750 mm and 1500 mm respectively. The diameter of the press rolls is 70 mm and the distance is 220 mm (see Fig.4.13).

Test results using the CETS technique are presented in chapter 5 (section 5.2).

4.3.3 CONCLUSIONS

LEFM analysis has been discussed for thin sheets under combined extension and bending stress condition. A stress intensity type fracture criterion is postulated which differs significantly from existing fracture criteria. An experimental set-up for studying fracture behaviour of thin metal sheets under combined extension and bending stress condition has been developed.

4.4 PFSTS (PRESSURIZED FUSELAGE SKIN TEST SYSTEM)

As mentioned before, a study on the influence of the internal pressure of an aircraft fuselage on the stress intensity of a longitudinal crack is of great interest. It is a complex problem due to the stress biaxiality and the bulge phenomenon. It was theoretically shown by Riks[16] and Ansell[17], that the bulge factor of a longitudinal crack in a pressurized fuselage depends not only on the geometrical parameters and the material response, but also on the internal pressure itself. Despite full scale tests conducted on almost every modern transport aircraft and some tests carried out on sections of fuselages, the pressure dependency of the bulge factor was not known for several reasons. The most important reason is that during a full-scale test of a fuselage, only one internal pressure was used (usually the maximum operating pressure differential). The influence of the internal pressure was not studied.

The aim of the PFSTS is to develop a test system for studying the bulge phenomenon under various realistic test conditions, including different internal pressures and stress biaxialities. There are many details involved in the design of the PFSTS, but only the main features of the test system will be discussed in this section.

4.4.1 COMPONENT TEST AND FULL SCALE TEST

It was the loss of human life which forced engineers to conduct full scale fatigue test on aircraft with a pressurized fuselage. As mentioned in chapter 2, after the accidents with the Comet I aircraft, the British RAE (Royal Aircraft Establishment) decided that a fatigue test on the pressurized fuselage was needed. The fuselage was pressurized in a water tank with the wings protruding through cut outs in the tank sides. The reason that water was used instead of air, was because of the explosive character of an air pressurized fuselage when the crack became unstable. A flexible seal between each wing and cut out edge retained the water inside the tank and allowed the aircraft to move and deflect under water. The loads applied to the fuselage were the internal pressure and the wing and tail loads. The time for a complete flight was approximately 2.5 minutes. A similar test set-up was used for the development of The Bristol Britannia type 100[18]. A general view of the test set-up is shown in Fig.4.15. The same technique was used in the fifties and sixties for fuselage full scale tests.

In Fig.4.16, a typical water tank test set-up with the external load introductions is shown (Fokker F-28 main fuselage full scale fatigue test). Fuselage component panel developments were carried out by Douglas in a so-called "water cycle test machine" (Fig.4.17) and in an "air tank test set-up" (Fig.4.18). The air tank set-up consisted of a steel air tank made in two sections connected by an aluminium section representing the fuselage structure. The short end of the tank of the steel tank was free to move axially to ensure the same axial stresses that would exist in the fuselage. An opening at the top of the simulated fuselage structure was used for mounting the development test panel. A typical test panel is shown in Fig.4.19. The overall concept was to perform a fatigue test in the water cycle fixture to develop and propagate fatigue cracks and then transfer the panels to the air tank fixture for residual strength testing.

In the late 1960's, the pressure medium was changed from water to air which is definitely more realistic because of the compressibility of the air. A photograph of such a set-up is shown in Fig.4.20 (DC-10 full scale fatigue test). The fuselage is fully packed with foam-plastics in order to speed up the pressurization and to limit the damage of unstable failure (explosive decompression). A component test set-up also using air as a pressure medium is

60

shown in Fig.4.21 (SAAB 340 fuselage development program).

The main advantage of such systems is that a realistic component simulation is possible. However, the boundary conditions of the test specimens are problematic (stiff attachments).

4.4.2 PFSTS (Pressurized Fuselage Skin Test System)

For studying the bulge phenomenon, it was decided to build a simple test system to simulate the most important loading stresses and boundary conditions around a longitudinal crack in the fuselage skin. After several development modifications, a so-called PFSTS (Pressurized Fuselage Skin Test System) has been realized which consists of three subsystems: (1) the test device itself, (2) the pressure control system and (3) the time controller (see Fig.4.22).

(1) test device

In the test device, a skin sheet of 500 mm x 1080 mm or a fuselage section of the same dimension can be tested under static or dynamic loads applied by internal air pressure on the specimen. The test device is designed in such a way that the SUPERBAT technique mentioned in section 4.2 can be applied for biaxial testing. The internal pressure differential can be varied between 0 bar and 2.5 bar for both static and dynamic loading conditions. The standard radius of the specimen is set to be 2000 mm. Specimens of smaller radii can be tested by changing the wedges where the grips are placed (as illustrated in Fig.4.23). The sealing of the system is realized by taping a plastic foil covering the whole inner side of the specimen including the grips (see in Fig.4.24). Because of the very small stiffness of the plastic foil compared to the specimen, the sealing itself does not take any pressure load during the test. For a fatigue test, a cut-out is made in the plastic foil at the location of the crack allowing the air to flow freely through the crack. The foil is then sealed around the cracked area by means of taping. As a result of the air escaping from the pressurized box through the crack, there is a considerable noise production during the tests. Therefore, the test set-up is located in the basement of the laboratory.

(2) pressure control system

The pressure control system consists of the following parts: the air reservoir, the pressure controller, the control valve, the pressure transmitter and the pressure reducer. The pressure of the compressed air is approximately 6 bar. The maximum pressure in the air reservoir, which is the same as in the test device, can be controlled through the pressure controller. The pressure control system is able to maintain a pressure in the air reservoir with an accuracy of 0.01 bar. First, the test device is filled with the air from the air reservoir until an equilibrium between the pressures in the air reservoir and the test device has been reached. The pressure is then brought to the desired value by the air supply. A typical pressure wave shape is shown in Fig.4.25. The ripples in these air pressure curves reflect the fact that the pressure in the test device is brought up by the reservoir first and then reaches it desired value by the air supply.

(3) time controller

The home-built time controller regulates the time intervals of the electrical valves in such a way that when one valve is in the closed position the other one is in the open position. In order to get a reasonable test frequency, the test compartment is filled with wood. This considerably reduces the volume inside the test compartment. Due to the capacity of the air reservoir, the air supply and the volume of test device itself, the highest test frequency which can be reached is 0.25 Hz (period time of 4 seconds). The time controller monitors the air pressure in the test device through the pressure sensor. It will interrupt the fatigue test when the maximum pressure is not reached. The number of the fatigue cycles is counted by the time controller.

As indicated in Fig.4.22, the actual stresses in the specimen can be measured by strain gauges on the outer surface of the specimen before a saw-cut is made into the center of the specimen. For some specimens the strain records were continued during the fatigue tests. As expected, the shape of the stress waves corresponds well with the shape of the air pressure. The stress level agrees well with the hoop stress formula ($\sigma_{hoop} = \dfrac{PR}{t}$) for sheet specimens. Bending of the sheet at the grips was found to have a negligible effect on the stresses in the center of the specimen.

4.4.3 CONCLUSIONS

A simple, unique test system (Fig.4.26) has been developed which is able to simulate the most important loading stresses and boundary conditions around a longitudinal crack in the fuselage skin. In the so-called PFSTS (Pressurized Fuselage Skin Test System) both static and fatigue tests can be carried out on a thin metal sheet or a curved skin panel under realistic loading conditions. The system simulates the internal differential pressure of modern transport aircraft using compressed air instead of incompressible water as a pressure medium. The test compartment is designed in such a way that the test area is accessible for visual inspection and displacement measurements of the crack. The system gives an excellent opportunity for studying the bulge-out phenomenon under well defined loading conditions. Compared to the full scale tests of a complete fuselage section, the system provides an economical way for selecting, qualifying and testing a new skin material.

Test results with the PFSTS are presented in chapter 5 (section 5.3).

REFERENCES

1. **Beaver, P.W.** "Multiaxial fatigue and fracture – A literature review", Structures Report 410, Department of Defense, Defense Science and Technology Organization, Aeronautical Research Laboratories, Melbourne, Victoria, Australia, July,1984

2. **Krempl, E.** The influence of state of stress on low-cycle fatigue of structural materials: A literature survey and interpretive report, ASTM-STP-549, ASTM,1974

3. **Garud, Y.S.** Multiaxial fatigue: A survey of the state of the art, *J.of Testing and Evaluation.* JTEVA. Vol.9, May 1981, pp.165-178

4. **Love, A.,** A treatise on the mathematical theory of elasticity. Fourth ed. (First Amer. Printing), Dover Publ., 1944, p.209.

5. **Williams, M. L.,** "Surface stress singularities resulting from various boundary conditions in angular corners of plates under bending", *Proceedings, First U.S. National Congress of Applied Mechanics,* June 1951, pp.325-329.

6. **Williams, M.L.,** "The bending stress distribution at the base of a stationary cracks", *Journal of Applied Mechanics,* Vol.28, Trans.ASME, Vol.83, Series E, Mar.1961, pp.78-82.

7. **Sih, G.C., Paris, P., and Erdogan, F.,** "Crack tip stress intensity factors for plane extension and plate bending problems", *Journal of Applied Mechanics,* Vol.29, Trans.ASME, Vol.84. Series E, June 1962, pp.306-312.

8. **Knowles, J.K., and Wang, N.M.,** "On the bending of an elastic plate containing a crack", *Journal of Mathematics and Physics,* Dec.1961, pp.223-236.

9. **Hartranft, R.J., and Sih, G.C.,** "Effect of plate thickness on the bending stress distribution around through cracks", *Journal of Mathematics and Physics,* Vol.47, Sep.1968, pp.276-291.

10. **Williams, M. L., and Owens, R. H.,** "Stress singularities in angular corners of plates having linear flexural rigidities for various boundary conditions", *Proceedings, Second U.S. National Congress of Applied Mechanics,* ASME, June 1954, pp.407-411.

11. **Ang,D.D., and Williams, M.L.,** "Combined stress in an orthotropic plate having a finite crack",*Journal of Applied Mechanics,* Vol.28, Trans.ASME, Vol.83, Series E, Sep.1961, pp.372-378.

12.Williams, M. L., Invited discussion of "An experimental investigation of the crack tip stress-intensity factors in plates under cylindrical bending", by Erdogan, F., Tuncel, O., and Paris, P.C., GALCIT SM 62-19, California Institute of Technology, Mar.1962.

13.Swedlow, J.L., and Williams, M.L., "A review of recent investigation into fracture at GALTIC", ARL 64-175, Wright-Patterson Air Force Base, Oct.1964.

14.Folias, E.S., "A finite line crack in a pressurized spherical shell", *International Journal of Fracture Mechanics,* Vol. No.1, Mar.1965.

15.Wynn, R.H., and Smith, C.W., "An experimental investigation of fracture criteria for combined extension and bending", *Journal of Basic Engineering,* Dec.1969, pp.841-849.

16.Risk, E. Bulging cracks in pressurized fuselage: a numerical study, NLR MP 87058 U, National Aerospace Laboratory NLR, The Netherlands.

17.Ansell, H. Bulging of cracked pressurized aircraft structure, LIU-TEK-LIC-1988:11, Thesis no.138, Institute of Technology, Dept. of Mech. Eng., S-581 83 Linköping, Sweden.

18.Morgan, W.H., The fatigue test failure of a pressurized fuselage (Britannia type 100), Royal Aircraft Establishment, Technical Report 70241, Dec.1970.

19.Swift, T., Damage tolerance in pressurized fuselages, Douglas Paper 7768, June 1987.

20.van Beek E.J., Fatigue testing of the F.28 "Fellowship", Paper in Aircraft Fatigue-Design, Operational and Economic Aspects. Proc. 5th ICAF Symposium, Melbourne, May 1967. Pergamm Press Australia, 1972, pp.65-98.

Chapter 5 Test results on monolithic aluminium sheets

5.1 Bi-Axial test (SUPERBAT)

5.1.1 Test results

Two uniaxial and two biaxial CA fatigue tests have been carried out on both 1.55 mm Al 7075-T6 bare and 1.2 mm Al 2024-T3 Alclad sheets. The biaxial tests are conducted with the SUPERBAT technique described in section 4. The specimen dimensions are: width 300 mm and length 500 mm. The specimens used for the biaxial tests are the same as for the uniaxial tests except for the steel stiffening elements in the test area. The tests are conducted in a computer controlled material test system (Amsler).

The biaxiality in the test area of the SUPERBAT specimens was measured with strain gauges before the saw-cut starter notch was made in the specimen. The biaxiality of all SUPERBAT specimens turned out to be about 0.24. The lengths of the starter notch are $a_0 = 4.0$ mm and $a_0 = 1.5$ mm for the 2024-T3 and 7075-T6 specimens respectively. A constant-amplitude (CA) fatigue load with $\sigma_{max.} = 100$ MPa and $\sigma_{min.} = 0$ MPa (R=0) was applied on all specimens.

The test results are shown in Fig.5.1 to Fig.5.4. Scatter is low and a difference between the crack growth behaviour of the materials under uniaxial and biaxial loading conditions can not be observed. All cracks grew in the direction perpendicular to the direction of the maximum loading stress (length direction of the specimen). Crack branching did not occur. All cracks in the SUPERBAT specimen behaved exactly in the same way as the cracks in the uniaxial tests specimens.

5.1.2 Discussion

The crack growth rates of SUPERBAT specimens and the uniaxial specimens are almost identical for both Al alloys. At relatively small crack lengths (5 mm < a < 15 mm) slightly more scatter was found for the Al 7075-T6 specimens (see Fig.5.4). Some more scatter was also found in biaxial tests on

cruciform steel specimens conducted by Kitagawa *et al*[1] and. Brown and Miller[2]. Fig.5.5 shows the test results of Kitagawa *et al* [1] on Welten 60. It was concluded by the authors that no effect of stress biaxiality could be observed, if a crack is sufficiently large and the stress level is low. Similar conclusions were drawn by Brown and Miller[2] based on the results (Fig.5.6 and Fig.5.7) of cruciform steel specimens tested at various stress levels.

It was pointed out by Kitagawa *et al* that a significant effect of stress biaxiality can occur in the case where a crack is relatively small and the stress level is relatively high. However, for a wide rang of materials, including Al 2024-T351, Al 7075-T7351 and various types of steel, it seems that the effect of stress biaxiality is negligible unless the cracks are small (a < 10 mm in most cases) and the maximum applied stress (σ_1) is higher than 0.4 to 0.5 times the yield strength of the material. In the latter case, the effect of stress biaxiality is considered to be the result of a change in the crack tip plastic zone due to higher biaxial stresses.

For the present bulge out study, the interest is focused on the half crack length range between 10 mm and 150 mm and a maximum stress level not exceeding 150 MPa, which is significantly smaller than the stress levels for which biaxial stress effects were found. Under these conditions, the effect of stress biaxiality on the crack growth behaviour of aluminium sheets can be disregarded.

5.1.3 CONCLUSIONS

CA fatigue tests with the SUPERBAT technique have shown that there is no effect of stress biaxiality on fatigue crack growth in both Al 2024-T3 Alclad and Al 7075-T6 bare aluminium alloy sheets. This is in good agreement with the literature. Although the half crack lengths reached in the SUPERBAT tests were limited to about 30 mm, it is believed, that the absence of a stress biaxiality effect will also apply to larger crack lengths. For the present bulge out study, the biaxiality effect need not be considered.

5.2 COMBINED BENDING AND EXTENSION (CETS)

5.2.1.1 STATIC TEST RESULTS

Two Al alloys (Al 7075-T6 bare and Al 2024-T3 bare) and two thicknesses (0.5 mm and 1.0 mm) of each were tested with the CETS system described in the previous chapter. The specimens were originally flat. Central cracks were simulated by narrow saw-cuts (width 0.3 mm) with a half-crack length of 10 mm, 20 mm, 30 mm and 40 mm respectively.

The specimens were then placed in the test fixture CETS (see section 4.3) and loaded to failure in tension (see Fig.4.14) in a home-built 6-tons material test system.

The test results are summarized in Table 5.1 and in Figs.5.8 a,b,c and d.

Several central cracked flat tensile specimens (W = 160 mm) were also tested in order to determine the K_c of the materials. Net-section-yielding was found for Al 2024-T3, whereas almost similar K_c-values were found for the two thicknesses of Al 7075-T6, namely, $K_c = 73$ MPa$\sqrt{m}$ for t = 1.0 mm and $K_c = 72$ MPa$\sqrt{m}$ for t = 0.5 mm.

Stable crack extension was not measured during the tests. Considerable "bulge-out" of the crack edges was visually observed during the tests.

5.2.1.2 DISCUSSION

As mentioned in chapter 4, three different types of fracture criteria can be considered, namely, the point-type criteria, the energy-type criteria and the average stress-intensity-factor-type criterion. Preliminary calculations using both point-type-criteria (Eqs.(4.13) and (4.14)) and the energy-type- criteria (Eqs.(4.15) and (4.18)), have shown that these criteria give erroneous predictions of the fracture tensile loads. As an illustration, calculation results are shown in Table 5.2.

Strictly speaking, Eqs.(4.25) and (4.26) (stress-intensity-type criterion) were derived for an infinite central cracked sheet. A finite width correction factor must be applied for the test specimens used in this study. Eq.(4.26) can be rewritten as follows:

$$C_e \bar{\sigma}_e \sqrt{\pi a} + C_b \frac{1}{\sqrt{3}} \frac{1+\nu}{3+\nu} \bar{\sigma}_b \sqrt{\pi a} = K_c \qquad (5.1)$$

For a central cracked flat tensile specimen with a finite width W, the Feddersen correction factor can be used,

$$C_e = \sqrt{\sec \frac{\pi a}{W}} \qquad (5.2)$$

Wilson and Thompson[3] calculated (FEM) a correction factor for plate bending. It can be shown that the results are also well fitted by Eq.(5.2). Hence,

$$C_b = C_e \qquad (5.3)$$

and Eqs.(4.25) and (4.26) can be applied to our test results.

As stated by Schijve[4], the Irwin plastic zone correction must be incorporated when calculating K_c-values. Corrected K-values can be obtained by substitution of

$$a_{corr.} = a + r_p \qquad (5.4)$$

where

$$r_p = \frac{1}{2\pi} \left(\frac{K}{\sigma_{0.2}} \right)^2$$

The residual tensile strength (σ_e) of a finite width flat specimen loaded under combined extension and bending condition can then be calculated according to

$$\bar{\sigma}_e = \frac{K_c}{\sqrt{\pi(a_0 + r_p)} \sqrt{\sec \frac{\pi(a_0 + r_p)}{W}}} - \frac{1}{\sqrt{3}} \frac{1+\nu}{3+\nu} \bar{\sigma}_b \qquad (5.5)$$

where

$$\bar{\sigma}_b = \frac{tE}{2R}$$

$$r_p = \frac{1}{2\pi} \left(\frac{K_c}{\sigma_{0.2}} \right)^2$$

Considering Eq.(5.5), the contribution of the bending stress to the residual tensile strength can be expressed in an equivalent tensile stress $\bar{\sigma}_{e_{eq.}}$

$$\bar{\sigma}_{e_{eq.}} = \frac{1}{\sqrt{3}} \frac{1+\nu}{3+\nu} \bar{\sigma}_b$$

Substitution in Eq.(4.26) gives

$$\bar{\sigma}_e = \bar{\sigma}_c - \bar{\sigma}_{e_{eq.}} \qquad\qquad (5.6)$$

For a constant R value $\bar{\sigma}_b$ is constant and thus $\bar{\sigma}_{e_{eq.}}$ is constant. In the Feddersen diagram it implies that the residual strength curve moves to a lower level with a constant amount $\bar{\sigma}_{e_{eq.}}$, see Fig.5.9.

A bending stress field can thus be treated as an extensional stress field when there is sufficient tensile stress to keep the crack open.

Very satisfactory predictions for both Al 7075-T6 bare and Al 2024-T3 bare can be made by using Eq.(5.5). This is clearly illustrated by Figs.5.10 a to h for 7075-T6. It is most remarkable that the predictions are still very satisfactory for 2024-T3 in Figs.5.10 i to p, in spite of the net section yield behaviour.

It can be concluded that the stress-intensity-type-criterion (Eq.4.26) as postulated in this paper gives the most accurate predictions for static combined bending and extension tests as compared to the theories discussed before. It is the opinion of the author that the average stress-intensity-type criterion (Eq.4.26) must be used when static combined extension and bending of thin metal sheets is involved.

5.2.2.1 CA-Fatigue Test Results

Constant amplitude fatigue tests were carried out with the CETS system. Thin 2024-T3 bare and 7075-T6 bare aluminium alloy sheet specimens were tested under a constant-amplitude sine wave fatigue load of σ = 60±60 MPa. Originally flat specimens of 160 mm in width, 550 mm in length and 1.0 mm or 0.5 mm in thickness were forced to take different radii (R = 130 mm, 375 mm, 750 mm,

1500 mm respectively). The tests were carried out in a computer-controlled fatigue test machine with a frequency of 15Hz. Several flat specimens were also tested under the same tensile fatigue load of $\sigma = 60\pm60$ MPa as reference tests. The starter notches are simulated with a $2a = 3.0$ mm narrow saw-cut. A detailed description of the tests is given in reference 6.

The test results are summarized in Fig.5.11 to 5.15. For technical reasons, no results were obtained for 1 mm thick sheets tested with a curvature R = 130 mm (crack initiation and crack growth in the specimen occurred at the press rolls).

5.2.2.2 DISCUSSION

In chapter 4, a concept has been developed for predicting the residual tensile strength of a central cracked monolithic specimen loaded in combined bending and extension. The basic assumption of the theory was that the tensile load will be sufficient to keep the crack open. In that case, the stress intensity factor at the crack tip can be calculated according to the theory described in chapter 4.

For R=0 CA fatigue, which is the case in this study, part of the crack edges will not open during the fatigue process due to the compressive stresses introduced by the bending of the specimen. The theory mentioned above is thus not valid for R=0 CA fatigue under combined bending and tensile loads. The aim of this study is to investigate the possible influence of bending stress to the fatigue behaviour of sheet material.

From Figs.5.11 to 5.14 it can be seen that the crack growth rates of the specimens tested under curvatures R = 750 mm and R = 1500 mm are practically identical to the crack growth rate of the flat specimens for both alloys. It should be pointed out that the bending stress is not a cyclic stress, but a static stress, whereas the tensile load is cyclic. For R = 375 mm and R = 130 mm, there is a slight tendency that the crack growth rate decreases with increasing curvature (smaller bending radius). This may be due to the phenomenon which can be called "partial crack closure due to bending". This so-called "partial crack closure due to bending" is a phenomenon which is not

widely known. It is different from the Elber *"crack closure"* mechanism which is a result of plastic deformation at the crack tip throughout the whole thickness of the specimen. However, *"partial crack closure"* due to the bending radius is a result of the compressive stress acting at the compression side over the full width of the specimen (see Fig.5.16). The mechanism of fatigue crack growth under this condition is not known. It will not be discussed any further in the present study.

5.2.2.3 CONCLUSIONS

It can be concluded from the results of the R=0 CA-fatigue tests carried out with the CETS system that the crack growth rate of thin (t ≤ 1.0 mm) monolithic aluminium alloy sheets (Al 2024-T3 and Al 7075-T6 bare) under combined static bending and cyclic tension fatigue load is identical to the crack growth rate of a flat specimen under the same tensile fatigue load, when the radius of curvature R is large, say larger than 750 mm. For smaller curvature radii (R ≤ 375 mm) the crack growth rate tends to decrease with decreasing radius of curvature, which is thought to be the result of *"partial crack closure due to bending"*.

For an aircraft fuselage structure, the radius of curvature is usually larger than 1500 mm, which means that the effect of the bending stress on the crack growth rate of the skin sheet can be left out of consideration.

5.3 PRESSURIZED FUSELAGE SKIN TESTS

5.3.1 REFERENCE TESTS (FLAT PANEL)

A reference test was carried out on a flat panel of Al 2024-T3 Alclad, 500 mm in width and 1.2 mm in thickness. The test was conducted in a 20-tons MTS-material testing machine. Anti-buckling guides were used to prevent buckling of the crack edges during the test. The CA-fatigue load was σ_{max} = 106.6 MPa and σ_{min} = 0 MPa (R=0). A starter-notch of 2a = 3.0 mm was made in the center of the specimen by means of a saw-cut. The test frequency was 10 Hz. The test results are presented in Fig.5.17 as a crack growth (a-N) curve.

In reference 7, a similar test was carried out on the same material and the same specimen geometry. The result of the test is the solid curve in Fig.5.18. The present test results are practically identical. The crack growth data in Fig.5.18 will be used as the reference data for the bulge-out study in this report.

5.3.2 Test results PFSTS (curved panels)

5.3.2.1 Constant-amplitude fatigue tests

Constant amplitude fatigue tests were conducted on 1.2 mm thick 2024-T3 alclad specimens using the home-built pressurized fuselage skin test system, PFSTS, described in the previous chapter. Both uniaxial and biaxial fatigue tests were carried out. For the biaxial tests, the SUPERBAT technique was used. The specimen geometry is shown in Fig.5.19. The dimensions are the same as for the uniaxial test specimens, but the steel strips were added for preventing the lateral contraction. The biaxiality in the test area was measured by means of strain gauges. The biaxiality ratio was found to be 0.24 (χ = 0.24 = $\sigma_{transvers}/\sigma_{hoop}$). The radius of curvature was 2000 mm for all tests. Two maximum internal pressures were used, namely p_{max} = 0.35 bar and p_{max} = 0.55 bar[1]. The minimum internal pressure was p_{min} = 0 for all tests. The test frequency was 0.25 Hz (pressure cycle of 4 seconds). The test conditions are summarized in Table 5.3.

The specimens were originally flat and forced to take the radius of curvature of 2000 mm by means of bending. The starter notch (saw-cut) was introduced in the specimen after it was clamped onto the test fixture. The crack lengths were measured during the test by means of visual observation.

The test results are shown as crack growth curves in Figs.5.20 and 5.21, as crack growth rate curves in Figure 5.22, and as da/dN-ΔK curves in Figs.5.23

---

[1] The pressure sensor was modified during the tests. After the modification the internal pressure was slightly higher than the originally fixed pressure of p=0.35 bar or p=0.55 bar. As a consequence some tests were conducted with p=0.36 bar or p=0.56 bar.

and 5.24. A comparison between the results of different tests is made in Fig.5.25. Some trends are easily recognized, which apply to crack growth in curved panels loaded under internal pressure:

— Crack growth is faster than in flat panels loaded by the same cyclic hoop stress without any air pressure effects (Figs.5.23 and 5.24).

— Biaxiality has a small but systematic effect. The biaxiality (χ = 0.24) reduced the crack growth rate if compared to uniaxial loading (χ = 0). (Fig.5.25).

— The internal pressure had a systematic effect on the crack growth rate. The crack growth rate as a function of ΔK was larger for a higher pressure level.

The ΔK-values for the curved specimens were calculated from the applied hoop stress σ_{hoop} and the half-crack-length a through the formula $\Delta K = \sigma_{hoop} \sqrt{\pi a} \sqrt{\sec\frac{\pi a}{W}}$ where W is the width of the specimen. It implies that the ΔK-values for the curved specimens given in Fig.5.23 to Fig.5.25 are in fact the stress intensity factors for specimens in the flat condition. It does not account for the bulge-effect due to internal pressurization. Empirical stress intensity factor for the curved specimens can be derived from the crack growth rate da/dN through the similarity concept, which will be described later in this chapter.

5.3.2.2 MEASUREMENTS ON THE DEFORMATION FIELD AROUND THE CRACK

As mentioned in chapter 3, the bulge-out phenomenon can be studied by considering the out-of-plane deformation field around the crack. According to the theory outlined in chapter 3, there is a direct relationship between the out-of-plane deformation field around the crack and the bulge factor β_b (Eq.3.33). For this reason, measurements are carried out on a uniaxially loaded curved specimen at various crack lengths.

The specimen used is the same as that for the uniaxial CA fatigue tests. The specimen is cycled to obtain a crack of a certain length. The fatigue test is then temporarily interrupted for the deformation measurements.

A sketch of the measuring system is shown in Fig.5.26. The out-of-plane deformation of the sheet is measured with a displacement transducer which is

connected to a rigid frame. It can move in both the tangential and the transverse direction of the curved sheet. At the location of the crack, the displacement transducer is situated perpendicular to the tangent of the curvature of the specimen. When the displacement transducer moves away from the crack in the tangent direction of the sheet, the measured displacement differs slightly from the actual radial displacement of the sheet. The error will be less than 0.3% due to the large curvature of the sheet (see Fig.5.27). Compared to the accuracy of the measuring device, which is about 0.01 mm, this error can be ignored.

Detailed deformation fields can be recorded by moving the displacement transducer at different crack lengths and internal pressures. The out-of-plane displacements can then be determined by comparing the displacement fields around crack to the global radial displacement of the sheet.

In Figs.5.28 and 5.29, the out-of-plane deformation fields of two cracks (a = 25.65 mm and a = 44.9 mm) under an internal pressure p = 0.55 bar are shown. The influence of internal pressure on these deformation fields are shown in Figs.5.30 and 5.31.

In Fig.5.32 the out-of-plane deformations of the center of the crack w_o are shown as a function of the half-crack-length a for three values of the internal pressure. The influence of the internal pressure is also illustrated in Fig.5.33, where w_o is plotted as a function of the internal pressure p.

5.3.2.3 EVALUATION OF THE FATIGUE TEST RESULTS

As mentioned in paragraphs 5.1, a biaxial stress field does not influence the crack growth behaviour of flat thin aluminium sheet. The influence of the bending stresses on the crack growth behaviour is also found to be negligible if the radius of curvature, which induces the bending stresses, is larger than 1500 mm (see paragraph 5.2). It can thus be assumed that the influences of these two factors on the crack growth behaviour can be disregarded for the PFSTS test results. The differences of the crack growth behaviour between the reference tests (flat specimens) and the curved specimens loaded by internal pressure can only be caused by the bulge phenomenon. The bulge-factor β_b can thus be determined by comparing the da/dN-ΔK curves of the PFSTS tests to the curve of the reference flat specimen tests by means of the similarity concept.

In reference 8 a detailed description of the similarity concept can be found.

It starts from the idea that: *similar conditions, applied to the same system, will cause similar consequences.*

For the comparison of two fatigue cracks it implies:

$$\left\{ \begin{array}{l} \textit{the same K-cycle,} \\ \textit{the same enviroment} \end{array} \right\} \textit{ applied to } \left\{ \begin{array}{l} \textit{the same material} \\ \textit{of the same thickness} \end{array} \right\}$$

$$\textit{will cause the same } \left\{ \textit{crack exten sion da/dN} \right\}$$

With this concept empirical K factors can be determined for curved panels, and bulge factors can thus be obtained. The procedure is outlined in Fig.5.34.

In Figs.5.35 to 5.38 the bulge-factors β_b are plotted as a function of the half-crack-length a for all test conditions. The lines marked with 'prediction' in these figures are predicted curves based on the theory developed in chapter 3 as discussed below. The predicted curves are compiled in Fig.5.39. Because the predicted curves do represent the empirical results rather well, it may be concluded from Fig.5.39 that an increased pressure level reduces the bulge factor. A more significant effect is caused by the biaxiality, which reduces β_b considerably.

5.3.2.4 OUT-OF-PLANE DEFORMATION

In chapter 3 a theory has been outlined for the calculation of the bulge factor of a longitudinal crack in a thin-walled cylinder loaded by internal pressure. In this theory it has been found that the additional energy due to bulging available for the crack extension can be approximated by $\frac{1}{3} \cdot p \cdot s_1 \cdot s_2 \cdot dw_0$ (see Eq.3.30) where s_1 and s_2 indicate the dimensions of the bulge area and dw_0 is the increment of the out-of-plane deformation at the center of the crack due to crack extension da. It is found from the measurements on the bulge deformation that the values of s_1 and s_2 are approximately constant for different internal pressures p and equal to about 2 and 2.5 times the half-crack-length a respectively (see Figs.5.28 to 5.31). These values of s_1

and s_2 (s_1= 2a and s_2= 2.5a) will be used for further evaluation of the test results.

According to the theory developed in chapter 3, the bulge-factor β_b can be calculated with Eq.3.33. Substitution of s_1 = 2a and s_2 = 2.5a in this equation gives:

$$\beta_b = \sqrt{1 + \frac{5Eta(dw_0/da)}{3\pi pR^2}} \qquad (5.7)$$

In this equation all constants are known, but dw_0/da must still be obtained. From the test results shown in Fig.5.32 the increment of the out-of-plane deformation at the center of the crack dw_0 due to crack extension da can be calculated. Four dw_0/da values are calculated by measuring the slope of the curve at the various a value. The results are presented in Fig.5.40 as a function of the half-crack-length a. It is found that the results can well be fitted by the following equation (see Fig.5.40):

$$\frac{dw_0}{da} = 0.316 \cdot \tanh\left(0.06 \cdot \frac{R}{t} \cdot \sqrt{\frac{pa}{Et}}\right) \qquad (5.8)$$

Substitution in Eq.(5.7) gives:

$$\beta_{b_{uniaxial}} = \sqrt{1 + \frac{5}{3\pi} \cdot \frac{Eta}{R^2 p} \cdot 0.316 \cdot \tanh\left(0.06 \cdot \frac{R}{t} \cdot \sqrt{\frac{pa}{Et}}\right)} \qquad (5.9)$$

With this equation the bulge factor can be calculated for a large thin-walled cylinder with a longitudinal crack, loaded by internal pressure and no loading stress parallel to the crack (uniaxial loading, χ = 0). Predictions with Eq.(5.9) are compared to the test results in Figs.5.35 and 5.36. The agreement is good.

Biaxial loading has a significant influence on the crack growth behaviour of the curved specimens. For similar test conditions, the bulge-factor of a specimen under biaxial loading was found to be significantly lower than for a specimen loaded under a uniaxial stress only (see Fig.5.39). Because of the

presence of the steel strips on the biaxial specimens, it was not possible to conduct measurements on the out-of-plane deformation of the specimens under biaxial loading. However, visual observations during the tests have shown that the out-of-plane deformation around a crack under biaxial loading is much smaller as compared to the deformation under uniaxial loading. As a consequence also dw_0/da in Eq.(5.9) will be much smaller. Good predictions of β_b under biaxial loading were obtained by dividing dw_0/da in Eq.(5.7) by $\sqrt{1+18\chi}$, which leads to:

$$\beta_b = \sqrt{1 + \frac{5}{3\pi} \cdot \frac{Eta}{R^2 p} \cdot \frac{0.316}{\sqrt{1+18\chi}} \cdot \tanh\left(0.06 \cdot \frac{R}{t} \cdot \sqrt{\frac{pa}{Et}}\right)} \qquad (5.10)$$

The comparison between predictions and test results in Figs.5.37 and 5.38 confirms that Eq.(5.10) fits the test results very well. For $\chi = 0$ Eq.(5.10) reduces again to Eq.(5.9).

In summary, the bulge phenomenon of a thin-walled cylinder with a longitudinal crack, loaded under internal pressure, can be considered to be local out-of-plane deformation around the crack, introduced by the internal pressure and the curvature. The bulge-factor β_b is a non-linear function of the geometrical parameters (R,t), the Young's modulus of the material (E), the half-crack-length (a) and the loading conditions (p,χ) as shown in Eq.(5.10).

5.3.3 Application of Eq.(5.10) to Results from the Literature

5.3.3.1 Non-Linear FEM Results

Using a non-linear FEM code, Riks[9] calculated bulge-factors of an unstiffened thin-walled cylinder containing a longitudinal crack loaded by internal pressure. The biaxiality of the stress field was $\chi = 0.5$. The bulge-factors were calculated through the energy-release rate G which was obtained by calculating the total potential energies for half-crack-lengths a_i and $a_i+\Delta a$. The influence of the internal pressure p on the bulge-factor β_b was investigated.

78

Eq.(5.10) will now be applied to Riks' cylinder (R = 1650 mm, t = 1 mm, Al alloy). The results are presented in Figs.5.41 and 5.42. The predictions by Eq.(5.10) agree well with the FEM results except when the internal pressure reduces to zero (Fig.5.42). In this extreme case, the Folias' solution (see chapter 3 Eq.(3.14)) will give the correct prediction.

Using the same computer code, similar calculations were carried out by Riks and den Reijer[10] for a different configuration. Bulge-factors of a small range of the half-crack-length a were calculated. It can be seen in Fig.5.43 that the predictions given by Eq.(5.10) are again close to the FEM results.

Another non-linear FEM code was developed by Ansell[11]. Bulge-factors were calculated for an unstiffened thin-walled cylinder containing a longitudinal crack. The influences of crack length a and internal pressure p on the bulge-factor were studied. Some of the calculation results are presented in Figs.5.44 and 5.45 together with the predicted curves obtained with Eq.(5.10). The predicted curves in Figs.5.44 and 5.45 give higher bulge-factors as compared to the FEM calculation results found by Ansell. This discrepancy might be due to the calculation method adopted by Ansell. In his calculations, two different bulge-factors were computed for one crack, namely the so-called bending-bulge-factor and the stretching-bulge-factor. It was found by Ansell that it was difficult to incorporate the bending-bulge-factor into the stretching-bulge-factor. Because the bending-bulge-factor was small compared to the stretching-bulge-factor, the bending-bulge-factor was then ignored and the stretching-bulge-factor was treated as the only bulge-factor in his considerations. This might be a reason for the discrepancies in Figs.5.44 and 5.45.

5.3.3.2 FUSELAGE WITH FRAMES AND LONGERONS

Swift[13] investigated the pressurization of fuselage structures with one-bay and two-bay cracks (see Fig.5.46). When the crack tips of a two-bay crack were midway between the frames, the bulge-effect was not influenced by the presence of the frames (the bulge-factor equals that of an unstiffened cylinder). On the other hand, the bulge-effect seemed to damp out when the crack tips approached the frames. Based on these observations Swift suggested that the

damping of the bulge-effect due to the presence of the frames could be expressed as a cosine function of the half-crack-length a. Swift also suggested that for a two-bay crack (cracks starting from the center frame) with the frame intact, the crack could be treated as two separate cracks each of length 2a. The so-called frame Damping-Factor (D.F.) was supposed to have the following form:

$$D.F._{two-bay crack} = \frac{1}{2} \cdot \left[1 + \cos\pi(1 - \frac{4a}{L}) \right]$$

(5.11)

where L denotes the frame spacing.

As stated by Swift, <u>this damping-factor must be applied to the maximum bulge-factor expected in the bay.</u> That is the case when the crack tip is midway between the frames (2a = L/2).

For two-bay cracks in a stiffened pressurized fuselage structure with the central frame intact, the bulge-factor β_b can thus be calculated by substituting 2a = L/2 in Eq.(5.10) and combining Eq.(5.10) with Eq.(5.11). Hence,

$$\beta_b = \sqrt{ 1 + \frac{5}{3\pi} \cdot \frac{Et\frac{L}{4}}{R^2 p} \cdot \frac{1}{\sqrt{180\chi+10}} \cdot \tanh\left(0.06 \cdot \frac{R}{t} \cdot \sqrt{\frac{pL}{4Et}} \right) \cdot \frac{1}{2} \cdot \left(1 + \cos\pi(1 - \frac{4a}{L}) \right) }$$

(5.12)

Based on Swift's consideration, Mor[14] suggested the following damping-factor for one-bay cracks:

$$D.F._{one-bay crack} = \frac{1}{2} \cdot \left[1 + \cos\frac{2a\pi}{L} \right]$$

(5.13)

<u>which should be applied to the bulge-factor corresponding to the half-crack-length a.</u>

For one-bay cracks in a stiffened pressurized fuselage structure, the bulge-factor β_b can thus be expressed as follows:

$$\beta_b = \sqrt{1 + \frac{5}{3\pi} \cdot \frac{Eta}{R^2 p} \cdot \frac{1}{\sqrt{180\chi + 10}} \cdot \tanh\left(0.06 \cdot \frac{R}{t} \cdot \sqrt{\frac{pa}{Et}}\right) \cdot \frac{1}{2} \cdot \left(1 + \cos(\frac{2\pi a}{L})\right)} \quad (5.14)$$

It should be noted that Swift's observation was made on DC-10 test panels with a relative large longeron spacing, and the damping effect of the longerons was not taken into account in Eqs.(5.11) and (5.13). Because the bulge phenomenon is dominated by the local out-of-plane deformation as stated in the previous section, the presence of longerons will certainly influence the bulge deformation around the crack if the longeron spacing is small compared to the crack length. However, it is not possible to include the effect of longerons into the context of the present analysis, which led to Eq.(5.10).

Moreover, Eqs.(5.11) and (5.13) are essentially empirical. The cosine shape of the damping function is arbitrary. The reason why Eqs.(5.11) and (5.13) are used here is purely because of lack of alternatives.

Predictions with Eq.(5.14) will now be compared to FEM calculation results of Lemaitre *et al*[12]. Based on non-linear energy release rate calculations, Lemaitre *et al*[12] investigated the influences of the shell parameters R and t, the longeron spacing S and the internal pressure p on the bulge-factors β_b for a number of stiffened fuselage configurations. The cracks considered in their calculations were one-bay cracks starting midway between the frames and the longerons. In these calculations, the fuselage skin sheet was assumed to have no radial displacement at the locations of the frames and the longerons. The FEM calculation results for a frame spacing L = 508 mm and a longeron spacing S = 200 mm are compared with the predictions according to Eq.(5.14) in Figs.5.47 to 5.49. Despite the arbitrary character of the damping-factor, satisfactory predictions are found. The influences of the shell parameters R and t and the internal pressure p found by Lemaitre *et al* agree well with the predictions of Eq.(5.14).

The influence of the longeron spacing S is clearly shown in Fig.5.50 where the FEM results of three different longeron spacing S are compared to the prediction given by Eq.(5.12). A significant reduction of the bulge-factor is found for the small longeron spacing S = 100 mm. Because Eqs.(5.12) and (5.14) do not account for the longeron spacing, Eq.(5.12) fails to predict the

correct bulge-factors for the low S-value. It should be expected that a small longeron spacing will reduce the bulge-factor.

Additionally, Lemaitre *et al* also calculated the bulge-factor for another fuselage configuration containing a one-bay crack starting midway between the frames and the longerons (aluminium skin sheet, R = 835 mm, t = 0.8 mm, a = 75 mm, p = 0.35bar, χ = 0.5, L = 430 mm, S = 200 mm). The bulge-factor found by their FEM calculations was β_b = 2.05. The bulge-factor for this fuselage configuration according to Eq.(5.14) is β_b = 1.93, which is rather close to the FEM result.

Riks[9] also studied the bulge problem of a fuselage structure containing both frames and longerons. He used a non-linear FEM code developed for the unstiffened cylinders. Unlike Lemaitre, Riks allowed radial displacements of the frames and the longerons. The cracks started midway between the frames and the longerons. Two longeron spacings (S = 150 mm and S = 300 mm) were used. The calculation results are compared to the prediction of Eq.(5.14) in Fig.5.51. It seems that despite the large longeron spacings the influence of the longerons is significant. The bulge-factors for S = 300 mm are higher than for S = 150 mm. This agrees with the expected influence of the longerons as mentioned above. It should be noted that Riks' results show an asymmetric a-effect contrary to the cosine equations assumed above. No explanation can be given for this behaviour.

Parameter studies on bulge factors of two-bay cracks in different stiffened pressurized fuselage configurations were also made by Ansell[11]. Non-linear FEM programs developed for the unstiffened cylinders were used. Frames and longerons were allowed to have radial displacement. The center frame was considered to be intact.

The calculation results are compared to Eq.(5.12) (see Table 5.4). Very good agreement is found for the cracks with the crack tip situated midway of the bay (2a = 250 mm). For other cracks, the bulge-factors predicted by Eq.(5.12) are still close to the FEM results. The discrepancy may be a result of the arbitrative character of the cosine shape of the damping-factor used in Eq.(5.12). Nevertheless, Eq.(5.12) still produced acceptable predictions for this very complicated two-bay crack situation.

In summary, it can be concluded that predictions of Eqs.(5.10), (5.12) and (5.14) agree well with the non-linear FEM results. For unstiffened cylinders, Eq.(5.10) gives accurate predictions. The agreement between the predictions of Eq.(5.14) and the FEM results of Lemaitre *et al* for one-bay cracks is also quite good. However, Eq.(5.14) is unable to predict the effect of the longeron spacing, which can be very large as shown by the results of Riks (Fig.5.51) and Lemaitre (Fig.5.50). In the case of a two-bay crack, the agreement between Eq.(5.12) and FEM results of Ansell is good for cracks if the crack tip is midway between the frames, while acceptable predictions are still obtained by Eq.(5.12) for other crack lengths.

5.3.3.3 RESULTS OF FULL-SCALE FUSELAGE TESTS

Results of Swift (DC-10)

The most frequently used empirical formula for calculating the bulge-factor is undoubtedly Swift's bulge formula:

$$\beta_b = 1 + 5 \cdot \frac{2a}{R} \tag{5.15}$$

This formula was found based on results of both residual strength tests and fatigue tests on DC-10 fuselage development panels. It should be noted that Eq.(5.15) does not contain the internal pressure p, which has a significant influence on the bulge-factor as shown by Riks, Ansell and Lemaitre *et al*, as well as our own test results, Moreover, the biaxial stress ratio χ, which has a considerable influence on the bulge behaviour as shown also by our test results, is not present in Eq.(5.15).

Swift's Eq.(5.15) is compared to our Eq.(5.10) for the DC-10 configuration including the pressure p. The result is shown in Fig.5.52. A very good agreement between the two equations is found. However, it will be shown in the next section of this chapter that Swift'sequation is only valid for fuselage configurations and loading conditions which are close to those of the DC-10 (R/t, χ and p).

Swift & Wang[17] reported fatigue test results of three DC-10 fuselage development test panels made of 7075-T73 material. The results covered two one-bay cracks and one two-bay crack. The test results and the test conditions are presented in Fig.5.53. In Table 5.5 the bulge-factors according to the da/dN-ΔK curves are compared to the prediction values. Again, good agreement has been found.

Results of Schwarmann (Airbus)

Schwarmann[15] reported fatigue test results of a pressurized fuselage structure. Three different crack configurations were considered (see Fig.5.54):

(1) crack A (crack located in the skin sheet between two intact frames);

(2) crack B (crack located in the skin sheet below a frame. The strip and part of the castellation were cut);

(3) crack C (crack located in the skin sheet below a longeron).

The fuselage structure was loaded by CA internal pressure with a maximum pressure differential p = 0.47 bar. The test results are collected in Figs.5.55 to 5.57. The crack growth rates are calculated from the crack growth curves in these figures. The bulge-factors are then determined by using the procedure described in Fig.5.34. For crack B, the half-crack-length a used in the calculations is taken as half of the crack length situated between two neighboring frames. Corresponding equations are used for the prediction values of the bulge-factor (Eq.(5.14) for crack A and Eq.(5.12) for crack B). The crack growth data of the flat panel tests mentioned in paragraph 5.3.1 are used as the reference data. The results are summarized in Table 5.6. The predicted bulge-factors for crack A and crack B agree extremely well with the test results. For crack C no predictions can be made, since the prediction method does not account for the influence of the longerons in the structure. It can be seen from the "bulge-factors" of crack C that the crack, which is located just below a longeron, behaves like a flat sheet. This can be expected since the bulge deformation of the crack is completely suppressed by the longeron.

Results of Barrois (SN 601 A "Corvett")

Full-scale fatigue tests on a SN 601 A "Corvette" fuselage were carried out by Barrois[16]. The tests were conducted under repeated internal pressures with maximum values of 0.35 bar to 0.57 bar. A two-bay crack and a one-bay crack, both located in the rear section of the fuselage were tested. The radius of curvature of the fuselage skin at the locations of the cracks was R = 850 mm. Another one-bay crack, which was located in the front section of the fuselage, was also tested. For this crack, the skin sheet was double-curved. The radius of the front fuselage section was slightly smaller than R = 850 mm.

The fatigue tests were started with a maximum internal pressure of p = 0.35 bar. After a certain number of cycles, the maximum pressure was then increased to p = 0.4 bar, and again to p = 0.45 bar, p = 0.5 bar and p = 0.57 bar. Crack growth was recorded by means of visual measurements.

The skin material was Alclad A-U4G1-T3, which is similar to 2024-T3 Alclad.

In order to determine the actual stress intensity factors of the cracks, CTOD measurements were also carried out for al cracks under an internal pressure of p = 0.4 bar. The stress intensity factor K was then calculated through the CTOD values. It was assumed by Barrois[15] that the K values of the cracks under a different pressure was proportional to $p(a)^{1/2}$. This assumption, however, having the present knowledge of the non-linearity of the problem, is incorrect. Hence, only the measured K-values for p = 0.4 bar are used here for comparison.

In Table 5.7 the bulge-factors according to the crack growth rates and the stress intensity measurements are compared to the predictions. For the calculations of β_b the results of da/dN-ΔK curves of 1.2 mm flat 2024-T3 Alclad specimens were used again. The cracks in the two-bay crack situation are treated as two cracks each of length 2a. It can be seen from Table 5.7 that the scatter of the bulge-factors β_b is large, which is probably due to the low accuracy of the crack growth measurements of the tests. As mentioned above, the stress intensity measurements carried out by Barrois are only valid for p = 0.4 bar. The bulge-factors for p = 0.4 bar according to the stress intensity measurements $\beta_{b,K}$ agree well with the predicted values of $\beta_{b,pred.}$.

It can be concluded that the test results, which can be found in the

literature so far, are well predicted by the Eqs.(5.10), (5.12) or (5.14) in all cases.

5.3.3.4 DISCUSSION

The results of the present chapter suggest that the bulge-phenomenon can be described by a fracture mechanics analysis of the bulge deformation around a longitudinal crack in a thin-walled cylinder loaded under internal pressure. The influences of the shell parameters, the stress biaxiality and the internal pressure on the bulge-factors can be well described by Eq.(5.10). By using the damping-factors (Eqs.(5.11) and (5.13)), Eqs.(5.12) and (5.14) satisfactorily predict the bulge-factors of stiffened fuselage structures. However, the equations do not account for the influence of the longerons.

The theory developed in this report is based on fracture mechanics considerations of the bulge phenomenon supplemented with experimental determinations of the influences of the parameters. The theory agrees well with the fatigue test results conducted by the present author as shown in Figs.5.35 to 5.38, except for small crack length (a < 10 mm). In the latter case the predicted bulge-factors are always smaller than the test results. The exact reason of this discrepancy is not fully understood. Nevertheless, very good predictions can be made for larger crack lengths (a > 10 mm), which are relevant for the aircraft industry.

It is interesting to note that the bulge formula of Swift (Eq.(5.15)), with its extremely simple form, works quite well for structures similar to the DC-10 configuration.
For a modern pressurized fuselage, the maximum normal operating differential pressure p is often in the order of 0.57 bar (Boeing 707, Boeing 747, Airbus 300,310,320 etc.), which is also the maximum normal operating differential pressure of the DC-10. Moreover, the design hoop stresses of these aircraft are also quite similar, i.e. about 85 MPa, which is partly related to the fatigue resistance of the skin material of the modern fuselage structures (commonly 2024-T3 Alclad). So the R/t ratio of these aircraft will be about R/t = 1500 (R/t ratio of DC-10 is 1672.22). For a stress biaxiality

of χ = 0.5, Swift's formula is compared to Eq.(5.10) in Fig.5.58. It can be seen that the equations agree very well with one another. However, for other stress biaxialities (see Fig.5.59) and internal pressures (see Fig.5.60), Swift's formula can give erroneous predictions. For modern aircraft fuselage structures, Swift's formula can be used to predict bulge-factors, if the stress biaxiality is about 0.5. However, Eqs.(5.10), (5.12) and (5.14) are more complete and cover a wider range of parameters. Figs.5.59 and 5.60 show that the stress biaxiality χ and the internal pressure p have a significant influence on the bulge-factors. This is important for aircraft designers because the stress biaxialities in the fuselage structures are not always equal to 0.5. For the crown section of a fuselage, an equi-biaxial stress field (χ = 1) is likely to exist. In this case, Swift's formula will give erroneous bulge-factors.

References

1. Kitagawa, H., Yuuki, R., Tohgo, K. and Tanabe, M., "ΔK–Dependency of Fatigue Growth of Single and Mixed Mode Cracks Under Biaxial Stress", *Multiaxial Fatigue, ASTM STP 853*, K.J. Miller and M.W. Brown, Eds., American Society of Testing and Materials, Philadelphia, 1985, pp.164–183.

2. Brown, M.W. and Miller, K.J., "Mode I Fatigue Crack Growth Under Biaxial Stress at Room and Elevated Temperature", *Multiaxial Fatigue, ASTM STP 853*, K.J. Miller and M.W. Brown, Eds., American Society of Testing and Materials, Philadelphia, 1985, pp.135–152.

3. Wilson, W.K., and Thompson, D.G., "On the finite element method for calculating stress intensity factors for cracked plates in bending", *Engineering Fracture Mechanics,* 1971, Vol.3, pp.97–102.

4. Schijve, J., The effect of low sheet thicknesses on the fracture toughness of an Al-alloy (7075-T6), Report LR-425, April 1984, Faculty of Aerospace Engineering, Delft University of Technology, Delft, the Netherlands.

5. Wynn, R.H. and Smith, C.W., "An experimental investigation of fracture criteria for combined extension and bending", *Journal of Basic Engineering,* Dec. 1969, pp.841–849.

6. Kroon, S.J., Stress intensity type prediction of crack growth rates in thin aluminium alloy sheets under combined bending and tensile C.A. fatigue stress. TZ-Report July 1989, Faculty of Aerospace Engineering, Delft University of Technology, The Netherlands.

7. Kruijff de, R., ARALL as crackstopper material. Thesis-report, Vakgroep B2 Faculty of Aerospace Engineering, Delft University of Technology, Delft, The Netherlands, Oct. 1985.

8. Schijve, J., Lecture Notes on Fatigue, Static Tensile Strength and Stress Corrosion of Aircraft Materials and Structures. Report LR-360, Delft University of Technology, Delft, The Netherlands, Oct.1982.

9. Riks, E., Bulging cracks in pressurized fuselage: A numerical study. NLR MP-87058-U, National Aerospace Laboratory NLR, The Netherlands, 1987.

10. Riks, E. and Reijer den, P.J., A finite element analysis of cracks in a thin walled cylinder under internal pressure, NLR TR-87021-U, National

Aerospace Laboratory NLR, The Netherlands, Jan.1987.

11.**Ansell, H.,** Bulging of cracked pressurized aircraft structure. LIU-TEK-LIC-1988:11, Institute of Technology, Dept of Mech Eng, S-581 83 Linköping, Sweden.

12.**Lemaitre, J.** *et al,* "Fracture mechanics analysis of pressurized cracked shallow shells", *Engineering Fracture Mechanics,* 1977, Vol.9, pp.443-460.

13.**Swift, T.,** "Design of redundant structures", *AGARD-LS-97,* pp.9-1 - 9-23,

14.**Mor, H.,** "Crack propagation analysis of longitudinal skin cracks in a pressurized cabin", 26th Israel Annual Conf. on Aviation and Astronautics, Tel Aviv, Feb.1984.

15.**Schwarmann, L.,** "Crack propagation analysis of pressurized fuselage structure", *AGARD-AG-257,* Practical Applications of Fracture Mechanics, edited by Harold Liebowitz, 1980, pp.3-93.

16.**Barrois, W.,** "Practical use of the 'equivalent' measured stress intensity factor to control fatigue crack propagation rates in aircraft full-scale fatigue tests-first assessment on the method in testing of a pressurized aircraft fuselage", *Engineering Fracture Mechanics,* 1975, Vol.7, pp.673-688.

17.**Swift, T. and D.Y., Wang,** "Damage tolerance design-Analysis methods and test verification of fuselage structure", *Air Force Conference on Aircraft Fatigue,* Miami Beach, Florida, From Wood *et al.* (Eds) Proceedings, AFFDL TR-70-144, Wright-Patterson Air Force Base, Ohio, Sept.1970.

CHAPTER 6 ARALL, TESTS ON A NEW AEROSPACE STRUCTURAL MATERIAL

6.1 BRIEF INTRODUCTION ON ARALL

The development of a new generation of aircraft is significantly influenced by new materials. The driving force behind such developments is the ever lasting incentive of reducing aircraft operating costs without impairing the aircraft safety level. Fuel consumption and maintenance costs are two decisive aspects of the "direct operating costs" (DOC). Continuous efforts have been made to design aircraft structures in new materials in order to obtain a significant weight saving combined with minimum maintenance. During the last twenty years, much attention was paid to two families of new structural materials: new aluminium alloys, such as Al-Li alloys and powder metallurgy alloys, and composite materials. The breakthrough of Al-Li alloys and of powder metallurgy alloys is still uncertain. Large weight savings and extensive utilization of composites for primary parts of the structure are expected already for some decades. For several reasons an extensive application is still not yet realized for civil aircraft.

For an optimal structural design there is an obvious need for new materials which combine high strength, low density and high modulus of elasticity with improved toughness, corrosion-resistance and fatigue properties. Carbon fiber and aramid fiber composites almost cover all these demands, except for fracture toughness, which is an important argument for still using the aluminium alloy 2024-T3 in todays aircraft primary structures, especially so if fatigue is a design criterion.

In 1978 the basic ideas of ARALL as a highly fatigue resistant material were generated in the laboratory of Materials and Structures of the Faculty of Aerospace Engineering (Delft University of Technology). It implied that with ARALL (ARamid ALuminium Laminates) an ideal combination of metals and composites should result in a material, which combines the favourable properties of the two components, without sharing their individual disadvantages. Developments of ARALL materials have led to a family of new structural materials with superior fatigue properties as compared to the conventional aluminium alloys, combined with good mechanical, corrosion and workshop properties[1-5].

ARALL is a laminate (Fig.6.1) of thin Al-alloy sheets and fiber layers impregnated with an epoxy adhesive. Originally aramid fibers were used only, but later advanced glass fibers have been adopted also, while the application of carbon fibers in now under investigation. ARALL laminates is a trade name used by ALCOA for ARALL with aramid fibers. GLARE is another trade name used by AKZO for ARALL with R-glass fibers. The principal benefit of the hybrid composite is the ability to impede and self-arrest fatigue crack growth by fibers parallel to the cyclic loading. If a crack has been initiated in the aluminium alloy layers, some limited delamination will occur at the interfaces between the epoxy and the fibers, That will accommodate stress redistribution from the metal to unbroken fibers in the wake of the crack. Crack bridging provided by the strong fibers, constrains crack opening, and thus reduces the driving force for crack growth in the metal layers (Fig.6.2)[9].

Though originally developed for fatigue resistance, ARALL material displays a range of impressive property improvements over those of monolithic high strength aluminium alloys. These attractive characteristics include: 9 - 16 % lower density than aluminium alloys; an unusually high static strength if compared to the 7075 and 2024 aluminium alloys; machining properties comparable to those of metals (e.g. ARALL and GLARE can be cut and sawed, holes can be drilled, riveting is possible); the outer metal layers give protection against fiber/resin system damage by moisture, thermal attack, lightning and impacts; damping is superior to monolithic aluminium. A summary of several engineering properties of ARALL is given in Table 6.1. In this report attention will be mainly focused on ARALL laminates with unidirectional aramid prepregs.

6.2 THE FATIGUE FAILURE MECHANISM IN ARALL

A brief description will be presented here on the fatigue failure mechanism as it was observed by Marissen[7], Verbruggen[8] and Roebroeks[6]. This is necessary to understand the test results described later.

As said before the high fatigue resistance of ARALL is primarily a result of crack bridging by unbroken fibers. If fatigue cracks are growing in the

Al-alloy sheets, while the fibers remain intact (see Fig.6.3 a and b), the stress intensity at the crack tip of the fatigue crack will be significantly reduced. It may become smaller when the crack is growing, because crack opening is drastically reduced by the unbroken fibers. However, the load carried by the cracked area of the sheets must now be transmitted by the crack bridging fibers. As a consequence substantial shear stresses will occur between the fibers and the adhesive rich layer. The prepreg layers in ARALL are usually characterized by a central "fiber rich" part and two thin "fiber poor" or "adhesive rich" layers between the fiber rich part and the adjacent Al-alloy sheets, see Fig.6.4. As a consequence of the shear stresses some delamination between the fiber rich layer and the adhesive rich layer is unavoidable. If the fibers do not fail the growing fatigue crack is surrounded by an elliptically shaped delamination area (Fig.6.3 a).

If the fibers at the minimum of the cyclic load go into compression, the cyclic load can induce fiber failure, especially if aramid fibers are used. Fiber failure then occurs not at the tip of the fatigue crack, but somewhat behind the tip of the crack (in the wake of the crack). Fatigue crack growth is still considerably slower, but an optimal ARALL is not obtained. In this case the delamination area will increase when the crack is growing (Fig.6.3 c). Compression in the fibers can be avoided by prestraining ARALL, i.e. straining ARALL sheets to a small plastic strain (e.g. 0.5%) in the AL-alloy sheets. After this process a residual stress system is obtained with tension in the fibers and compression in the Al-alloy sheets. A superior crack growth resistance is then achieved becaus fiber failure does not occur and crack growth arrest is possible. Another way to avoid fiber failure is to adopt R-glass fibers instead of aramid fibers. The adhesion between glass fibers and the adhesive is much better than for aramid fibers. Moreover, glass fibers are much more resistant if loaded into compression. As a consequence fiber failure in the glass fibers has rarely been observed, and prestraining is no longer necessary to avoid fiber failure. Actually, the process of fiber failure and avoiding fiber failure is more complex than indicated above, because of microcracking in the adhesive and deterioration of the fiber-matrix coherence[6].

92

Another fracture mechanism is indicated as "fiber splitting". It implies a splitting failure along the fibers in the loading direction. When the crack is growing in the Al-alloy sheets, cracking also occurs in the adhesive matrix. It can lead to high shear stresses between the matrix and the fibers. As a kind of crack branching the crack in the adhesive matrix can grow along the fibers. Crack branching in the vertical direction is known to be favourable, because it significantly reduces the stress intensity in the fibers ahead of the broken fibers. As a result it may stop fiber failure. This has been observed indeed. An increasing delamination area, after fiber splitting, may be followed by a decreasing delamination area (Fig.6.3 d) because fiber failure has stopped.

Delamination areas can easily be observed after termination of the fatigue test. An Al-alloy sheet is removed by a chemical milling process. Delaminated areas are then visible by a different colour (i.e. a lighter colour), caused by microcrazing of the adhesive (see Figs.6.7 and 6.8).

6.3 PROBLEM AREAS FOR FUSELAGE APPLICATION

During the last decade much attention is paid to the damage tolerance evaluation of the aircraft fuselage with a pressurized fuselage shell structure. Since the design of the first jet transport aircraft, the tangential loading of the fuselage shell structure has more than doubled due to the increase of the fuselage diameter and higher cabin pressures. One of the most important aspects of designing an aircraft fuselage shell structure is to consider skin fatigue cracks resulting from the pressurization cycle once every flight. The selection of the material and the design stress level must be made in such a way, that fatigue cracks will be discovered within a certain inspection period prior to reaching a critical crack length.

Since the start of ARALL at the end of the 70's, ARALL has been widely regarded as a family of highly damage tolerant materials with a high weight saving potential. After extensive testing of specimens, joints and small components a full-scale ARALL aircraft lower wing skin structure was designed, built and successfully tested under a flight-simulation load history[2]. A weight saving of more than 30% was achieved. International attention is now focused on the application of ARALL as an aircraft fuselage skin material.

Yet, several questions concerning the basic design principles and material properties for this application have still to be answered. As explained before, the stress conditions in a modern pressurized fuselage skin structure are rather complicated due to the internal pressurization of the structure and the secondary effects associated with this internal pressurization, such as the bulging-effects, biaxial stress field, bending effects etc. For the application of a new fuselage skin material, it is very important to know how those effects contribute to the crack growth behaviour of the material under service load conditions.

At the moment, the crack growth mechanism of ARALL laminates is studied in the Materials and Structures Laboratory of the Faculty of Aerospace Engineering in Delft. Several crack growth models concerning different aspects of the crack growth behaviour of ARALL exist. Unfortunately, it is still difficult to predict the ARALL behaviour under conditions, which include crack edge bulging and stress biaxiality. It is thus essential to investigate the influences of those effects before designing an ARALL fuselage skin structure. For that purpose the investigation reported in the previous chapter was extended to deal with the behaviour of ARALL.

The potential application of ARALL as a fuselage skin material has initiated another development. ARALL with unidirectional fibers can be fully satisfactory for the lower wing structure. Wing bending induces a highly dominant tension loading direction. In a pressurized fuselage, however, a biaxial loading is obviously present. Moreover, the fuselage skin has riveted joints in the longitudinal and the circumferential direction. Further, fuselage bending can change the direction of the main principal stress in some parts of the fuselage structure (e.g. in the crown section). Good properties in more than one direction are desired. In view of the anisotropic properties of ARALL with unidirectional fibers (see Table 6.1, the UD ARALL version), there is need for a more isotropic ARALL. For this purpose GLARE 2R33 50/50 has been developed. It has 50% of the fibers in one direction and the other 50% in the perpendicular direction. The improvement of properties in the transverse (LT) direction is clearly illustrated by the data in Table 6.1. Some fatigue tests on the 50/50 version were carried out as part of the present investigation.

6.4 EXPERIMENTS AND TEST RESULTS

In previous chapters biaxial tests and the tests on curved panels were described. the SUPERBAT specimen (section 4.2) was developed to introduce a moderate stress biaxiality by preventing the Poisson contraction. The CETS (Curvature Effect Testing System) was introduced to test curved specimen under combined tension and bending, and the PFSTS (Pressurized Fuselage Skin Test System) was designed to test curved panels under cyclic internal air pressure. The same testing equipment and types of specimens have been used to investigate fatigue cracks in ARALL. The number of tests is limited, because insufficient ARALL material was available. Moreover, testing ARALL in the PFSTS is rather time consuming, due to the low cyclic frequency and the high fatigue resistance of ARALL. A survey of the tests is given in Table 6.2.

It may be noted here that the classical cruciform specimens for biaxial testing will offer still more problems for ARALL than for monolithic aluminium alloys, because of the uniaxial fibers, which are discontinuous in such a specimen in one of the two loading directions. Problems at the corners of the cruciform specimen should be expected.

6.4.1 EFFECT OF STRESS BIAXIALITY

Tests were carried out on the SUPERBAT specimen shown in Fig.6.5. The lateral restraint is obtained by heavy steel strips. The stress biaxiality ratio χ in the test area was measured with strain gauges. The result was $\chi = 0.28$.

Two uniaxial and four biaxial R = 0 constant amplitude fatigue tests have been carried out on 0.82 mm thick ARALL sheet (UD ARALL 2H32 with Aramid fibers). Scatter of the test results is very low. The test results are shown in Fig.6.6 together with the test results of monolithic 2024-T3 aluminium sheets. The crack growth behaviour of the monolithic Al alloy under uniaxial loading is the same as that under biaxial loading, see chapter 5. However, the ARALL specimens loaded under the biaxial stress field show a considerably longer fatigue life than the uniaxially loaded ARALL specimens, see Fig.6.6.

After the fatigue tests, the aluminium layers around the delamination areas were removed by means of chemical milling in order to investigate the shape of

the delamination area in the prepreg layer. The delamination areas are shown in Fig.6.7 and Fig.6.8 for uniaxially and biaxially loaded specimens respectively. Apparently the delamination area in the uniaxially loaded specimen is significantly different from that of a biaxially loaded specimen. There are two reasons for the different behaviour:

First, the delamination area of the biaxially loaded specimen is considerably smaller than that of the uniaxially loaded specimen (compare Fig.6.7 to Fig.6.8) which results in a lower crack growth rate[6]. This can be explained as follows:

A study by Marissen[7] on the "load flow" in a cracked ARALL sheet with a delamination area has shown that there are three "load flows" in that area (Fig.6.9). As stated in reference 7, the load flow 2 (part 2 in Fig.6.9) introduces a peel stress on the interfaces between the aluminium layers and the fiber layer, which is the most important cause of the delamination growth. As a consequence of this load transfer (load flow 2) the aluminium layers in the delamination area will deform outwards from the fiber layer (out-of-plane deformation of the aluminium layers in the delamination area, which has been frequently observed during tests on ARALL in the laboratory, see also Fig.6.3 b). The biaxial stress field limits this out-of-plane deformation, which leads to a smaller delamination area. A smaller delamination area of ARALL will result in a lower stress intensity at the crack tip in the Aluminium alloy sheets and thus to a lower crack growth rate[8].

Secondly, it can be seen in Fig.6.8 that the delamination area of the biaxially loaded specimen shows more fiber splitting as compared to the uniaxially loaded specimen. This is due to the transverse loading of the prepreg layer (tensile stress perpendicular to the fiber direction). It promotes the fiber splitting mechanism which is considered to be in favour of ARALL. As mentioned before (section 6.2) the fiber splitting results in a redistribution of the stress field, which will delay fiber failure in the delamination area. That results in a lower crack growth rate of ARALL[6].

Recently, other versions of ARALL material have been developed, such as GLARE with R-glass fibers with both unidirectional or cross-ply prepregs, see Table 6.1. Because this material was not available in time, the effect of stress

biaxiality on the crack growth behaviour of this material could not yet be studied. It is believed, however, that crack growth under biaxial loading conditions will be slower than for ARALL with unidirectional aramid fibers. The glass fibers will not fail and the effect of limiting the out-of-plane deformation of the aluminium layers in the delamination area will still be present.

6.4.2 EFFECT OF BENDING STRESSES

During the assembling of an aircraft fuselage, the skin sheets are usually bent to take the local curvature of the fuselage. This process introduces a bending stress field in the fuselage skin sheets. For a conventional aluminium alloy the bending stress field will increase the stress intensity factor when a crack is present (see section 5.2). This may result in a higher crack growth rate and reduce the fatigue life of the structure. To investigate the bending effect the test set-up "CETS" (Curvature Effect Test System) was developed as described in section 4.3.2, see also Fig.4.3. An originally flat ARALL sheet is forced to take a predetermined curvature by placing the sheet between a curved block and two press-rolls. Blocks are available with radii of 130 mm, 375 mm, 750 mm and 1500 mm respectively.

Two materials (ARALL 2H32 and 7H32[1]) have been tested. The thickness of the specimens is 0.82 mm. The starter-notch is simulated by a narrow saw-cut (width 0.3 mm) with a half-crack length of 1.5 mm. The notch is perpendicular to the fiber direction of the specimens. The specimen is then placed in the test fixture and a constant amplitude fatigue load of $\sigma = 75 \pm 75$ MPa is applied. The loading direction is the fiber direction of the specimen.

The test results are given ·in Fig.6.10 and Fig.6.11 for ARALL 2H32 and ARALL 7H32 respectively. Surprisingly, and in contrast with the fatigue test results of Al 2024-T3 in the same test fixture (see section 5.2.2), a higher initial bending stress (smaller radii of curvature) leads to a lower crack growth rate in ARALL. An examination of the delamination area of the ARALL specimens has

---

[1] Notation of ARALL see note of Table 6.1

shown (Fig.6.12) that different delamination shapes exist for the curved specimens as compared to the flat specimens. Moreover, the delamination shape of the outer side (tension side) of the curved specimen differs also from the shape of the inner side (compression side) of the same specimen (compare Fig.6.12 b to Fig.6.12 c). Fig.6.12 a shows the typical shape of a delamination area (also called a "Double-Tie" delamination area) of a flat specimen of ARALL with aramid fibers, loaded under R = 0 constant-amplitude fatigue stress, whereas, Fig.6.12 b shows a delamination area with a shape which is typical for ARALL with very limited fiber failure. Fig.6.12 c shows a delamination shape in between Fig.6.12 a and Fig.6.12 b (a detailed description of the delamination shapes in ARALL material is given in reference 6).

Observations of the cross-section of the specimens at the location of the crack are consistent with the different shapes of the delamination areas (see Fig.6.13. More fiber failure occurs at the inner side (compression side) of the curved specimens, whereas, most of the fibers at the outer side (tension side) remain intact ("*partial fiber failure in aramid prepreg*"). As discussed in section 6.2 compressive stresses will promote fiber failure, whereas tensile stresses will prevent fiber failure. As a consequence, a certain part of the fibers will remain intact in a curved specimen. Crack bridging is then more effective, and that explains why the crack growth rate is lower.

The influence of the bending stress on the crack growth behaviour of ARALL with aramid fibers under R=0 CA fatigue loading, is thus in favour of the material. A higher bending stress (i.e. smaller radius of curvature) results in a lower crack growth rate of the material. For GLARE laminates with R-Glass fibers, the effect of the bending stress on the crack growth rate of the material will probably be negligible, since no fiber failure is expected in these materials[6].

6.4.3 EFFECT OF BULGING

The significance of the "bulge-out" phenomenon for aircraft design has been discussed in previous chapters. In order to investigate this phenomenon, ARALL specimens have been fatigue tested in the pressurized fuselage skin test

system, PFSTS, described in section 4.4. In this test system, a curved panel is cyclically loaded with a realistic internal air pressure.

Tests were carried out on ARALL 2H32, ARALL 2H33 (both with aramid fibers) and GLARE 2R32 (with R-Glass fibers) panels of 1000 × 500 mm × mm. The thicknesses of the panels were 0.82 mm, 1.34 mm and 0.91 mm respectively. A saw-cut of 3 mm ($2a_0 = 3$ mm) was made in the center of the specimen to simulate a starter notch. The radius of curvature of the panels was 2000 mm. The panels were cyclically loaded from an internal pressure $p_{min} = 0$ bar to a maximum internal pressure of $p_{max} = 0.56$ bar. Transverse loading (preventing Poisson contraction) was not applied. The period of the loading cycles was 4 seconds (frequency of 0.25 Hz).

A summary of the test results is given in Fig.6.14 together with the test result of a monolithic 2024-T3 alclad sheet. A comparison between the crack growth curves for each ARALL material in the curved and in the flat condition is given in Fig.6.15 and Fig.6.16. The a-N curves for the flat specimens are adopted from reference 6.

It can be seen in Fig.6.15 that the crack growth curve for ARALL 2R32 tested in the curved condition is almost identical to the test result of a flat specimen with a similar tensile load. No influence of the bulge-out phenomenon is found. This is in strong contrast to the results of monolithic aluminium test panels (see chapter 5, section 5.3) where a significant influence of bulge-out has been found. This remarkable result can be explained because during the fatigue test of the ARALL 2R32 penal, no out-of-plane deformation of the crack edges has been observed. As shown in chapter 5, bulge-out is associated with the out-of-plane deformation of the crack edges. In the case of ARALL with R-Glass fibers, fiber failure will not occur during the fatigue process[6]. The R-Glass fibers will thus prevent any out-of-plane deformation of the crack edges. It is thus logical that no bulge-out effect was found with this material.

In Fig.6.16 the a-N curves of ARALL 2H32 and ARALL 2H33 under cyclic internal pressure are compared to the a-N curves of the same materials for flat panels. It shows that the crack growth behaviour of ARALL with aramid fibers loaded by

internal pressure is almost identical to that of the same material loaded in the flat condition.

In the case of ARALL 2H32, out-of-plane deformation of the crack edges (bulge-out) has been observed during the fatigue test. Nevertheless, no influence of the bulge-out on the crack growth behaviour was found. It is very likely that bulge-out (i.e. out-of-plane deformation) introduces a higher tensile stress in the unbroken fibers in the delamination area. A higher fiber stress will then result in a lower stress intensity of the crack in aluminium layers[7], and hence a lower crack growth rate is found. Apparently, it compensates for the unfavourable bulge-out effect. This may explain that the crack growth behaviour of ARALL 2H32 under internal pressure is still the same as for a flat panel.

Fig.6.16 also shows that the crack growth rate of ARALL 2H32 decreases after the crack length is approximately 60 mm. This is due to fiber splitting at a large crack length. A detailed explanation of this phenomenon is presented in reference 6 and is beyond the scope of this report.

For ARALL 2H33 the crack length reached during the tests is so small (a = 5 mm) that no bulge-out could be observed. As a consequence the crack growth behaviour of ARALL 2H33 under the test condition is similar to that of a flat specimen.

A residual strength test was carried out on one ARALL 2H33 specimen with a long central saw-cut of 2a = 200 mm. The saw-cut implies that that there are no crack bridging fibers. Although cutting the fibers of a large simulated crack is not a realistic simulation for a fatigue crack, it is relevant for damage tolerance requirements, which ask for considering penetrating impact by foreign objects, see next section. The internal pressure was manually increased until the specimen failed at a pressure of 0.61 bar. Considerable bulge-out was observed, but no stable crack growth occurred.

According to reference 9, the net residual tensile strength of flat ARALL 2H33 sheets is approximately 320 MPa independent of crack length and specimen width. In this test configuration, where the total crack length 2a is 200 mm and the specimen width is 500 mm, the gross residual tensile strength should be 320*(500-2*100)/500 = 192 MPa. This is much higher than the residual hoop stress found in the test, which is $\sigma_{cr.hoop}$ = pR/t = 0.0615*2000/1.34 =

91.79 MPa. The bulge-factor β_b is thus 192/91.79 = 2.09.

It is interesting to note that the bulge formula (5.10), derived for monolithic aluminium alloy sheets, predicts a bulge-factor of 2.18 for this test configuration, which is very close to the test value of 2.09. Apparently, for the residual strength of ARALL with aramid fibers there is a considerable influence of bulge-out for a large crack, as predicted by the bulge formula (5.10).

In summary, it can be concluded that bulge-out has no influence on the fatigue crack growth behaviour of ARALL material. For ARALL with aramid fibers, bulge-out of crack edges can be observed when fiber failure occurs and the crack length is large enough to show this out-of-plane deformation. However, this out-of-plane deformation does not result in a higher crack growth rate of the material. For ARALL with R-Glass fibers, no bulge-out effect is expected too, since the R-Glass fibers will always remain intact during the fatigue process.

A considerable bulge-out effect has been found under static load until failure of an ARALL panel with aramid fibers and a large crack (saw-cut) with all fibers broken. The bulge-out effect can be described by Eq.(5.10). No conclusion on residual strength can be drawn for ARALL with R-Glass or Carbon fibers, since such static tests have not yet been carried out on these materials.

6.5 ABOUT DAMAGE TOLERANCE DESIGN OF ARALL FUSELAGE STRUCTURES

For aircraft structural design, several criteria are of primary importance, especially the so-called damage tolerance design principles, which are outlined in the Federal Airworthiness Regulations (FAR) part 25 and in the Joint Airworthiness Requirements (JAR) 25.

In general terms, the damage tolerance concept includes three aspects: crack propagation, residual strength and damage detection, which are strongly interrelated. As shown in the previous sections, ARALL laminates have excellent fatigue properties even under severe loading conditions. Secondary aspects, such as biaxial loading, sheet bending and bulge-out, which play an important role in designing monolithic aluminium alloy fuselage skin

structures, are working in favour of ARALL laminates. As stated in reference 4, due to the excellent fatigue behaviour of ARALL, crack propagation and residual strength after fatigue are no more the most critical damage tolerance design factors. This is certainly true when R-Glass fibers are used instead of aramid fibers, which gives the material much better residual strength properties[6].

Numerical damage tolerance requirements for a specific aircraft fuselage will now be recapitulated to evaluate the experience of the present ARALL test series for such a practical problem.

The most important JAR (FAR) damage tolerance design criteria concerning fuselage structures were studied in reference 11. A brief summary of the criteria is given below.

1) Fatigue

Damages caused by fatigue and small accidental damage, including corrosion, manufacturing and servicing defects:

a) 100 mm skin crack in any direction or position;

b) 75 mm skin crack, plus a failed adjacent dependent element attached to the skin (e.g. stringer, frame, element of a multi-element frame or crack-stopper band);

c) 50 mm skin crack from the edge of a cut-out plus a small crack starting at the edge of the adjacent reinforcing element, if any (e.g. doubler or frame);

Minimum fatigue life after the above damage to which a safety factor of 3 must be applied:

skin and skin-joint visible from outside:	3000 flights (unfactored 9000 fl.)
skin and skin-joint not visible from outside:	6000 flights (unfactored 18000 fl.)
window frames and frames:	12000 flights (unfactored 36000 fl.)

Residual strength: 1.15Δp

(Δp = max. normal operating differential pressure)

(for circumferential cracks: 1.15Δp or limit load in flight)

2) Engine compressor or turbine disc break up, bird strike

Damage caused by one third of an engine compressor or turbine disc in any direction. The chance of a catastrophic failure due to the damage must be smaller than 1 to 20.

Minimum period during damage state: 1 flight.

Residual strength: $1.1\Delta p$.

3) Accidental damage caused by ground equipment

Initial damage:

a) 300 mm crack in any direction and position;

b) 200 mm skin crack, plus a failed adjacent dependent element attached to the skin (e.g. stringer, frame, element of a multi-element frame or crack stopper band).

(note: position of these initial damages is likely at the lower fuselage structure and 1m around door openings)

Minimum fatigue life in damaged state: 50 flights.

Residual strength: $1.1\Delta p$.

4) Corrosion

Initial damage: a) 300 mm crack in any direction and position;

b) 200 mm skin crack, plus a failed adjacent dependent element attached to the skin (e.g. stringer, frame, element of a multi-element frame or crack stopper band).

(note:for ARALL fuselage the following initial damages may be assumed:

lower fuselage structure: 1 aluminium layer corroded; length 300 mm.

upper fuselage structure: 1 aluminium layer corroded; length 200 mm.

see reference 11)

Minimum fatigue life in damaged state: 50 flights.

Residual strength: $1.15\Delta p$.

It has been concluded by W.Schijve[11] that the most critical damage tolerance design criteria for a longitudinal crack in an ARALL fuselage structure are:

1) 100 mm (2a) crack with fibers cut in the upper fuselage structure; residual strength: $1.15\Delta p; 15\Delta p$;

2) 300 mm (2a) crack with fibers cut in the lower fuselage structure; residual strength: $1.1\Delta p$;

3) damages caused by engine compressor or turbine disc break up, bird strike;

residual strength: $1.1\Delta p$.

For cases 1 and 2, the stiffening elements are assumed to be intact because of the excellent fatigue behaviour of the ARALL stiffening elements[11].

It is interesting to see whether ARALL can satisfy the above criteria. For that purpose ARALL will be considered as fuselage skin material for a modern wide body airliner, the Airbus 320 with R = 1975 mm, p = 0.57 bar and L = frame spacing = 500 mm. Due to lack of information caused by engine compressor or turbine failure and bird strike, the third criterion will not be considered. The calculations should lead to a comparison between required strength and available strength. For this purpose the following equation is used:

$$\text{required strength} = q \cdot \text{hoop stress} \cdot \beta_b \qquad (6.1)$$

The hoop stress is equal to pR/t. The damage tolerance requirements summarized above indicate q = 1.15 and q = 1.1 for the upper and lower fuselage structure respectively. The bulge factor β_b is calculated with Eq.(5.14) for a crack between two frames, and with Eq.(5.12) for a crack between the frames, but one crack tip has reached the frame.

The available strength is derived from the sharp notch (saw-cut) strength quoted in Table 6.1. It is conservatively assumed that the panel width is equal to the frame spacing L, which leads to:

$$\text{available strength} = \text{sharp notch strength} \cdot \left(\frac{L - 2a}{L} \right) \qquad (6.2)$$
$$\text{(gross stress)} \qquad\qquad \text{(net stress)}$$

The comparison between the required strength and the available strength is made in Table 6.3. It is done for two types of ARALL, viz. ARALL 2H33 with unidirectional aramid fibers, and ARALL 2R33 50/50 with R-glass fibers in two mutually perpendicular directions. The ratio between available strength and

required strength is defined as the reserve factor:

$$\text{reserve factor} = \frac{\text{available strength}}{\text{required strength}} \qquad (6.3)$$

Reserve factors larger than 1 indicate that there is still an extra margin of safety. The last column of Table 6.3 shows that the crack in the upper fuselage is far from critical, whereas the margins are much smaller for the crack in the lower fuselage. The table also shows that the margins for ARALL 2R33 50/50 are larger than for ARALL 2H33. For the latter material one reserve factor (0.93) is smaller than 1, which indicates insufficient residual strength.

The above analysis on damage tolerance aspects illustrates that ARALL with R-Glass fibers is the most suitable material for fuselage skin application. ARALL with UD aramid fibers gives insufficient residual strength in one case. Besides, ARALL with UD aramid fibers is not suitable for fuselage skin application because of its inferior engineering properties in the transverse direction (perpendicular to the fibers) of the material.

It is also interesting to note that studies carried out by W.Schijve[11] have shown that weight saving of about 30% can be achieved when using ARALL with aramid fibers as fuselage skin material. It is believed that application of ARALL with 50/50 R-glass fibers as fuselage skin material will lead to a comparable weight saving.

6.6 CONCLUSIONS AND REMARKS

In comparison to monolithic aluminium alloy sheets, ARALL laminates show very good fatigue and static test results under the fuselage test conditions which can be regarded as severe and realistic. The biaxial stress field improves the fatigue performance of ARALL laminates with aramid fibers. Combined cyclic tension and static bending have a negligible influence on the fatigue behaviour of monolithic aluminium alloy sheets, but in contrast to this behaviour it turned out to be favourable for ARALL laminates. The negative effect of bulge-out on the fatigue behaviour of monolithic aluminium alloy sheet is not present for ARALL material. The residual strength behaviour of

ARALL laminates with aramid fibers with a large saw-cut can be predicted with the bulge formulas found for monolithic aluminium alloy sheets. It is believed that this will also hold for GLARE laminates.

Study on the damage tolerance requirements shows that the most critical damage tolerance design criteria are the sharp notch (saw-cut) residual strength of ARALL material. Residual strength calculations have shown that GLARE laminates can meet this severe residual strength requirement with considerable weight saving (about 30%).

References

1. Vogelesang, L.B., R. Marissen and J. Schijve, "A new fatigue resistant material: Aramid Reinforced Aluminium Laminate (ARALL)", paper in *11th ICAF Symp.* Noordwijkerhout, The Netherlands, May 1981.

2. van Veggel, L.H., A.A. Jongebreur and J.W. Gunnink, " Damage tolerance aspects of an experimental ARALL F-27 lower wing skin panel". Proc. *14th ICAF Symp.,* Ottawa 1987, EMAS 1987, pp.465-502.

3. Vogelesang, L.B. and J.W. Gunnink, "ARALL, A Material for the Next Generation of Aircraft. A State of the Art", Report LR-400, Dept. Aerospace Eng., Delft University of Technology, The Netherlands, Aug.1983.

4. Gunnink, J.W. and M.L.C.E. Verbruggen and L.B. Vogelesang, "ARALL, A Light Weight Structural Material for Impact and Fatigue Sensitive Structures", Vertica Vol.10, No.2, 1986. pp.241.

5. Vogelesang, L.B., J.W. Gunnink, D. Chen, G.H.J.J. Roebroeks and A. Vlot, "New Developments in ARALL Laminates", *Second Specialists Conference on ARALL Laminates,* 25-26 Oct. 1988, Delft, The Netherlands.

6. Roebroeks, G.H.J.J., "Fiber failure mechanism of ARALL", to be published, Delft University of Technology.

7. Marissen, R., Fatigue Crack Growth in ARALL —— A hybrid aluminium-aramid composite material (crack growth mechanisms and quantitative predictions of the crack growth rates), Phd Thesis, LR Report-574, Delft University of Delft, June 1988.

8. Verbruggen, M.L.C.E., Aramid Reinforced Aluminium Laminates: ARALL, Phd Thesis, LR Report-503, Delft University of Technology, Nov. 1986.

9. Vermeeren, C.A.J.R., The ARALL Blunt Notch Behaviour, Master Thesis, Delft University of Technology, Oct. 1988.

10. Gunnink, J.W., Design studies of primary aircraft structures in ARALL laminates, Report LR-520, Delft University of Technology, June 1987.

11. Schijve, W., Investigation on the structural design of the Airbus A 320 fuselage with ARALL material (in Dutch), Master Thesis, Delft University of technology, 1983.

12. van Oost, R. Private communication. Delft University of Technology, Dec. 1989.

CHAPTER 7 SUMMARY AND CONCLUSIONS

Fatigue cracks in aircraft fuselages are a significant safety problem since the introduction of the pressurized passenger cabin. The explosion of the fuselage of two Comet aircraft in the early fifties was a most dramatic manifestation. Although we have learned much from these and similar accidents, the occurrence of fatigue cracks in fuselage shell structures is still problematic. Aircraft now are used longer and more intensively than in the past. Moreover, stress levels have been increased to save structural weight. As a consequence, the growth rate of fatigue cracks and the effect of cracks on the residual strength has to be considered as part of the airworthiness certification. Fracture mechanics is used for that purpose. However, longitudinal cracks in a pressurized fuselage offer special problems.

(1) The crack occurs in a **curved** thin sheet metal structure.

(2) The conditions are complex due to the **biaxial loading** and the **internal pressure**.

The fatigue crack edges bulge outwards (out of plane deformation) which considerably complicates the fracture mechanics analysis. Information in the literature, both theoretical and empirical, is rather limited. In the present study it is tried to analyze the problem. Test series were carried out with new test set-ups and the problem is also theoretically analyzed.

The problem area is introduced in chapter 1 and 2, followed by a survey of theoretical work in chapter 3. Three new test set-ups, designed as part of the present study, are described in chapter 4.

(1) The **SUPERBAT** specimen (SUPERBAT = Specimen Using Poisson Ratio Effect for BiAxial Testing) is a sheet specimen provided with stiff lateral bars to restrain the Poisson contraction if it is loaded in tension. As a consequence a biaxial stress field is obtained.

(2) In the **CETS** test set-up (CETS = Curvature Effect Test System) a sheet specimen is loaded in tension around a block with a fixed curvature. Blocks with different curvatures were used.

(3) Finally, the **PFSTS** test set-up (PFSTS = Pressurized Fuselage Skin Test System) was designed to load sheet specimens under hoop stress conditions by applying air pressure to the specimen. The SUPERBAT specimen was also used in this test set-up. A realistic simulation of the pressurized fuselage condition is thus obtained.

108

Results of static and fatigue tests carried out with the new equipment are presented and analyzed in Chapter 5. It includes measurements of the bulge out deformations around the crack in specimens loaded in the PFSTS. A new theoretical analysis, based on energy considerations, is offered in Chapter 3 with an additional evaluation in Chapter 5. It leads to equations to predict the bulge factor

$$\beta_b = K_{bulge}/K_{flat}$$

for pressurized fuselages. The bulge factor is the ratio of the stress intensity factor applicable to the fuselage and the stress intensity factor of a flat sheet with the same nominal stress intensity. The equations for β_b are semi-empirical because empirical results obtained for the bulge out deformation are used. The equations to predict β_b have been checked on our own results and on results from FEM calculations and full- scale tests as reported in the literature.

The problem of fatigue cracks in fuselages can also be solved by developing new fatigue resistant materials. This is now actively done in the Materials & Structures Laboratory of the Faculty of Aerospace Engineering in Delft. In the present study tests were carried out on these materials (ARALL and GLARE) with the new test equipment. The results are presented in Chapter 6, which is completed by a section on damage tolerance design of ARALL fuselage structures. The main results of the present study are summarized in the following conclusions.

effect of stress biaxiality

(1)   The advantage of the SUPERBAT specimen is that a biaxial stress field can easily be obtained in a test machine for uniaxial loading. The limitation is that the maximum biaxiality ratio is equal to the Poisson ratio. In general it will be slightly smaller. In the present tests a biaxiality ratio 0.24 was obtained (0.28 for ARALL specimens). The calculated ratio agrees very well with the measured value.

(2)   The stress biaxiality did not affect the fatigue crack growth behaviour in both Al 2024-T3 and Al 7075-T6 bare sheets. This is in good agreement with observations reported in the literature.

(3)   The effect of stress biaxiality on the CA fatigue crack growth behaviour in aluminium alloy sheets can be disregarded in bulge out studies.

effect of bending stress

(4) Specimens tested with the CETS equipment are subjected to constant bending stress and an applied tension load. The bending stress is depending on the radius of curvature used in the test. It affects the static strength and the fatigue crack growth, depending on the radius of curvature.

(5) The static tests revealed a systematic effect of the curvature on the residual strength. A smaller radius of curvature led to a lower residual strength.

(6) A theory is developed for predicting the static strength of thin aluminium sheets with a central crack, loaded under a constant bending stress and an increasing tension load. The theory gives more accurate predictions for the residual tensile strength of Al 7075-T6 sheets if compared to other prediction methods from the literature. For Al 2024-T3 sheets the theory still gives good predictions, although net section yielding does occur.

(7) Results of the R=0 CA fatigue tests with the CETS equipment show that the crack growth rate for thin Al-alloy sheets (t ≤ 1 mm) is identical to the crack growth rate for flat specimens if the radius of curvature is sufficiently large. As a consequence, the effect of bending stress on fatigue crack growth in skin sheet material of an aircraft fuselage can be ignored.

(8) For smaller radii (≤ 350 mm) the crack growth rate tends to decrease with a decreasing radius of curvature. This perhaps unexpected result is associated with a phenomenon *"partial crack closure due to bending"*. It is believed to be the result of the compressive stress acting at the compression side over the full width of the specimen. The phenomenon is different from the well known Elber's crack closure mechanism, which is due to plastic deformation in the wake of the crack.

(9) Bulge out of crack edges is observed during the CETS experiments, especially if a small radius of curvature is applied. Bulge out can occur even without an internal air pressure.

effect of bulge out

(10) Tests in the PFSTS under air pressure indicate significant bulge out deformations. The deformation field has been measured. It turns out to depend in a non-linear way on the applied air pressure. Moreover, it is highly sensitive to the biaxiality ratio. In comparison to uniaxial loading, the bulge out deformations are considerably smaller under biaxial loading. As a consequence the crack growth rate is smaller under biaxial loading.

(11) The experiments have shown that the bulge factor decreases with increasing internal pressure and stress biaxiality, and increases with increasing crack length.

(12) FEM calculations made for pressurized aircraft skin structures (Riks, Ansell, etc.) show that the linear theories on bulge out developed by Folias, Erdogan, etc. are invalid. The bulge out factor is a non-linear function of the geometrical parameters (R,t), Young's modulus, crack length and the loading conditions (p,biaxiality).

(13) A theory is developed in this report by considering the bulge out phenomenon from the fracture mechanics point of view, taking account of the non-linear effects associated with the non-linear deformations of the cylinder in the neighbourhood of the crack. The theory has led to an expression for a non-linear bulge factor with some terms, which have been experimentally determined.

(14) In general the theory agrees well with the results of the present author, and with FEM calculation results, and full-scale test results from the literature. The effect of fuselage frames can be accounted for by adopting a damping factor presented in the literature. However, the theory is unable to predict the effect of the longeron spacing on the bulge out effect.

(15) The bulge formula of Swift gives good predictions for fuselage structures similar to the DC-10 configuration (i.e. $p \cong 0.57$ bar and $R/t = 1500$) with a stress biaxiality ratio of 0.5. However, for other configurations Swift's formula gives erroneous bulge factors.

ARALL

(16) Test results show that stress biaxiality leads to a lower crack growth rate in ARALL laminates. There are two reasons: a biaxial stress field restrains the out-of-plane deformation, which leads to a smaller delamination area, and secondly, stress biaxiality enhances fiber splitting in the delamination area. Both mechanisms lead to a lower crack growth rate.

(17) The phenomenon of "partial fiber failure in aramid prepregs" has been observed in the CETS tests on ARALL specimens. The aramid fibers on the tension side of the specimen tend to remain intact during R=0 CA fatigue, more than on the compression side, which leads to a lower crack growth rate of the material under a combined static and cyclic tension load. A higher bending stress (i.e. a smaller radius of curvature) results in a lower crack growth rate. It is expected that this effect will be negligible for GLARE laminates, since fiber failure is not expected to occur in these materials.

(18) In contrast to monolithic aluminium sheets, bulge out has no influence on the crack growth behaviour of ARALL laminates. Bulge deformations of crack edges in ARALL 2H32 is observed when fiber failure occurs and the crack is long. However, this out-of-plane deformation does not result in a higher crack growth rate of the material.

(19) The influence of bulge out on ARALL laminates with a saw cut (all fibers broken) is the same as for a monolithic aluminium alloy sheet.

(20) The most critical damage tolerance design criteria are the sharp notch (saw cut) residual strength of ARALL laminates. In comparison with ARALL laminates, GLARE laminates are better fuselage materials in terms of damage tolerance requirements.

Epilogue

The present study illustrates the usefulness of a fracture mechanics analysis for the understanding of a complex crack problem, as well as to arrive at improved prediction equations. At the same time it must be admitted that it

does not contribute in itself to an improved knowledge of the fracture mechanisms involved. Such an improvement requires a detailed study of the fracture mechanism. The present investigation has indicated this to be especially true for such hybrid materials as ARALL and GLARE. Without information on concurrent, or even competing fracture processes, the application of fracture mechanics is unrealistic. In this respect the phenomenon "partial crack closure due to bending" and "partial fiber failure in ARALL laminates" should be studied further. In broader terms, continued research should be devoted to the prediction of damage tolerance properties of the fiber/aluminium alloy sheets laminates.

Acknowledgement

The author wishes to express his gratitude to the Production and Material Section (vakgroep B2) of the Faculty of Aerospace Engineering, Delft University of Technology, The Netherlands, for all facilities which were needed for performing the experimental work and finishing this thesis. The members of the design office and the instrument workshop of the Faculty of Aerospace Engineering are acknowledged for their excellent detailed engineering and workmanship.

Mr. E. Riks from the National Aerospace Laboratory (NLR) is thanked for useful discussions on the bulge-out phenomenon. Gratitude is due to Mr. C. Paalvast and Mr. A. Burgers for their assistance to carry out the tests, and to Mr. F. Oostrum who prepared the photographs. Mr. W. Spee and Mr. J. Sinke are thanked for their excellent drawing work. Mr. J. Snijder is acknowledged for his kind help and patience during the design and start-up of the experimental set-ups. His humour and positive way of looking at the experimental failures have certainly contributed to the success of the experiments.

I would specially like to express my thanks to Mr. L.B. Vogelesang for his advice and encouragement of my work, and for his more than amicable support for me and my family. His inexhaustible enthusiasm has inspired me to carry on the experiments which did not always run as they were planned.

I am most grateful to Professor J. Schijve for the indispensable supervision, criticism, advice, encouragement and discussions, and the many hours spent reading the manuscript which considerably improved the quality of this thesis. His most skilled and intuitive approach towards theoretical exercises and experimental layout was of great value for this research work.

Finally, I wish to thank all members of "vakgroep B2" and the students I have been working with. All of them have contributed to the excellent working atmosphere of the group, which I want to call the "B2-spirit". It stands for a scientific approach, good fellowship, enthusiasm and optimism, and last but not least, "gezelligheid".

Table 2.1 Summery of aircraft accidents involving fuselage fatigue
(data partly taken from ref.10)

aircraft type	accident date	remarks
D.H.Comet I (BOAC)	10 Jan 54	Mediterranean Sea of Elba, Italy. Fuselage fatigue failure
D.H.Comet I (BOAC)	8 Apr 54	Mediterranean Sea of Naples, Italy. Fuselage fatigue failure
Douglas DC-7 (Delta)	18 Jan 57	New Orleans, La. USA. Mild explosive decompression. Fuselage cracks in area of forward crew entrance & cargo doors
Boeing B-52 (USAF)	19 Jan 61	Monticello, Utah USA. Aft fuselage just forward of vertical stabilizer
Boeing B-52 (USAF)	24 Jan 63	Little Shanty Mountain, Maine USA. Aft fuselage just forward of vertical stabilizer
Boeing B-52 (USAF)	30 Jan 63	Mora, New Mexico USA. Aft fuselage just forward of vertical stabilizer
Lockheed C-130 (Canadian Forces)	15 Apr 66	Borden, Sask Canada. Explosive decompression of fuselage
Douglas DC-6B (Northeast)	24 Feb 67	North Holmdel, N.J. USA Fuselage: skin and attachments, 60" × 125" hole torn after crew compartment door
Boeing 707-349C	24 Sep 70	Enroute Shannon/London Loss of pressurization, fatigue of portion of external main cargo door skin
Boeing 747-? (?)	17 Feb 76	? Loss of pressurization while in flight, 40 in. (1m) skin crack under fairing

to be continued ...

115

Lockheed L-188 (Zantop)	18 Jan 80	Syracuse, N.Y. USA. Forward cargo door seperated. Door latch loop (fastener holes)
Airbus A310 (Thy)	? Jan 88	Ercan, Cyprus. Loss of cabin pressure. Fatigue.
Boeing 737-200 (Aloha)	28 Apr 88	Hawaii, USA. Sudden loss of entire forward upper fuselage section. Fatigue cracks in skin and stringers.
Boeing 747-100 (United)	Feb 89	Honolulu, USA. Sudden loss of cabin compression. Loss of forward cargo door. Cause: fatigue?

Table 3.1 λ-values of some aircraft with half-crack-length a

varying from 20 mm to 250 mm

aircraft type	$R_{max.}$ (mm)	$t_{min.}$ (mm)	λ a = 20 mm	λ a = 100 mm	λ a = 250 mm
B 707	1879.6*	1.02	0.826	4.130	10.325
B 727	1879.6*	1.02	0.826	4.130	10.325
B 737	1879.6*	0.91	0.874	4.372	10.931
B 757	1879.6*	1.02	0.826	4.130	10.325
B 747	3261.2*	1.80	0.472	2.360	5.901
DC-8	1866.9*	1.27	0.743	3.714	9.284
DC-10	3009.9	1.80	0.491	2.457	6.142
A 300	2819.4	1.60	0.538	2.692	6.731
A 310	2819.4	1.60	0.538	2.692	6.731
Fokker 50	1375.0	0.80	1.090	5.452	13.631
Fokker 100	1650.0	1.00	0.890	4.452	11.129

* Double lobe cross-section,

$$\lambda = \sqrt[4]{12(1-\nu^2)} \; \frac{a}{\sqrt{Rt}}$$

116

Table 5.1 Static failure stress of specimen tested under combined extension and bending (CETS)

material	t [mm]	R [mm]	a_0 [mm] 10.0	20.0	30.0	40.0
			σ_e [MPa]			
aluminium alloy 2024-T3 bare	0.5	130	304.2	254.7	212.6	160.5
		375	309.3	260.3	216.8	167.4
		750	314.6	264.8	220.4	173.9
		1500	316.4	270.6	226.3	181.3
	1.0	130	273.6	220.2	169.9	124.2
		375	282.3	251.6	199.7	152.2
		750	301.4	263.2	210.1	168.6
		1500	315.5	269.4	224.3	179.1
aluminium alloy 7075-T6 bare	0.5	130	327.5	228.4	174.2	127.6
		375	351.4	245.6	185.1	139.3
		750	361.0	257.3	195.4	151.5
		1500	368.5	263.4	199.8	157.6
	1.0	130	317.1	209.7	150.5	107.6
		375	340.2	235.0	175.3	132.6
		750	355.2	247.5	187.7	145.1
		1500	375.6	255.2	197.5	158.7

Table 5.2 Comparison between various prediction methods and test results for Al 7075-T6 bare specimens, $a_0 = 30.0$ mm (combined extension and bending)

t (mm)	R (mm)	Failure stress σ_u (MPa) test	Eq.(4.18) Wynn Smith [11]	Eq.(4.13) Ang Williams [7]	Eq.(3.14) Folias [10]	Eq.(5.5) present study
0.5	130	174.2	196.75 +12.9%	143.95 -17.4%	189.24 + 8.6%	167.36 - 3.9%
0.5	375	185.1	199.03 + 7.5%	180.13 - 2.7%	198.15 + 7.0%	188.25 + 1.7%
0.5	750	195.4	199.26 + 2.0%	189.73 - 2.9%	199.04 + 1.9%	193.79 - 0.8%
0.5	1500	199.8	199.31 - 0.2%	194.53 - 2.6%	199.26 - 0.3%	196.56 - 1.6%
1.0	130	150.5	188.90 +25.5%	88.66 -41.1%	155.21 + 3.1%	135.49 - 9.9%
1.0	375	175.3	198.19 +13.1%	161.03 - 8.1%	194.65 +11.0%	177.26 + 1.1%
1.0	750	187.7	199.12 + 6.1%	180.23 - 7.5%	198.25 + 5.6%	188.34 + 0.3%
1.0	1500	197.5	199.35 + 0.9%	189.83 - 3.9%	199.13 + 0.8%	193.89 - 1.8%
average error			+ 8.5%	-10.8%	+ 4.7%	- 1.8%

117

Table 5.3 CA Fatigue tests conducted with the PFSTS

	number of tests	
	uniaxial	biaxial $\chi = 0.24$
p = 0.35 bar	2	2
p = 0.55 bar	1	2

R = 2000 mm, t = 1.2 mm, f = 0.25Hz,
material: 2024-T3 Alclad

Table 5.4 FEM results of Ansell vs. Eq.(5.12)

R (mm)	t (mm)	2a (mm)	p (bar)	$\beta_{b,Ansell}$	$\beta_{b,Eq(5.12)}$	β-ratio Eq(5.12)/Ansell
2000	1.0	125	1.0	1.21	1.11	0.92
2000	1.0	250	1.0	1.47	1.45	0.99
2000	1.0	375	1.0	1.45	1.36	0.94
2000	1.0	125	0.6	1.26	1.16	0.92
2000	1.0	250	0.6	1.55	1.63	1.05
2000	1.0	375	0.6	1.57	1.53	0.97
2000	1.6	250	1.0	1.51	1.50	0.97
1000	0.5	250	1.0	1.96	1.83	0.93
1000	0.8	250	1.0	1.91	2.02	1.06

Two-bay cracks, Frame spacing L = 500 mm, Longeron spacing S = 200 mm,
Biaxiality χ = 0.5

Table 5.5 Test results Swift & Wang vs. predictions

a (mm)	χ	crack type	β	β
81.2	1.26	one-bay	1.33	1.14
106.4	1.26	one-bay	1.34	1.16
123.2	1.26	one-bay	1.32	1.17
116.2	0.10	one-bay	1.40	1.46
125.6	0.10	one-bay	1.41	1.46
127.8	0.10	one-bay	1.60	1.46
54.4	0.10	two-bay	1.27	1.29
62.8	0.10	two-bay	1.30	1.36
73.5	0.10	two-bay	1.29	1.44

R = 3010 mm, t = 2 mm, p = 0.705 bar, L = 508 mm, material 7075-T73

Table 5.6 Test results Schwarmann vs. prediction

	a (mm)	da/dN (mm/kc)	$\beta_{b,test}$	$\beta_{b,pred.}$	β-ratio pred./test
Crack A	30	3.2	1.20	1.20	1.00
	35	5.0	1.24	1.24	1.00
	40	7.8	1.27	1.28	1.01
	45	12.8	1.33	1.32	0.99
	50	19.3	1.36	1.36	1.00
	55	28.2	1.39	1.40	1.01
	60	54.1	1.47	1.43	0.97
Crack B left tip	15	0.65	1.11	1.05	0.95
	20	1.23	1.15	1.09	0.95
	25	1.90	1.16	1.14	0.98
	30	2.72	1.16	1.19	1.03
Crack B right tip	15	0.47	1.01	1.05	1.04
	20	1.00	1.09	1.09	1.00
	25	2.66	1.20	1.14	0.95
	30	6.50	1.41	1.19	0.84
Crack C left tip	30	1.70	1.03		
	40	2.78	1.01		
	50	4.41	1.00		
	60	9.38	1.08		
Crack C right tip	30	1.10	0.92		
	40	2.27	0.96		
	50	3.75	0.97		
	60	5.98	0.98		

Material: 2024-T3 Alclad, t = 0.8 mm, R = 1435 mm, p = 0.47 Bar, χ = 0.5
Frame spacing L = 508 mm, Longeron spacing S = 160 mm

Table 5.7 Results Barrois vs. predictions

p (bar)	L (mm)	a (mm)	da/dN (mm/kc)	β_b	$\beta_{b,K}$	$\beta_{b,pred}$
one-bay crack, front fuselage section						
0.4	260	76.3	3.0	1.56	1.61	1.51
0.4	260	76.47	1.0	1.18	1.61	1.51
0.45	260	76.95	10.6	1.83		1.48
0.45	260	77.68	7.9	1.71		1.47
0.5	260	78.82	10.0	1.61		1.44
0.57	260	80.57	19.9	1.60		1.40
0.57	260	82.28	15.0	1.50		1.39
two-bay crack, rear fuselage section, left crack tip						
0.4	430	37.75			1.66	1.60
0.45	430	37.85	2.35	1.86		1.57
0.45	430	38.1	4.28	2.13		1.58
0.5	430	38.5	3.43	1.82		1.55
0.57	430	38.9	5.55	1.77		1.53
0.57	430	39.2	4.09	1.65		1.53
two-bay crack, rear fuselage section, right crack tip						
0.4	380	37.75			1.66	1.62
0.45	380	37.85	2.35	1.86		1.59
0.45	380	38.05	2.85	1.94		1.60
0.5	380	38.35	1.71	1.54		1.57
0.57	380	38.72	1.66	1.33		1.54
0.57	380	39.17	3.63	1.60		1.55
one-bay crack, rear fuselage section						
0.35	380	76.45	4.4	1.95		1.86
0.35	380	77.95	3.1	1.78		1.87
0.4	380	78.53	14.5	2.17	1.80	1.82
0.4	380	79.57	13.0	2.11	1.80	1.82
0.45	380	81.0	26.0	2.11		1.79
0.45	380	82.68	16.4	1.92		1.79

R = 850 mm, t =0.8 mm, material Alclad A-U4G1-T3,
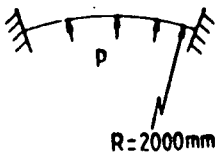
Table 6.1 Survey of some properties of ARALL and GLARE (recent results)

		Al alloys		ARALL(aramid)		GLARE (R-Glass)			
		2024 -T3 bare	7075 -T6 bare	1 7H33 UD	2 2H33 UD	1 7R33 UD	2 2R33 UD	3 2R33 50/50	4 2R33 70/30
Tensile ultimate strength, MPa	L	440	538	800	717	1239	1167	280	992
	LT	435	538	386	317	360	320	728	618
Tensile yield strength, MPa	L	324	483	641	359	550	400	320	360
	LT	290	469	331	228	340	230	320	260
Young's Modulus, GPa	L	72.4	71.1	67.6	68.1	64.7	64.7	57.5	56.4
	LT	72.4	71.1	48.3	49.0	49.2	50.2	57.5	50.3
Ultimate strain, %	L	13.6	8	1.9	2.5	4.6	5.1	5.1	5.1
	LT	13.6	8	7.7	12.7	7.7	13.6	5.1	5.1
Density, g/cm^3		2.78	2.78	2.33	2.33	2.52	2.52	2.52	2.45
Blunt notch, MPa (circular hole)	L	420	550	495	405	800	770	400	600
	LT	420	550	386	311	360	290	400	340
Sharp notch, MPa (saw cut)	L	320	350	377	362	720	660	360	540
	LT	320	350	250	250	230	230	360	305
Impact (crack initiation)		———		Comparable					
Fatigue C.A.		———		Better		Superior			
F.S.		———		Superior					
Corrosion fatigue		———		Superior					
Stress corrosion		———		Superior					
Pitting corrosion Cracking		———		Superior					
Bearing ultimate strength, MPa		890	1076	738	565	770	704	690	700
Workshop properties machining		———		Comparable (extra care)					
Sheet bending		———		Comparable		Lower (possible)			

Code ARALL and Glare:

L	=	Longitudinal direction
LT	=	Long.-Transverse direction
UD	=	Unidirectional fibers
50/50	=	50% of fibers in L direction
70/30	=	70% of fibers in L direction
2	=	2024-T3 Al alloy sheets
7	=	7075-T6 Al alloy sheets
H	=	high modulus aramid fibers
R	=	R-Glass fiber
33	=	3 Al alloy sheets of 0.3 mm in thickness each

Table 6.2 Summary of tests on ARALL specimens

Test set-up	Type ARALL (*)	Test condition	Results in Figure
SUPERBAT (Fig.6.5) flat specimen	2H32 (t=0.82 mm)	Uniaxial Biaxial(χ=0.28) σ=60±60 MPa	6.6
CETS	2H32 (t=0.82 mm) 7H32 (t=0.82 mm)	Tension+Bending σ=75±75 MPa R=1500 mm 750 mm 375 mm	6.10 6.11
PFSTS R=2000mm	2H32 (t-0.82 mm) 2H33 (t=1.34 mm) 2R33 (t=0.91 mm)	R=2000 mm p_{max}=0.56 bar (**)	6.14 6.15 6.16

(*) Codes: see note Table 6.1
(**) Flat specimens, uniaxially loaded, were tested in [6].

122

Table 6.3 Comparison between design stress and available strength for two types of ARALL calculated for an aircraft fuselage

ARALL	Structure and crack length	Type of crack (*)	Loca-tion	Local gross stress	β_b	Required strength (Eq.6.1)	Available strength (Eq.6.2)	Reserve factor (Eq.6.3)
2H33 aramid fibers t=1.34	upper fuselage 2a=100 mm	|—|		85	1.19	116.3	248	2.13
		| ⊣			1.24	121.2		2.05
	lower fuselage 2a=300 mm	|—|	1	77.3	1.30	110.5	124	1.12
			2	48.2	1.77	93.8		1.32
		| ⊣	1	77.3	1.57	133.5		0.93
			2	48.2	2.30	121.9		1.02
2R33 50/50 R-glass fibers t=0.91	upper fuselage 2a=100 mm	|—|		85	1.18	115.3	320	2.78
		| ⊣			1.22	119.3		2.68
	lower fuselage 2a=300 mm	|—|	1	77.3	1.32	112.2	160	1.43
			2	48.2	1.78	94.4		1.69
		| ⊣	1	77.3	1.52	129.2		1.24
			2	48.2	2.22	117.9		1.36

t in mm, Strength in MPa

(*) |—| crack between frames

   | ⊣ crack with one tip at frame

β_b - bulge factor

Location 1: σ_{hoop} = 77.3 MPa, $\sigma_{longitudinal}$ = 24.5 MPa, t = 1.2 mm

Location 2: σ_{hoop} = 48.2 MPa, $\sigma_{longitudinal}$ = 0 MPa, t = 1.8 mm

aft fuselage
construction

forward fuselage
construction

emergency exit

window construction

air conditioning and
toilet service doors
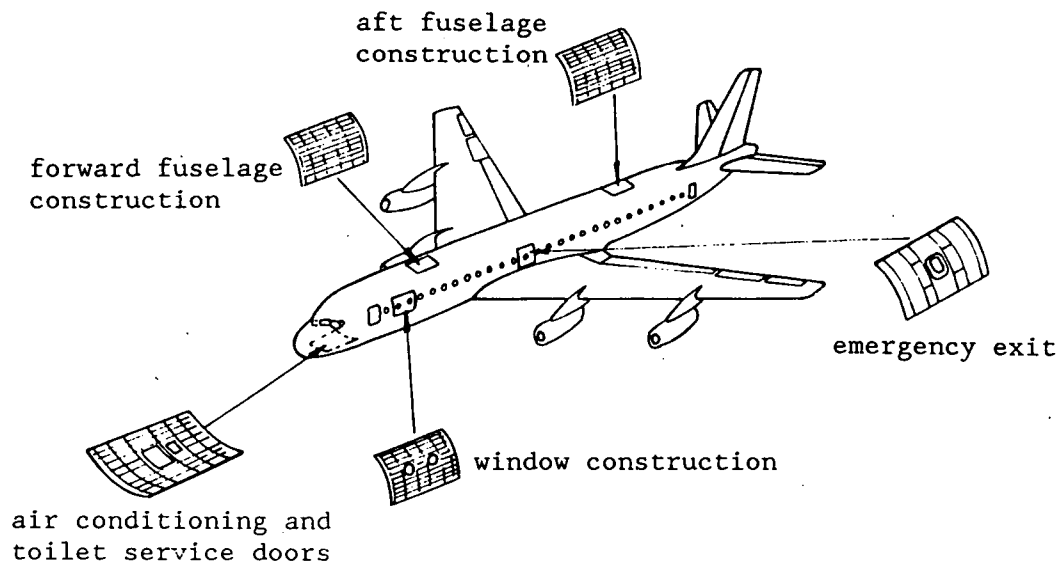
Fig.1.1 Fuselage fatigue test panels representing various areas of
the aircraft (After Swift, Douglas Paper 7768).

curved panel, four-way splice
basic structure, longeron to
frame connection fatigue tests

transverse splice
fatigue tests

longitudinal splice
fatigue tests

flat residual
strength test
panels

longeron-to-frame
connection fatigue
tests

pressure
bulkhead
tests

flat residual
strength test
panels

window belt
panel fatigue
tests
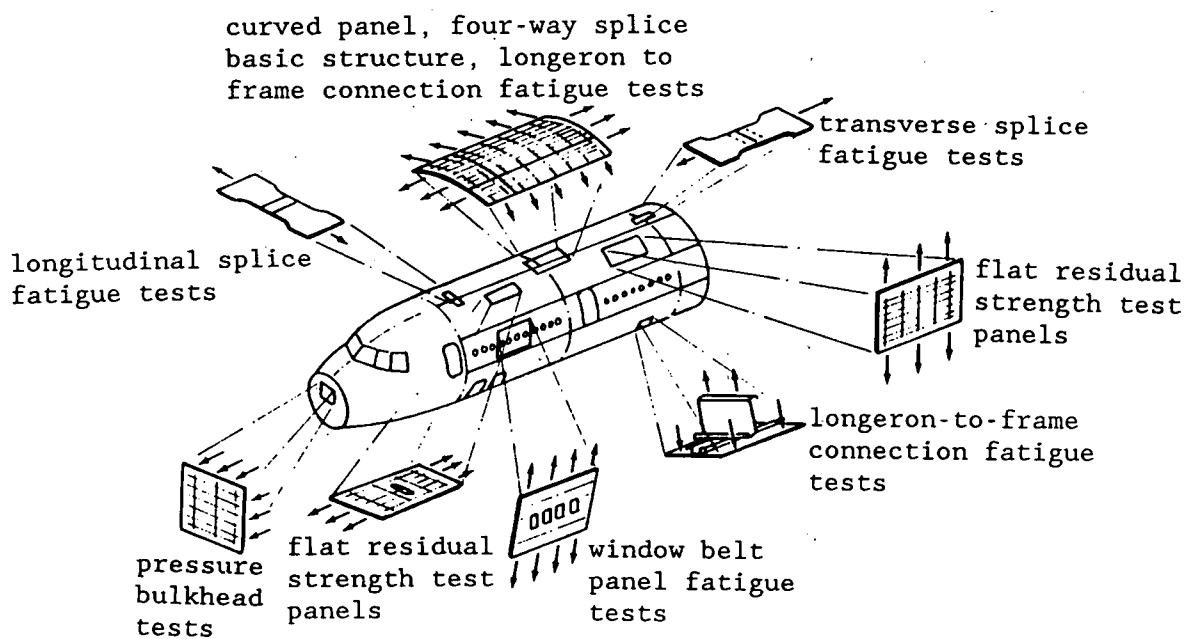
Fig.1.2 Fuselage fatigue development tests
(After Swift, Douglas Paper 7768).

125

one-bay longitudinal crack

two-bay circumferential crack
with broken longeron

DC-8
earlier aircraft
design goal

one-bay circumferential crack

two-bay longitudinal crack

DC-9

DC-10 damage tolerance design goals

DC-10
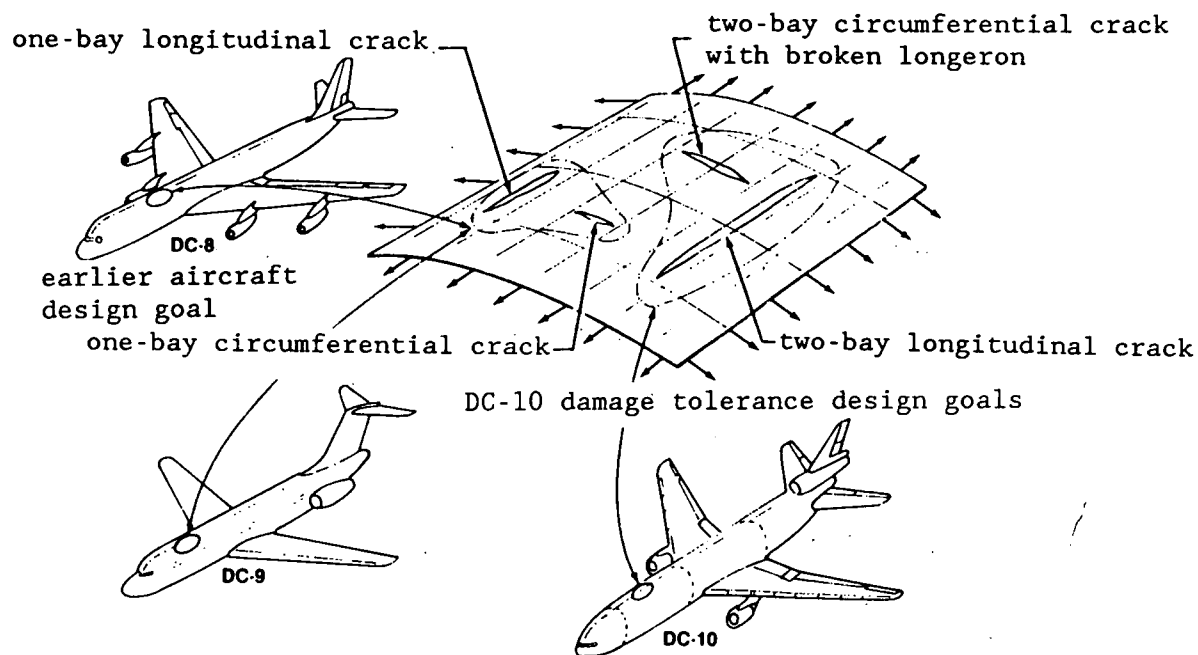
Fig.1.3 Damage tolerance design goals for fuselage skin
structures *(After Swift, Douglas Paper 7768)*

σ_{bulge}

bulge affects element
equilibrium and increases
as crack length increases

σ_{hoop} (zero due to crack)

hoop tension

bulge
radius

cabin pressure

crack length

shell radius
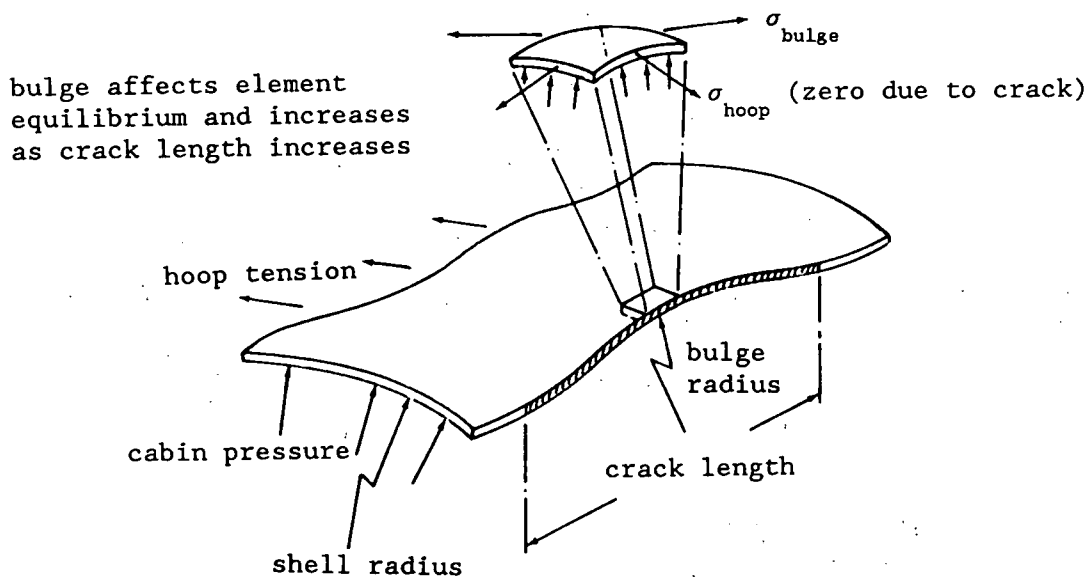
Fig.1.4 Bulging in a cracked cylindrical shell
(After Swift, Douglas Paper 7768)

126
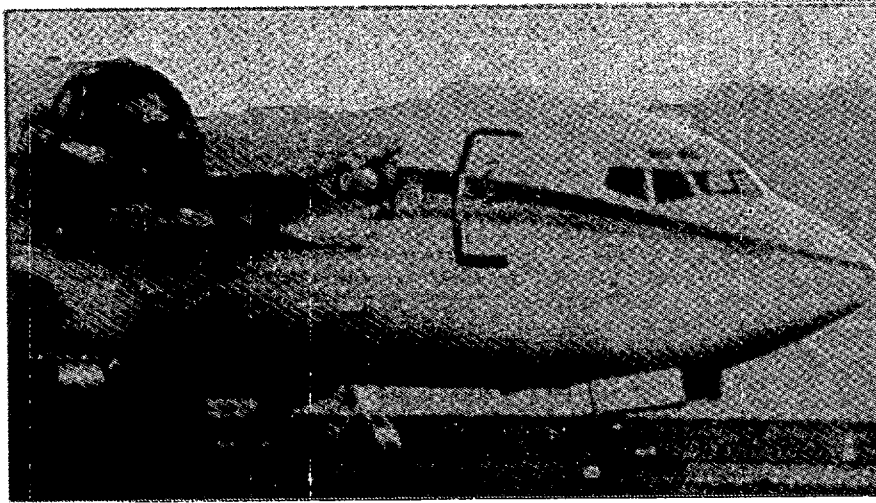
a Loss of the entire upper fuselage section (Aviation Week & Space Technology, May 9, 1988)
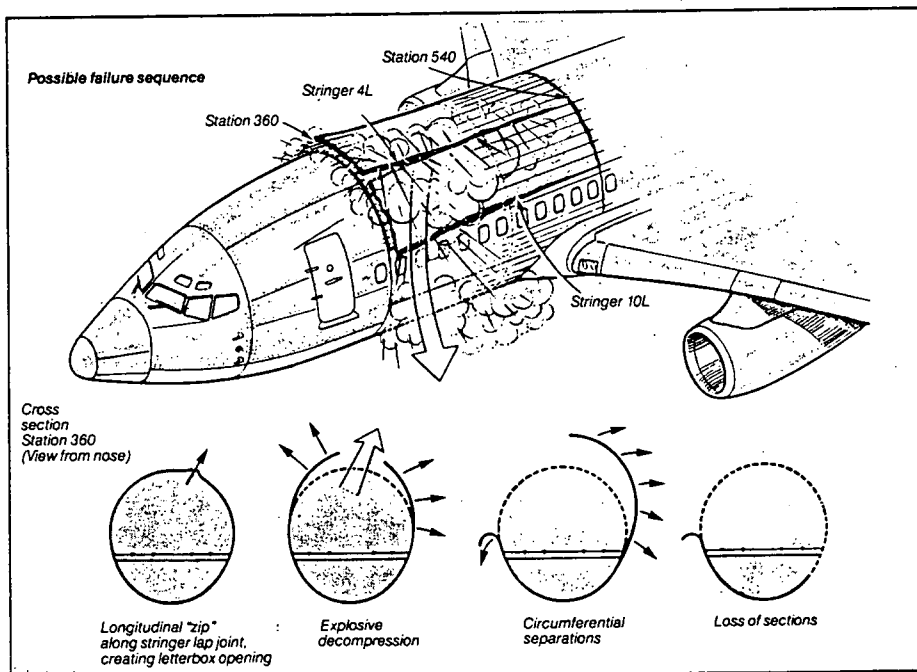
b Possible failure sequence as suggested by Flight International (3 Sep.1988)
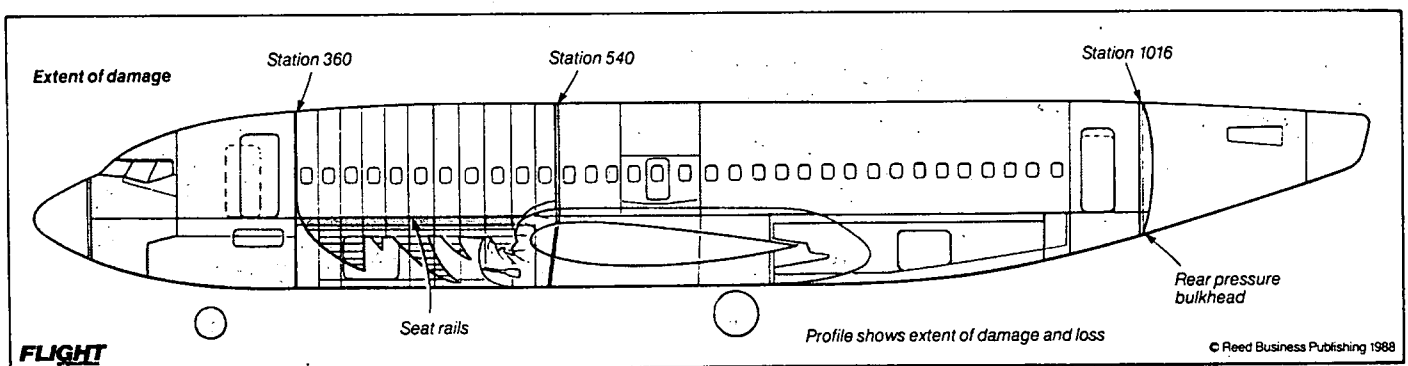
c Failure locatio. Extra lap-joint inspections required between stations 360 and 1016 (Flight International, 3 Sep.1988)

Fig. 2.1 Fuselage decompression of a high-life-time Aloha Airliner Boeing 737-200 on April 28, 1988.

127
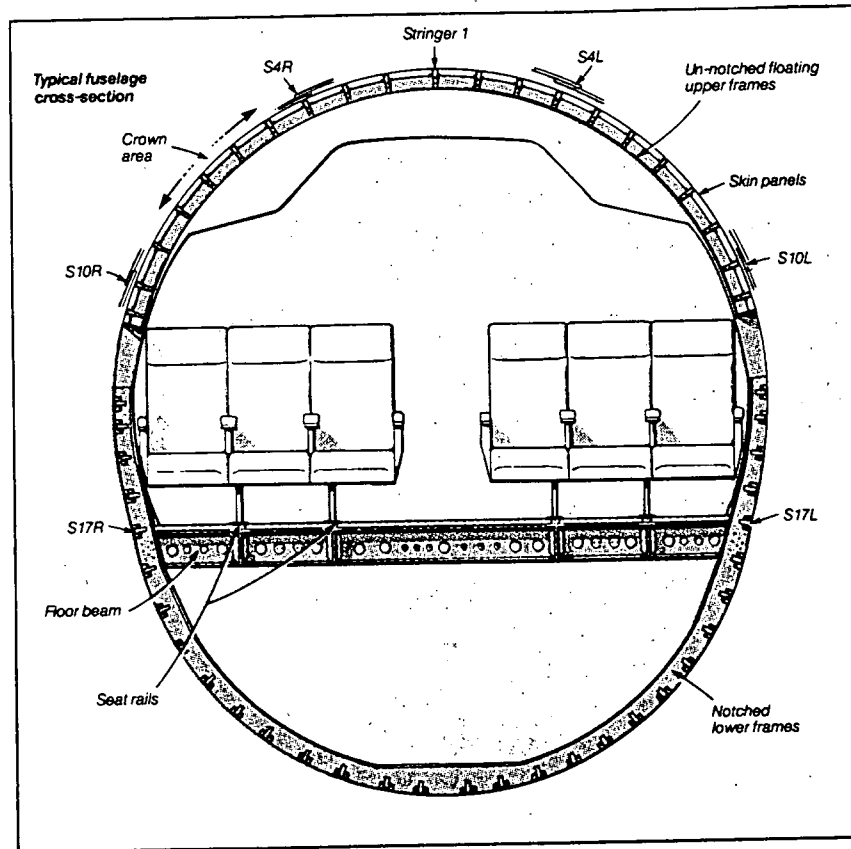
Fig. 2.2 Cross-section of the Boeing 737-200 fuselage. Locations of the critical stringers in the Aloha accident (Flight International, 3 Sep.1988).

Fig. 2.3 Comet I Yoke Peter, the first jet transport aircraft to enter scheduled airline service.

128
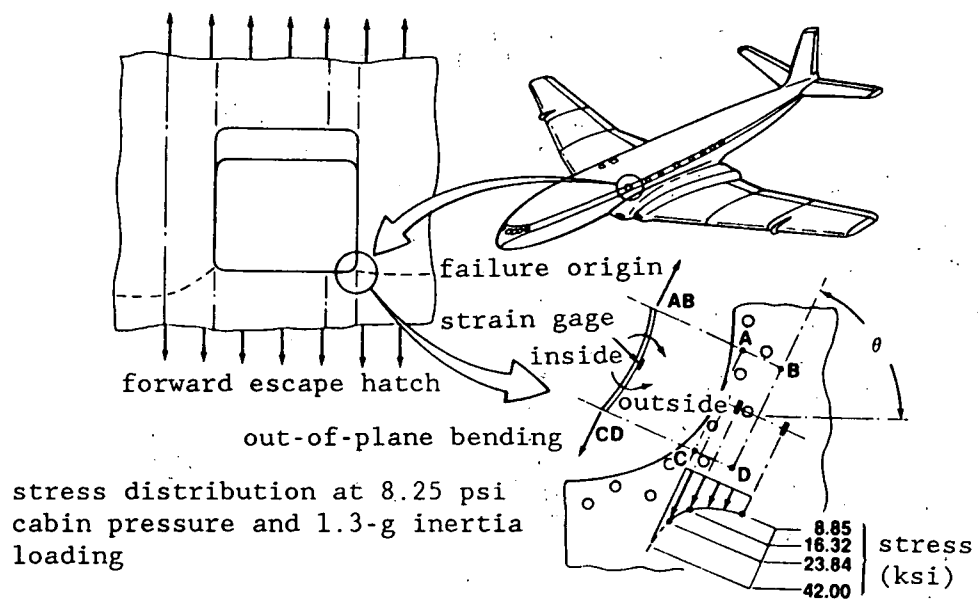
Fig.2.4 Probable failure origin — Comet I Yoke Uncle test
aircraft (After Swift, Douglas Paper 7768)
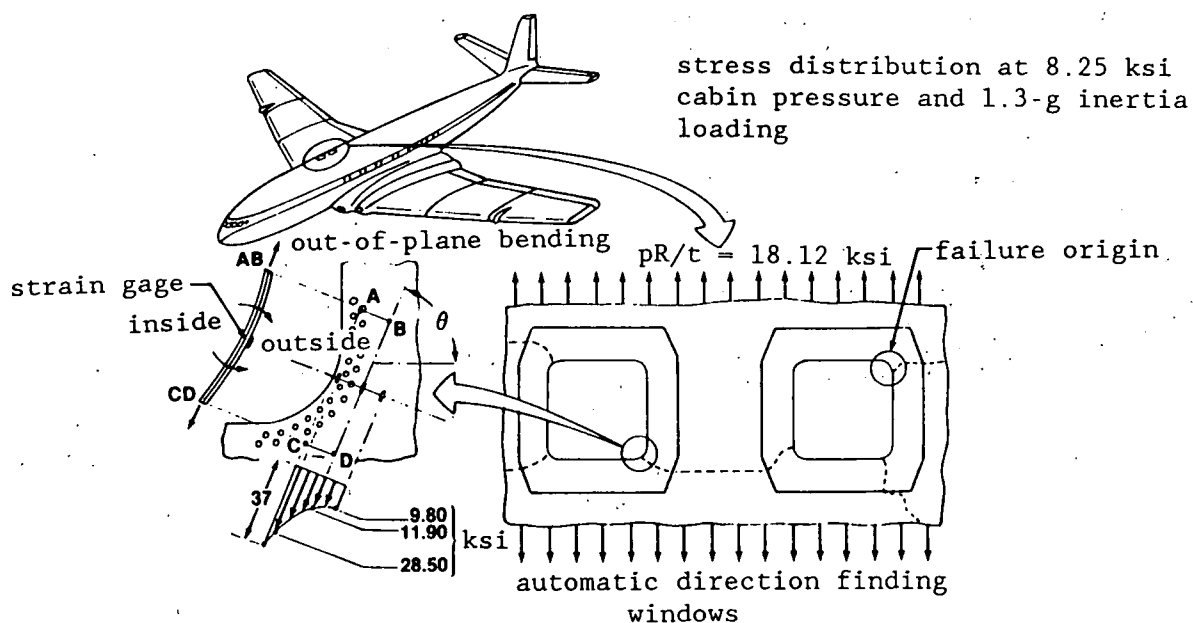
Fig.2.5 Probable failure origin — Comet I Yoke Peter
(After Swift, Douglas Paper 7768)
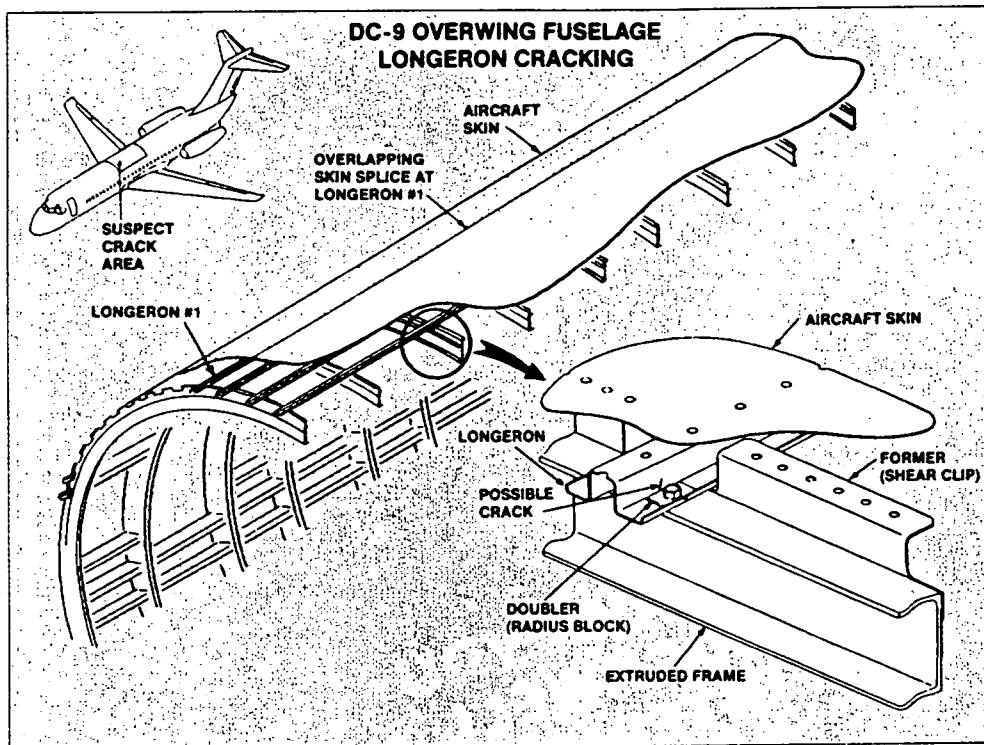
Fig.2.6 Upper fuselage fatigue cracking in DC-9
(Aviation Week & Space Technology, Nov.28,1988)
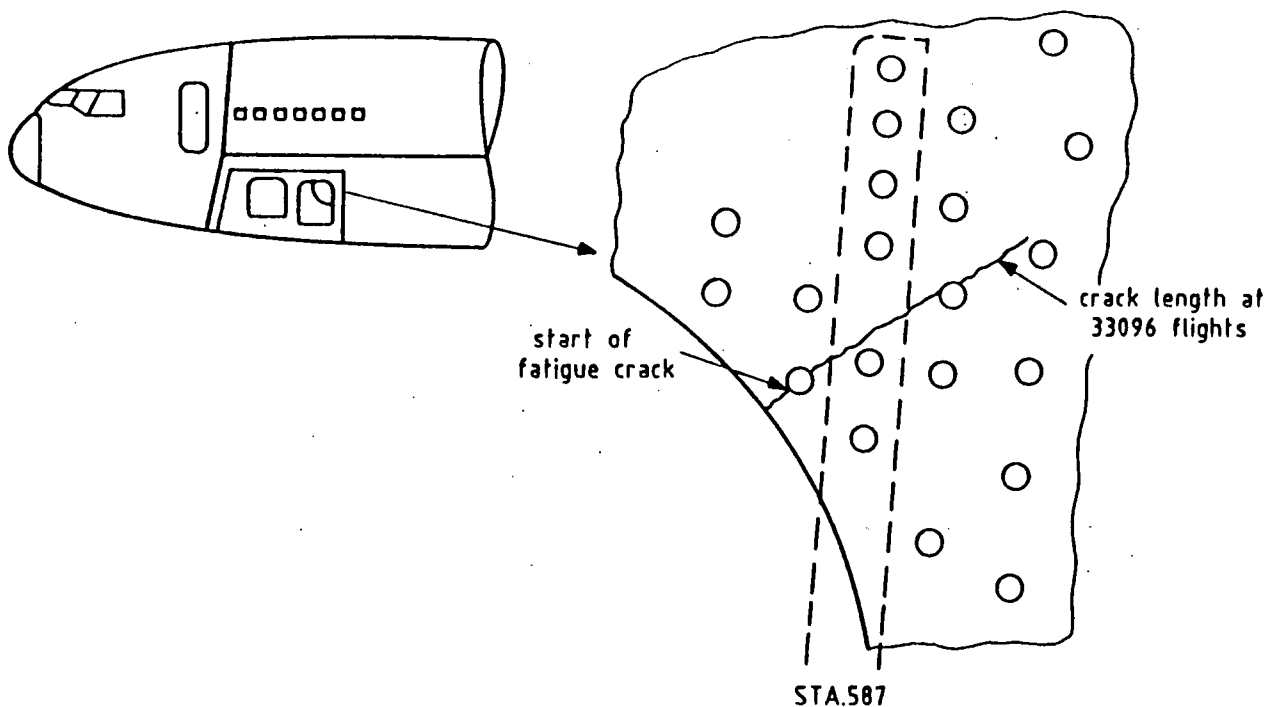
Fig.2.7 Early DC-10 fuselage skin cracking[11]

130
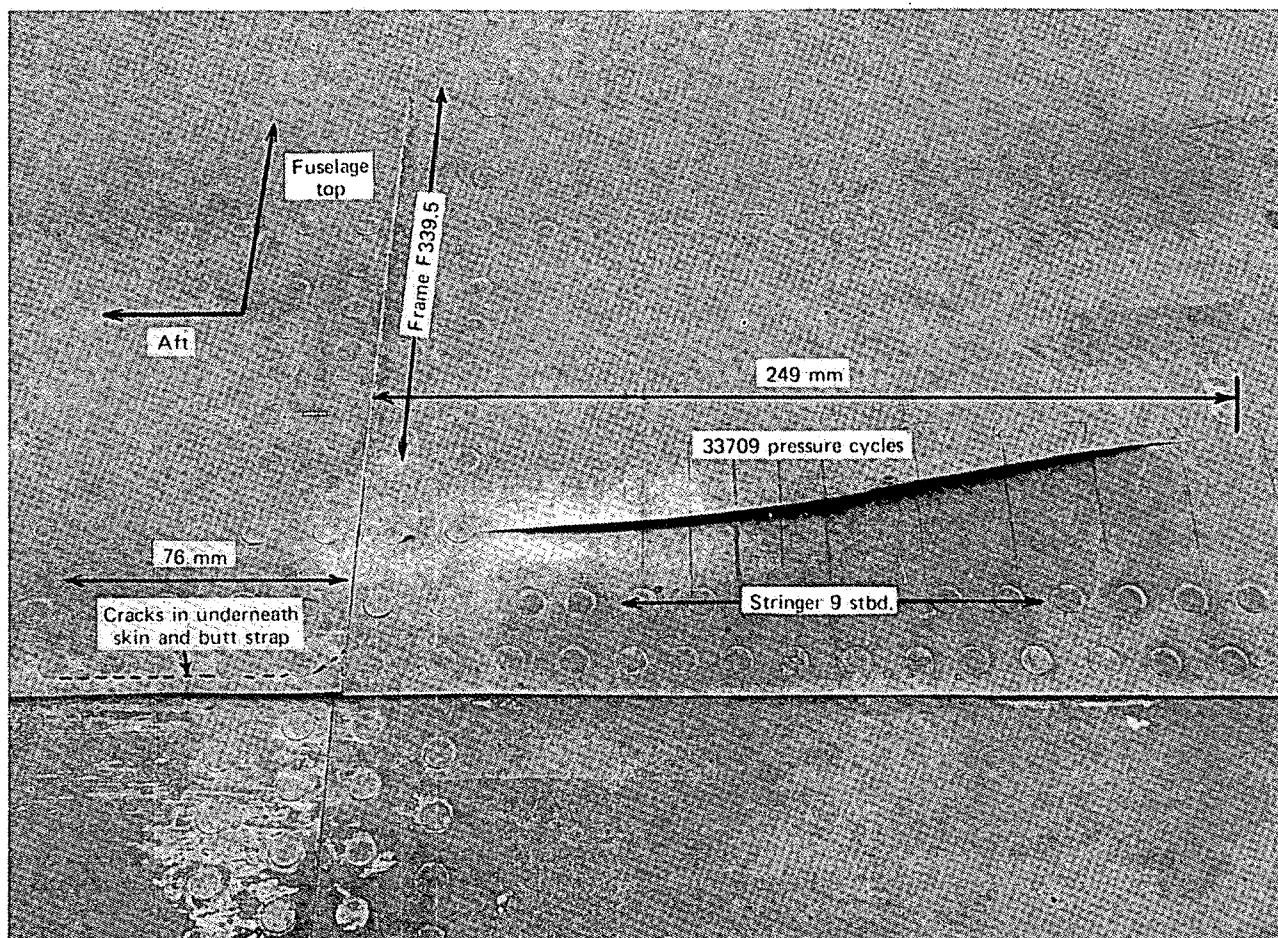
Fig.2.8 Fuselage fatigue cracks in the Britannia Type 100[12]
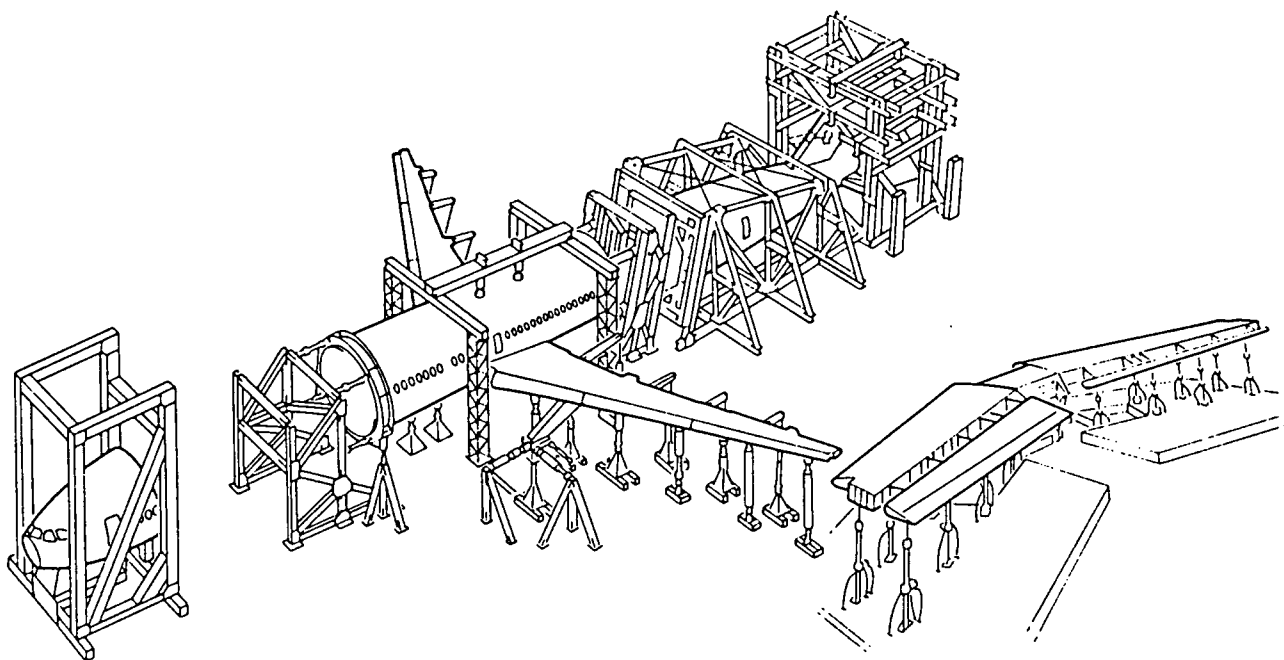
Fig.2.9 Airbus A310 full scale test arrangement[13]
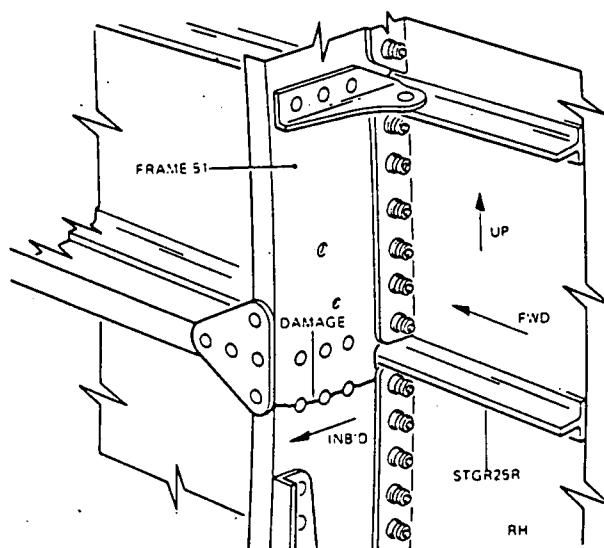
Fig.2.10 A310 fatigue damage at frame 51/stringer 25[13]
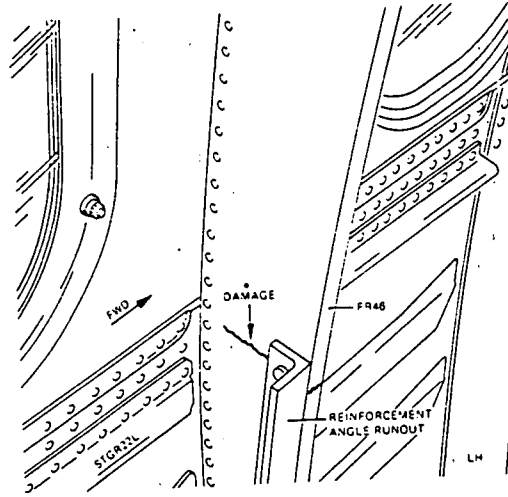
Fig.2.11 A310 fatigue damage at frame 46/stringer 22[13]
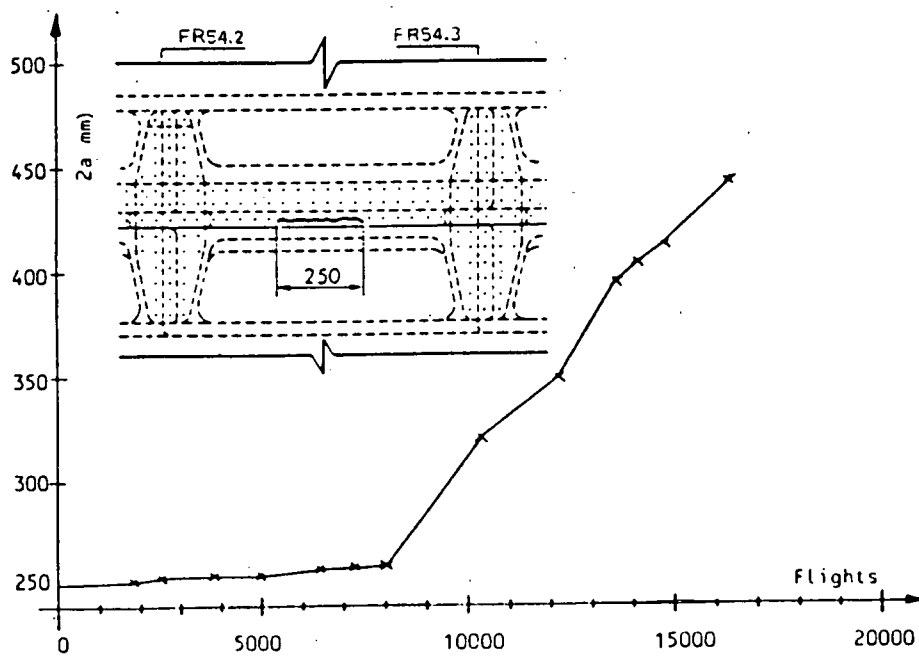
Fig.2.12 A310 mid bay damage at longitudinal fuselage lap joint[13]

•SAFE LIFE CONCEPT

slow crack growth structure

DAMAGE
•TOLERANCE
CONCEPT

fail-safe structure

multiple load path structure

dependent
(a common source of cracking exists in adjacent load path at on location)

independent
(no common source of cracking exists in more than a single load path at one location)

crack arrest structure

crack

load paths

crack

crack

load paths
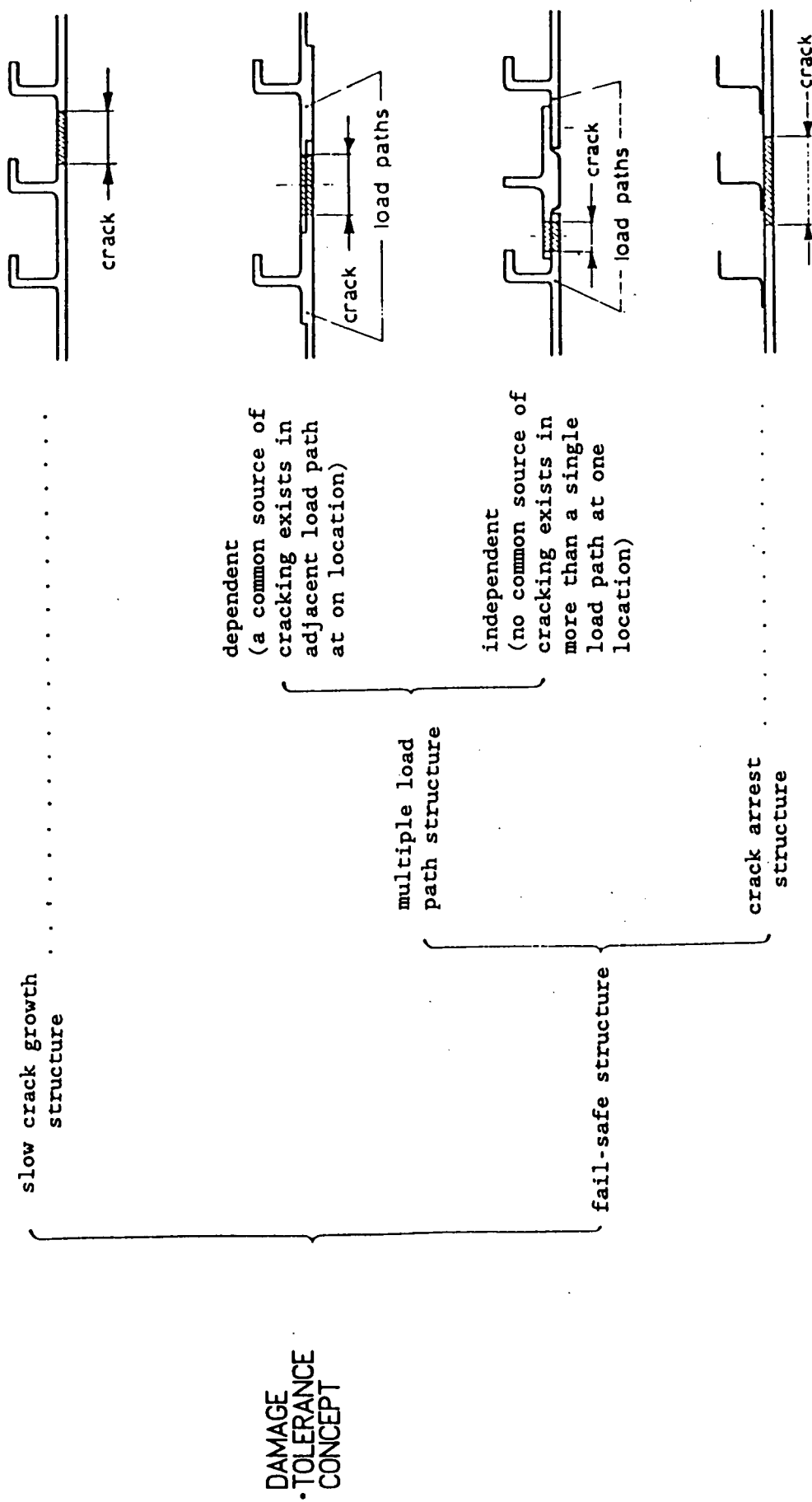
crack

Fig.2.13 Damage tolerance design features[23]
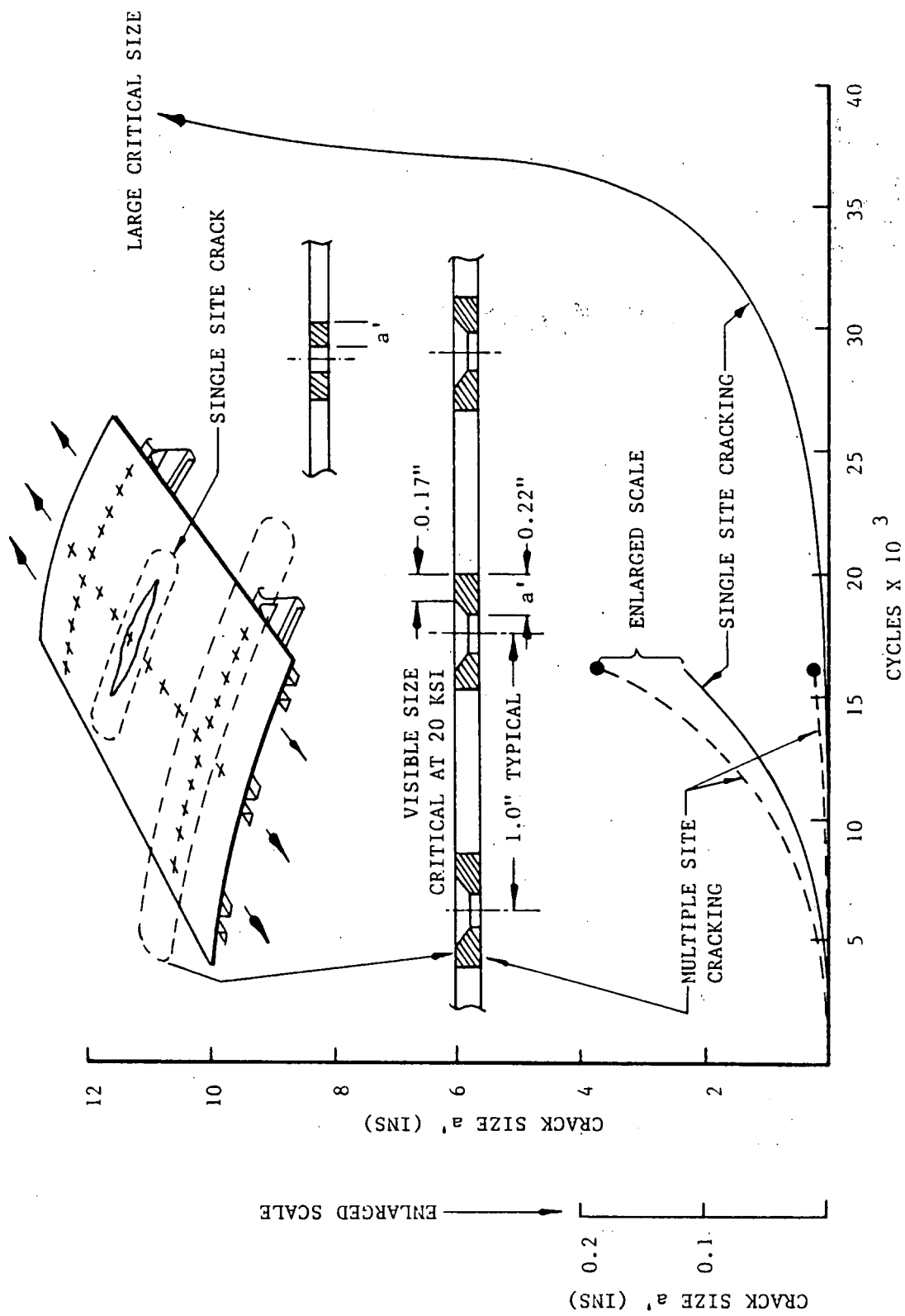
Fig.2.14 Comparison of multiple vs. single site cracking
in 2024-T3 material[24]

135
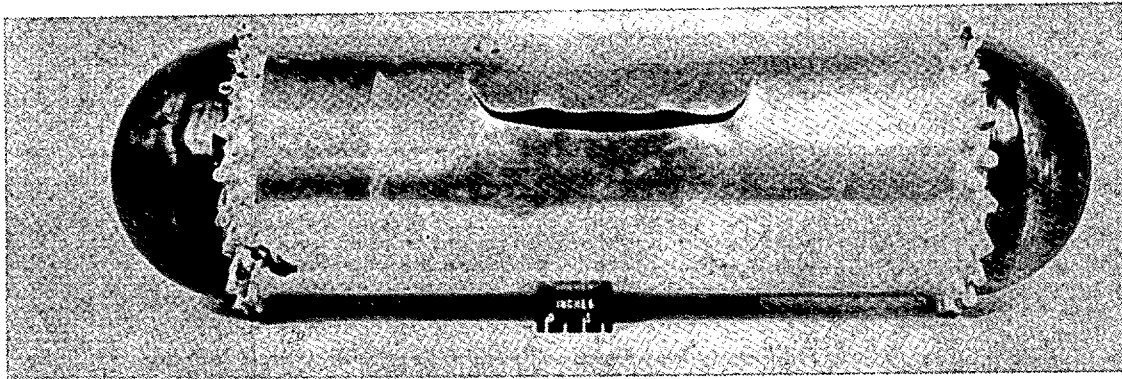
Fig.3.1 Peters & Kuhn's bursting test set-up[1]

cracked pressurized cylinder

section ABC showing rotation of crack edge
and resulting moment ahead of the crack
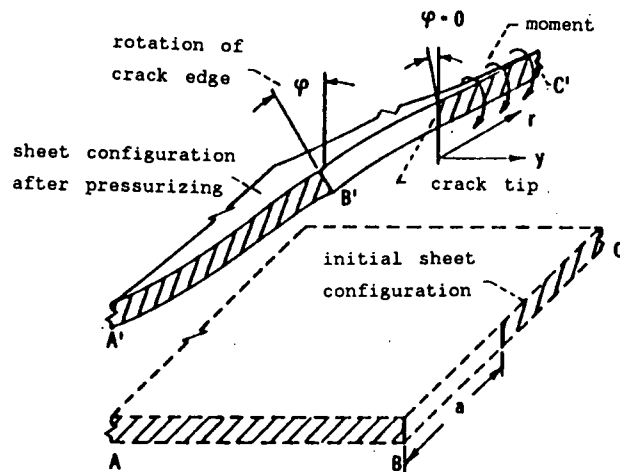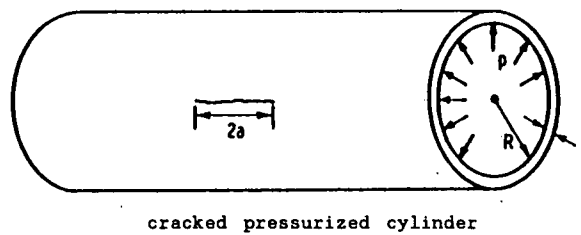
Fig.3.2 Bulge-out effect according to Anderson & Sullivan[2]
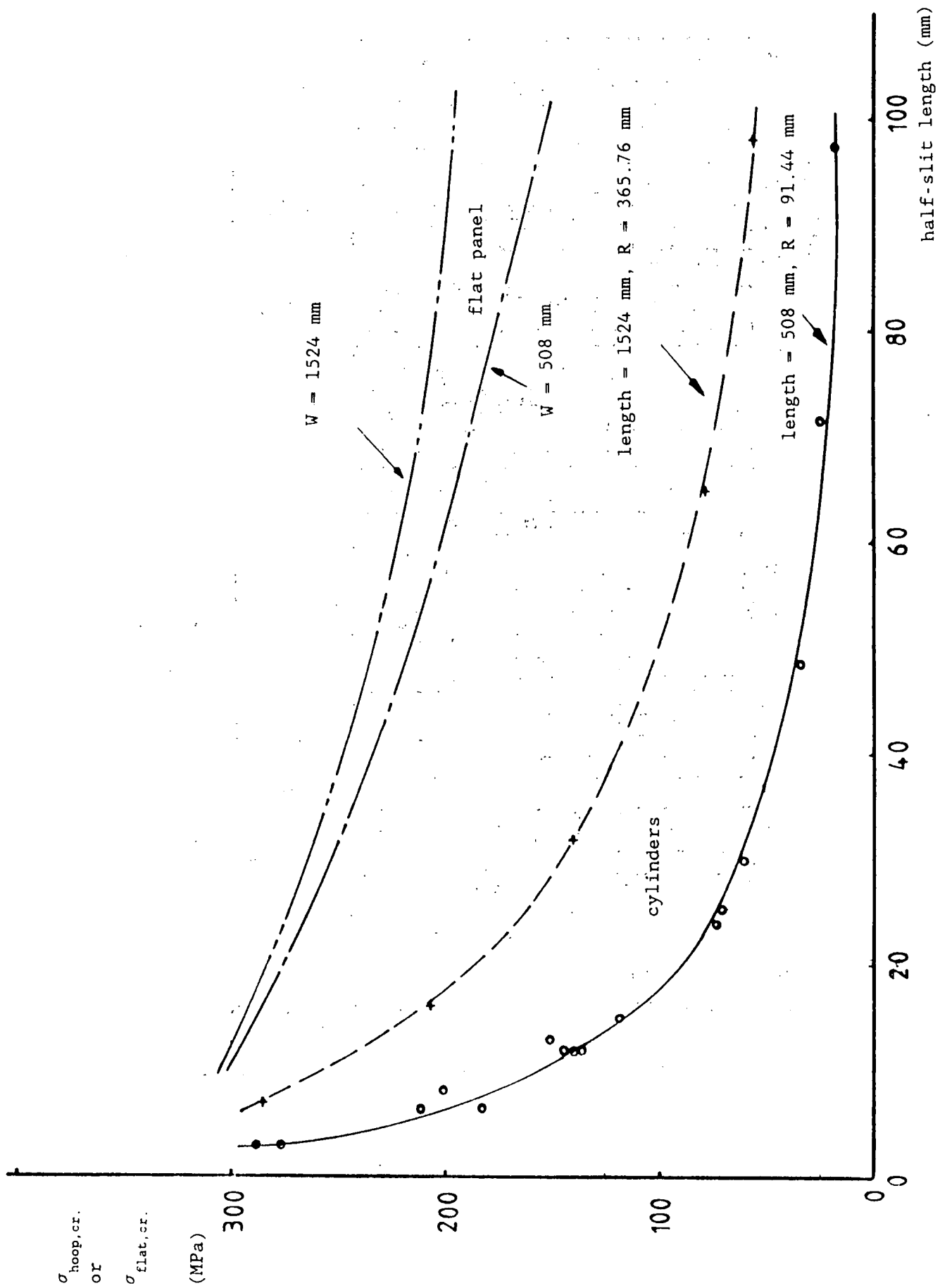
Fig.3.3 Bursting test results of Peters & Kuhn[1](material 2024-T3)
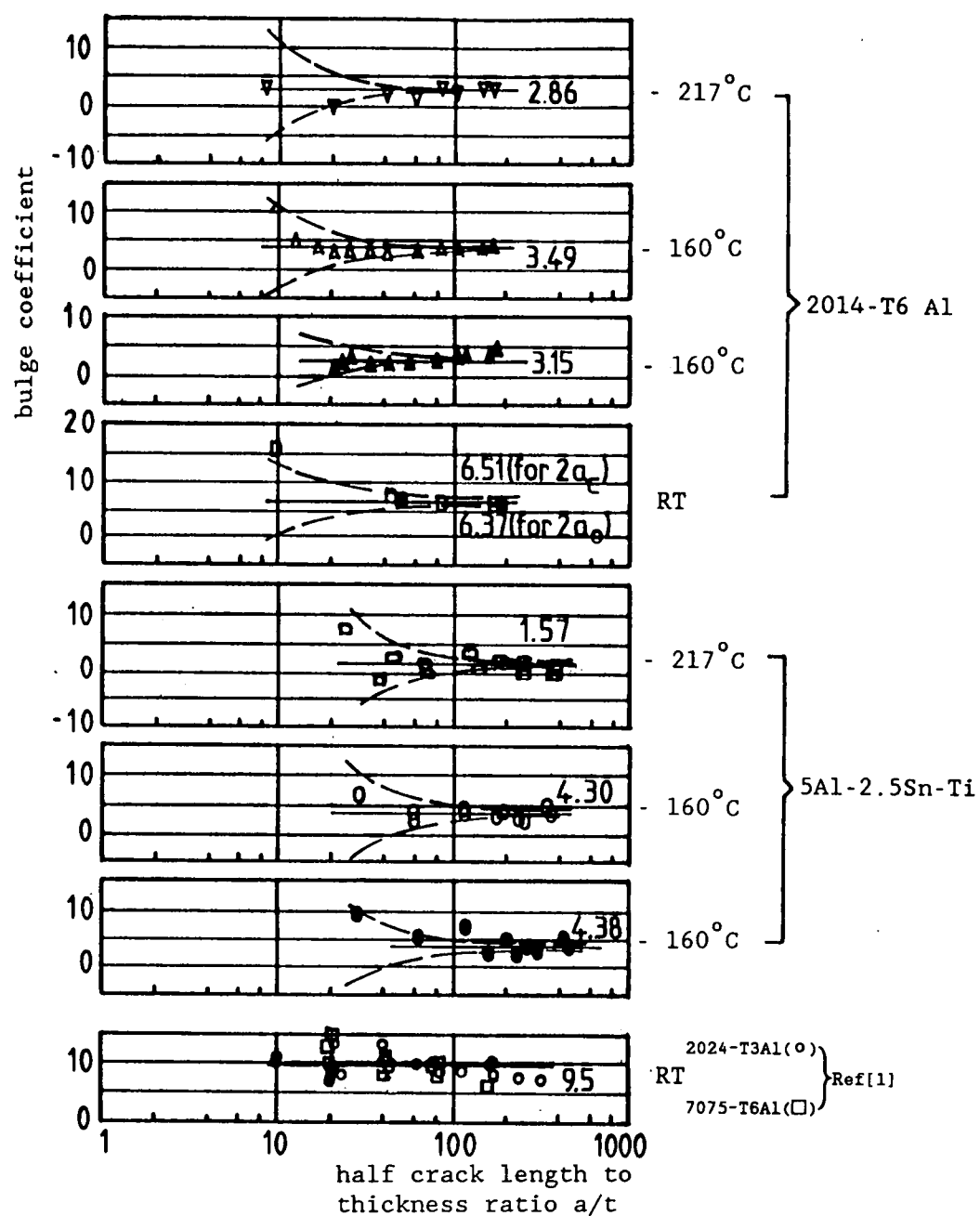
open   symbols denote $a = a_0$ ——— weighted average

solid symbols denote $a = a_c$ ·········· estimated scatter band

Fig.3.4 Bulge coefficients found by Anderson & Sullivan[2]
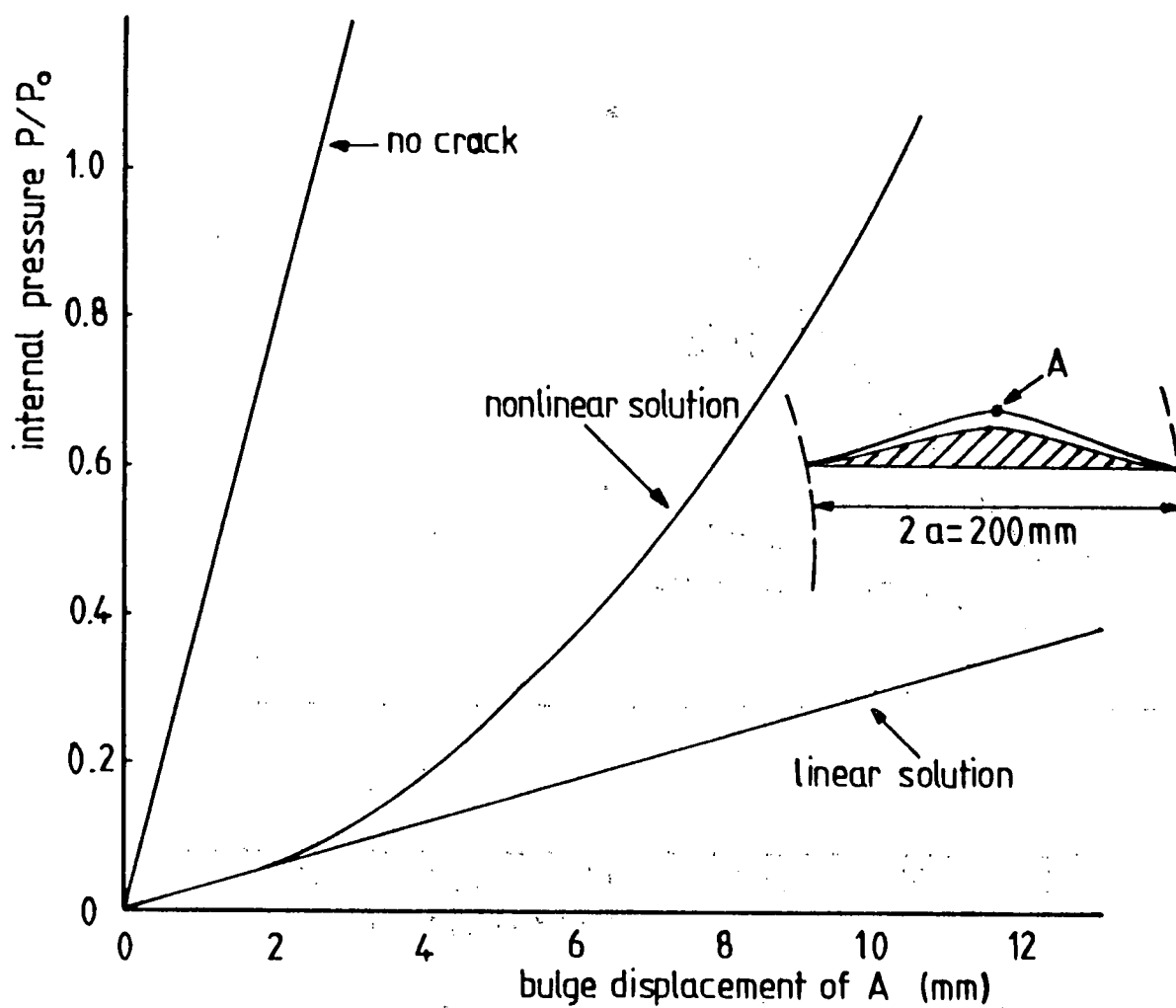
Po is the internal carbinpressure of a hypothetical transport aircraft

Fig.3.5 Bulge displacement at the center of a crack as a function
of internal pressure (After Riks[15])
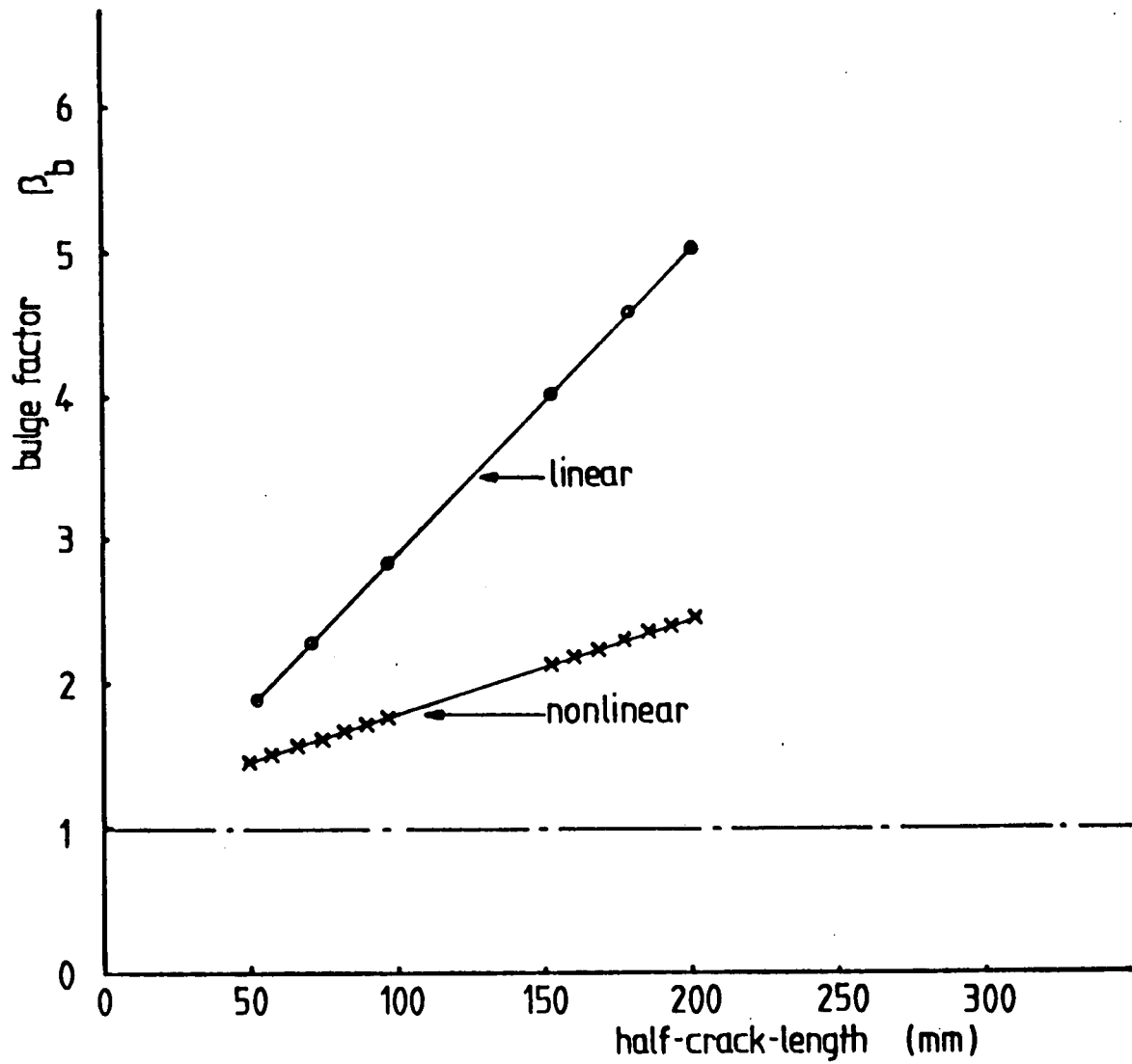
Fig.3.6 Bulge factor as function of half-crack length of unstiffened cylinder - linear vs. non-linear theory *(After Risk[15])*
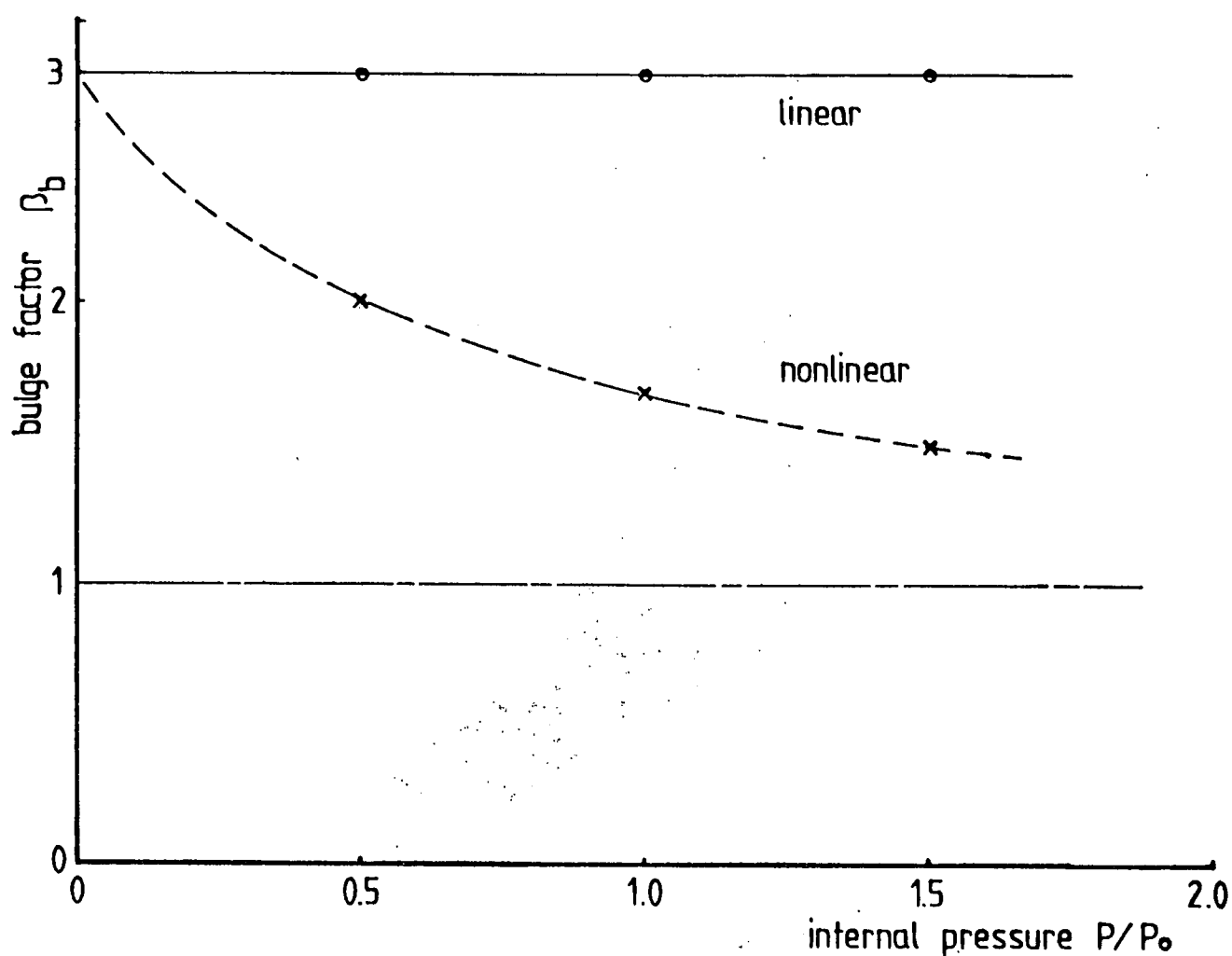
P₀ is the internal carbinpressure of a hypothetical transport aircraft

Fig.3.7 Bulge factor as function of internal pressure p
of unstiffened cylinder - linear vs. non-linear
theory (After Riks[15]).
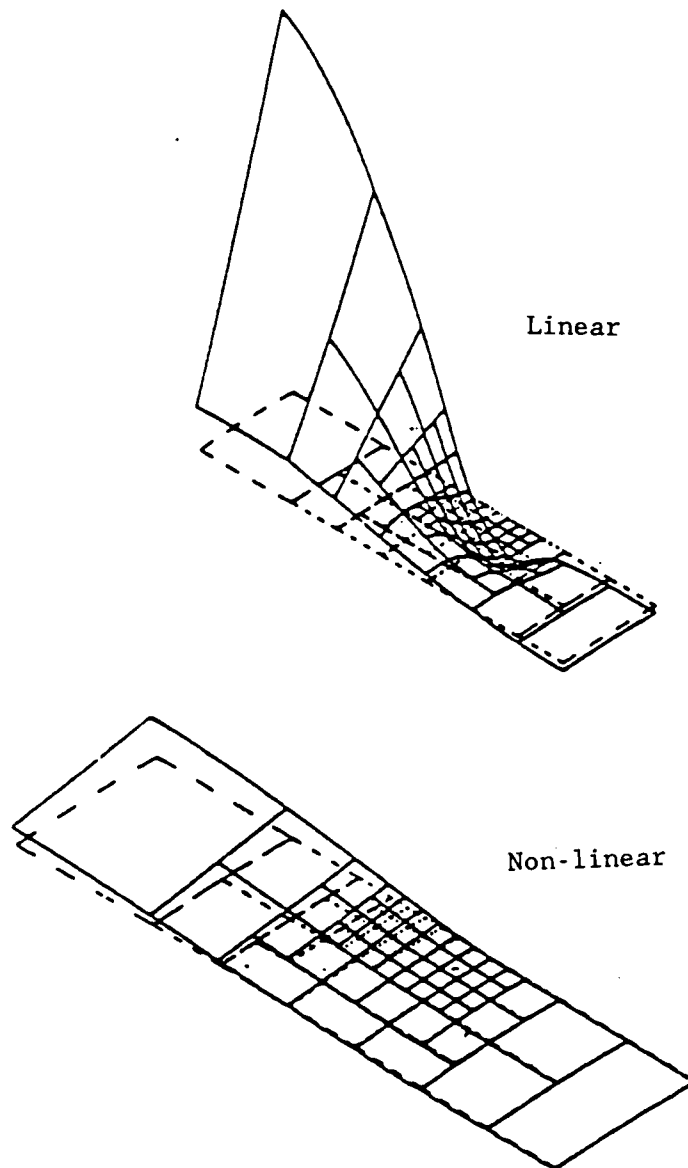
Linear

Non-linear

internal pressure p = 0.5 bar

Fig.3.8 Displacement field around the crack - linear vs. non-linear theory *(After Ansell[16])*

142

$$\lambda = \sqrt{12(1-\nu)^2} \ \frac{a}{\sqrt{Rt}}$$
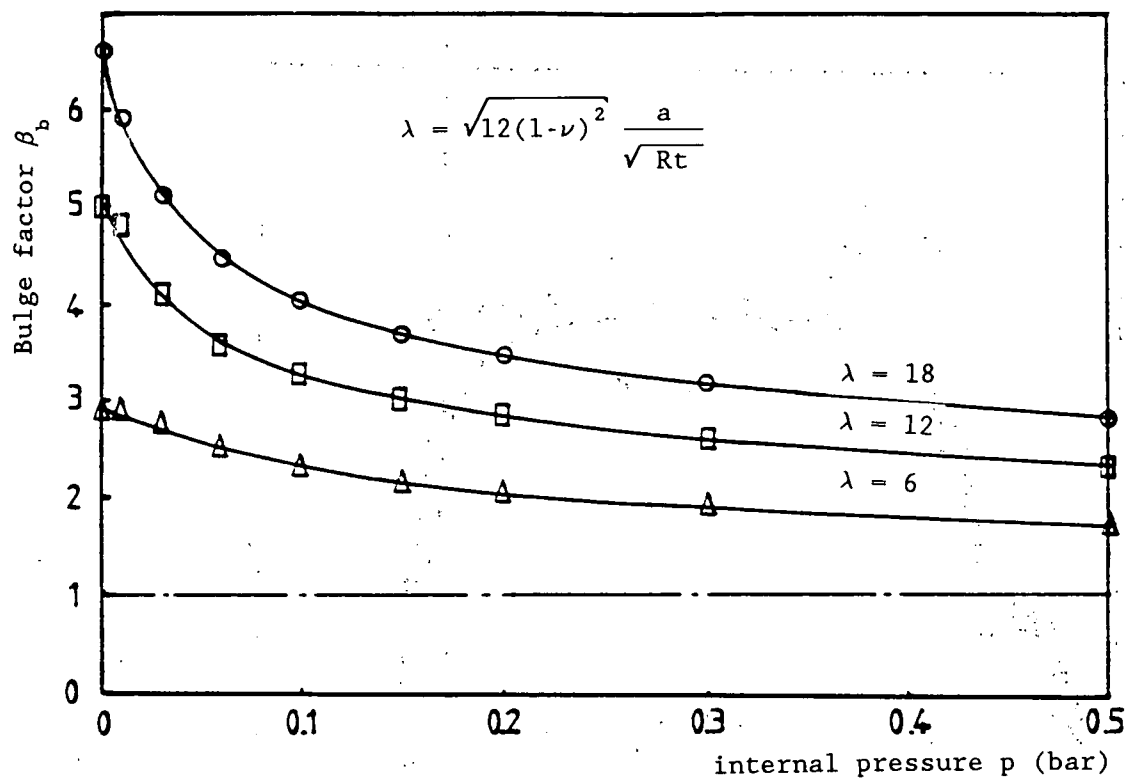
Fig.3.9 Bulge factor as function of internal pressure
(non-linear FEM results) *(After Ansell[16])*
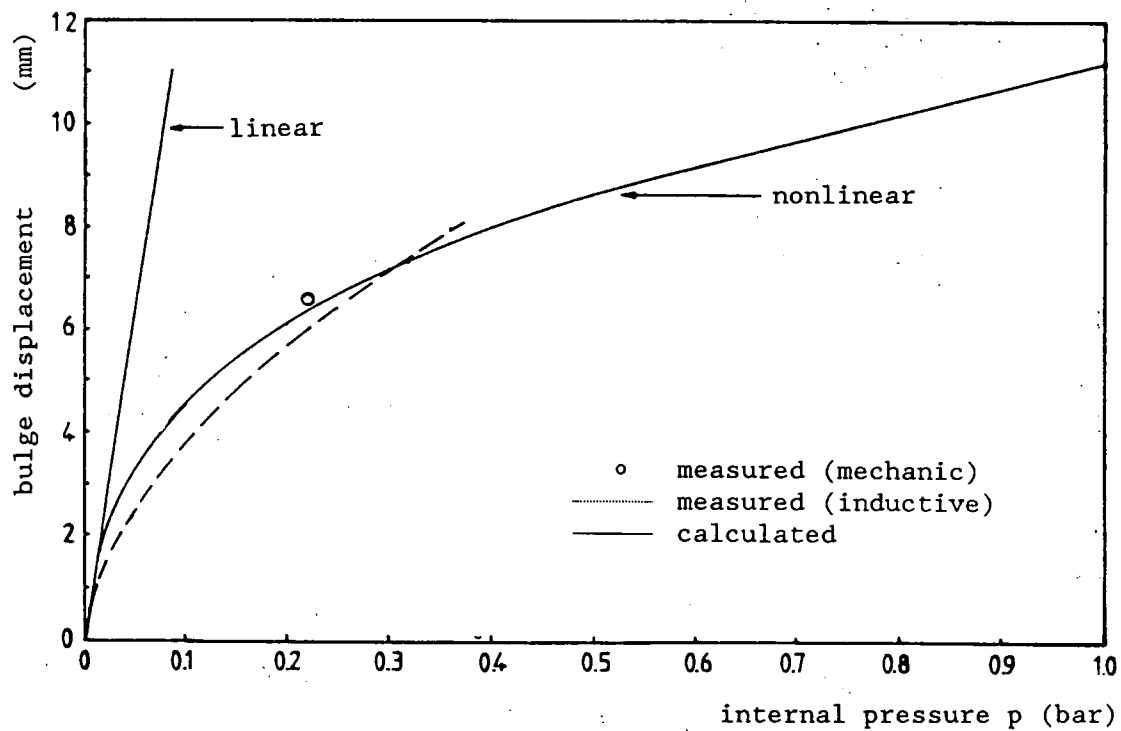
Fig.3.10 Non-linear behaviour of bulge displacement
(After Ansell[16])

143
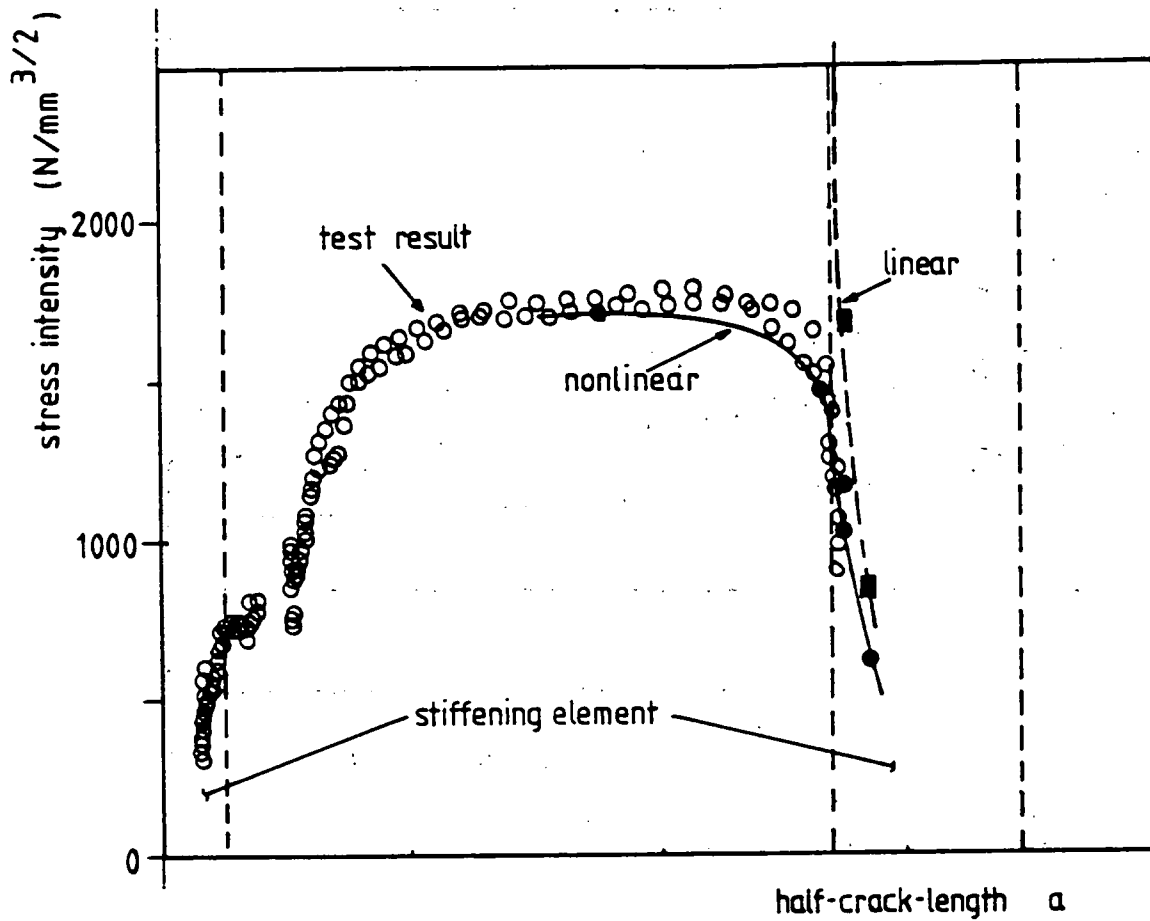
Fig.3.11 Comparison between calculated and test result of
a stiffened panel under internal pressure
(After Ansell[16])
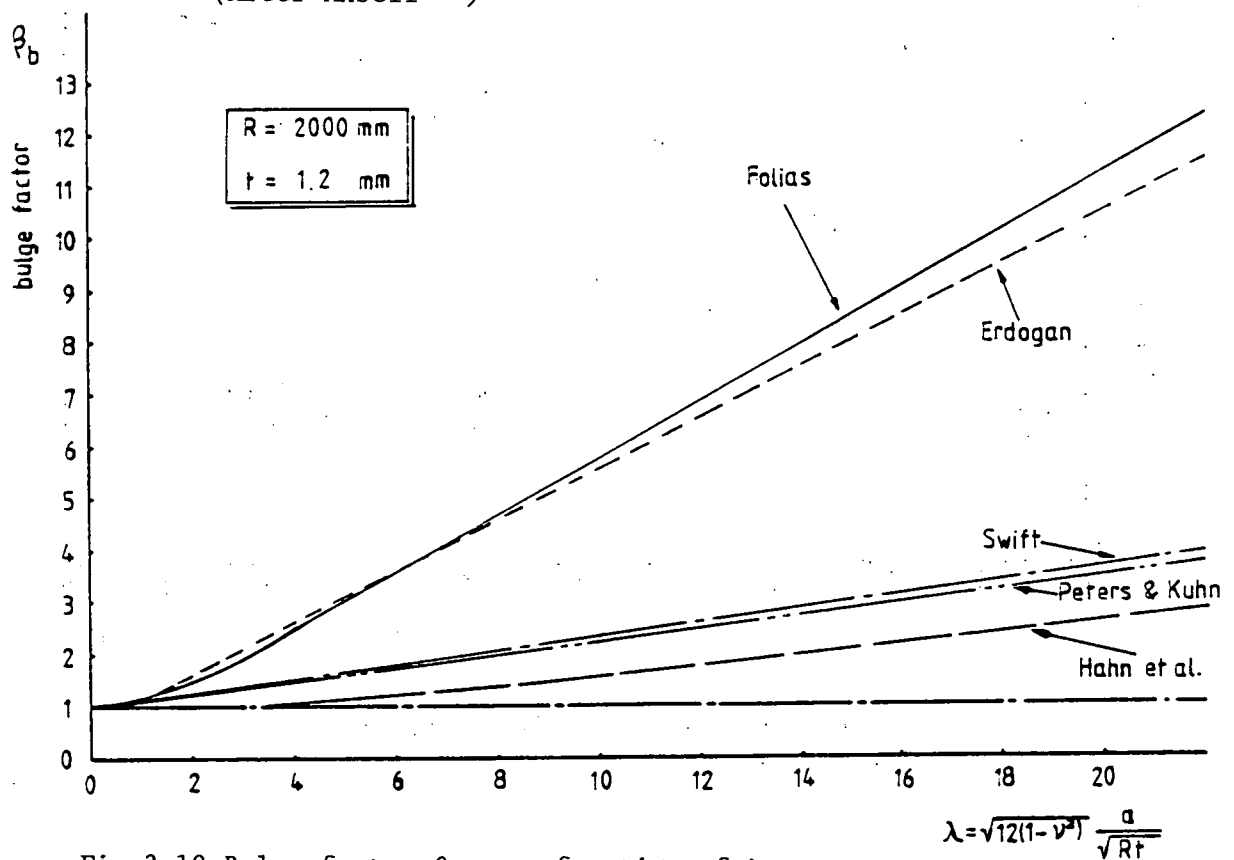
Fig.3.12 Bulge factor β_b as a function of λ
according to various predictions

144
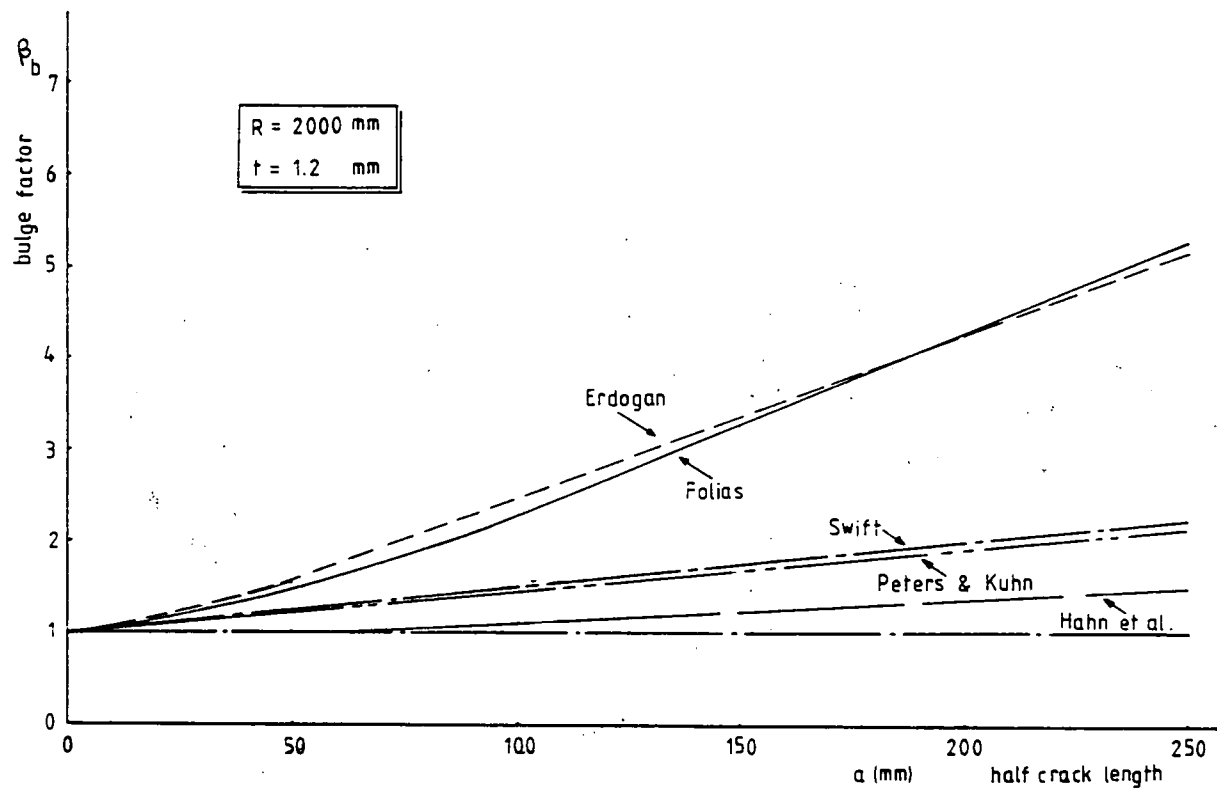
Fig.3.13 Bulge factor β_b as a function of a
according to various predictions
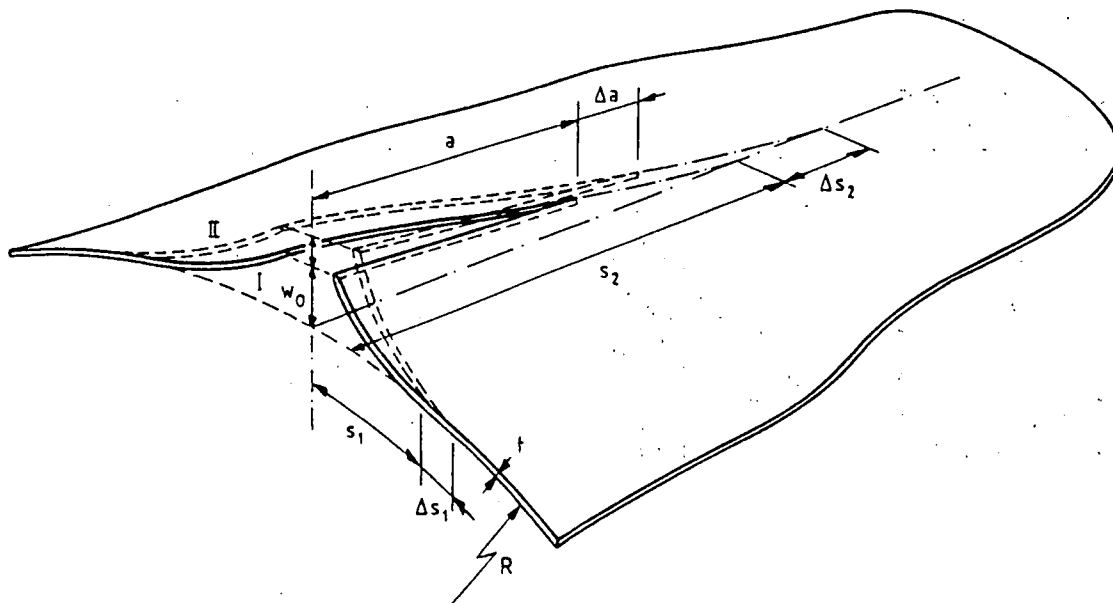
Fig.3.14 Deformation fields around a crack
with half-crack-length a (I) and
a+Δa (II). Half of the bulge area
has been sketched

145
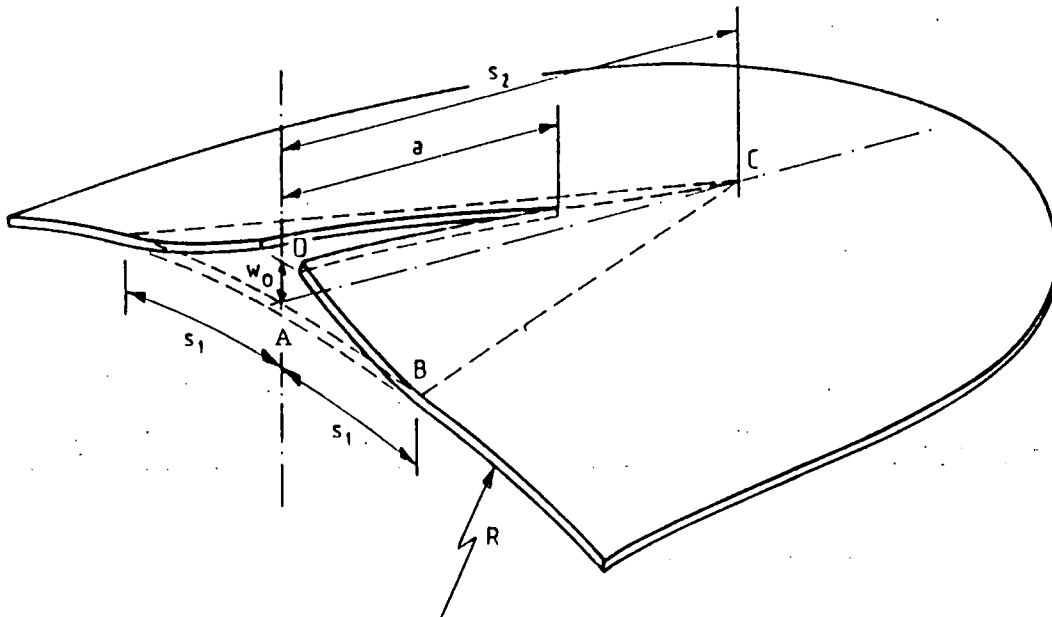
Fig.3.15 One half of the bulged area
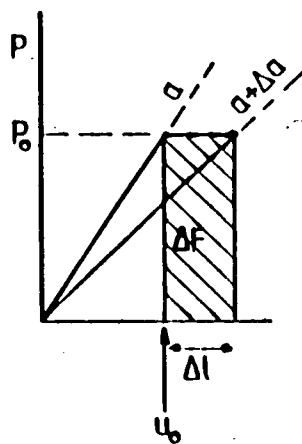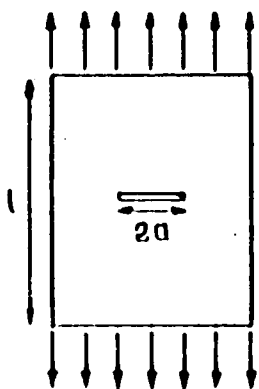
Fixed load, crack extension Δa

Work $F = P_0 \cdot \Delta l$

$$\Delta U = \frac{1}{2} P_0 (u_0 + \Delta l) - \frac{1}{2} P_0 u_0$$

$$= \frac{1}{2} P_0 \Delta l$$

$$\Delta F - \Delta U = \frac{1}{2} P_0 \Delta l = \Delta U$$

$$\Delta U = \frac{1}{2} \Delta F$$

Fig.3.16 Strain energy calculation for "Fixed-load" situation

146
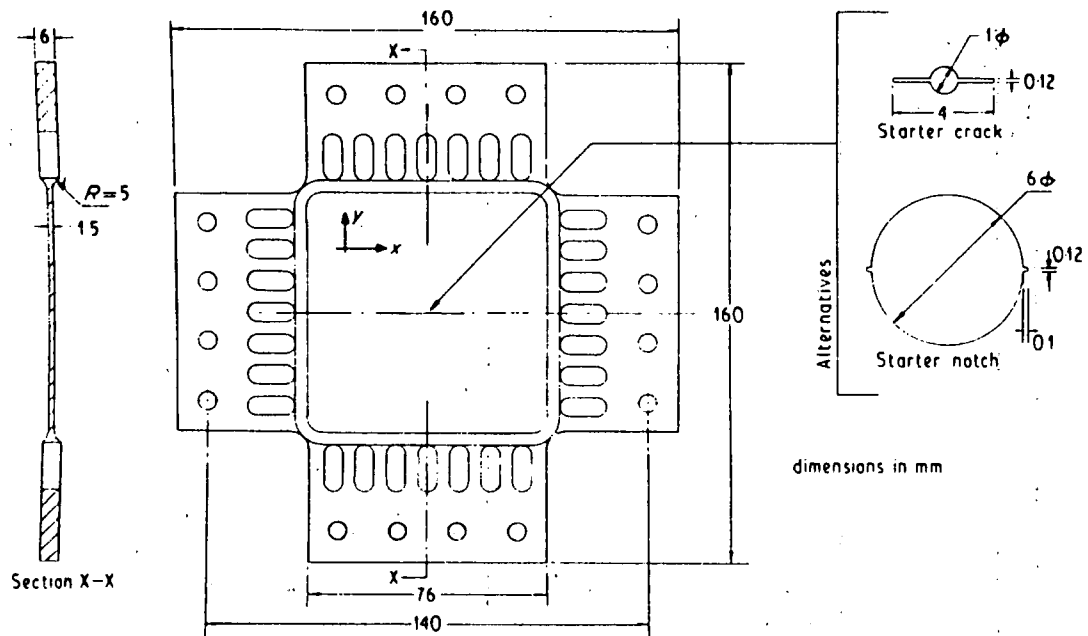
Fig.4.1 Cruciform shaped biaxial test specimen[1]
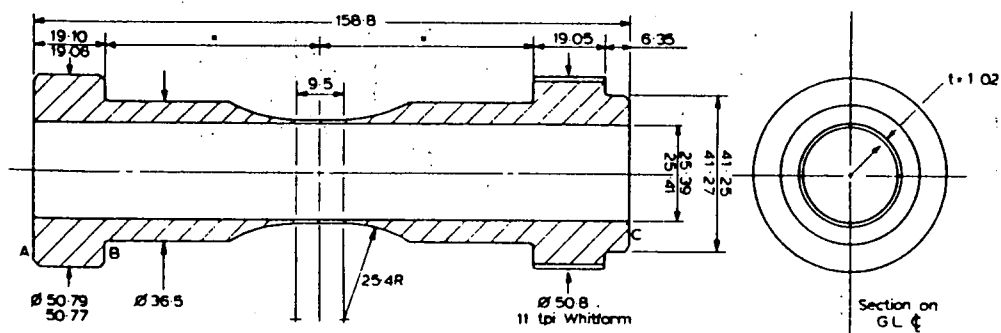
Fig.4.2 Thin-walled tubular biaxial test specimen[1]

147
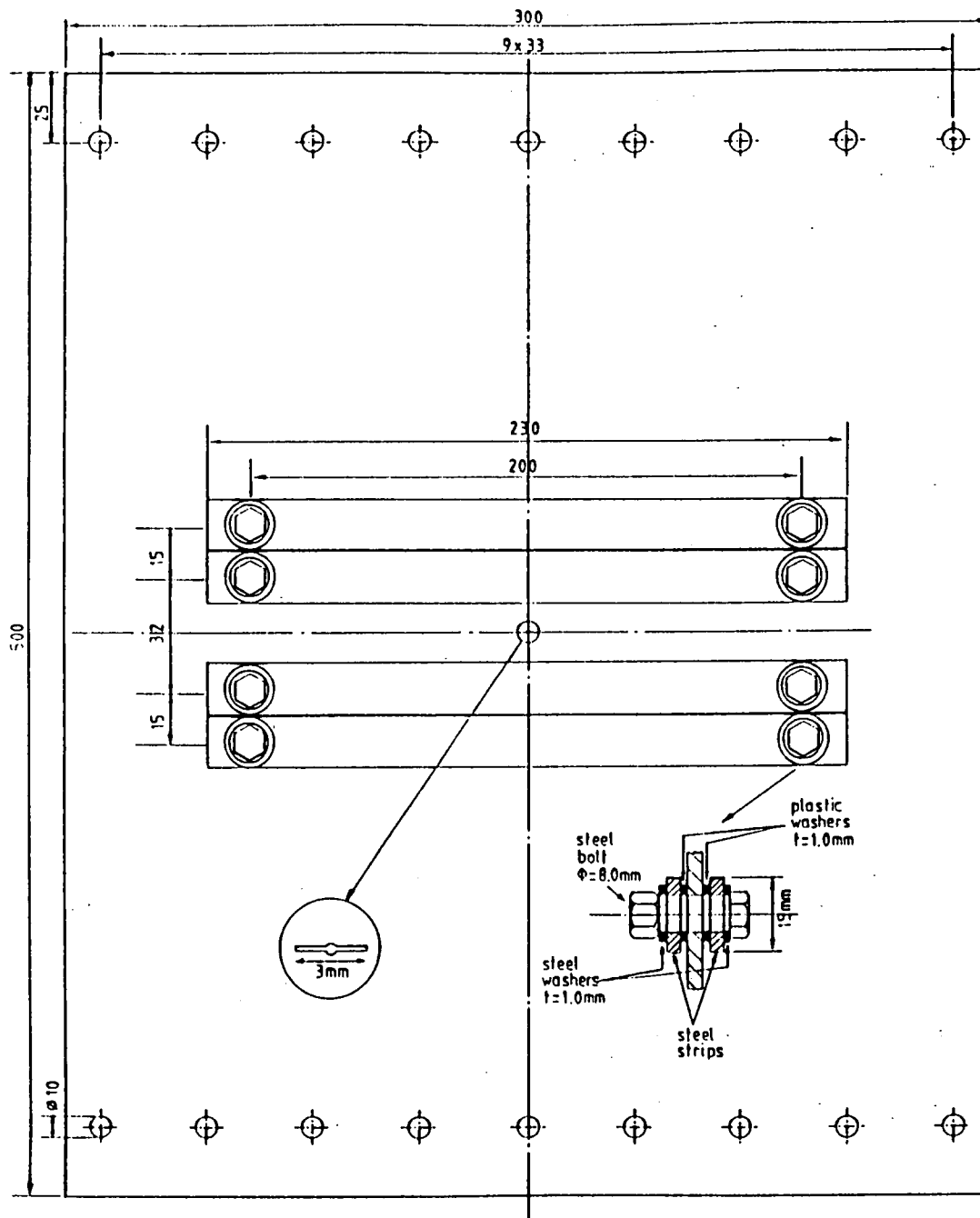
Fig.4.3 SUPERBAT

(Specimen Using Poisson Ratio Effect for Bi-Axial Testing)

143
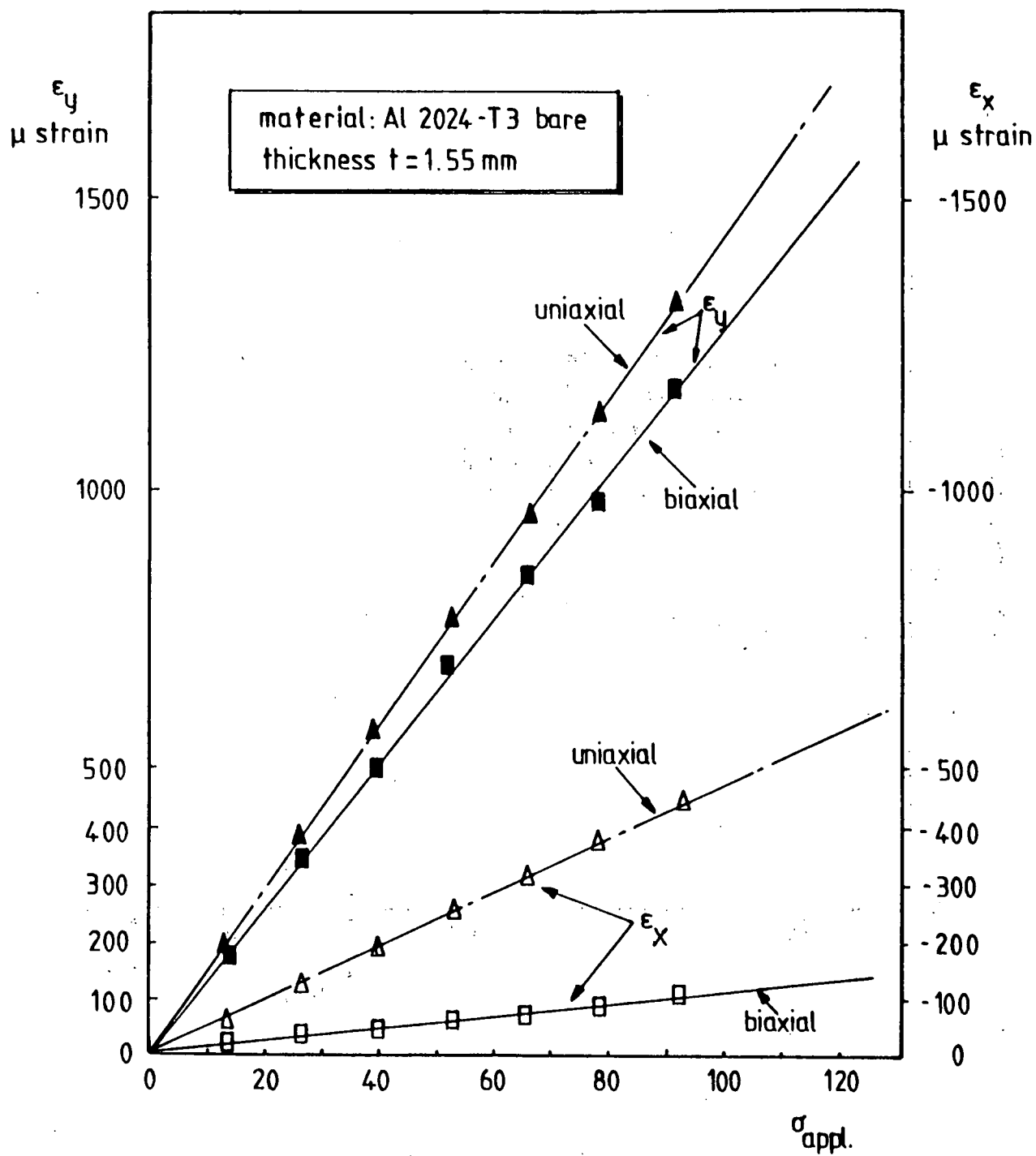
Fig.4.4 Results of strain-gauge measurements on a SUPERBAT specimen
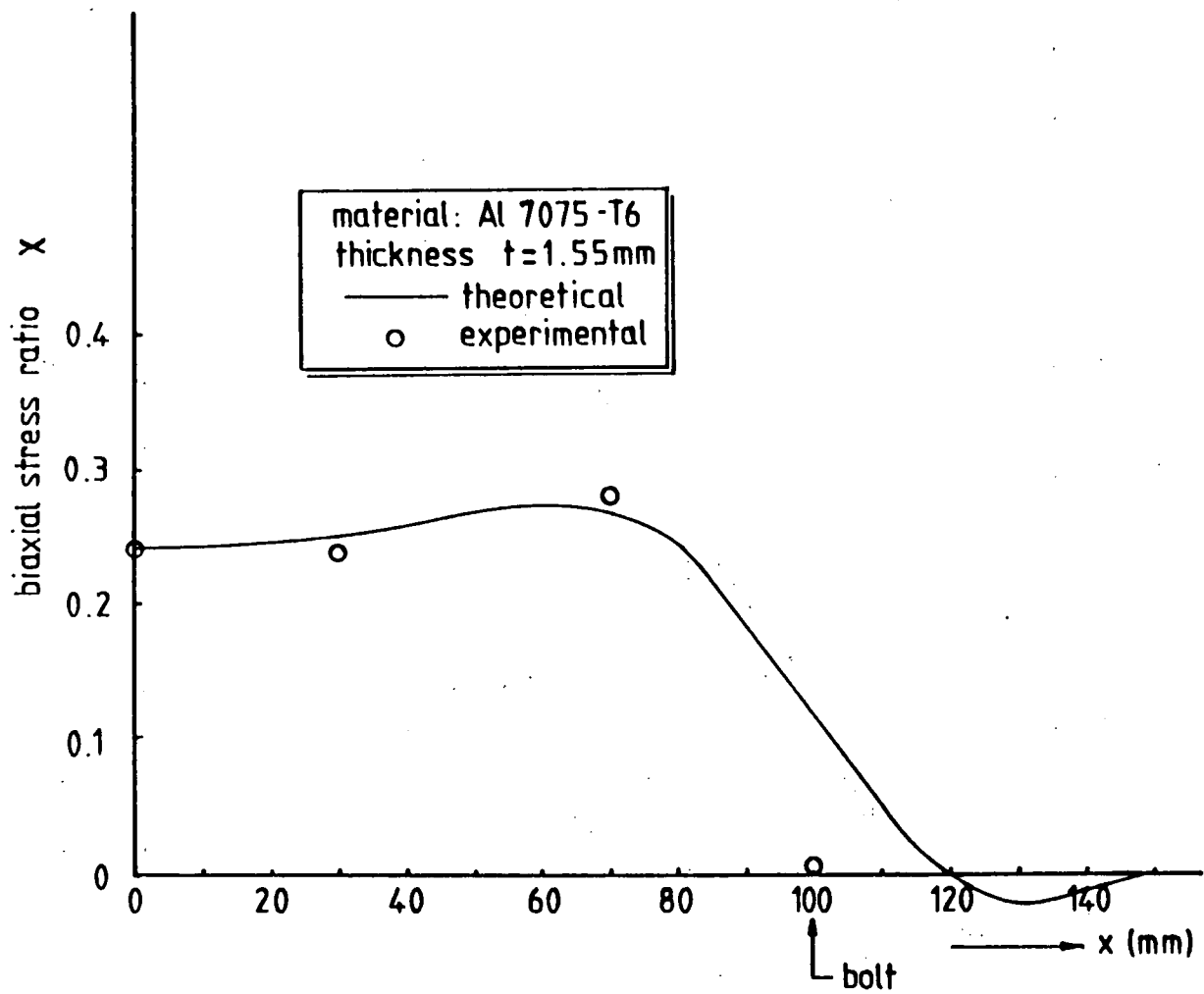
Fig.4.5 Comparison between theoretical and
experimental biaxial stress ratio χ
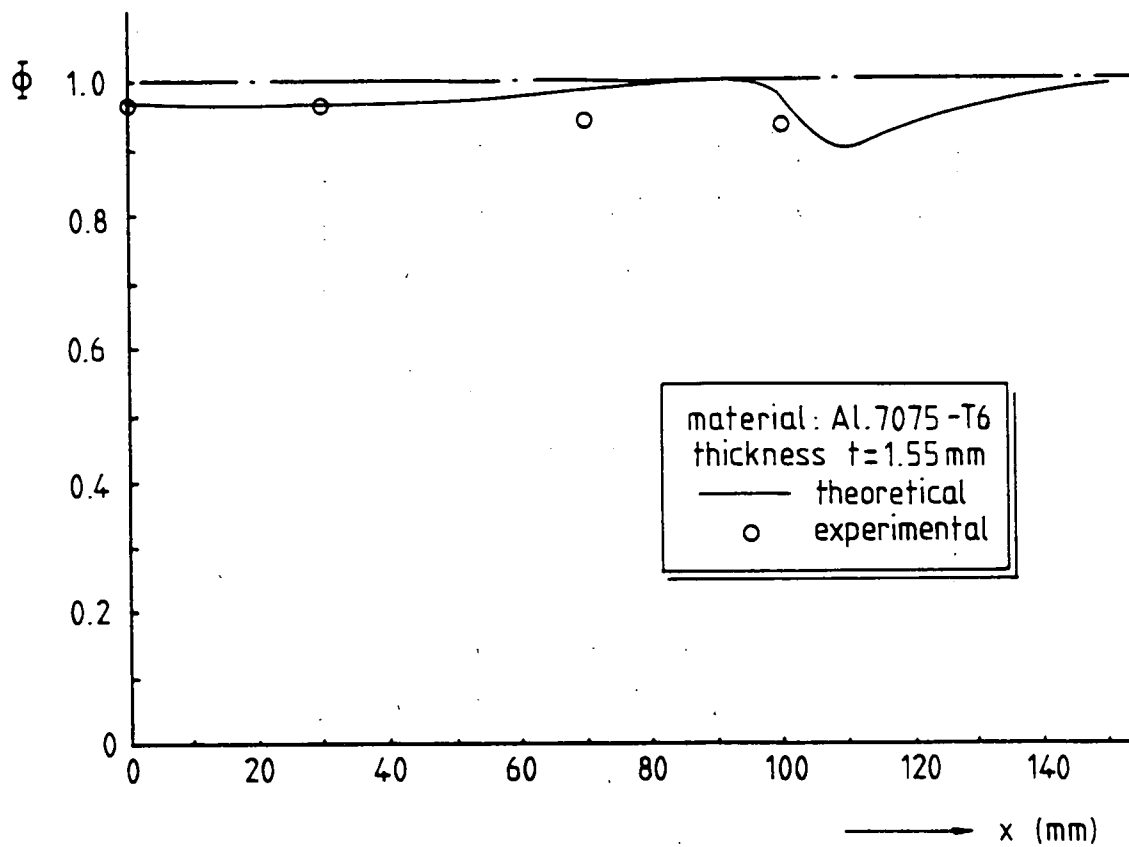
Fig.4.6 Comparison between theoretical and
experimental load-efficiency-factor Φ
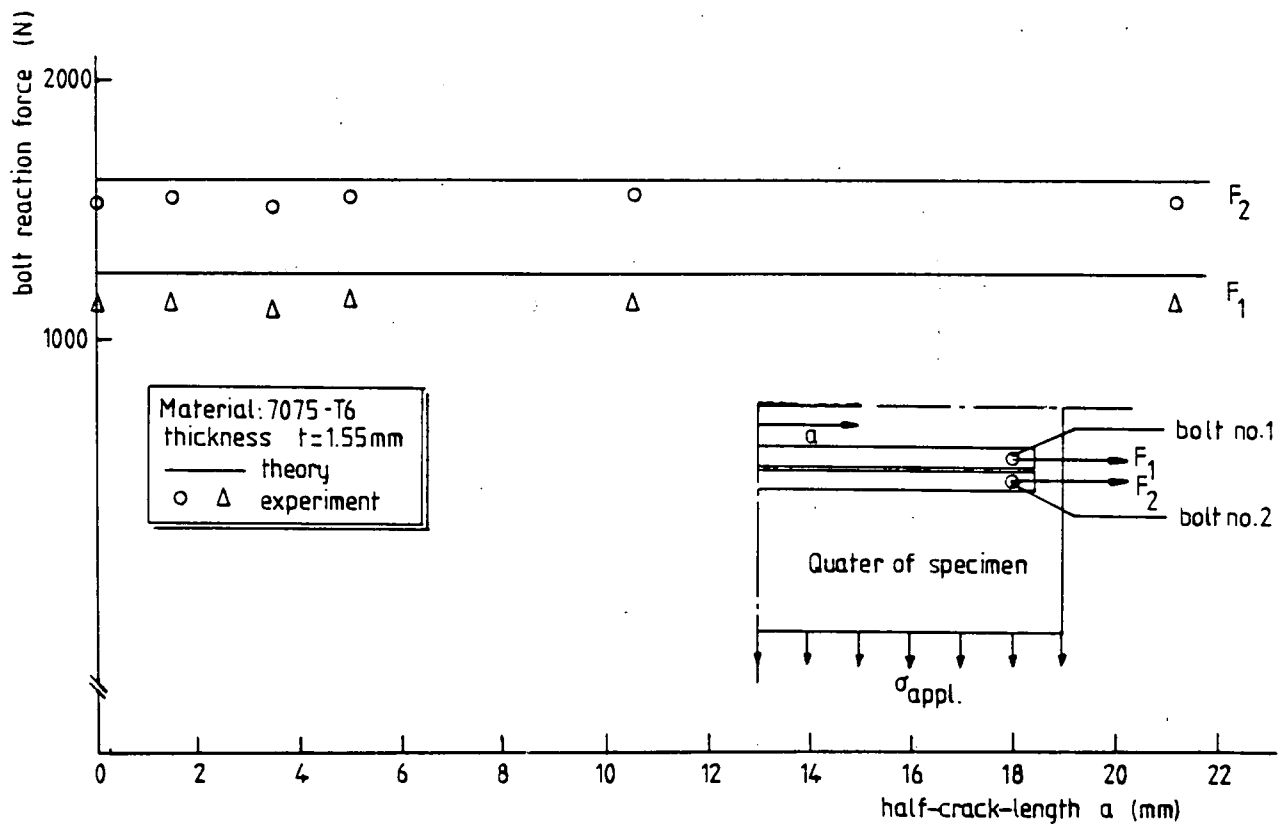
Fig.4.7 Comparison between theoretical and
and experimental bolt-reaction-force

151
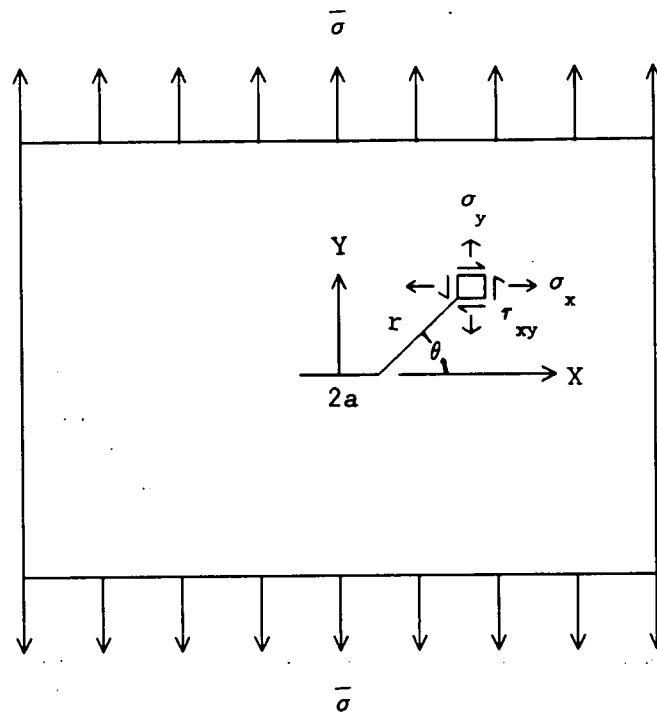
Fig.4.8 Extension of infinite cracked plate
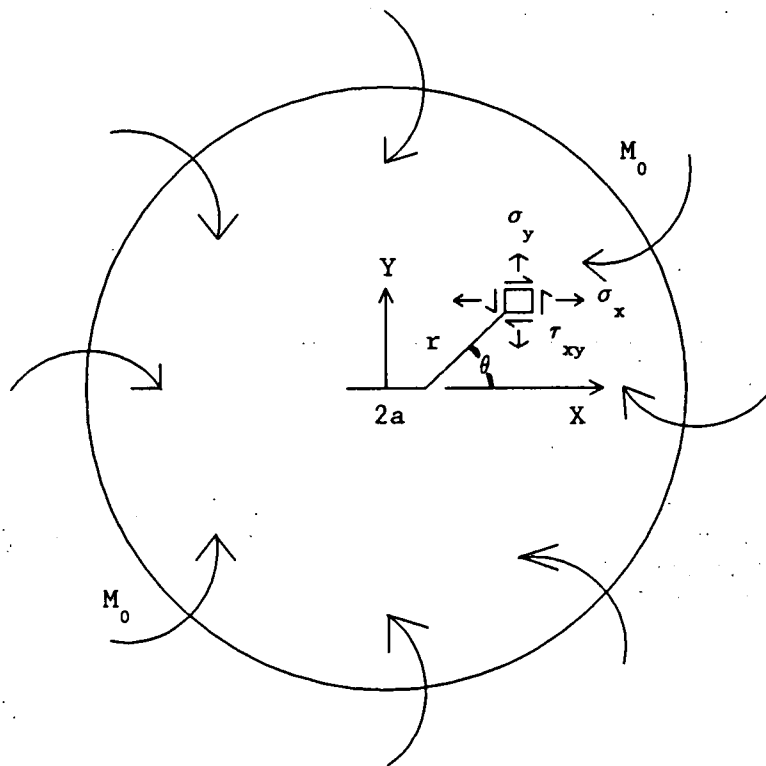
Fig.4.9 Uniform bending of infinite plate
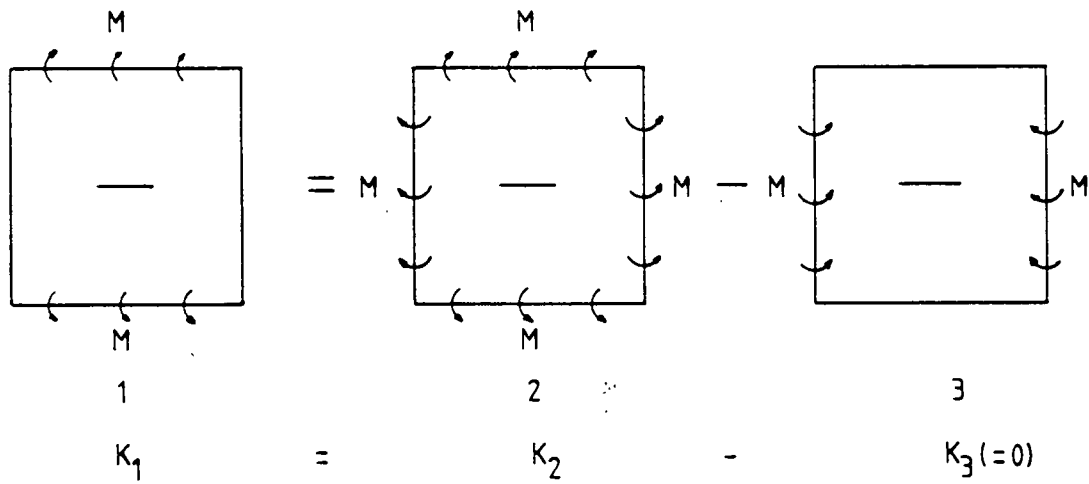
Fig.4.10 Superposition principle applied
to systems of bending moment
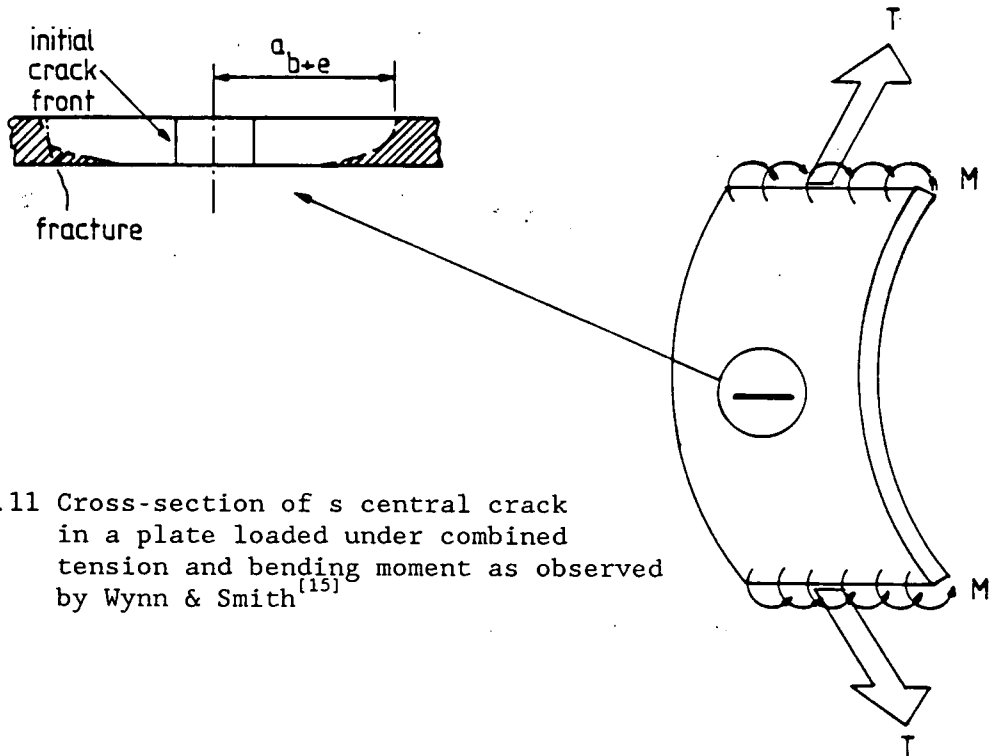
Fig.4.11 Cross-section of s central crack
in a plate loaded under combined
tension and bending moment as observed
by Wynn & Smith[15]

153
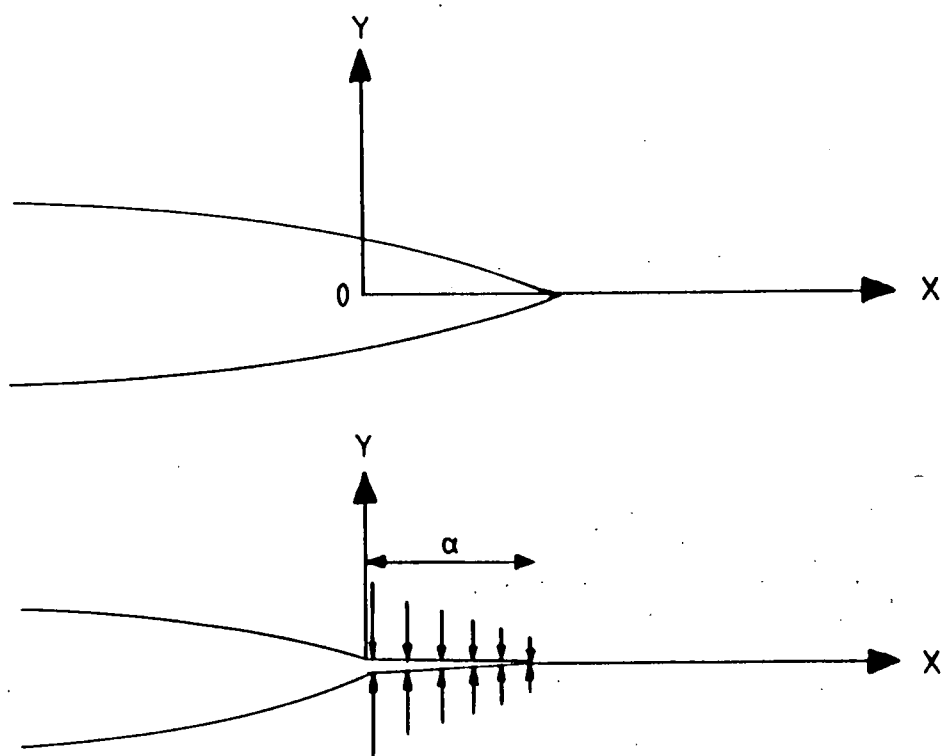
Fig.4.12 Strain-energy-release-rate calculation
according to Irwin

154
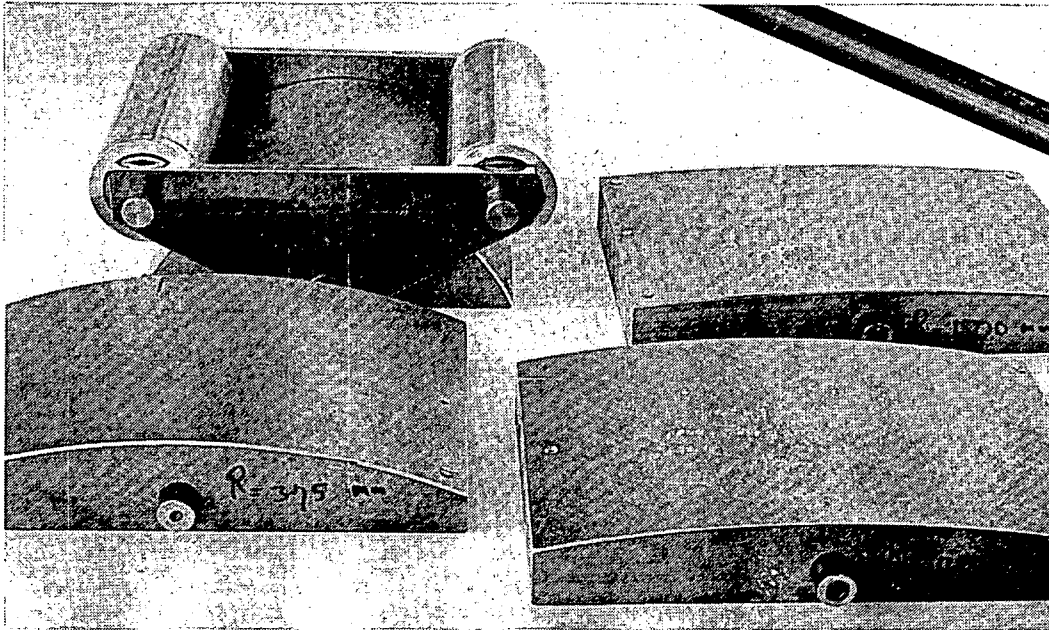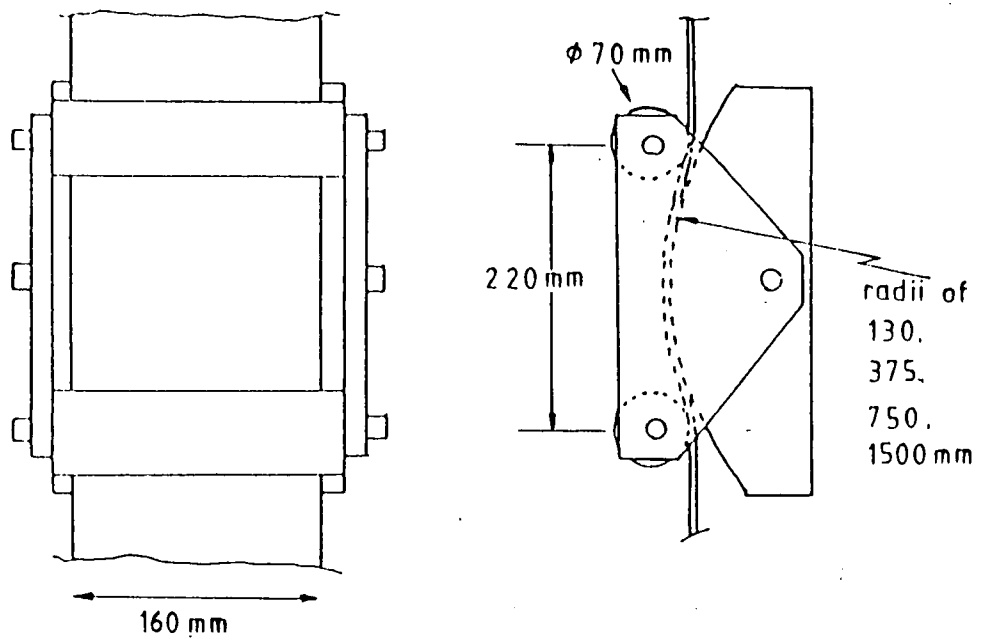
Fig.4.13 CETS (Curvature Effect Test System)
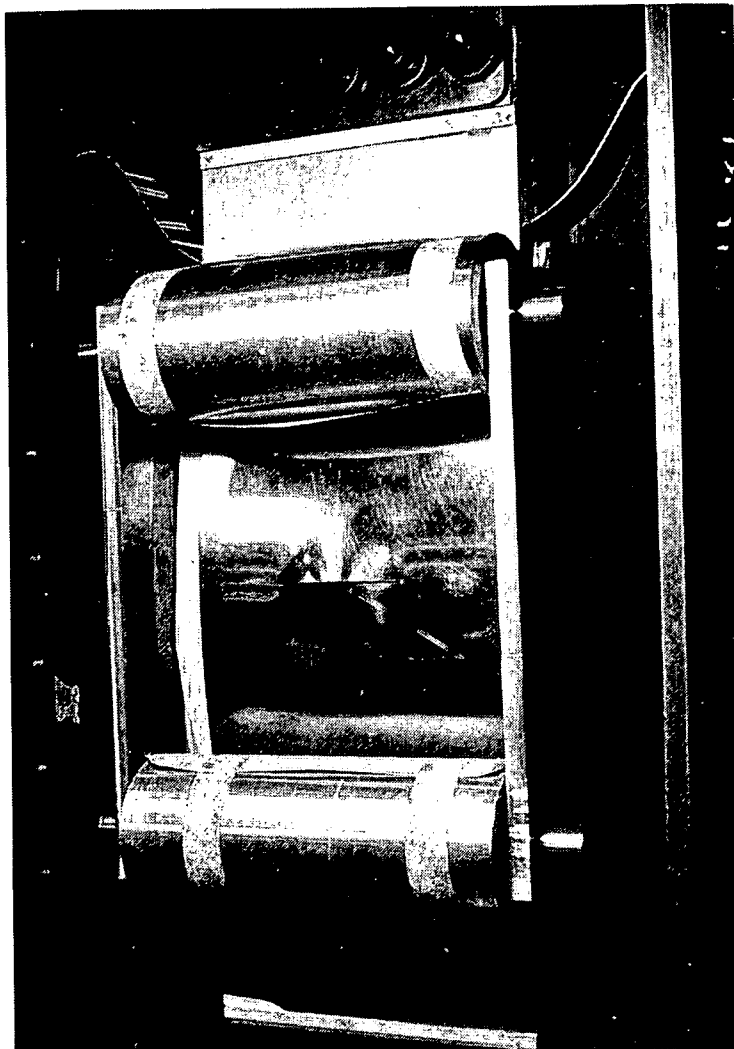
Fig.4.14 CETS showing bulge-out
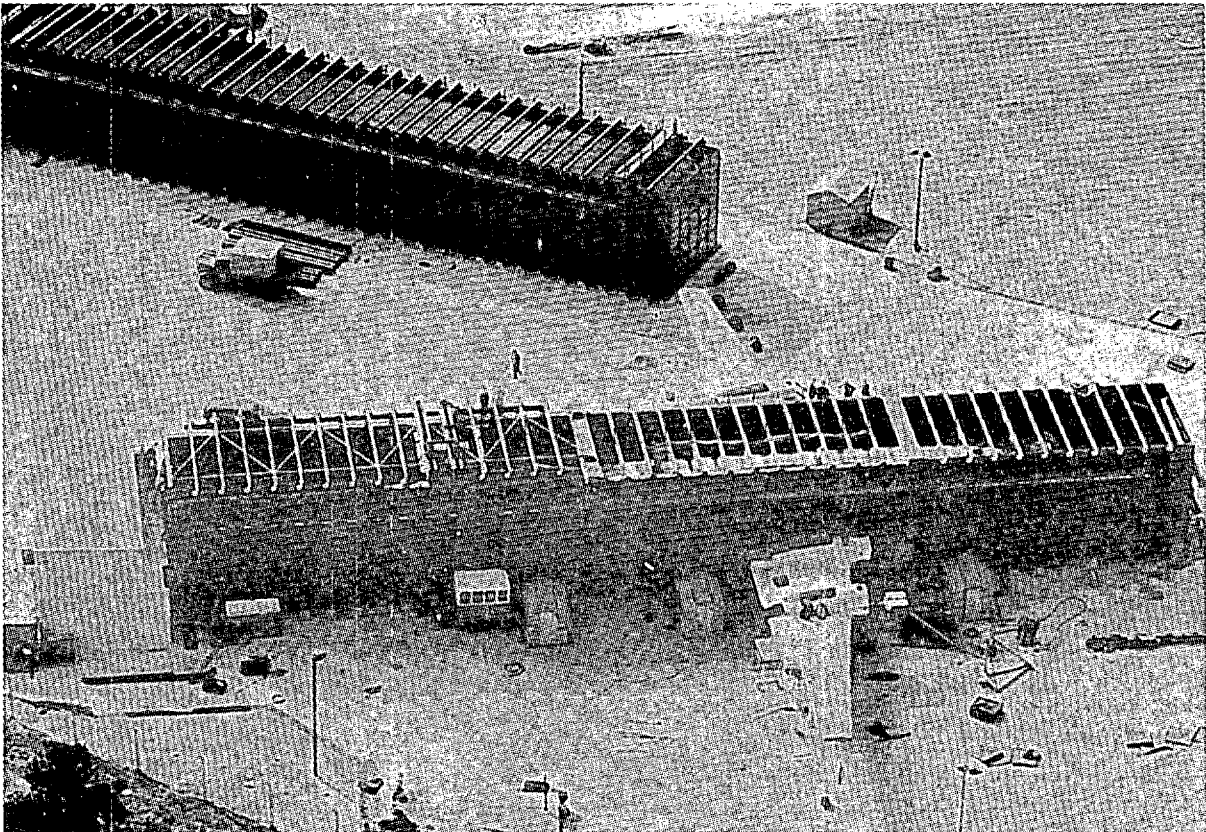
Fig.4.15 General view of Bristol Britannia type 100
        full scale fatigue test site *(after Morgan[18])*
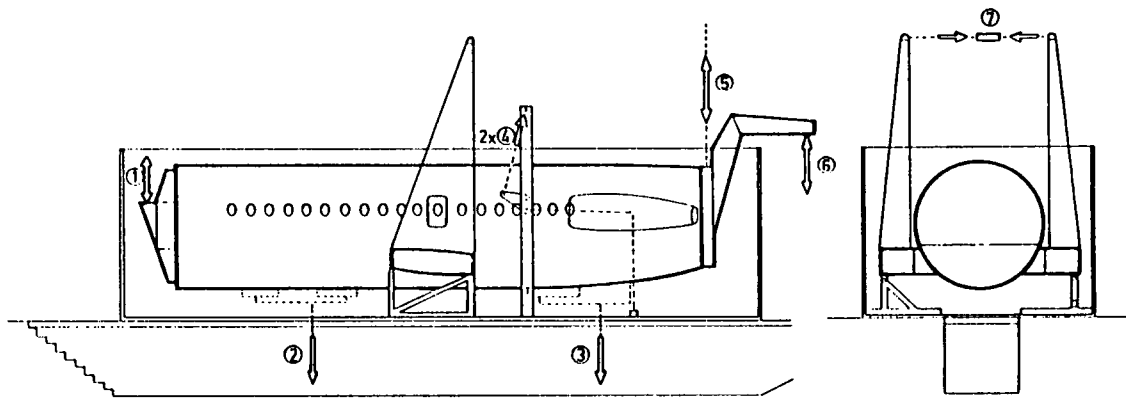
1 to 8: fatigue load applications

Fig.4.16 Fokker F-28 main fuselage full scale fatigue
test set-up (after van Beek[20])
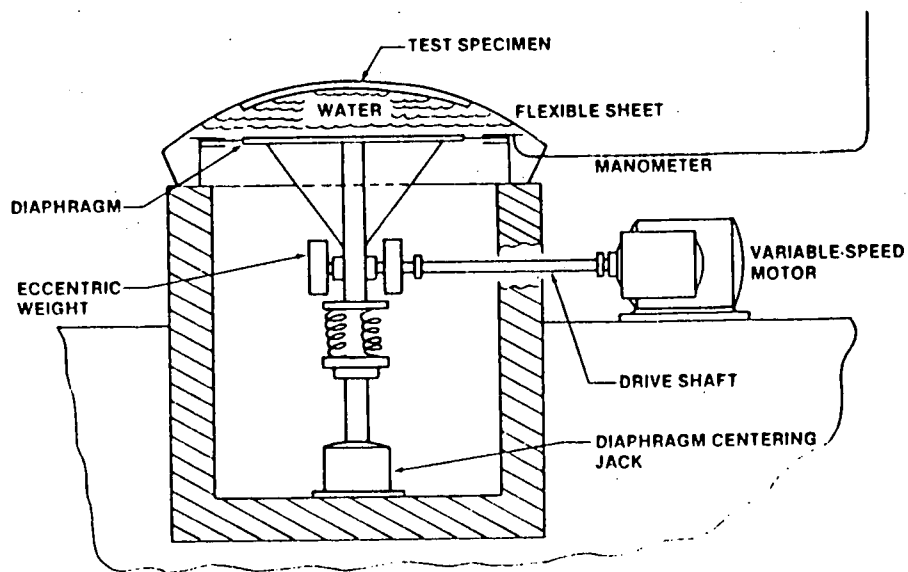
Fig.4.17 "Water cycle test machine" (after Swift[19])
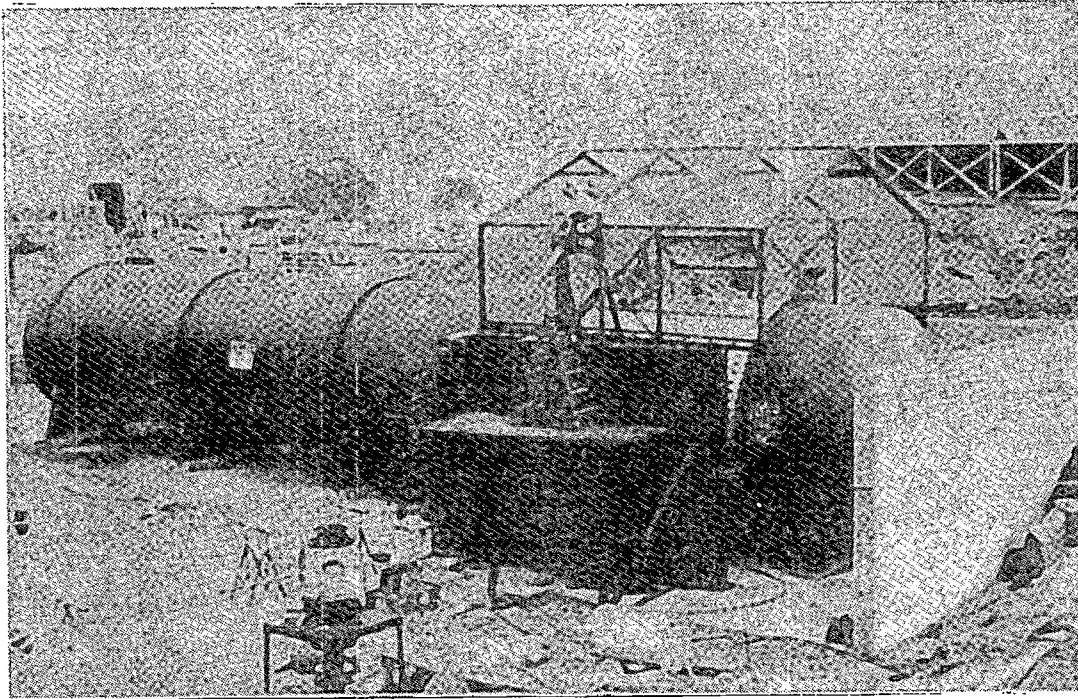
Fig.4.18 "Air tank test set-up" (after Swift[19])
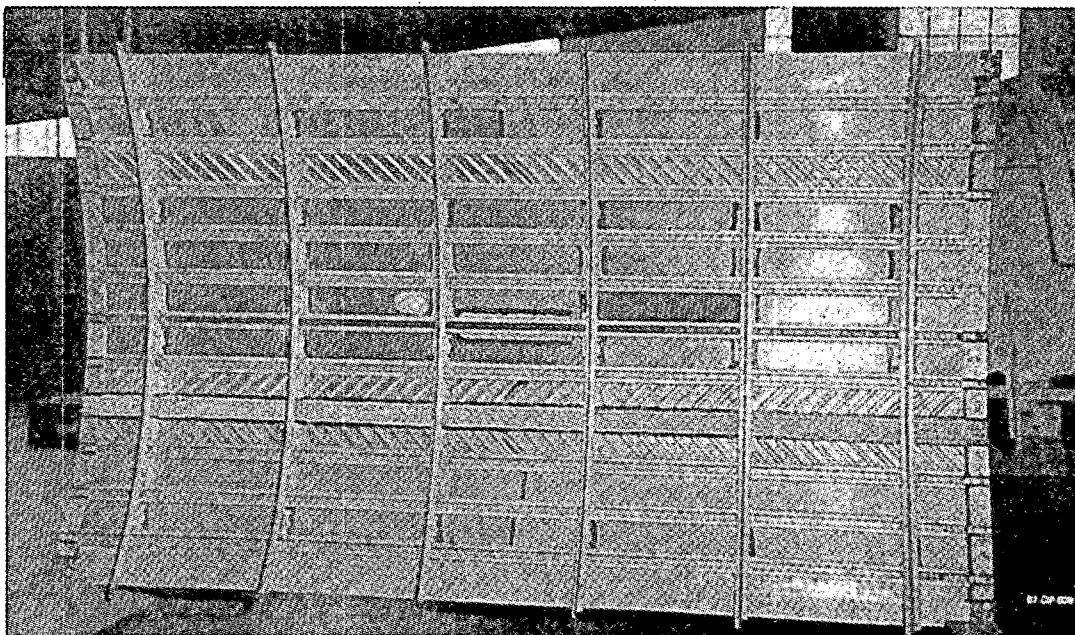
Fig.4.19 Typical curved panel tested in water cycle
and air tank fixtures (after Swift[19])

159
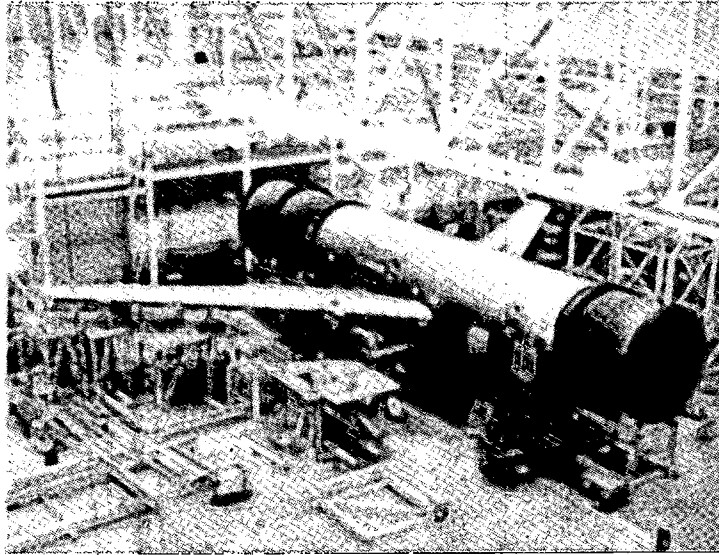
Fig.4.20 DC-10 wing and center section full scale
test set-up (after Swift[19])
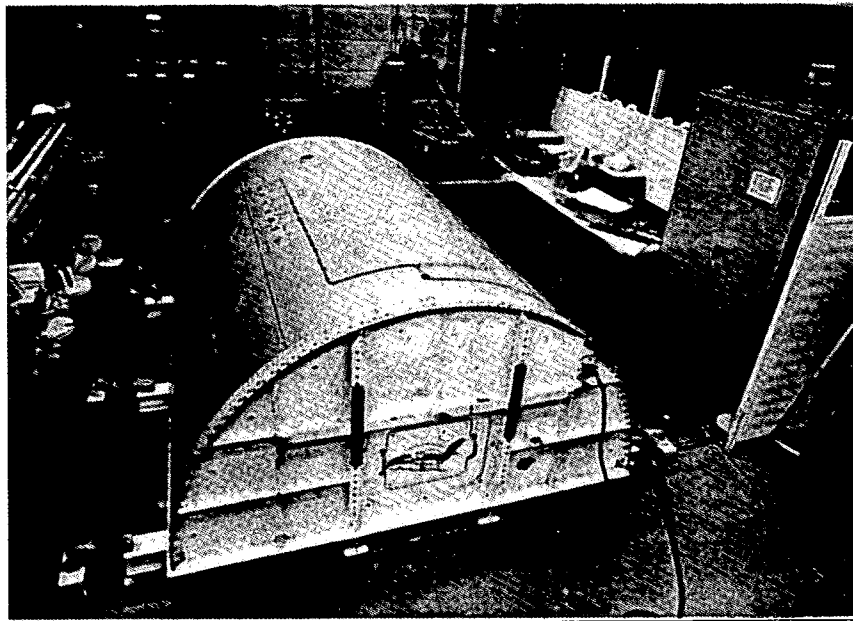
Fig.4.21 SAAB 340 fuselage development program
curved panel test set-up (after Ansell[17])

160
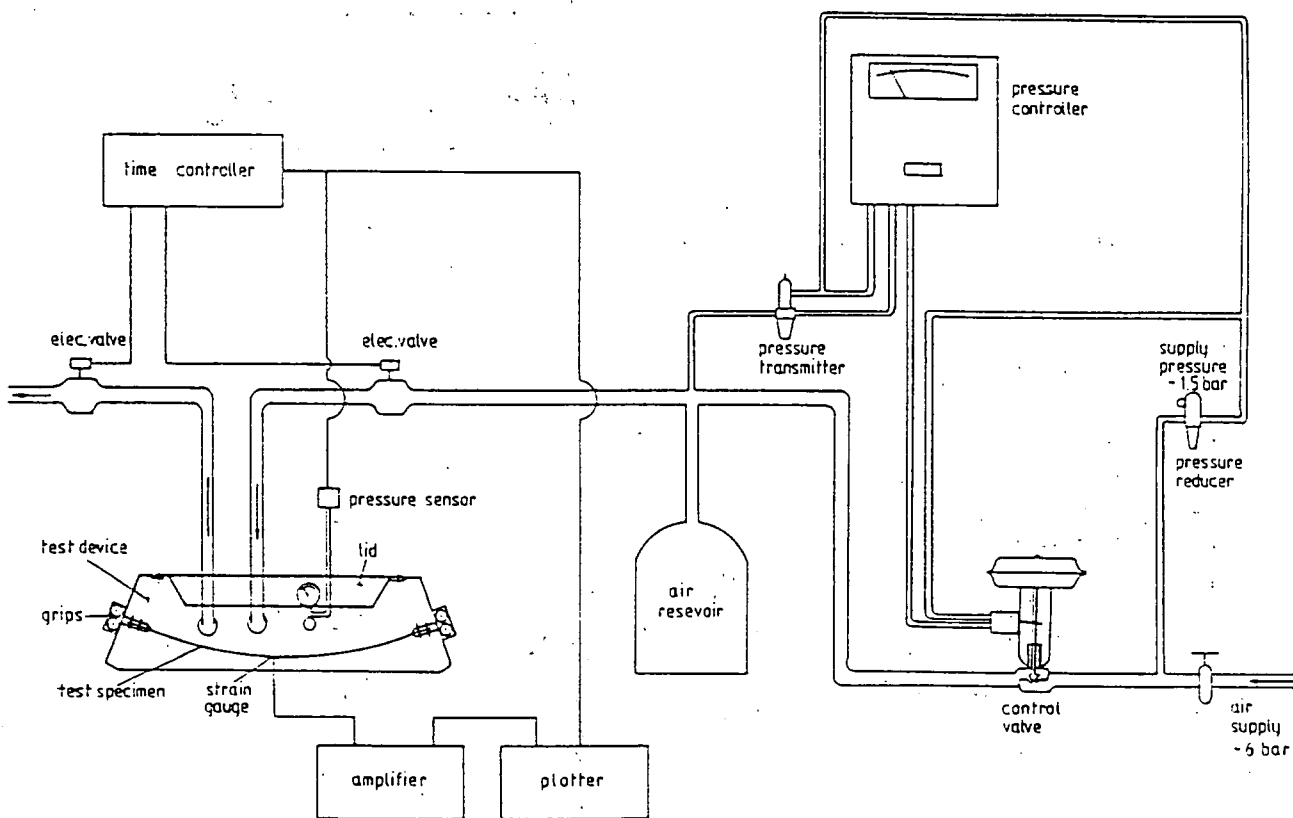
Fig.4.22 Arrangement of the PFSTS (Pressurized Fuselage Skin Test System)
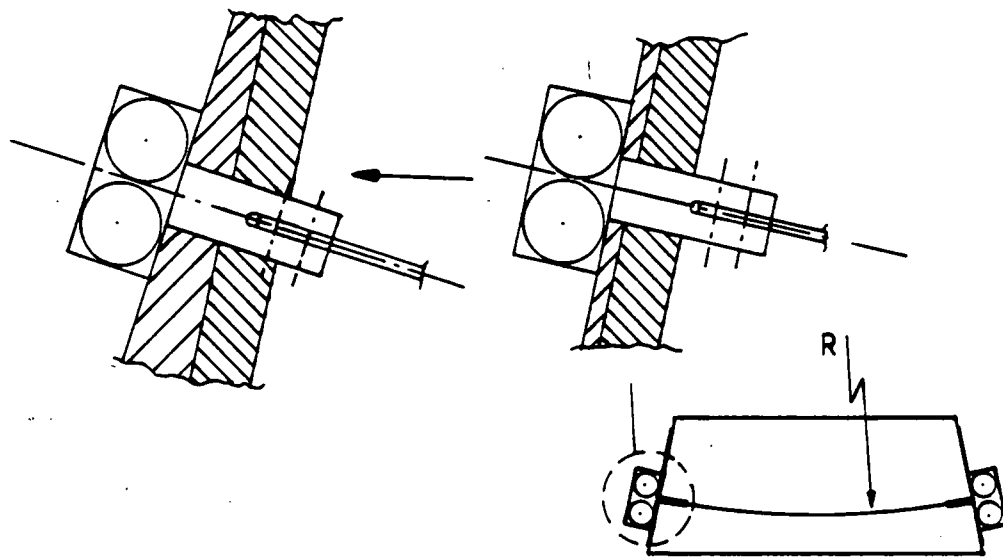
Fig.4.23 Varying radius of the specimen
by changing the wedges at the grips
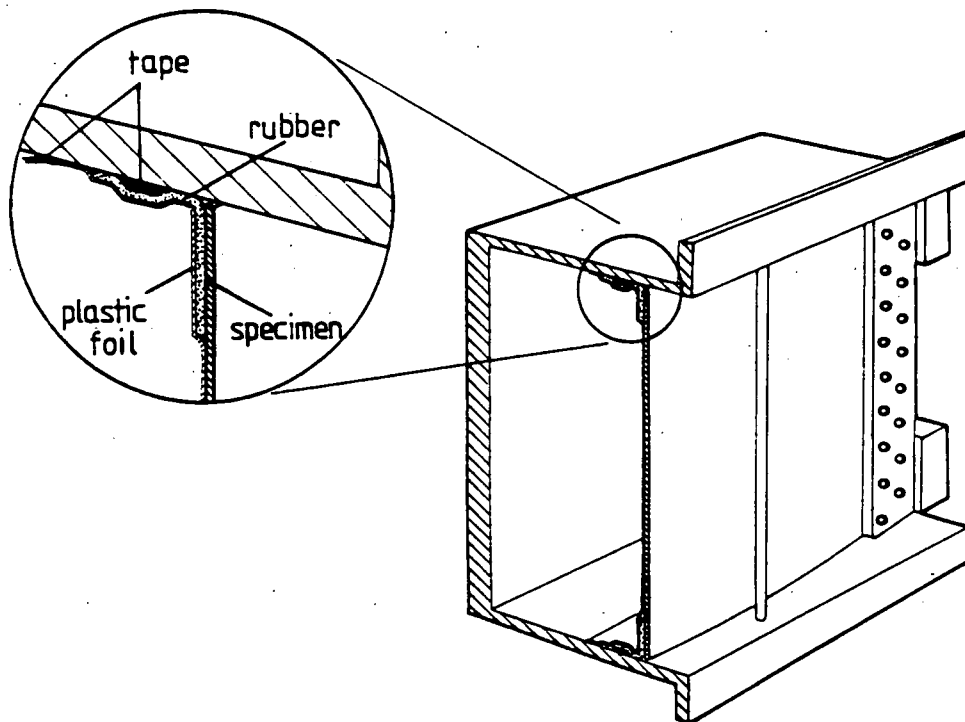
Fig.4.24 Sealing of the test system
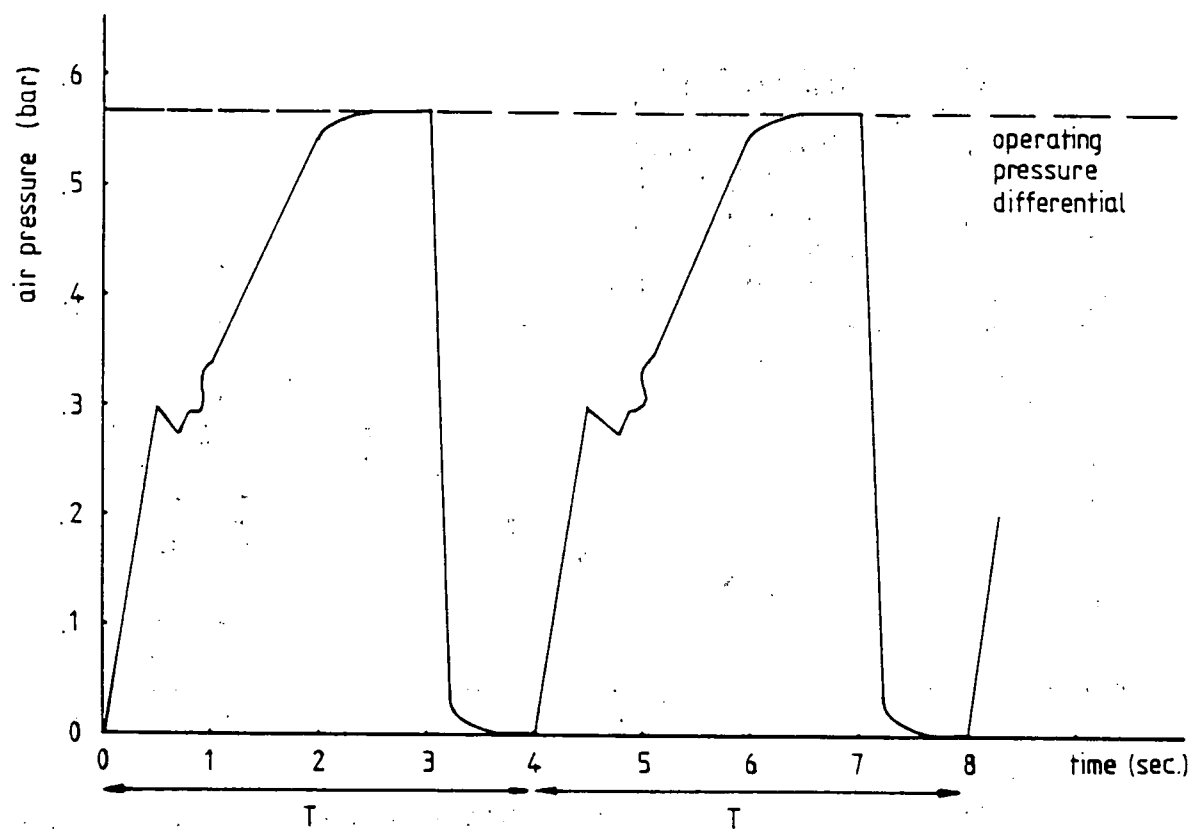
Fig.4.25 A typical pressure wave shape in PFSTS

Fig.4.26 The PFSTS

163
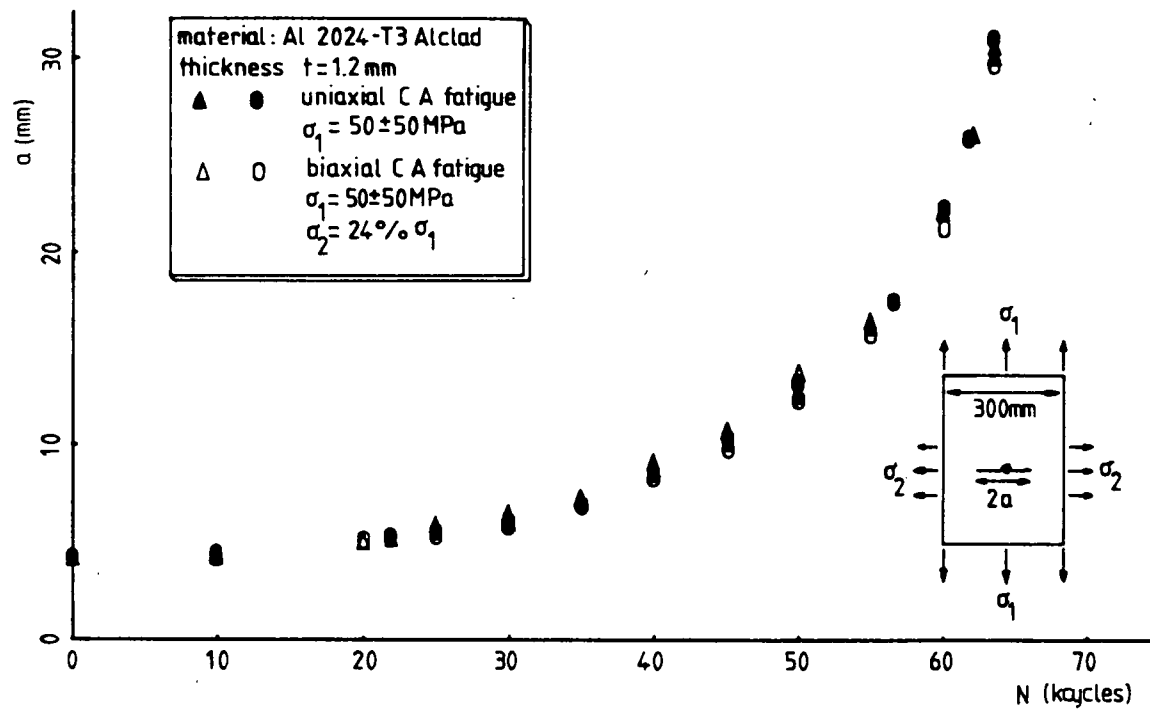
Fig.5.1 CA fatigue test results using SUPERBAT technique (2024-T3 Alclad)
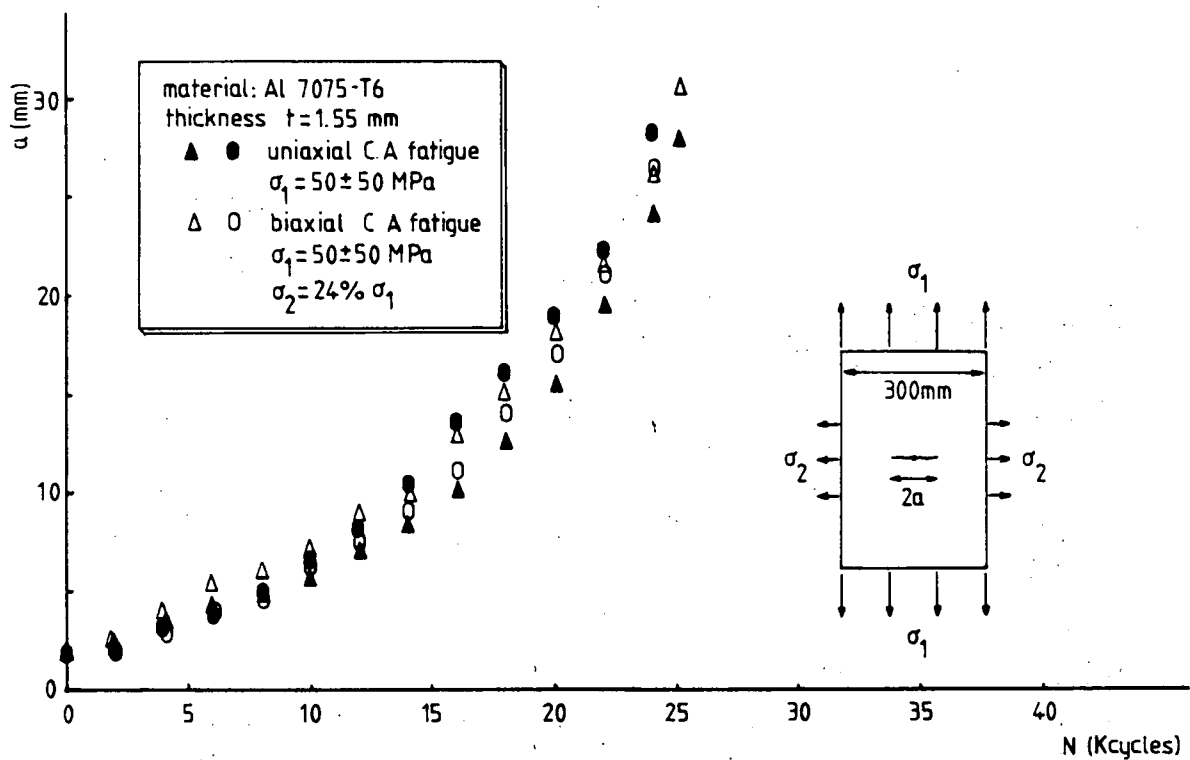
Fig.5.2 CA fatigue test results using SUPERBAT technique (7075-T6)

164

Fig. 5.3 da/dN-a curves for 2024-T3 Alclad

Fig. 5.4 da/dN-a curves for 7075-T6

crack growth rate da/dN (mm/cycle)

half-crack-length a (mm)

material: Al 2024-T3 Alclad
thickness t = 1.2 mm

+ △ uniaxial C A fatigue
      $\sigma_1 = 50 \pm 50$ MPa
o □ biaxial C A fatigue
      $\sigma_1 = 50 \pm 50$ MPa
      $\sigma_2 = 24\% \, \sigma_1$

300 mm

σ_1 σ_2 2a

material: Al 7075-T6
thickness t = 1.55 mm

+ △ uniaxial C A fatigue
      $\sigma_1 = 50 \pm 50$ MPa
o □ biaxial C A fatigue
      $\sigma_1 = 50 \pm 50$ MPa
      $\sigma_2 = 24\% \, \sigma_1$

300 mm

σ_1 σ_2 2a

crack growth rate da/dN (mm/cycle)

half-crack-length a (mm)

Fig.5.5 da/dN-ΔK curves for steel (Welten 60)
according to Kitagawa *et al*[1]
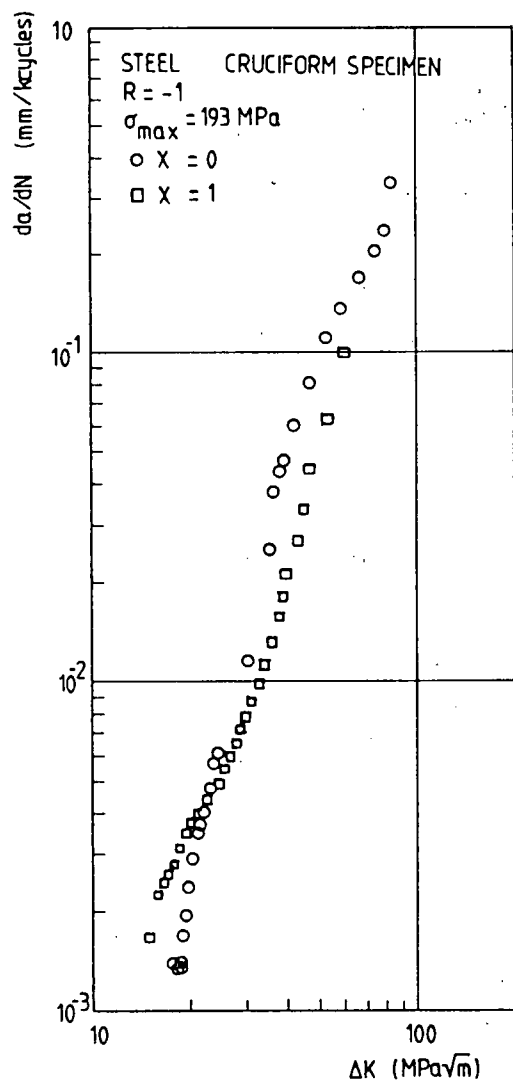
Fig.5.6 da/dN-ΔK curves for steel
according to Brown & Miller[2]
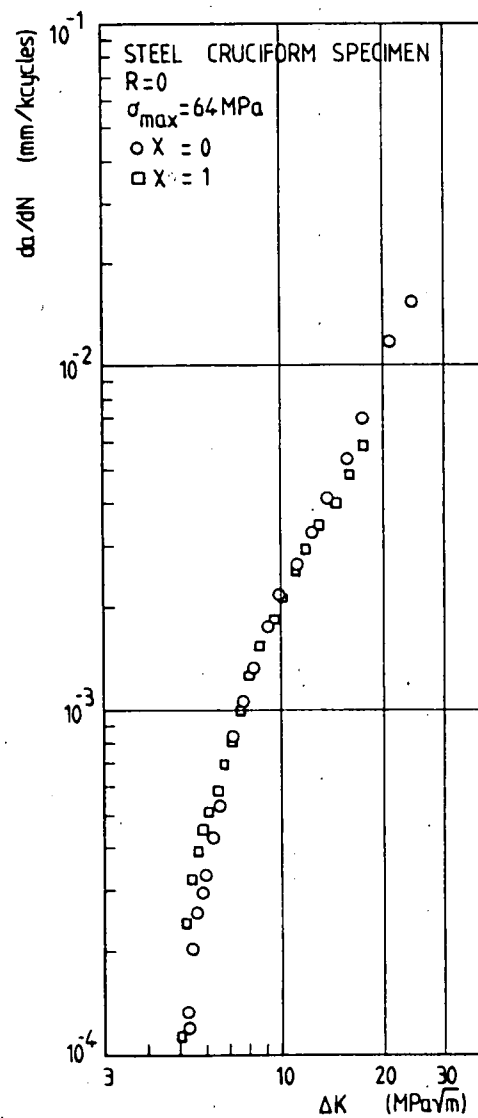
Fig.5.7 da/dN-ΔK curves for steel
according to Brown & Miller[2]
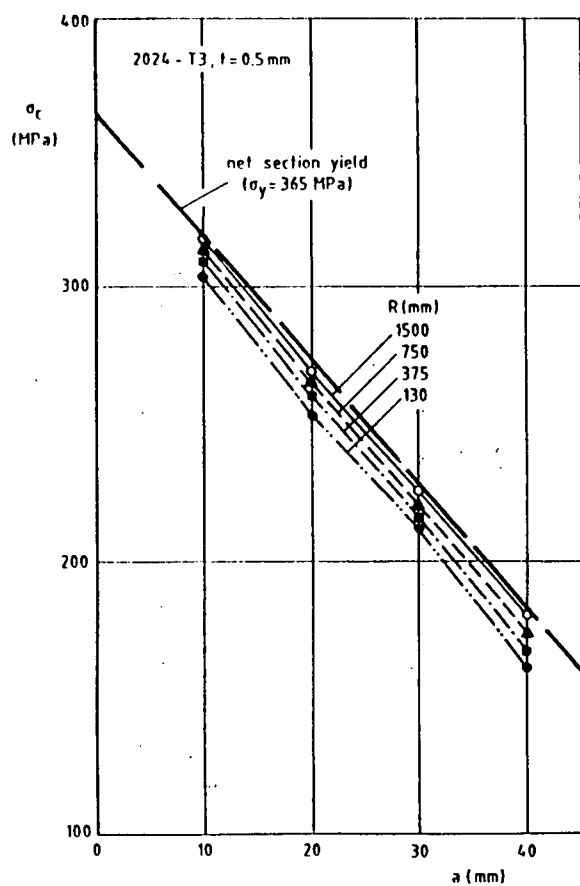
Fig.5.8a
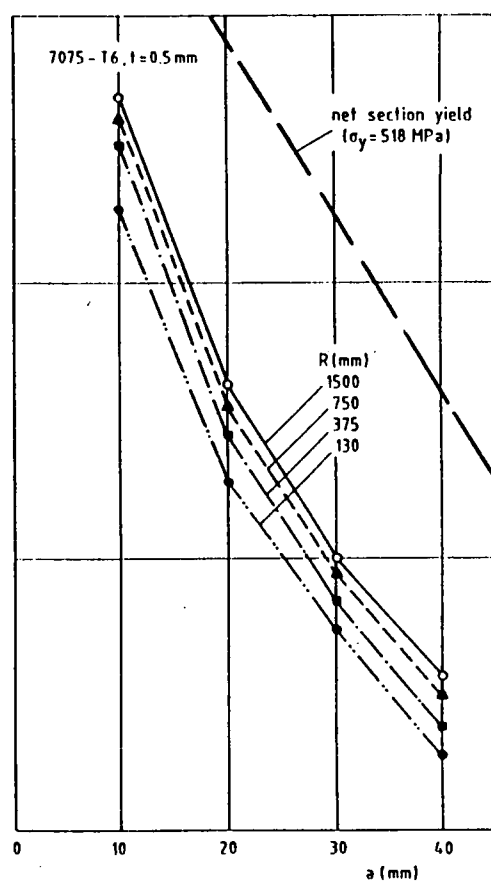
Fig.5.8d
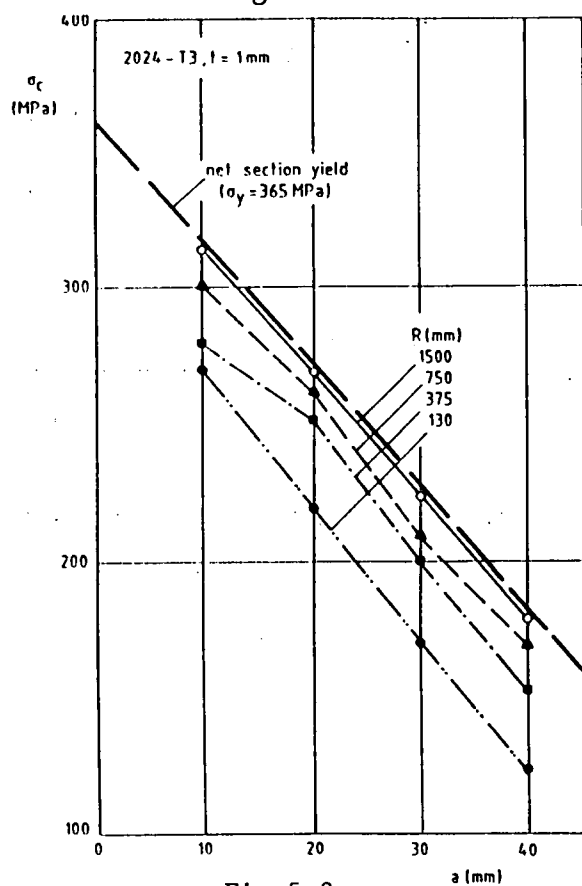
Fig.5.8c
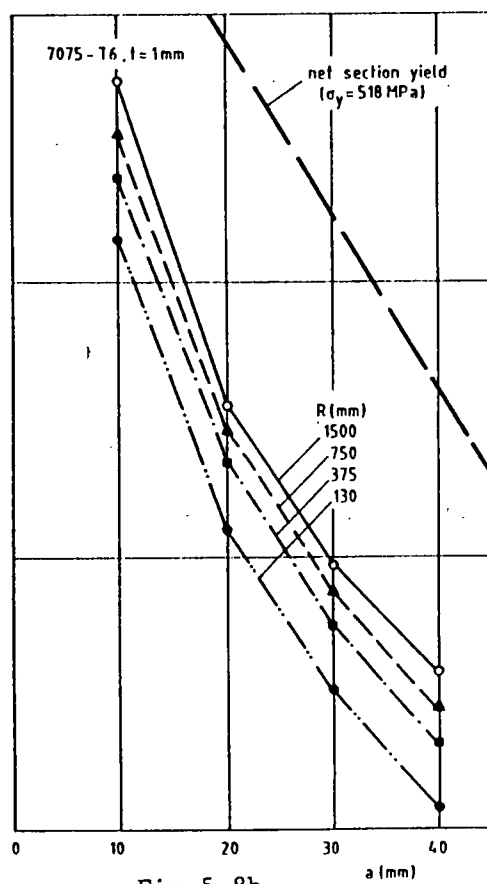
Fig.5.8b

Fig.5.8 Test results of CETS
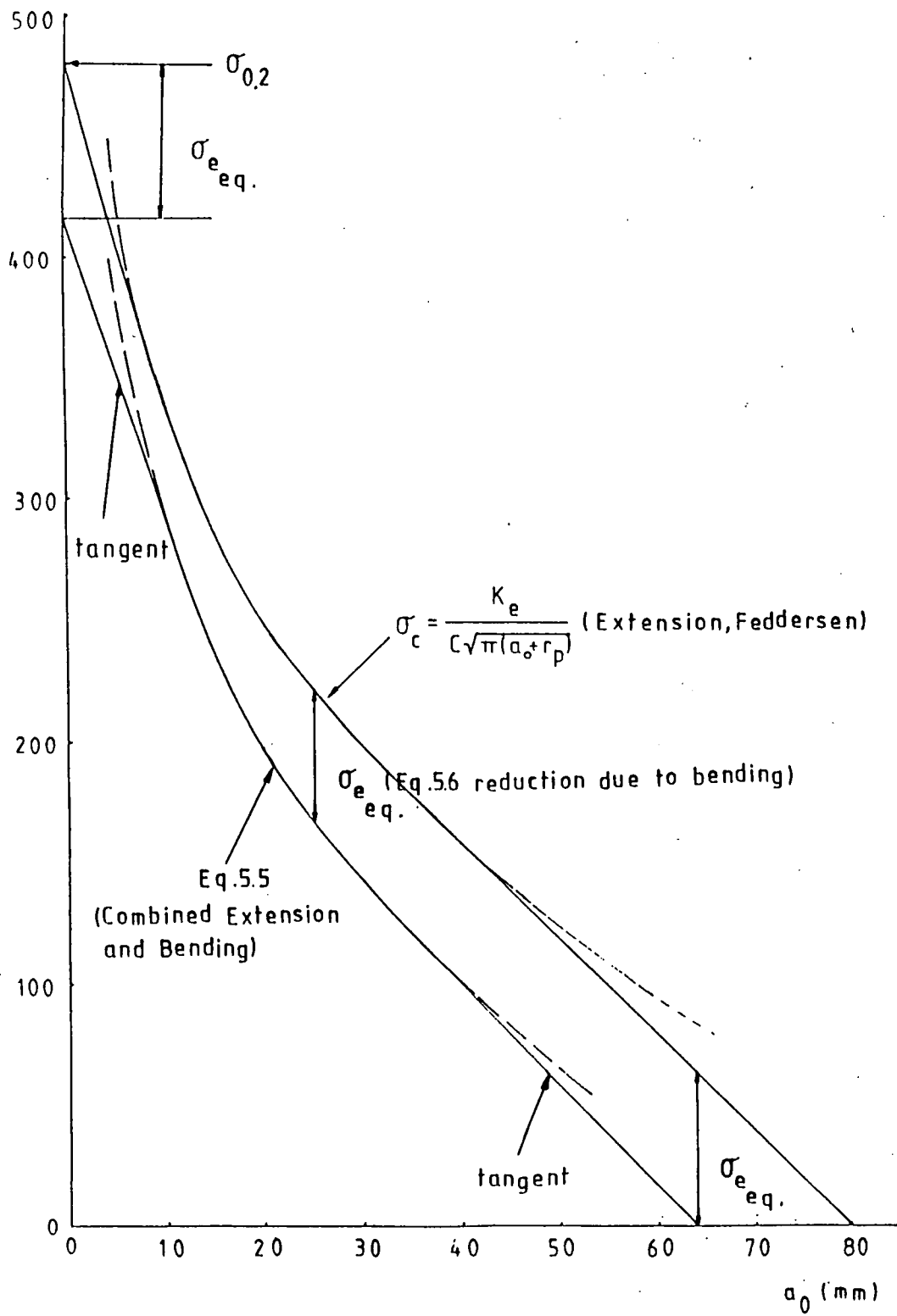
Fig.5.9 Representation of predictions in a
form similar to the Feddersen-diagram
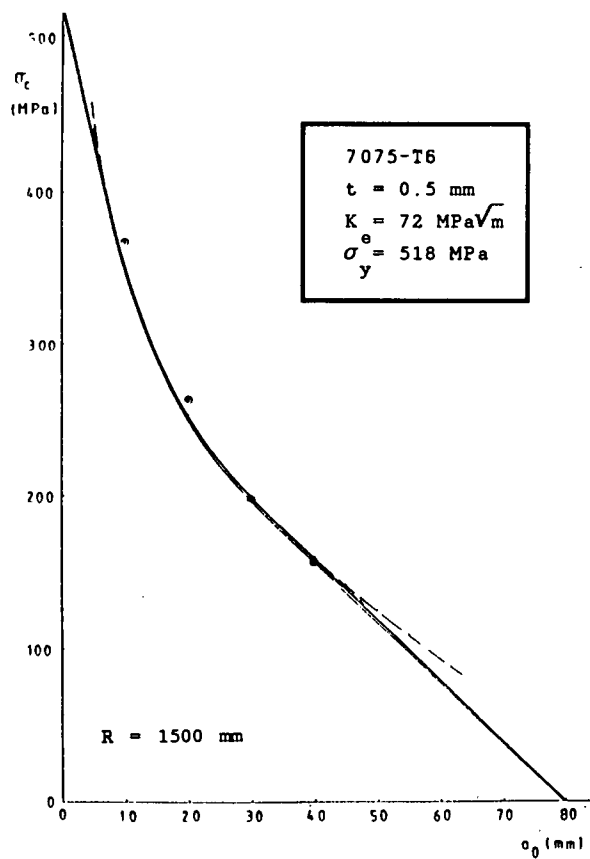
Fig.5.10a
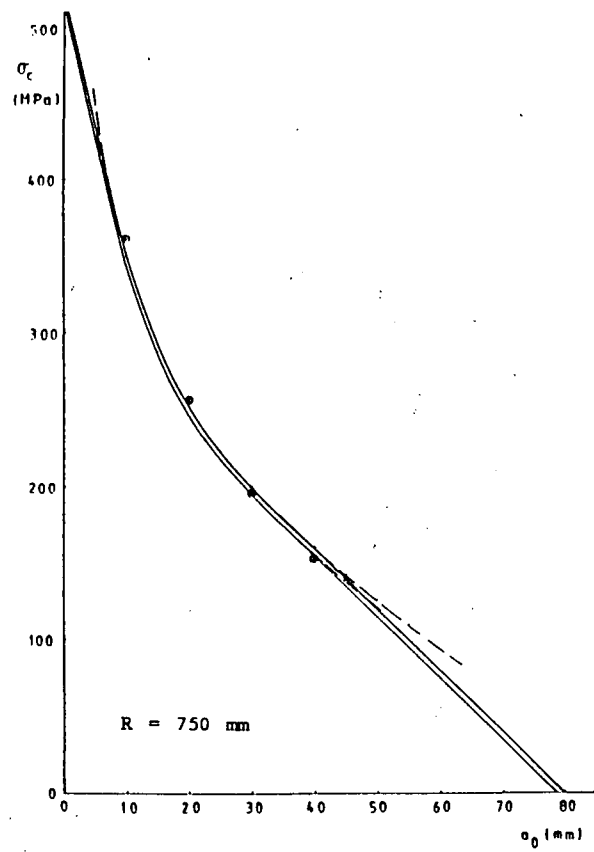
Fig.5.10b

Fig.5.10c

Fig.5.10d

170
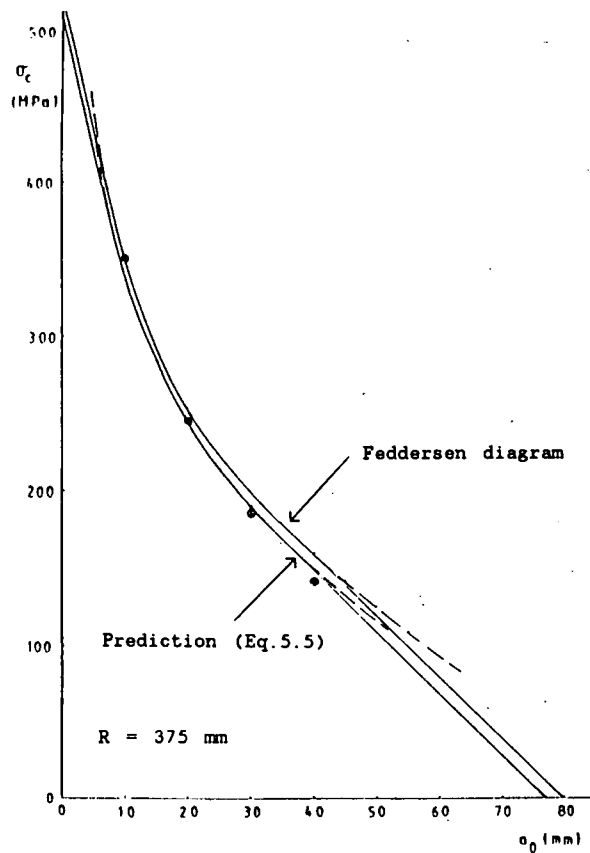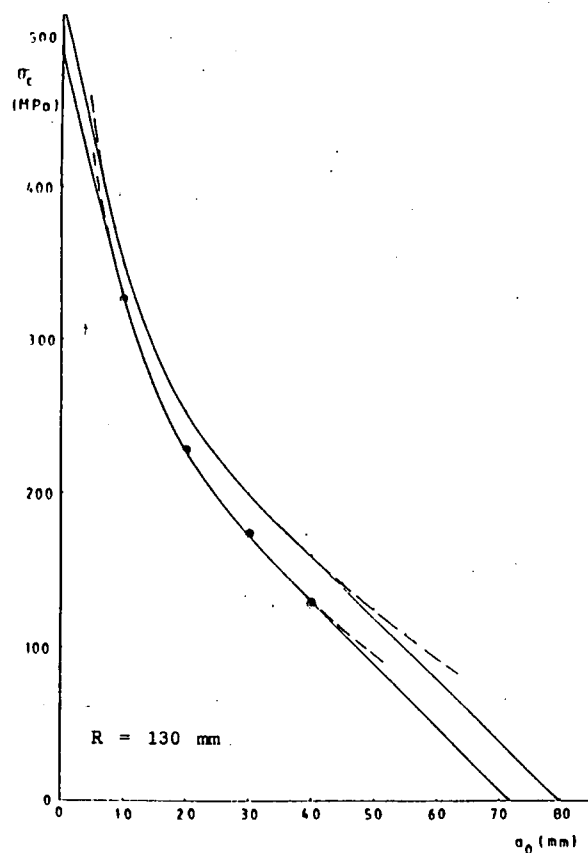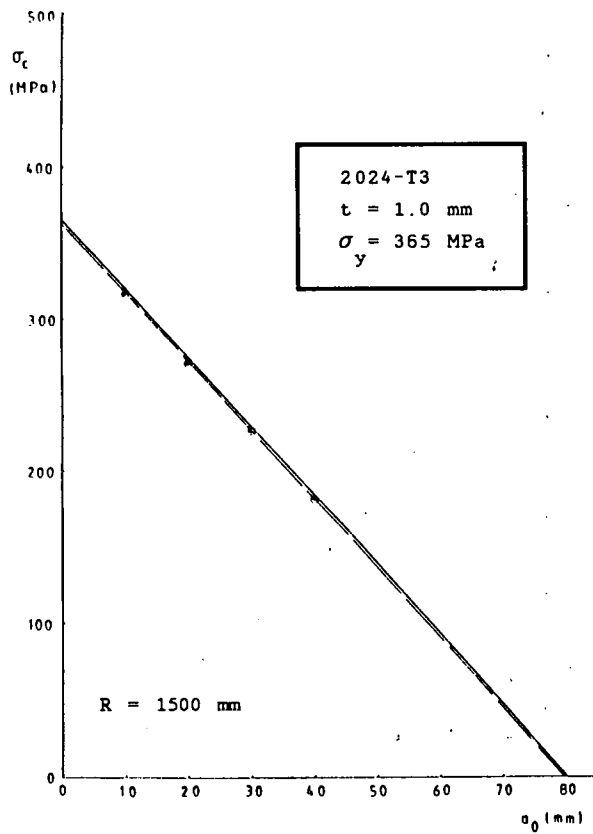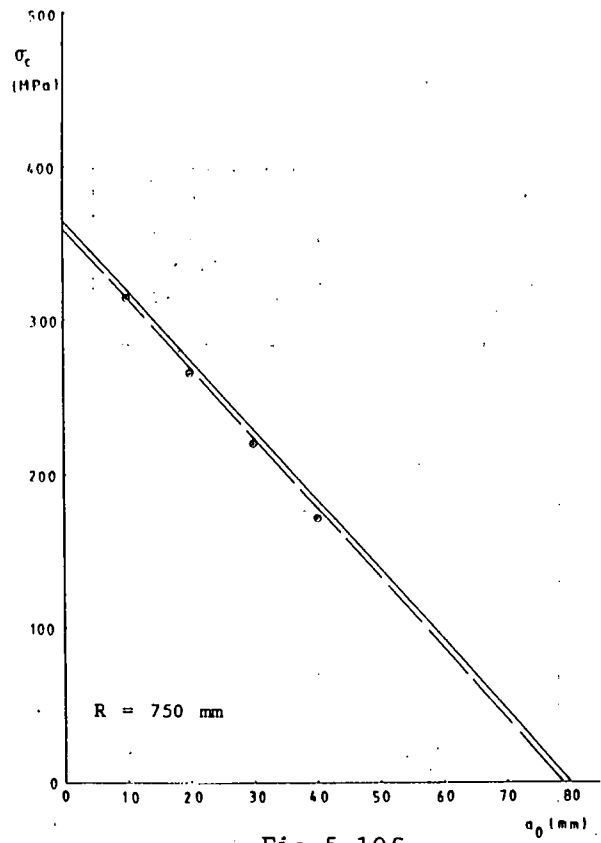
Fig.5.10e

Fig.5.10f

Fig.5.10g

Fig.5.10h

171

Fig.5.10i

7075-T6
t = 1.0 mm
K_e = 73 MPa√m
σ_y = 481 MPa

R = 1500 mm

σ_c (MPa)

a_0 (mm)

Fig.5.10j

R = 750 mm

Fig.5.10k

Feddersen diagram

Prediction (Eq.5.5)

R = 375 mm

Fig.5.10l

R = 130 mm

172
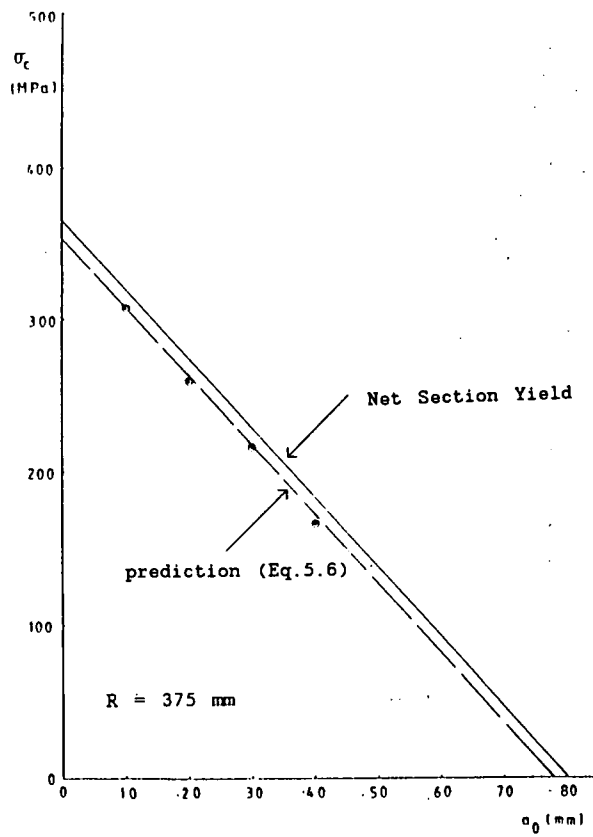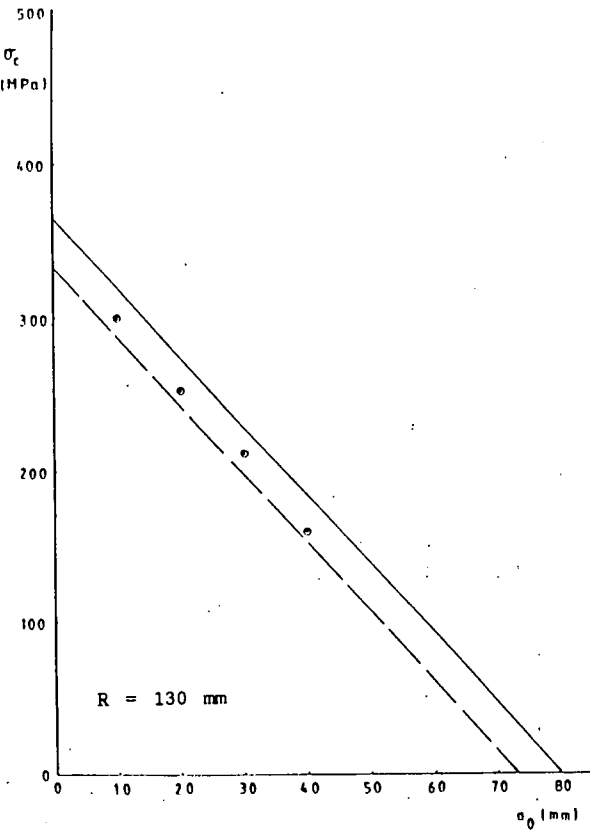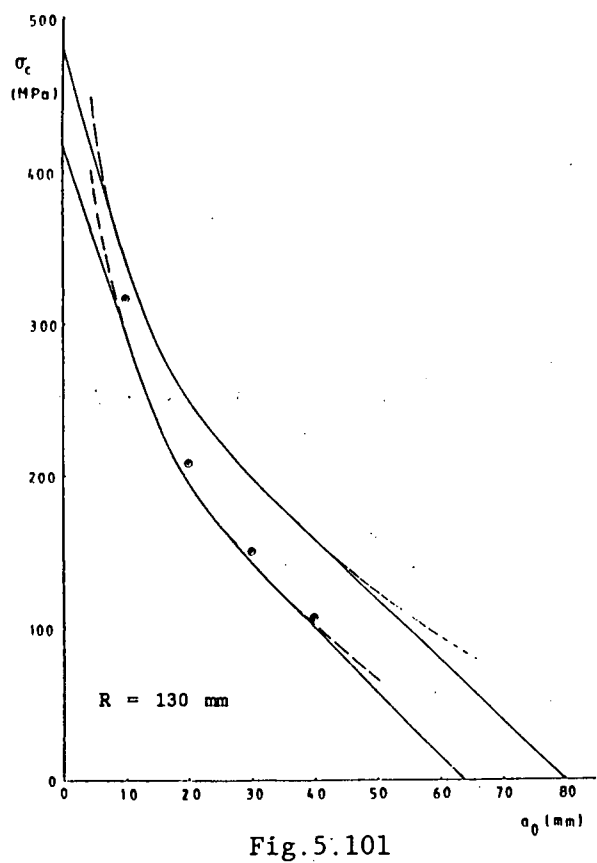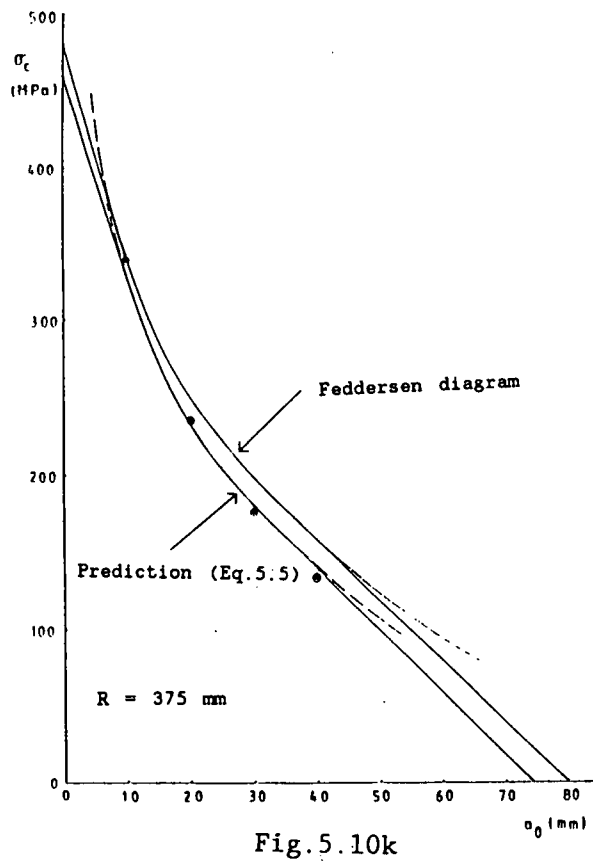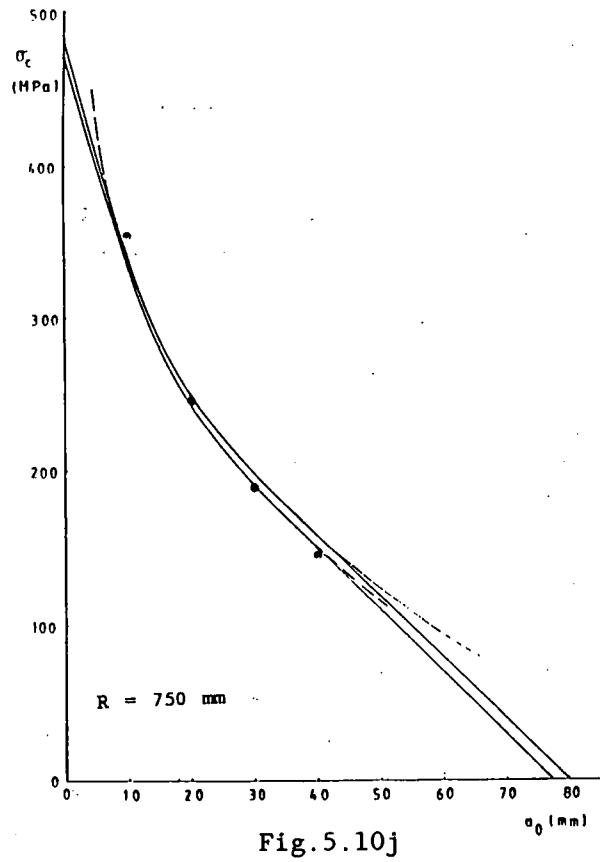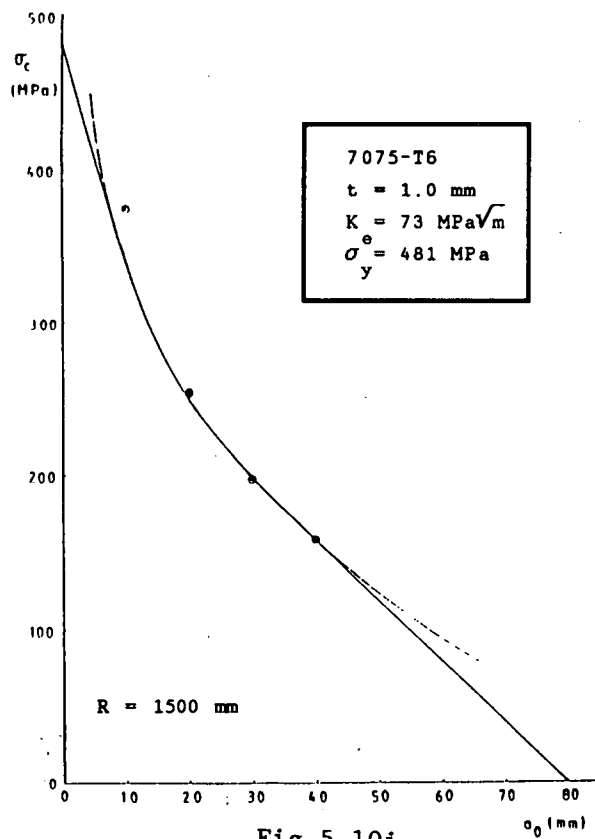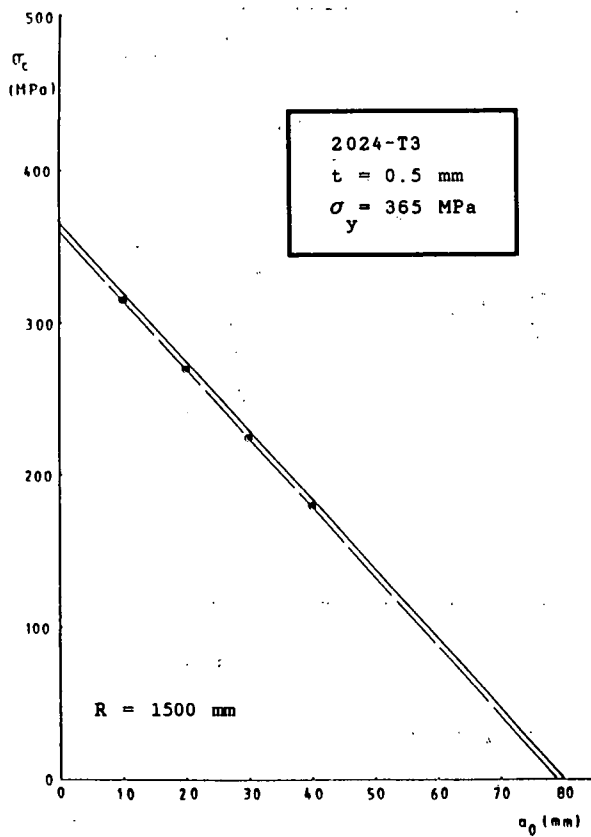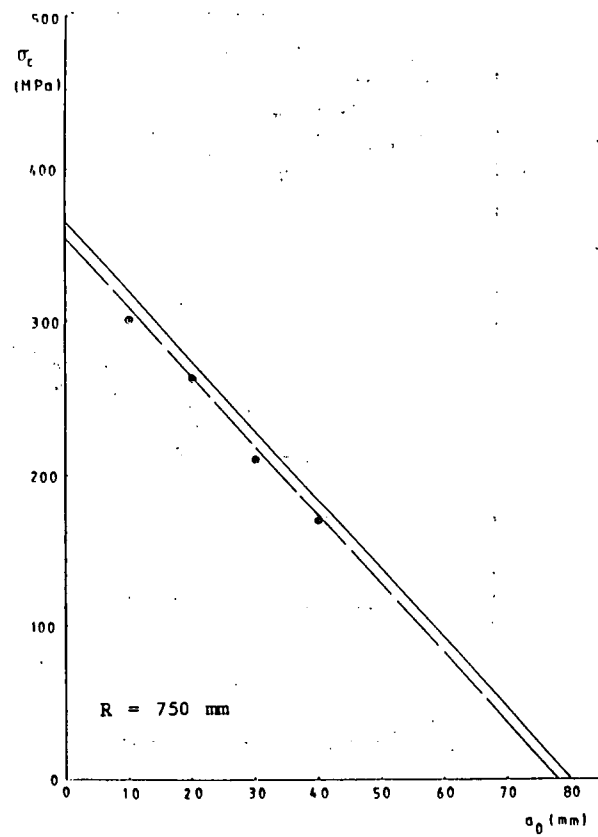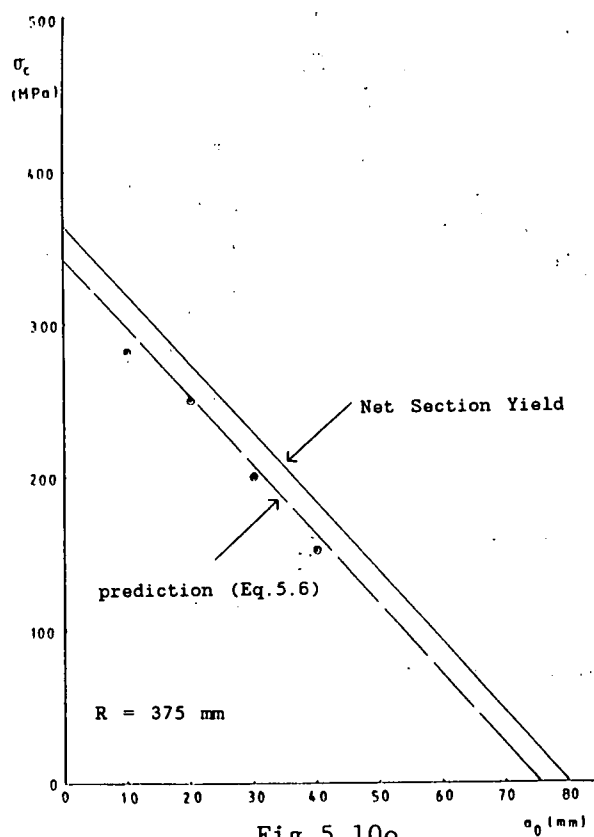
Fig.5.10m

Fig.5.10n

Fig.5.10o
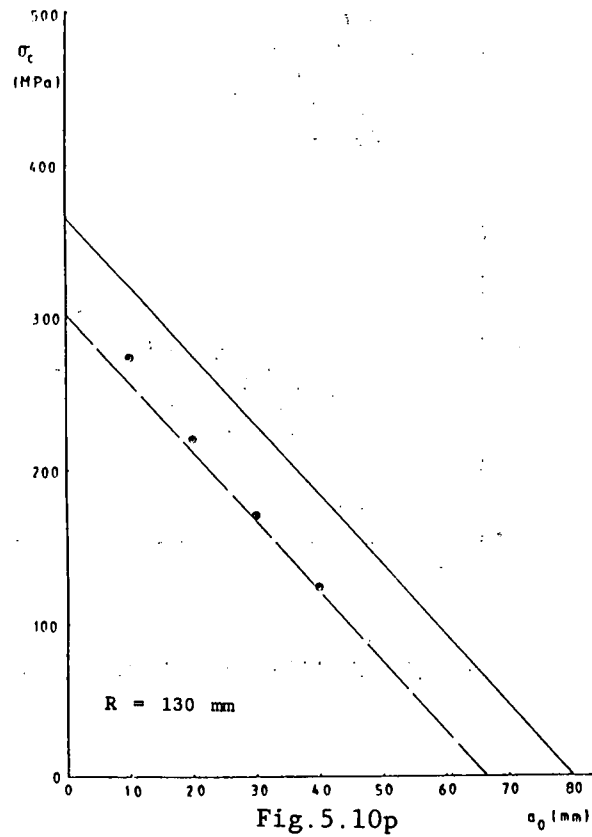
Fig.5.10p

Fig.5.10 Comparison between predicted residual strength
and test results of CETS
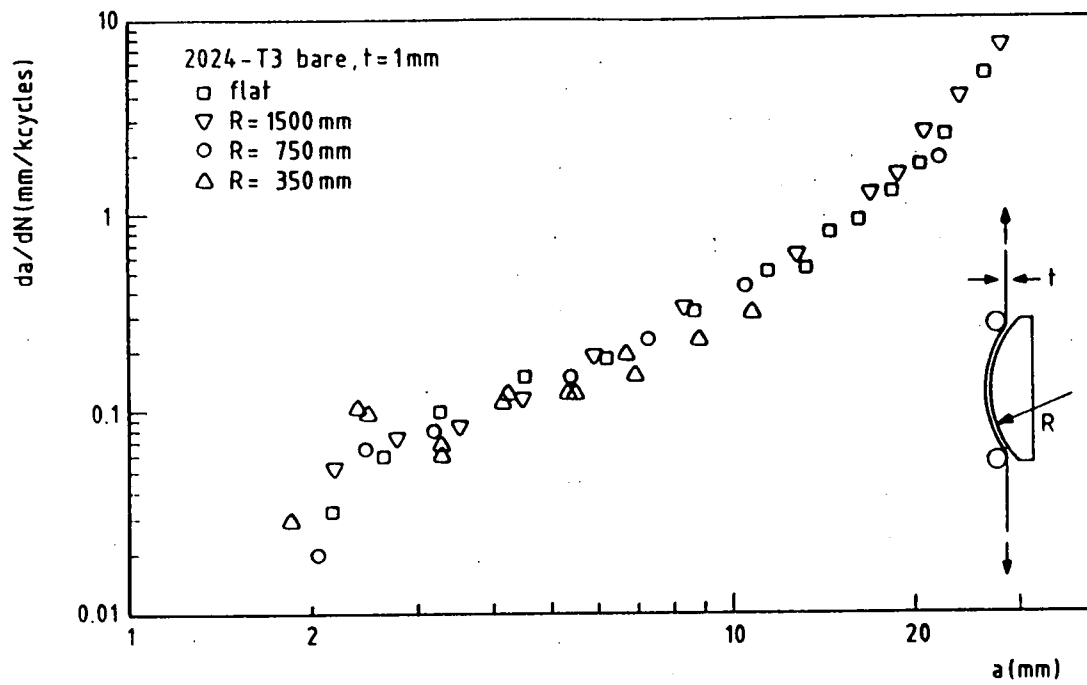
Fig.5.11 CETS CA fatigue test results for 2024-T3 t = 1.0 mm
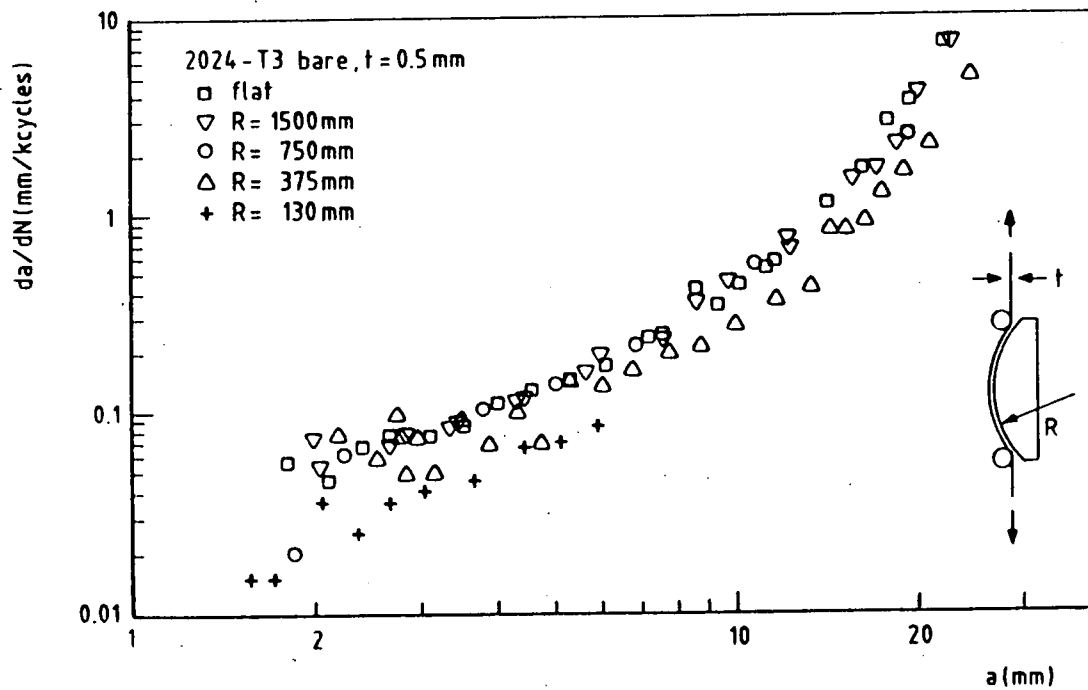
Fig.5.12 CETS CA fatigue test results for 2024-T3 t = 0.5 mm
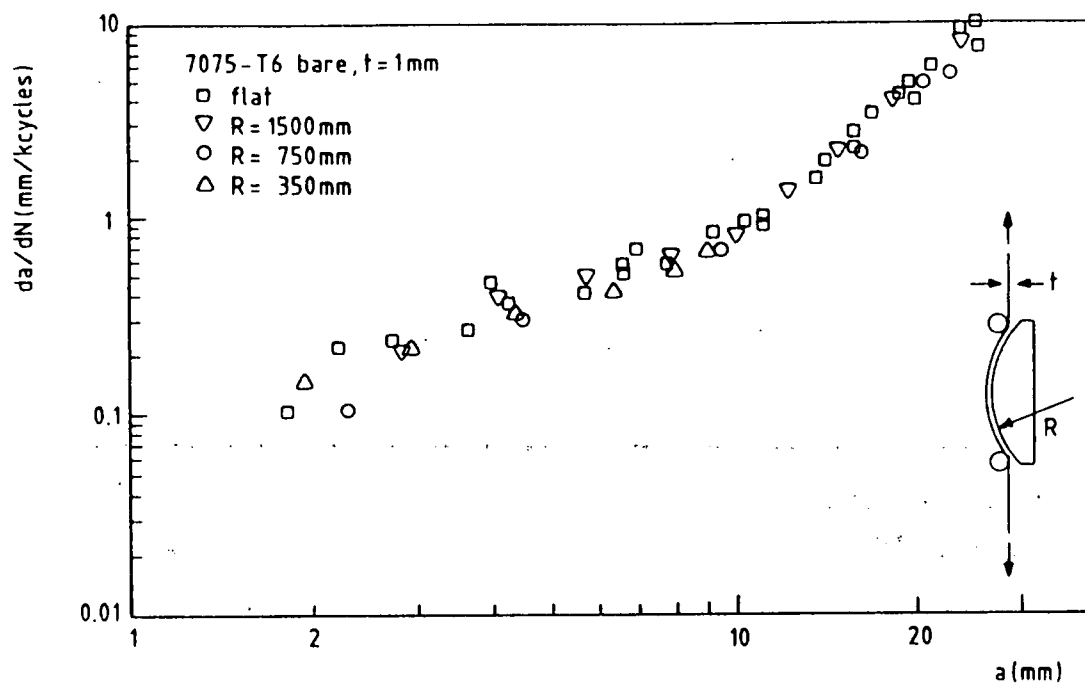
Fig.5.13 CETS CA fatigue test results for 7075-T6 t = 1.0 mm
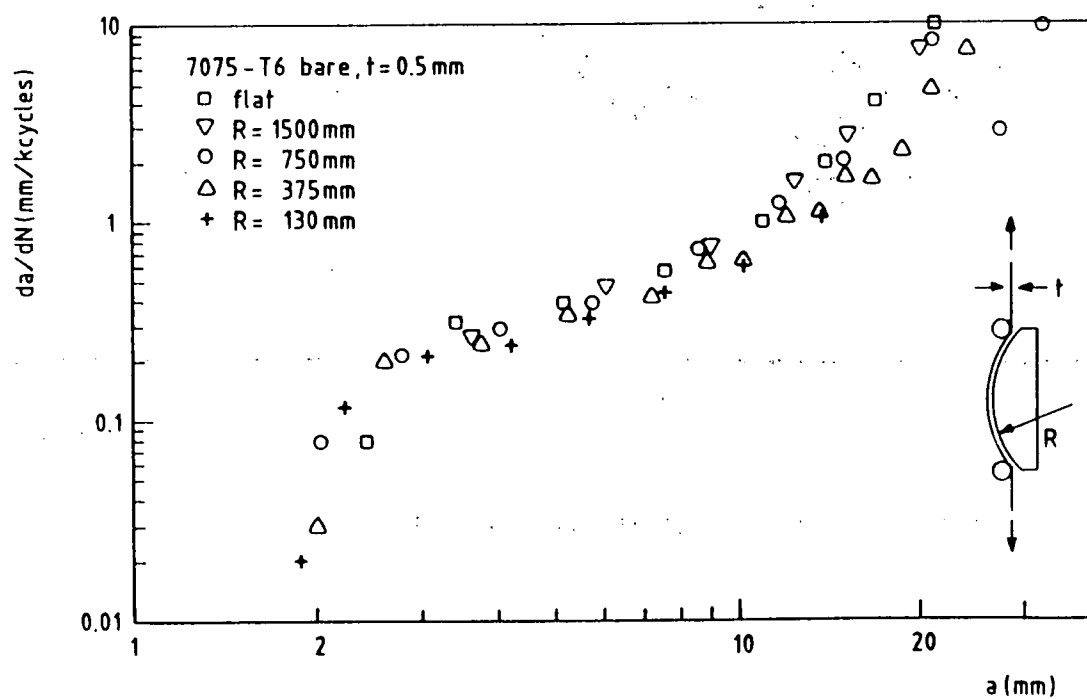
Fig.5.14 CETS CA fatigue test results for 7075-T6 t = 0.5 mm

175
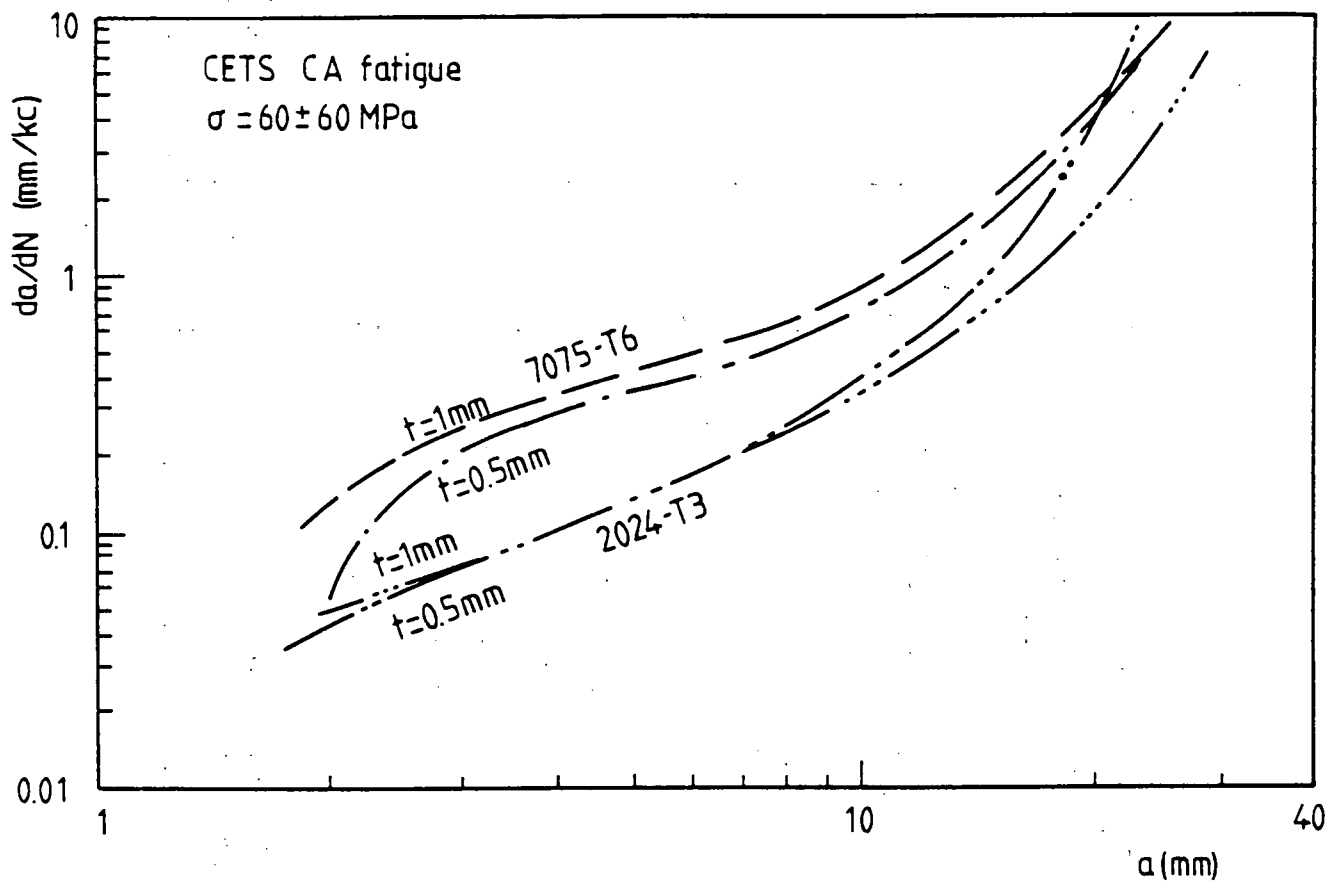
Fig.5.15 Average curves of figures 5.11 to 5.14
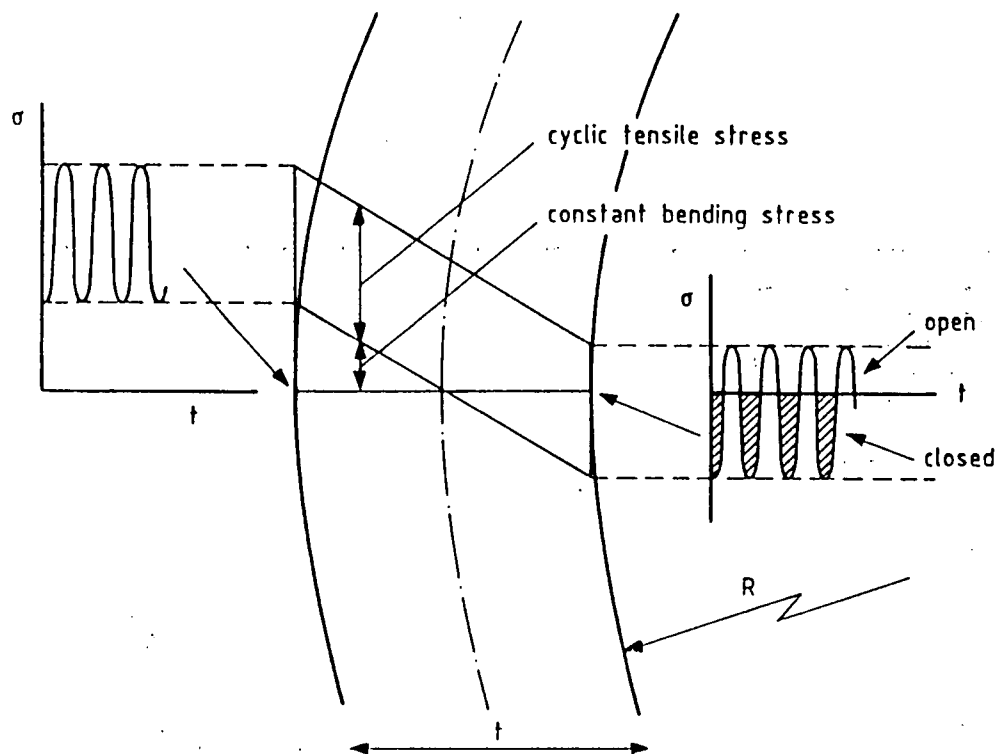
Fig.5.16 Partial crack closure in CETS due to constant bending
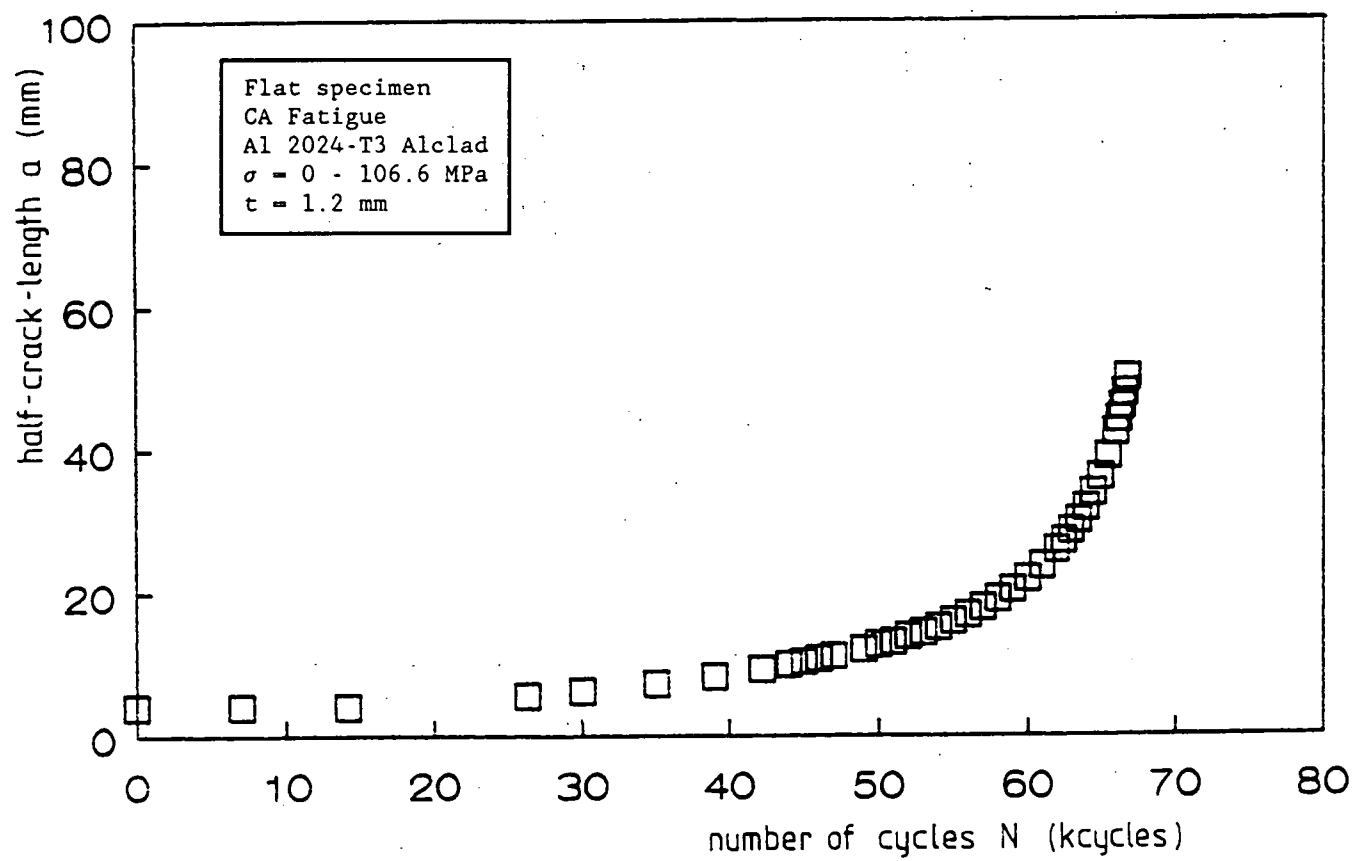
Fig.5.17 a-N curve of the reference test

178
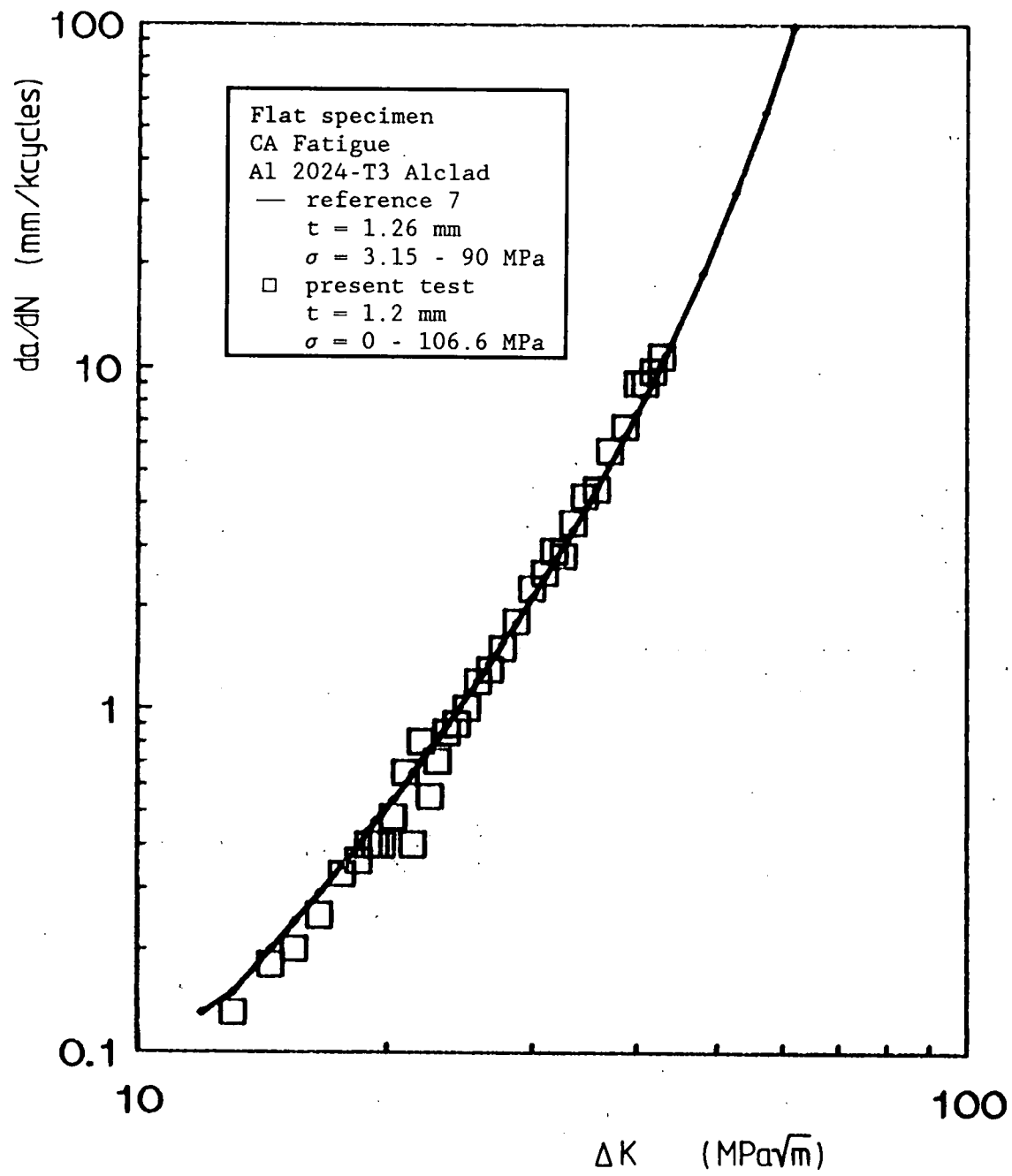
Fig.5.18 Comparison between da/dN-ΔK curves of
the reference test and the literature[7]
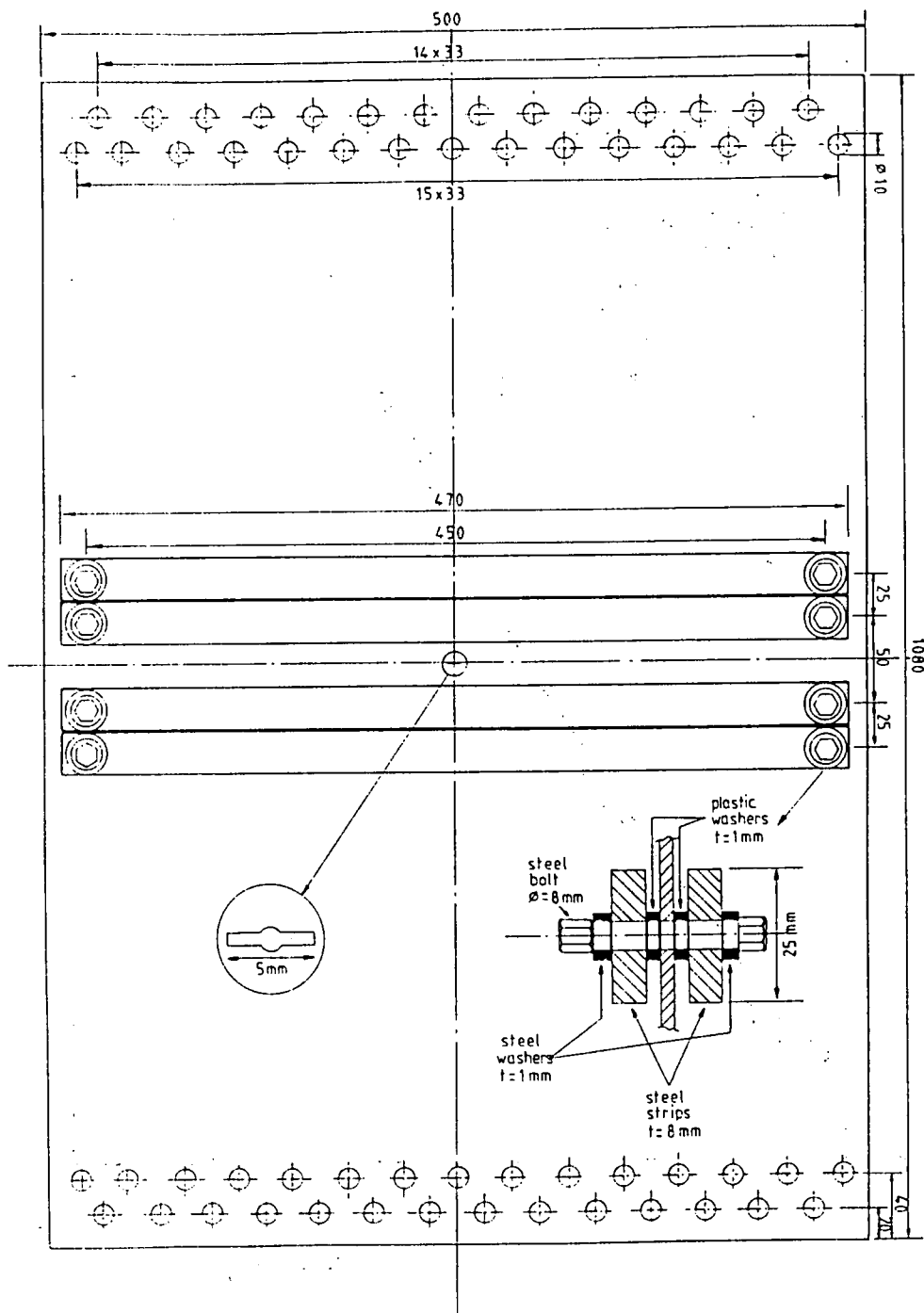
Fig.5.19 Specimen used for biaxial tests in PFSTS

180
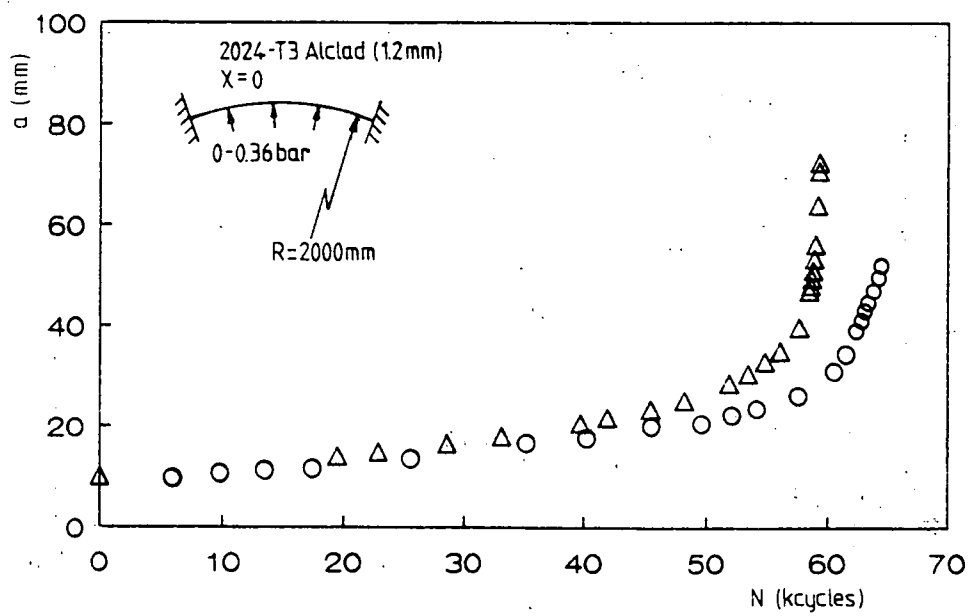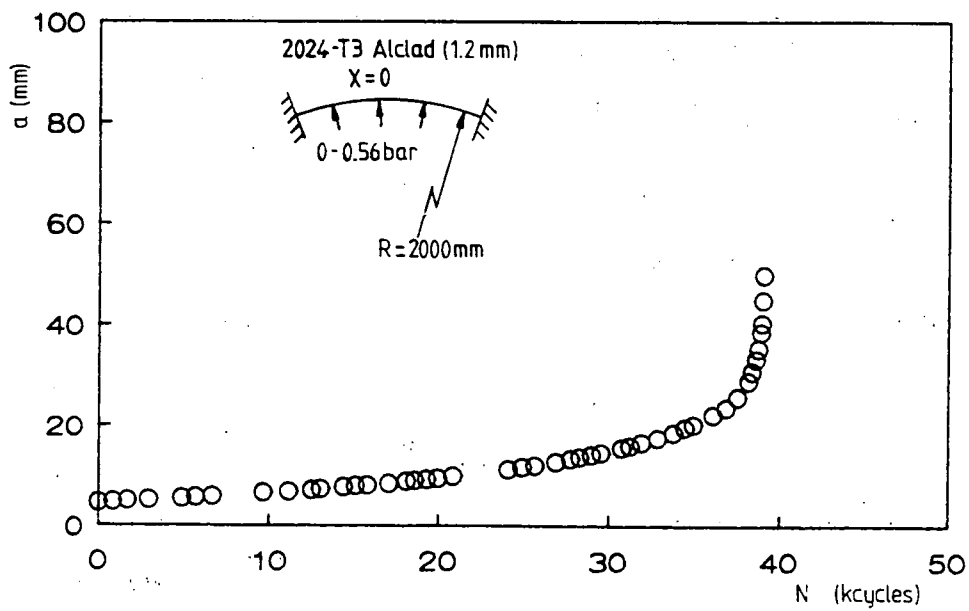
Fig.5.20a

Fig.5.20b

Fig.5.20 Crack growth curves of curved panels loaded
under cyclic air pressure, uniaxial loading

181
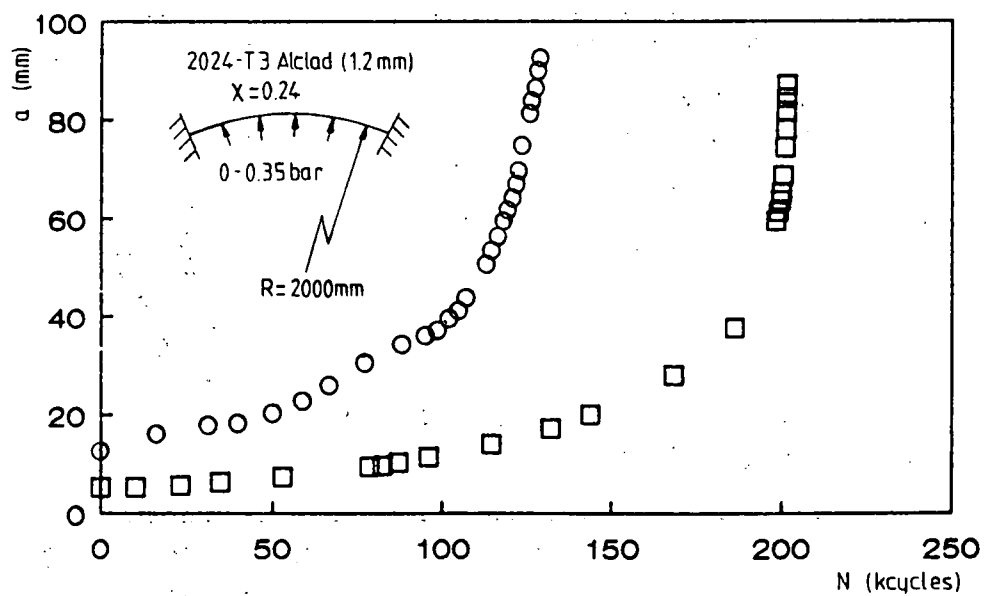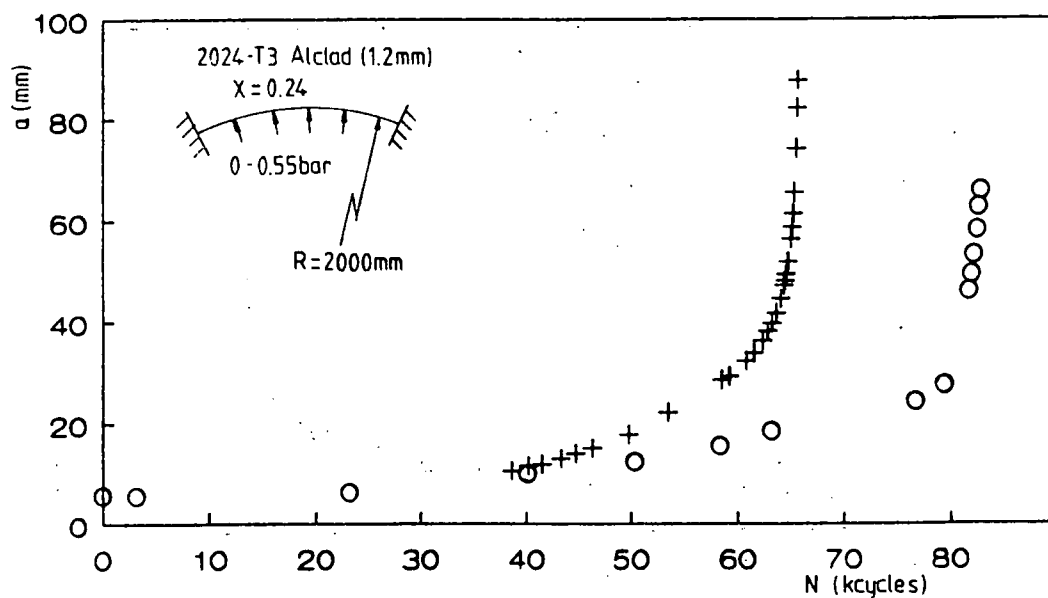
Fig.5.21a

Fig.5.21b

Fig.5.21 Crack growth curves of curved panels loaded
under cyclic air pressure, biaxial loading
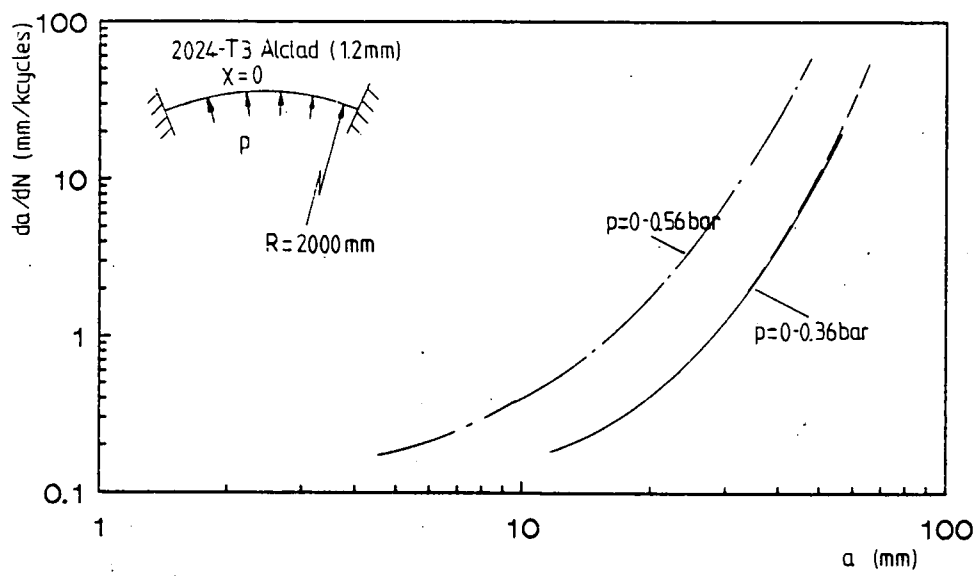
Fig.5.22a uniaxial loading
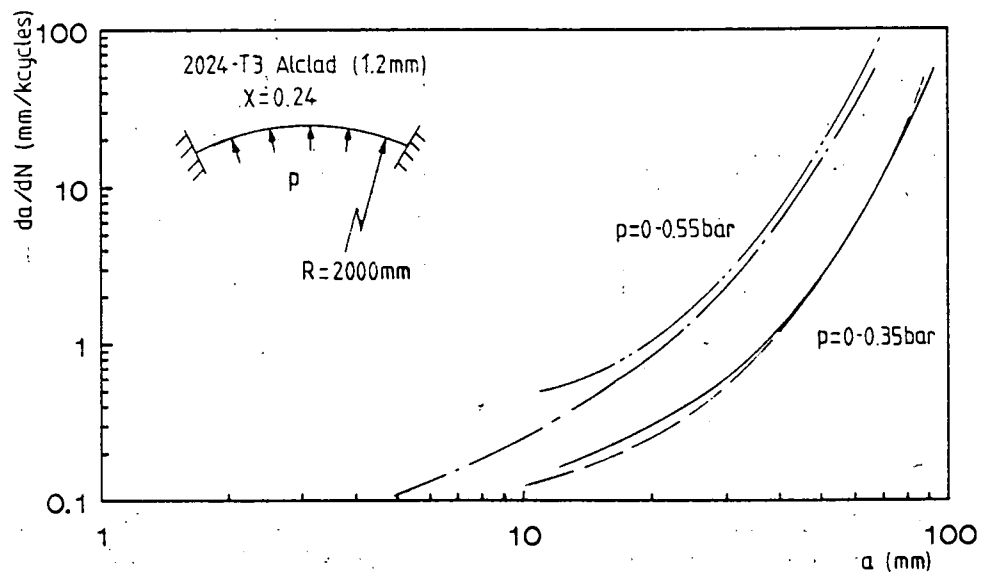
Fig.5.22b biaxial loading

Fig.5.22 Crack growth rates in curved panels
loaded under cyclic air pressure
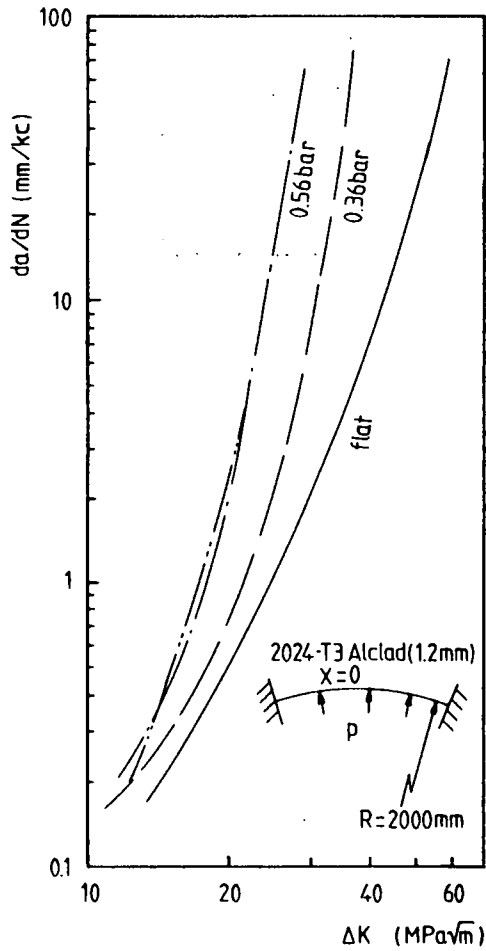
Fig.5.23 Crack growth curves of curved panels loaded under cyclic air pressure. Uniaxial loading.
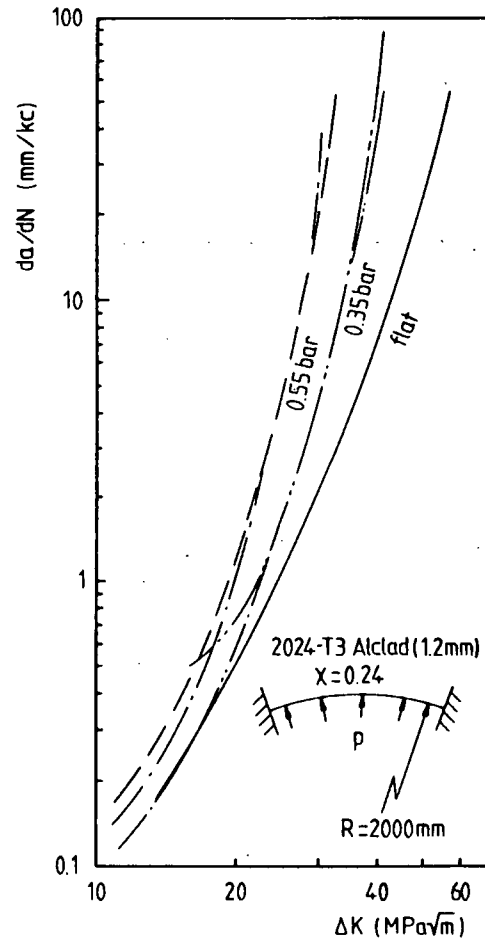
Fig.5.24 Crack growth curves of curved panels loaded under cyclic air pressure. Biaxial loading.
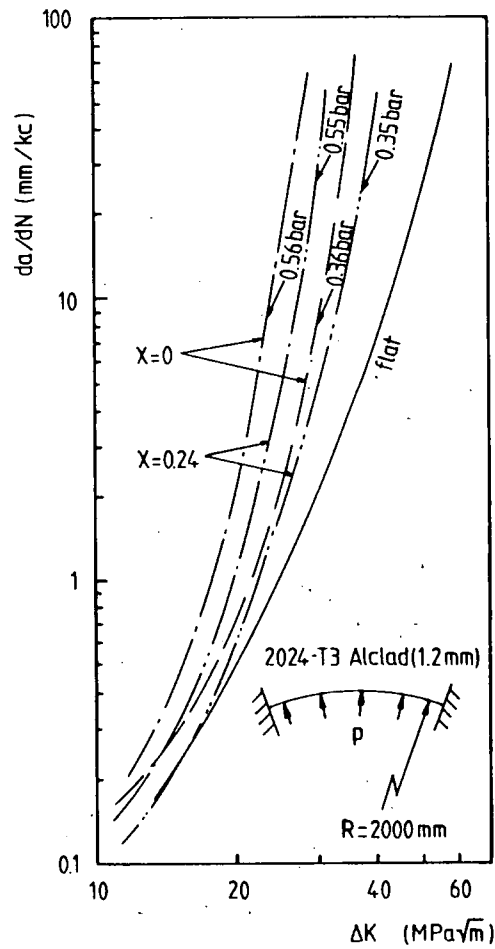
Fig.5.25 Comparison of crack growth rates in curved
panels under cyclic air pressure.
Effects of pressure level and biaxiality

135

signal of displacement
transducer

pressurized specimen
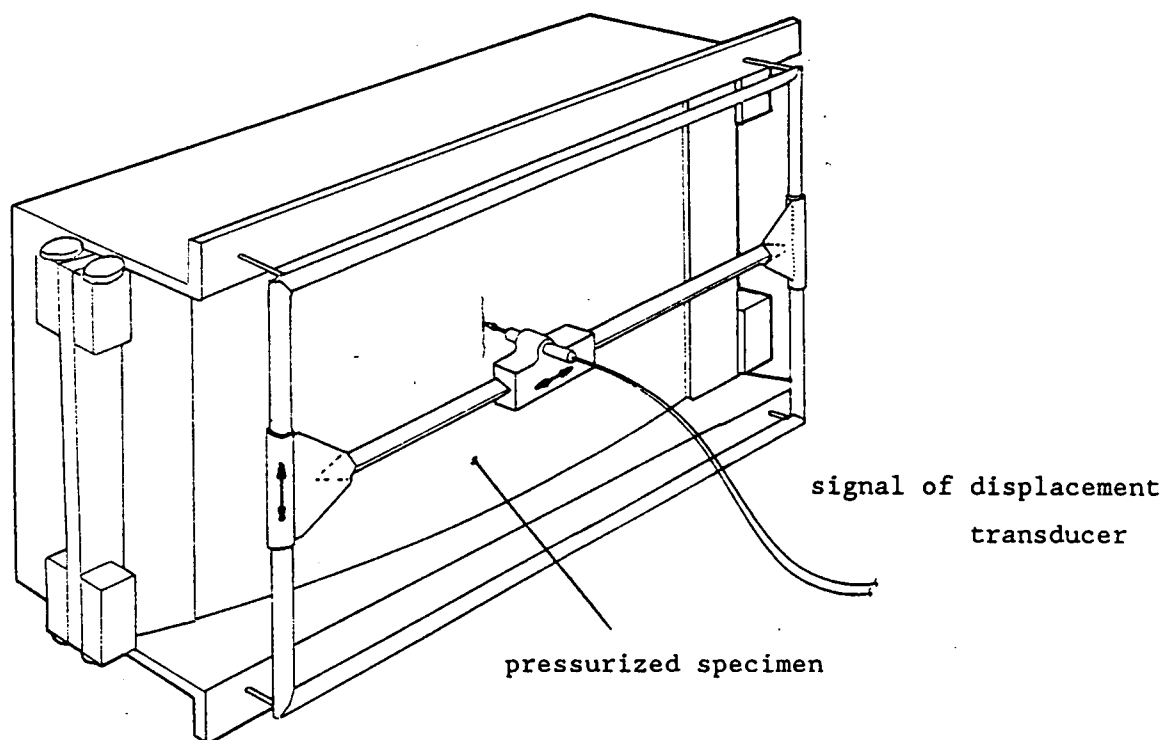
Fig.5.26 Sketch of arrangement for out-of-plane deformation measurements

150 mm

displament transducer

specimen

$\dfrac{AB}{AB'} \cong \cos \dfrac{150}{2000} = 1.0028$

location
of crack

B

B

A

R = 2000mm
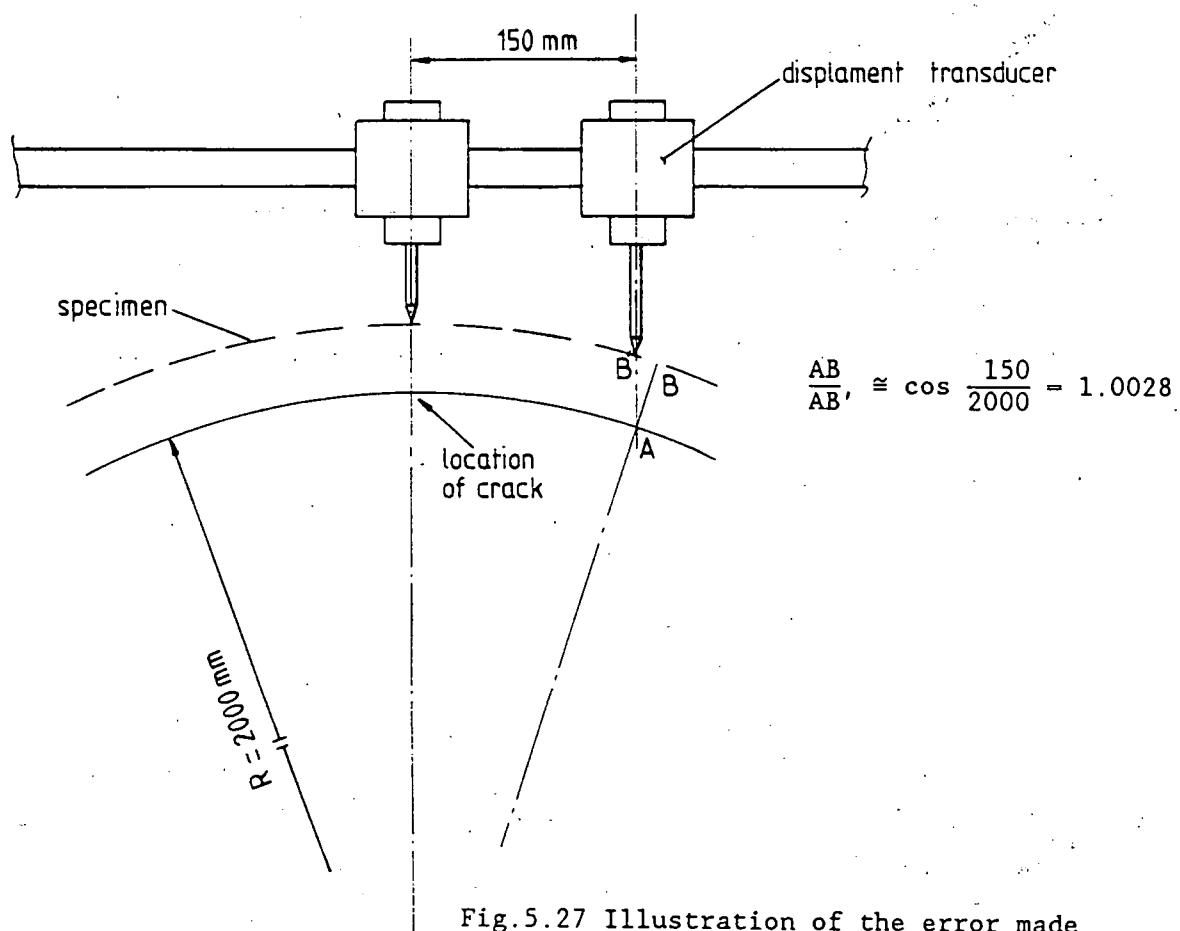
Fig.5.27 Illustration of the error made
during out-of-plane deformation
measurements
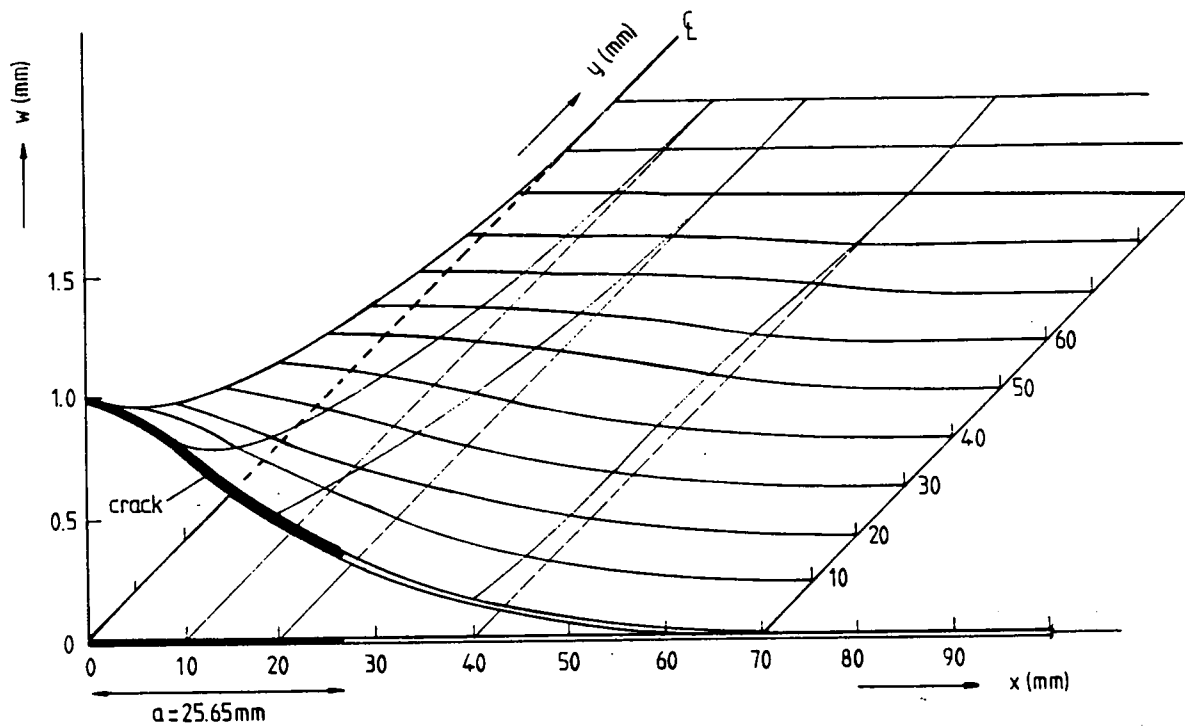
Fig.5.28 Out-of-plane deformation field around a crack of 25.65mm at p=0.55bar
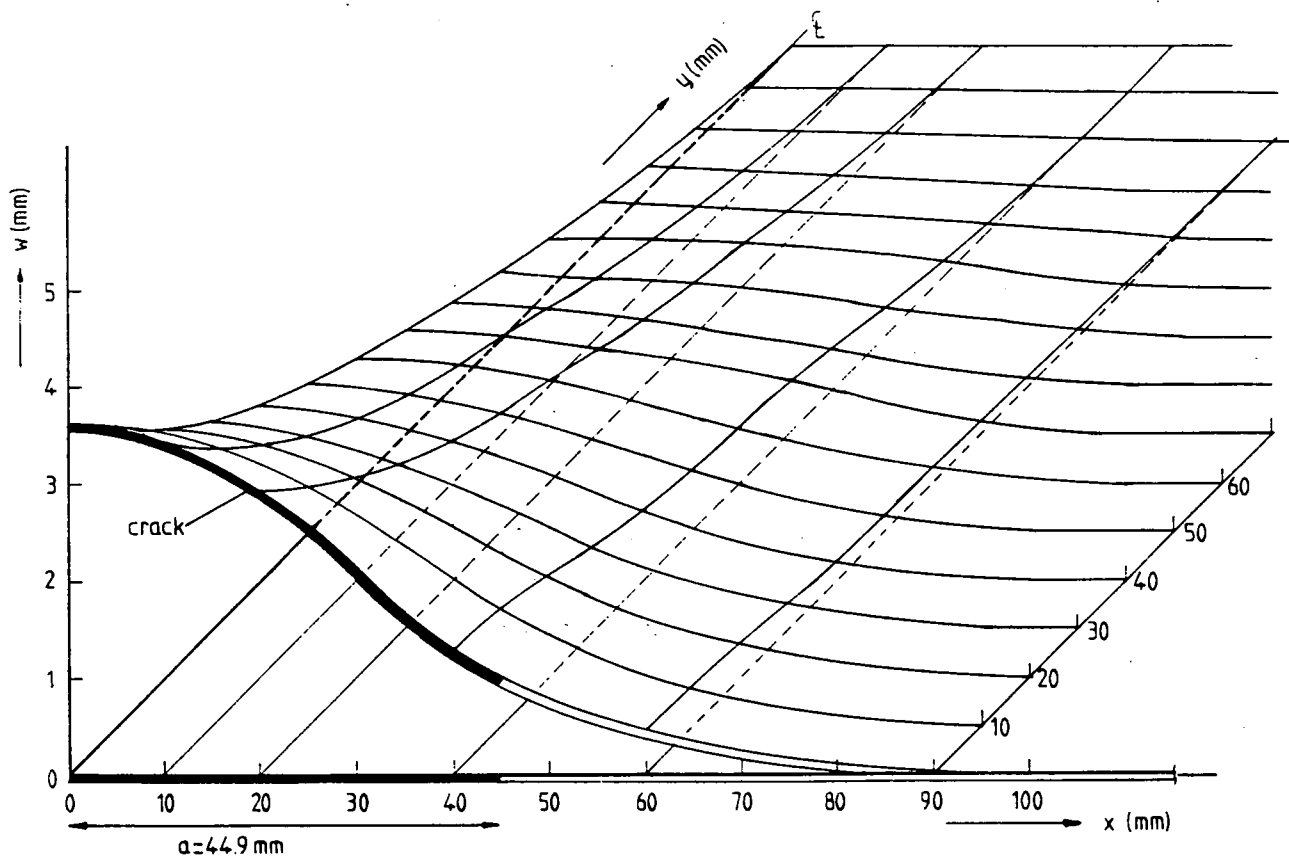
Fig.5.29 Out-of-plane deformation field around a crack of 44.9 mm at p=0.55bar
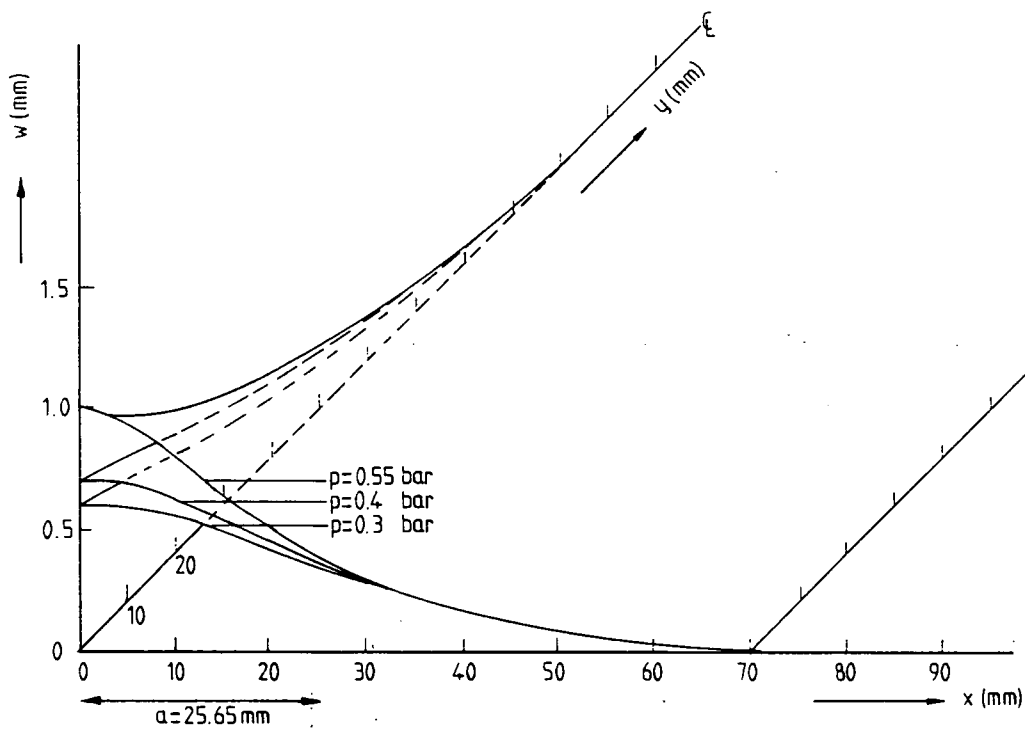
Fig.5.30 Influence of internal pressure on the out-of-plane
deformation field around a crack of 25.65 mm
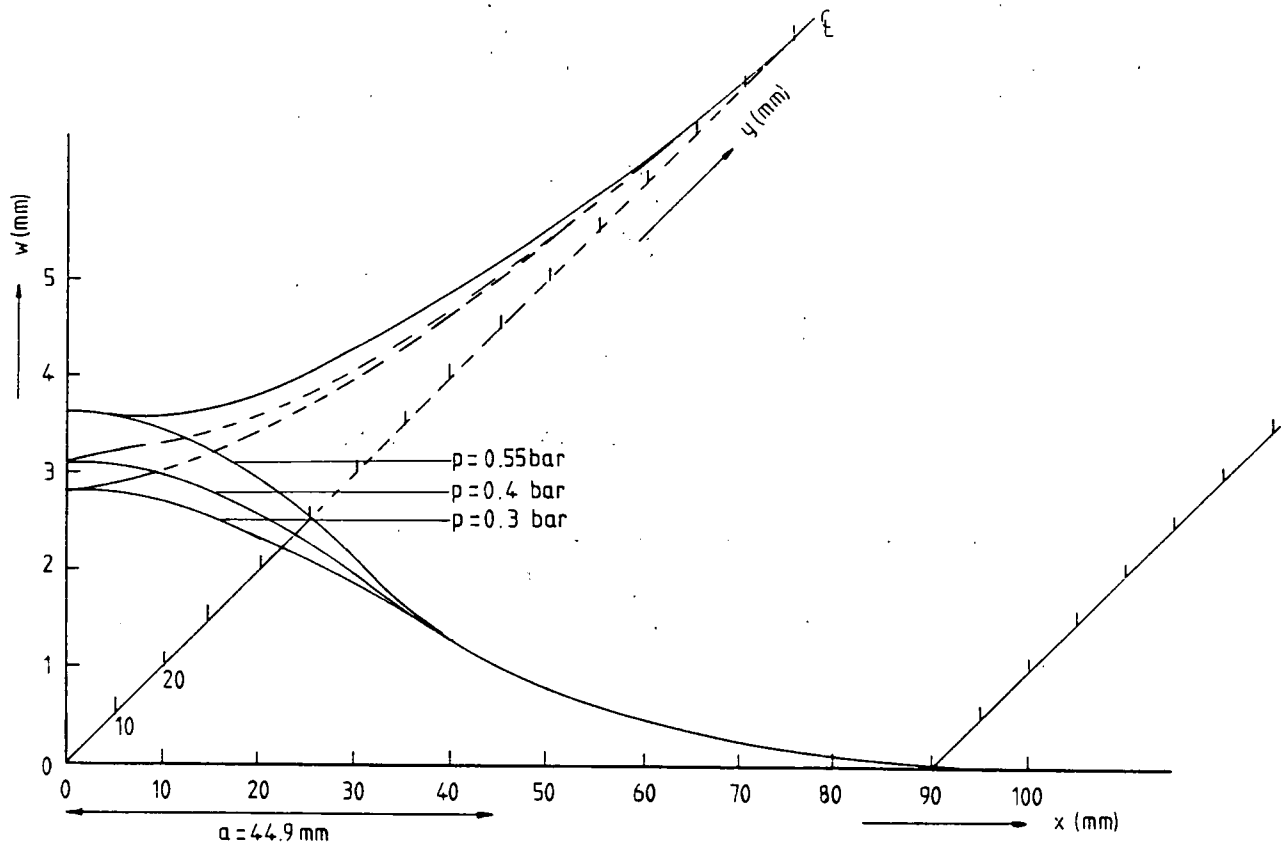
Fig.5.31 Influence of internal pressure on the out-of-plane
deformation field around a crack of 44.9 mm
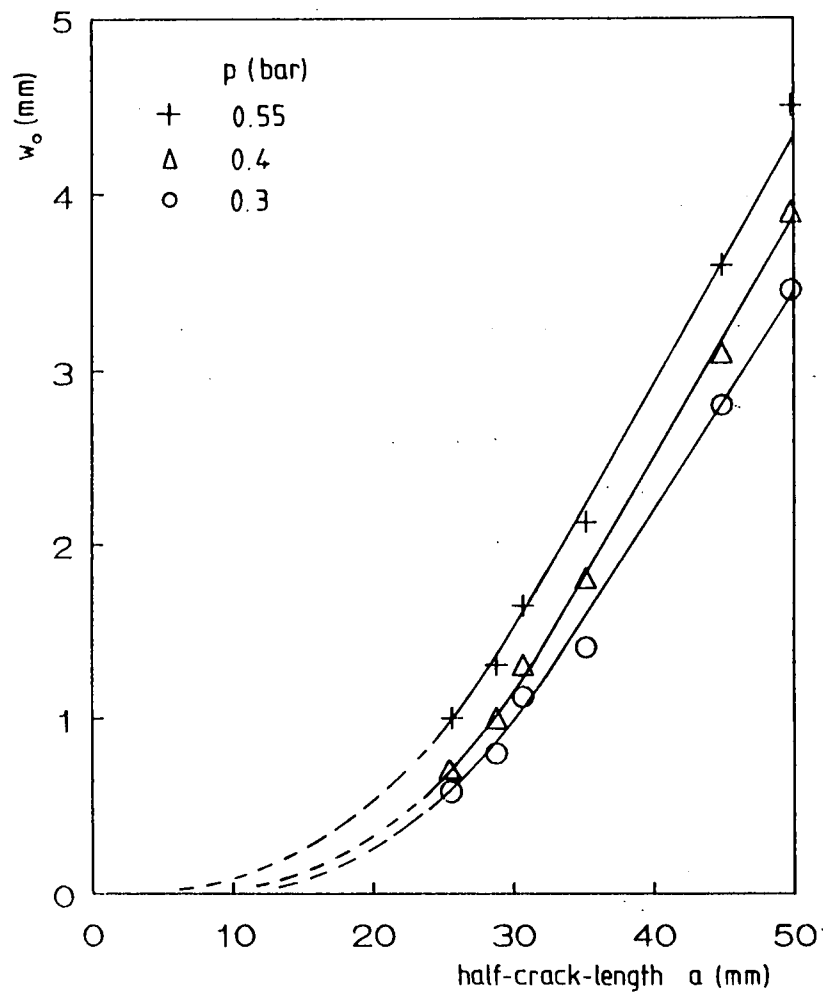
Fig.5.32 Out-of-plane deformation of the center
of the crack w_0 as a function of the
half-crack-length a

190
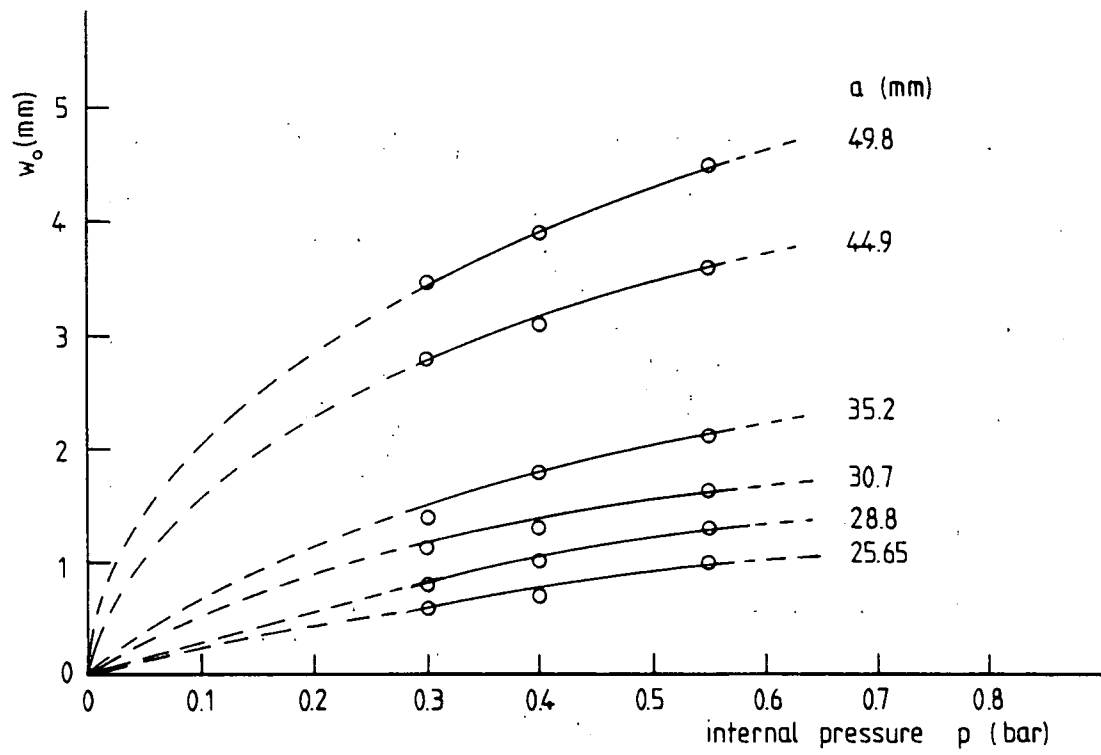
Fig.5.33 Out-of-plane deformation of the center of the crack w_0 as a function of internal pressure p
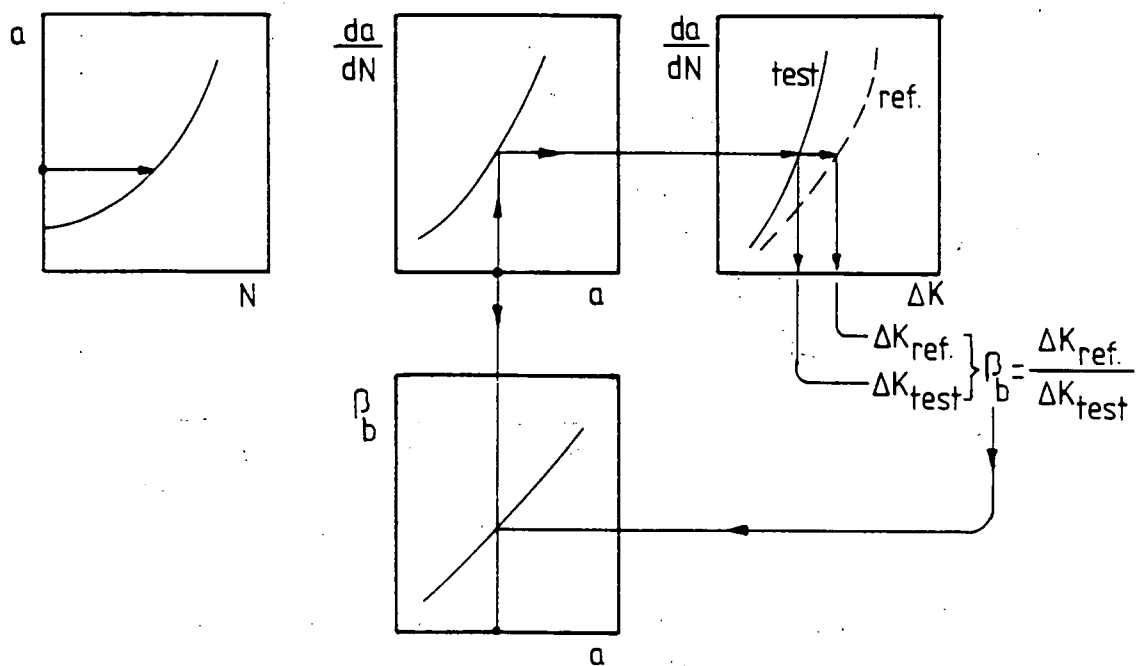
Fig.5.34 The similarity concept[8]
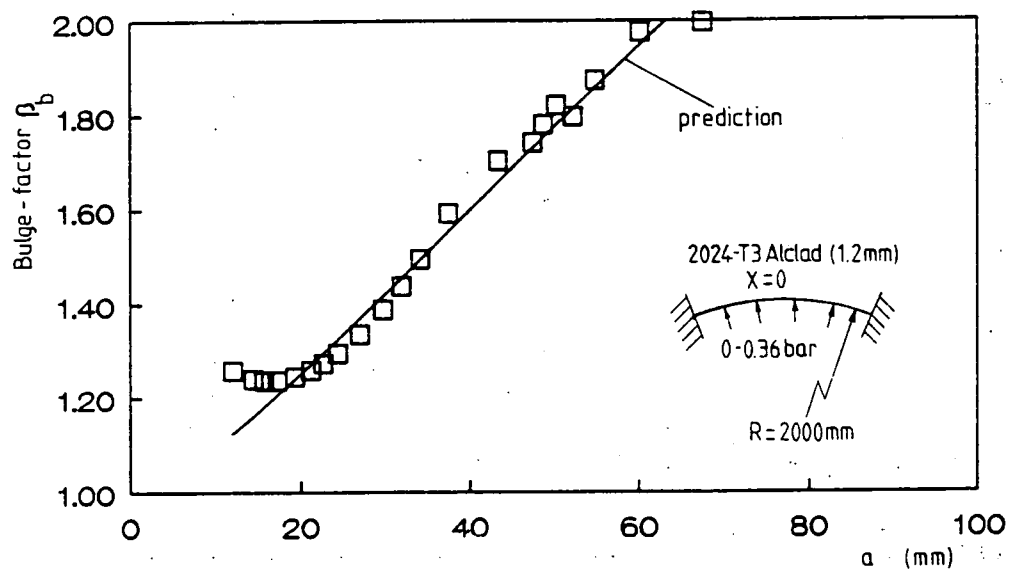
Fig.5.35a
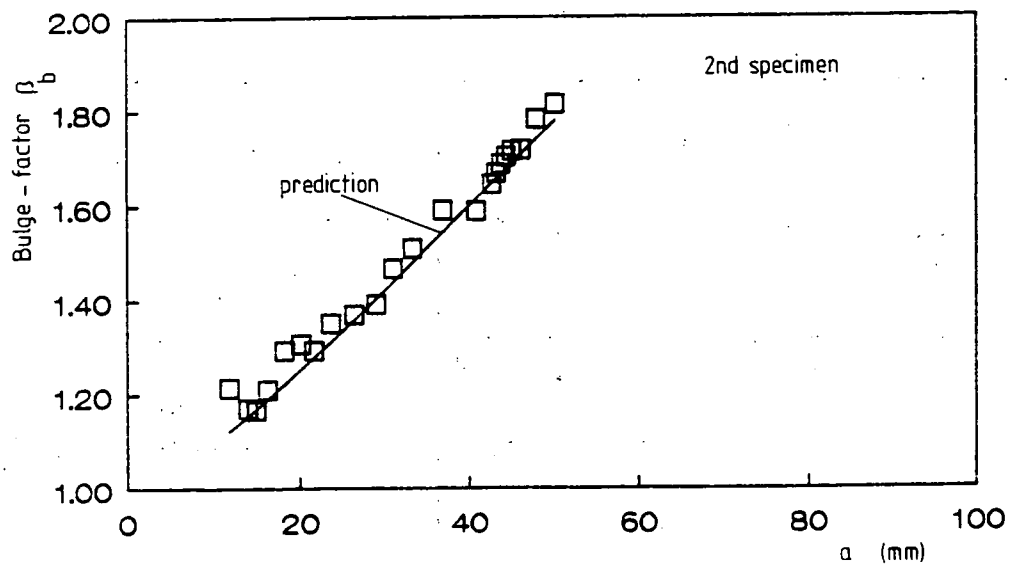
Fig.5.35b

Fig.5.35 Comparison between empirical and predicted bulge factors, uniaxial loading, $p_{max} = 0.36$ bar
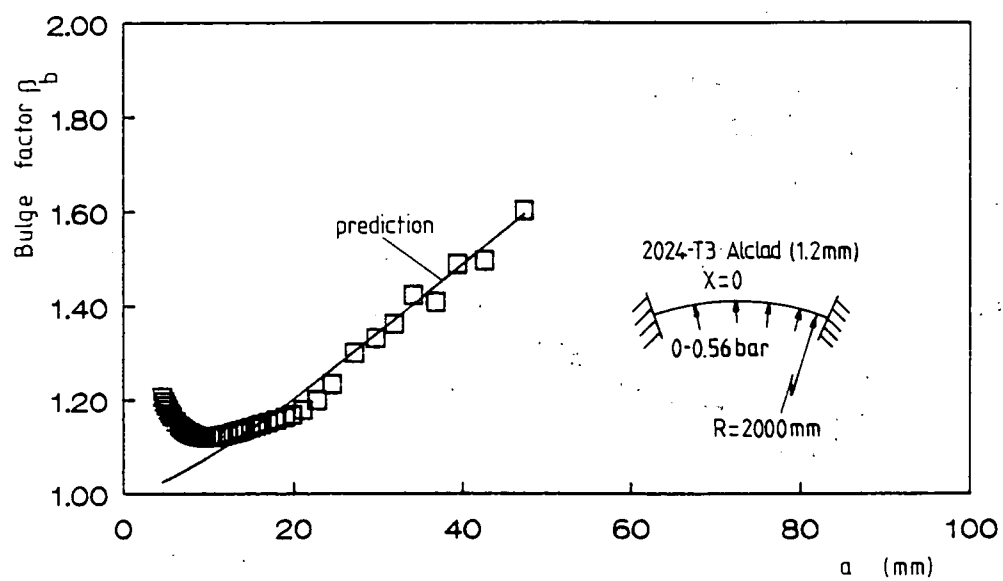
Fig.5.36 Comparison between empirical and predicted bulge factors, uniaxial loading, $p_{max} = 0.56$ bar
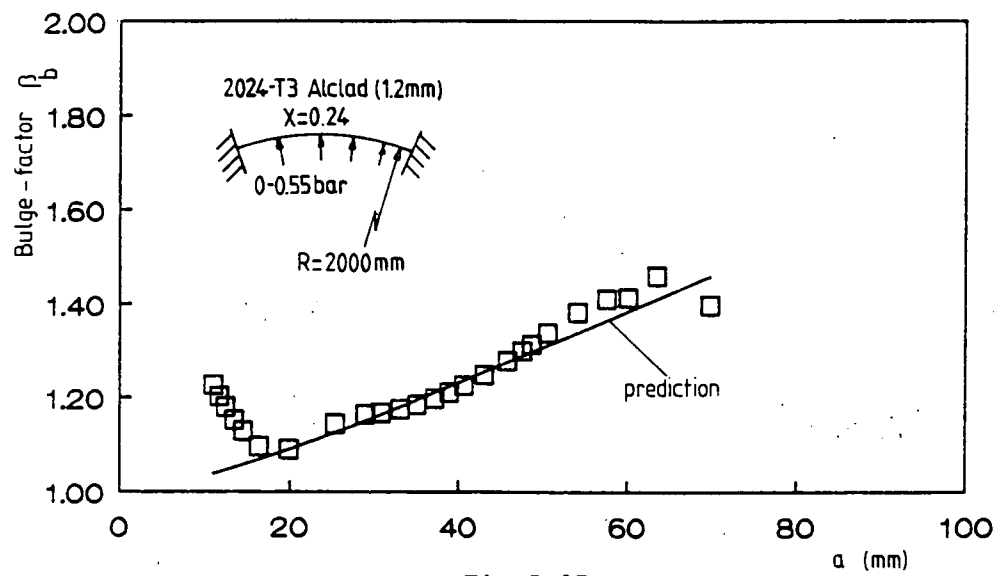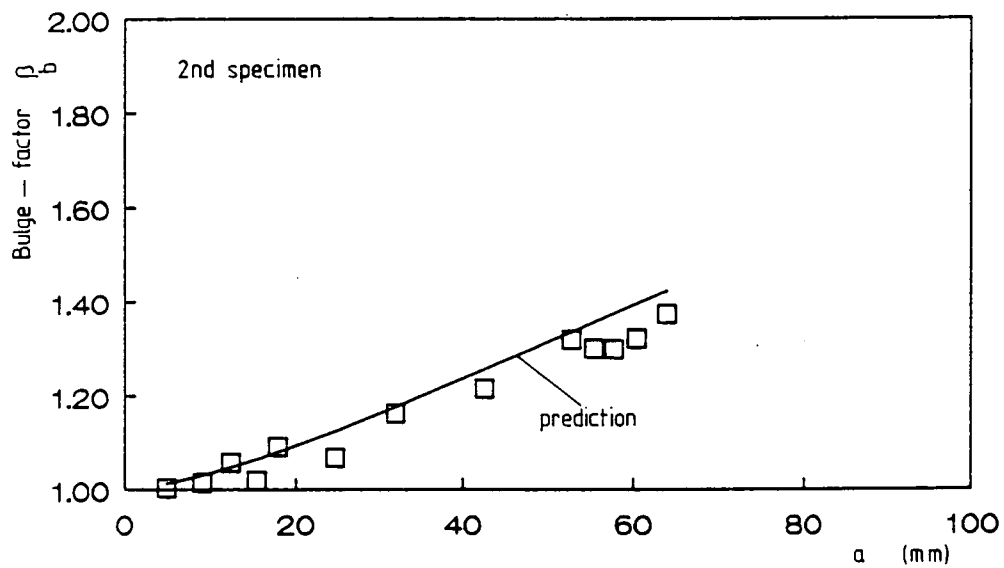
Fig.5.37a

Fig.5.37b

Fig.5.37 Comparison between empirical and predicted bulge factors, biaxial loading, p_{max} = 0.55 bar
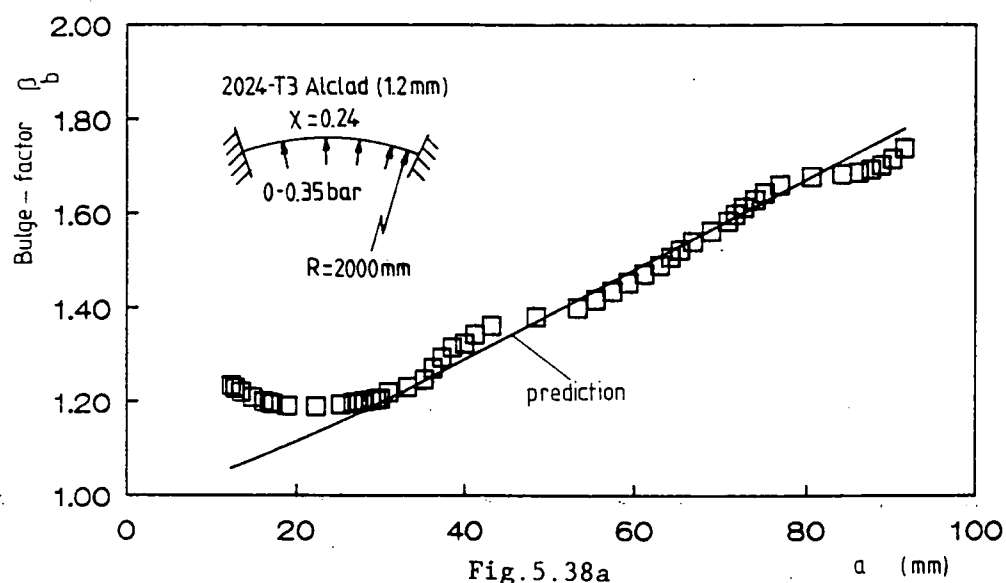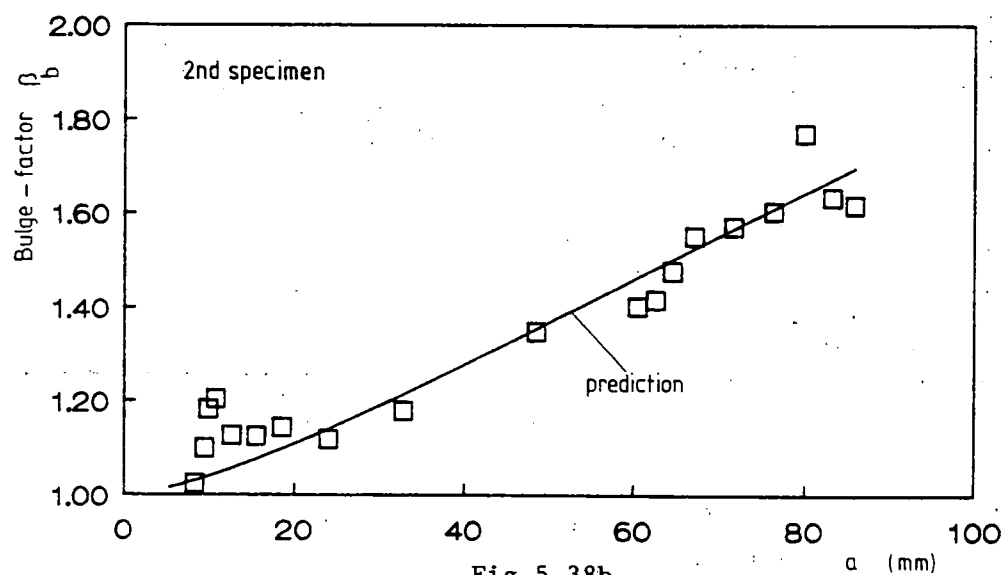
Fig.5.38a

Fig.5.38b

Fig.5.38 Comparison between empirical and predicted bulge factors, biaxial loading, p_{max} = 0.35 bar

195
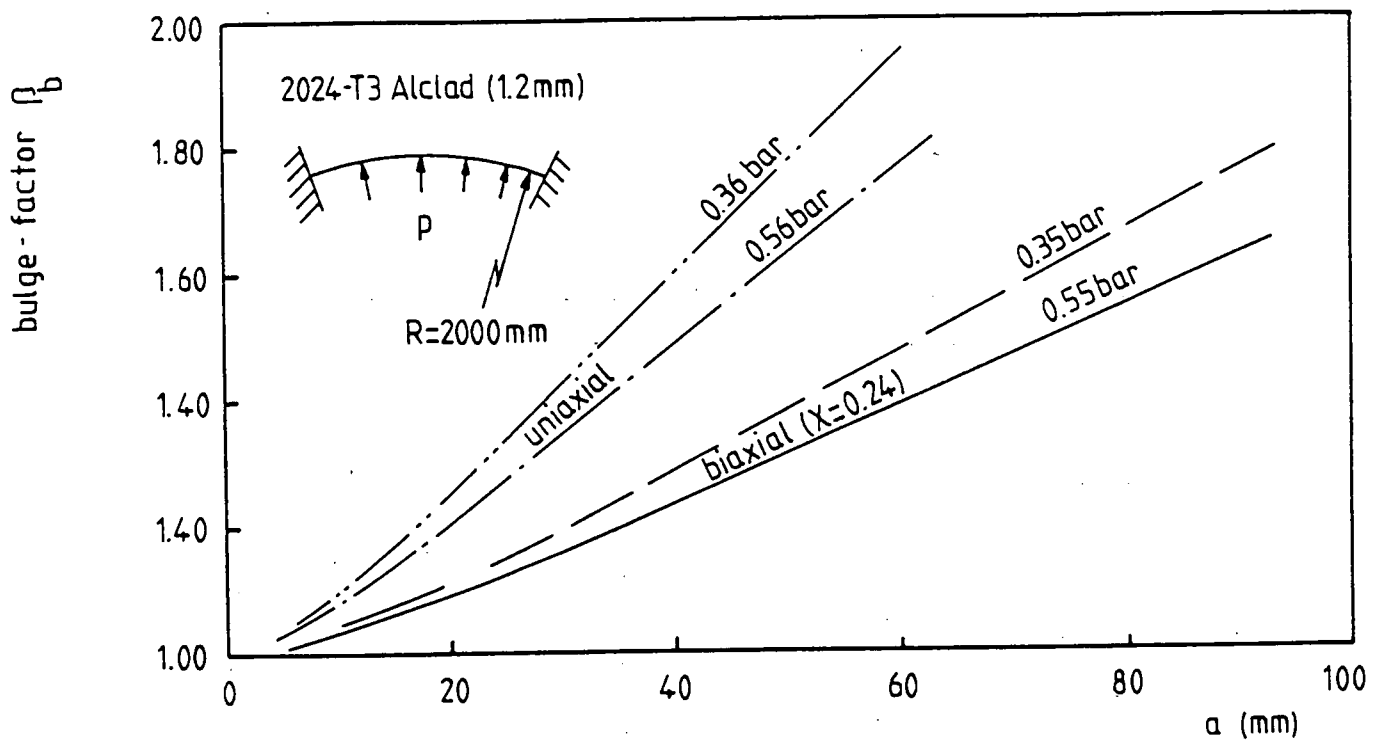
Fig.5.39 Effect of internal pressure and stress
biaxiality on bulge factor
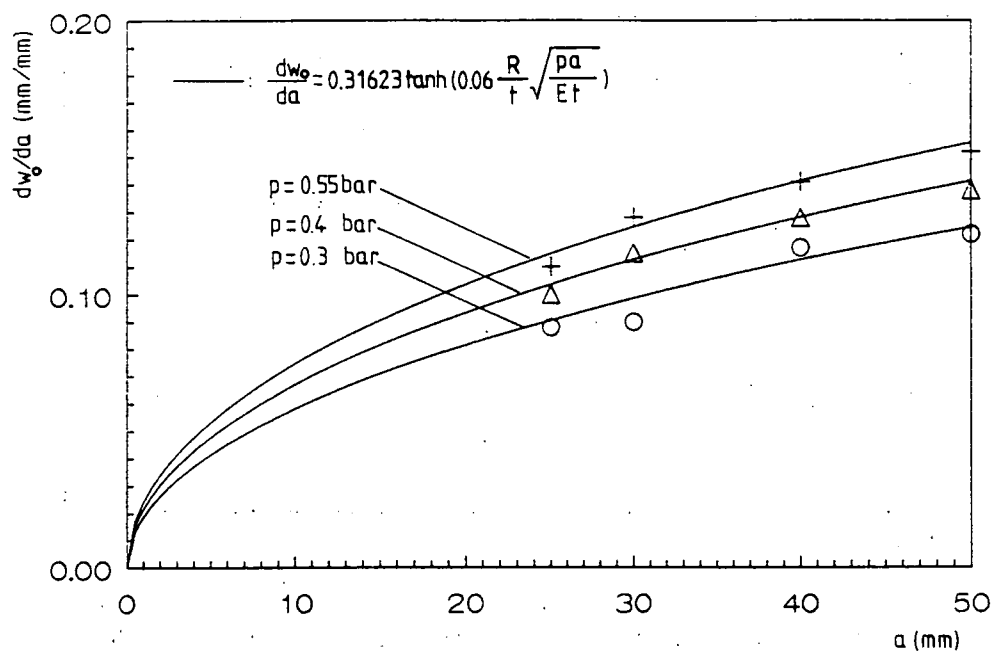
Fig.5.40 dw_0/da as a function of a
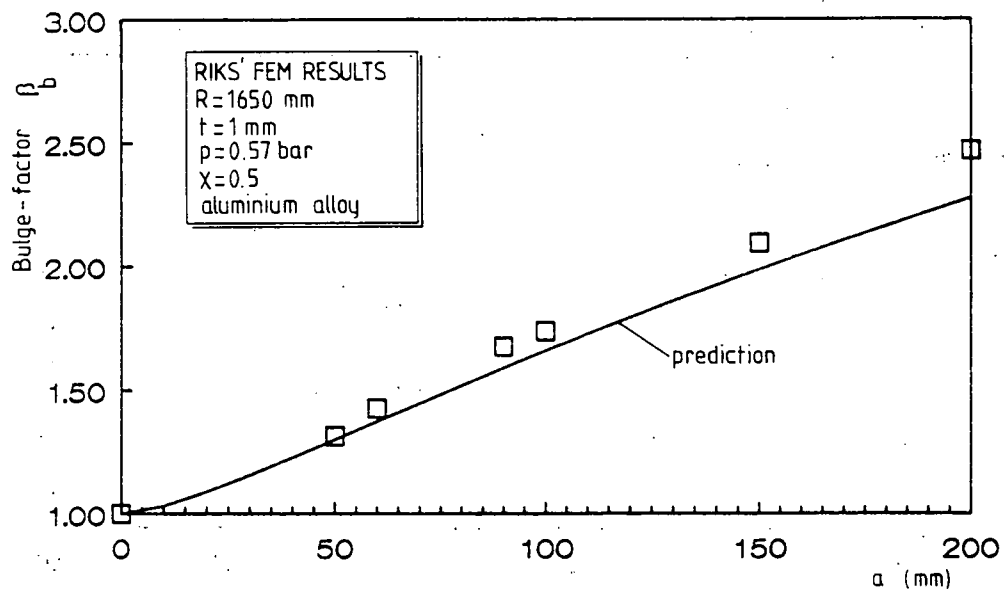
Fig.5.41 Comparison between Riks' FEM results and Eq.(5.10)

(bulge factor β_b vs half-crack-length a)

197
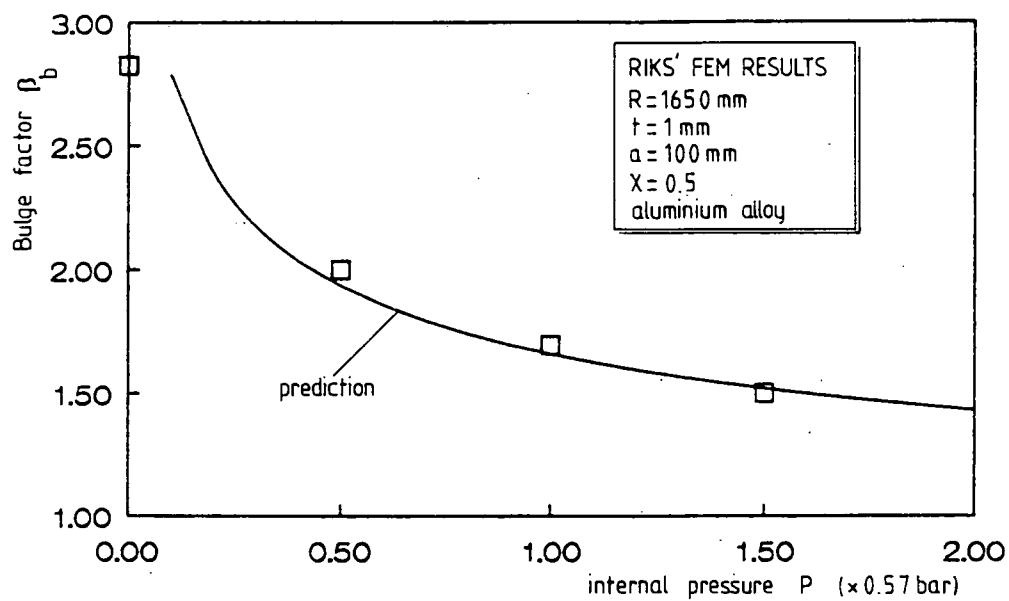
Fig.5.42 Comparison between Riks' FEM results and Eq.(5.10)

(bulge factor β_b vs internal pressure p)
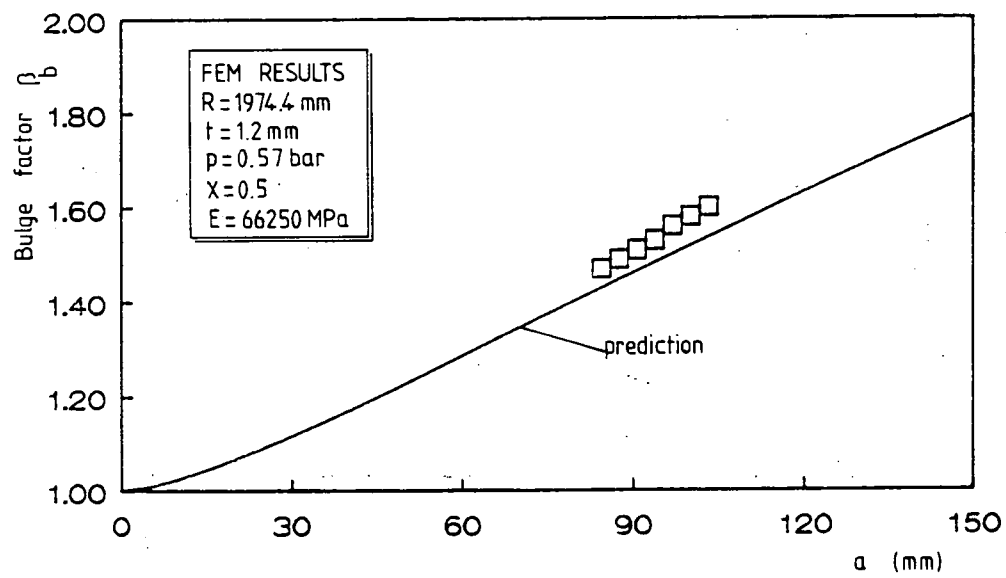
Fig.5.43 Comparison between FEM results from reference 10 and Eq.(5.10)

198
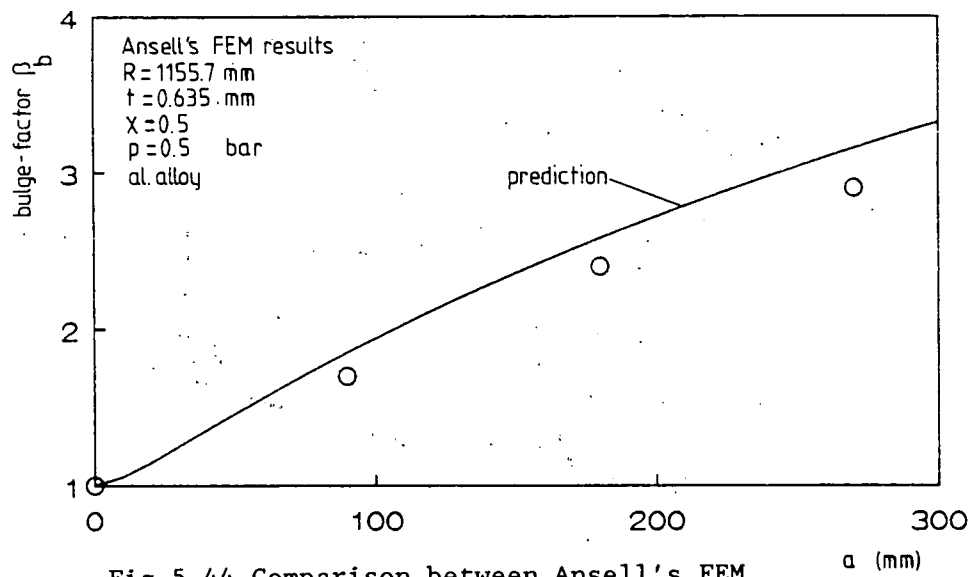
Fig.5.44 Comparison between Ansell's FEM

results and Eq.(5.10), p = 0.5 bar
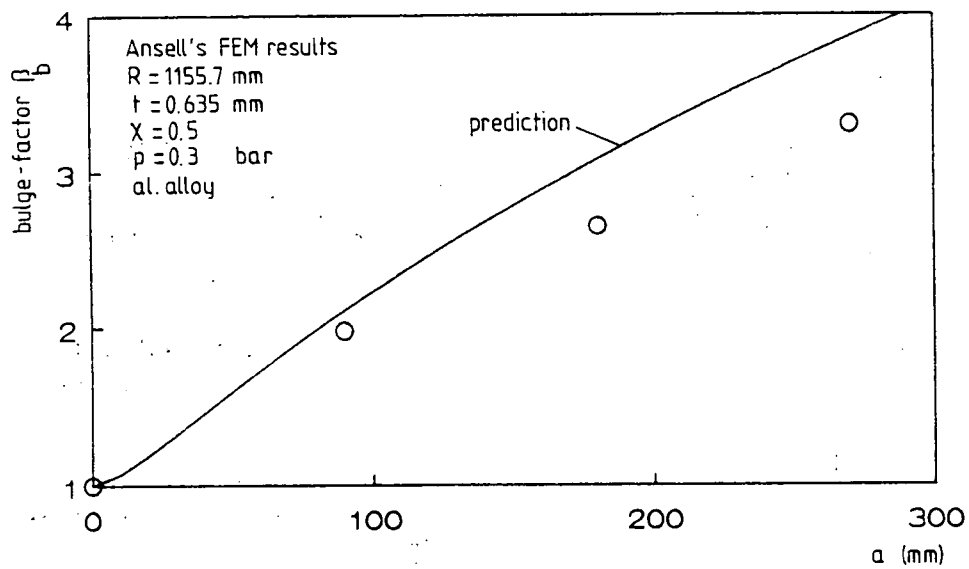
Fig.5.45 Comparison between Ansell's FEM

results and Eq.(5.10), p = 0.3 bar
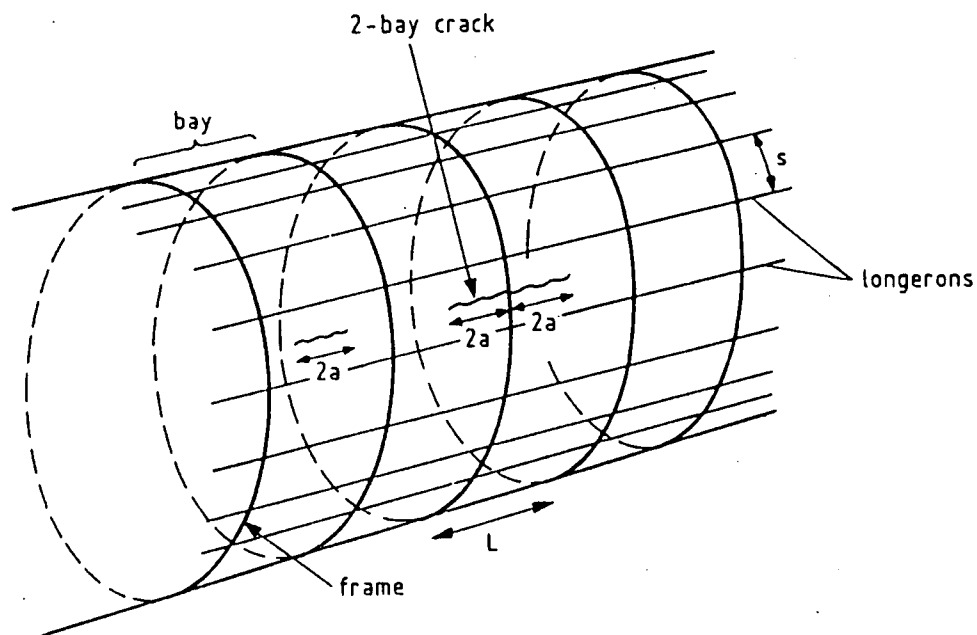
Fig.5.46 One-bay and two-bay crack
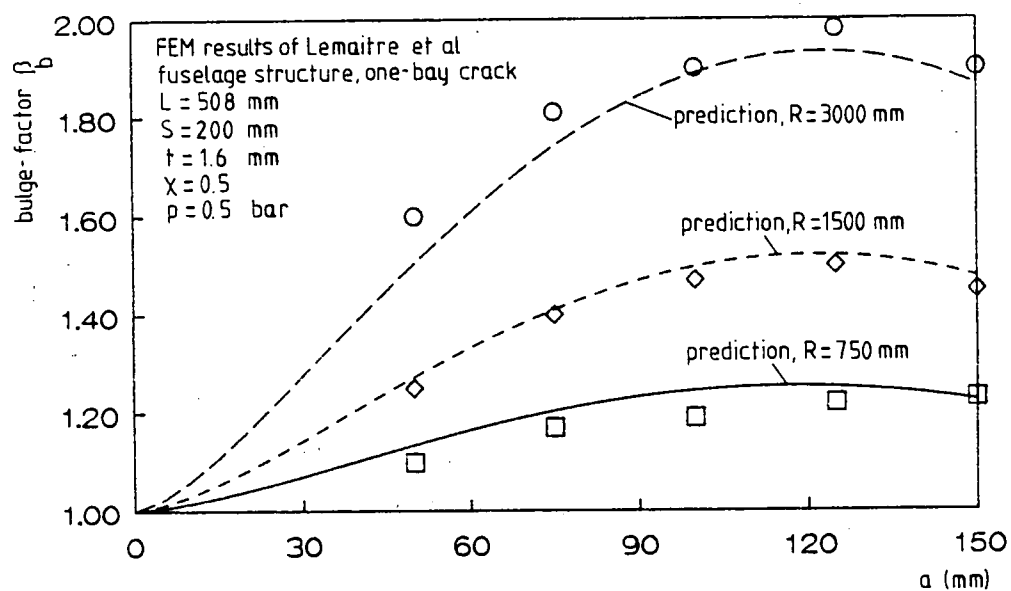
Fig.5.47 Comparison between Lemaitre's FEM
results and Eq.(5.14), effect of R

200
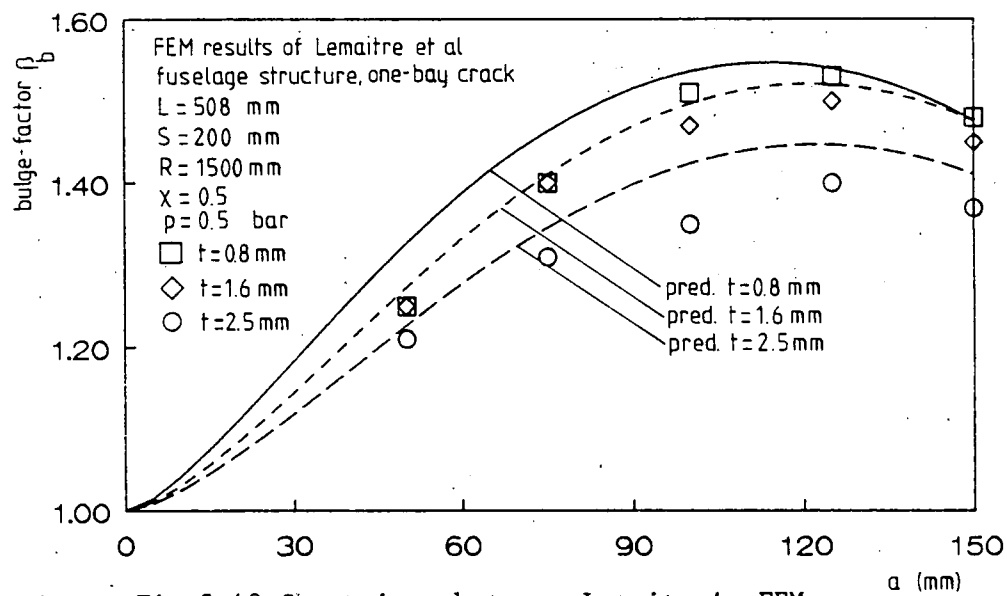
Fig.5.48 Comparison between Lemaitre's FEM

results and Eq.(5.14), effect of t
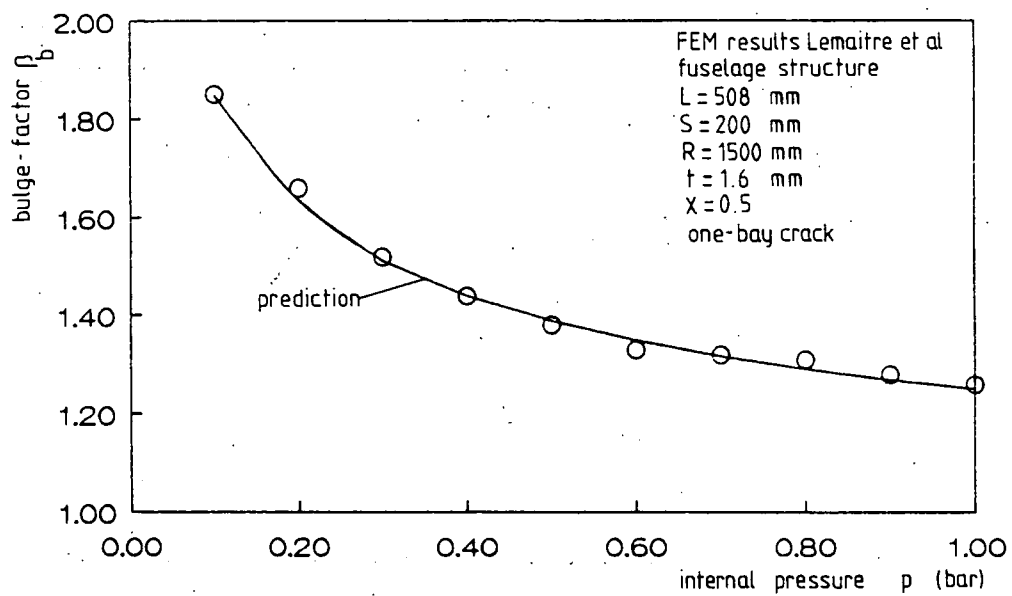
Fig.5.49 Comparison between Lemaitre's FEM
results and Eq.(5.14), effect of p

201
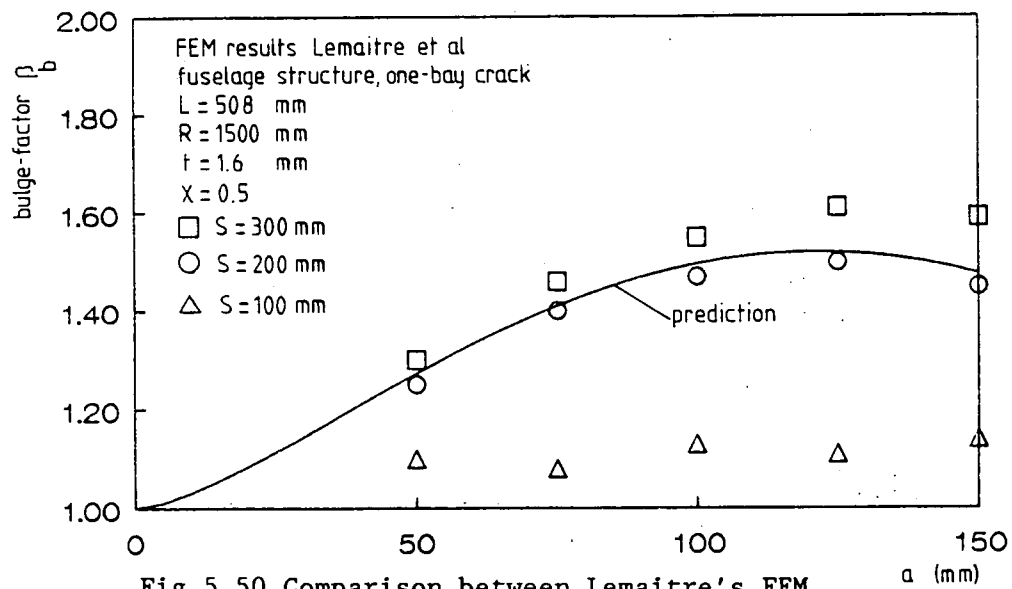
Fig.5.50 Comparison between Lemaitre's FEM
results and Eq.(5.14), effect of S
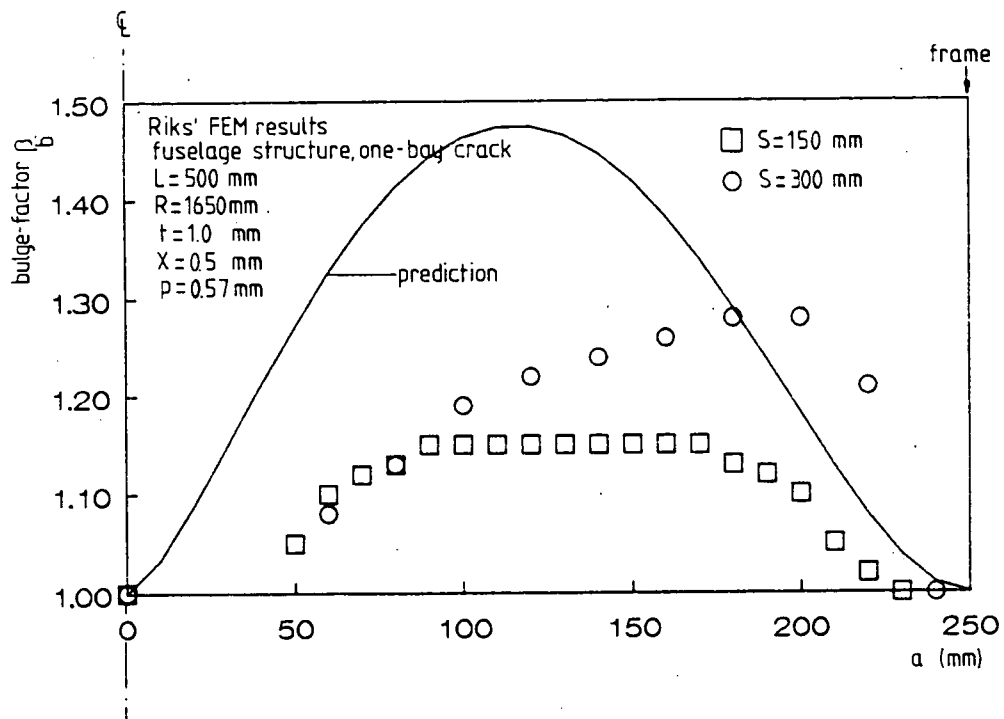
Fig.5.51 Comparison between Riks' FEM results and Eq.(5.14)
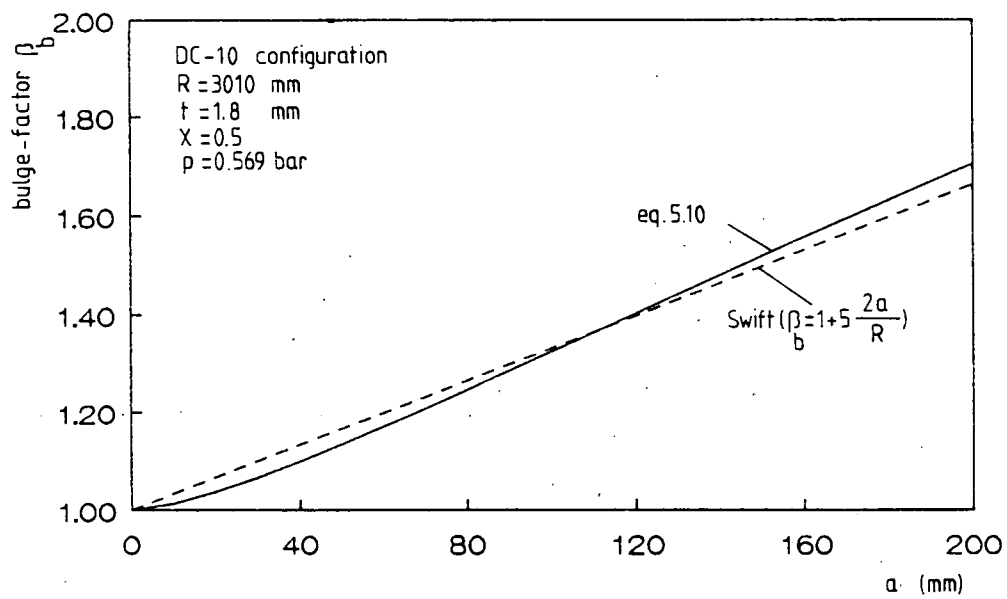
Fig.5.52 Comparison between Swift's formula and Eq.(5.10)
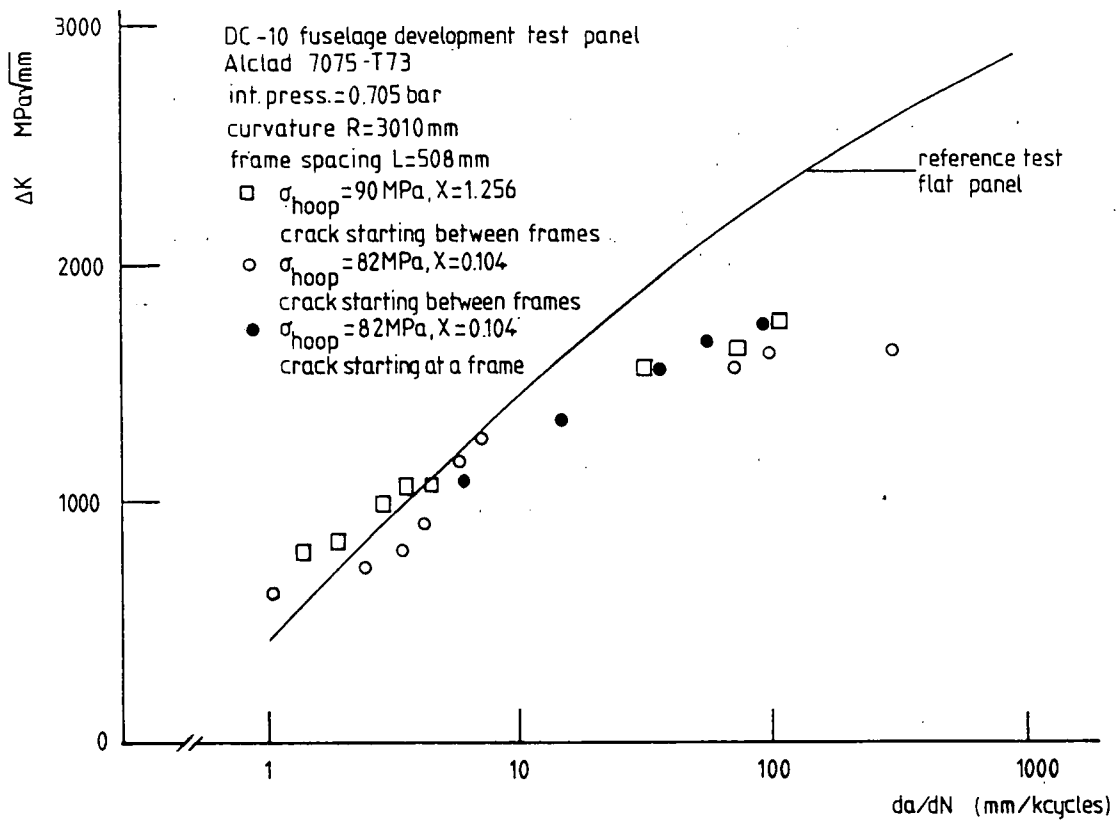
Fig.5.53 Test results of DC-10 fuselage development test panel[17]

203

TOTAL CRACK LENGTH = 2a
RADIUS OF CURVATURE = 1435 mm
SHELL THICKNESS = 0.8 mm
INTERNAL PRESSURE = 470 mbar
SHELL MATERIAL = 2024 – T 3

STRINGER

160 mm

CLIP

STRIP

FRAME

508 mm
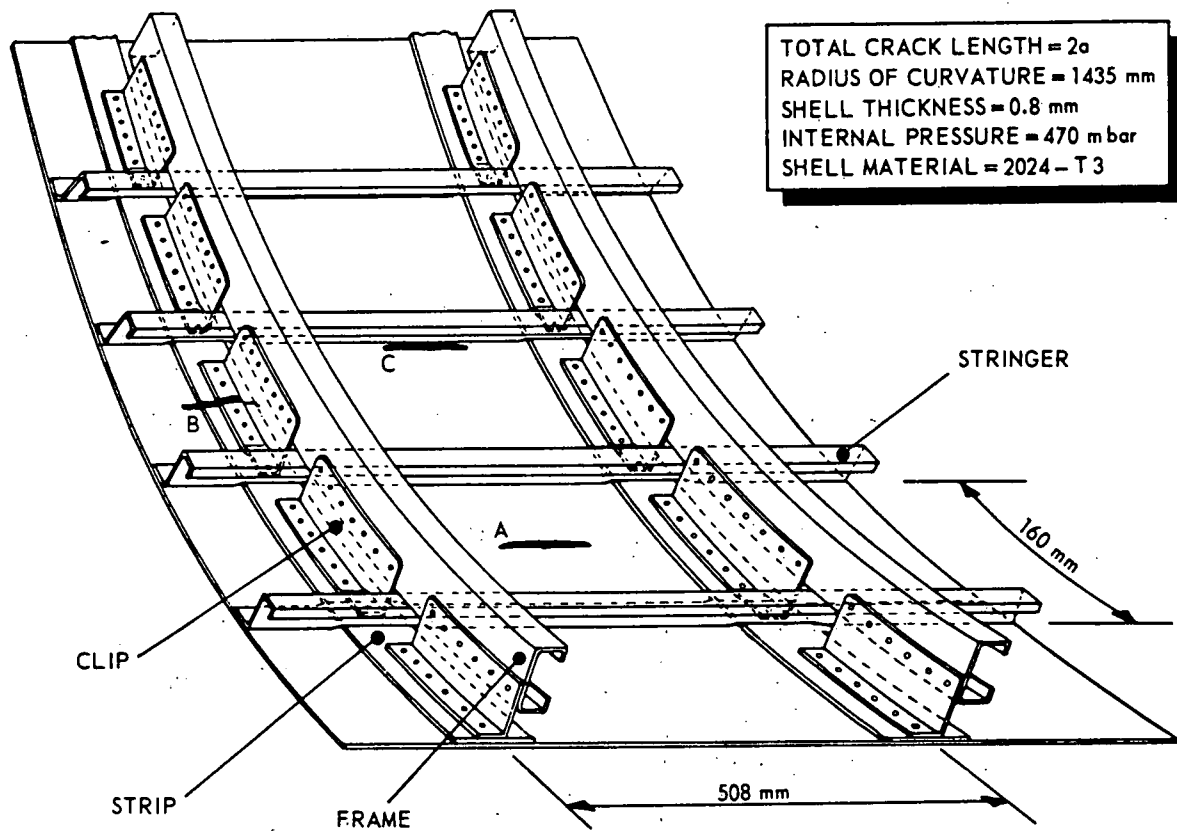
Fig. 5.54 Crack configurations of test
conducted by Schwarmann[15]

204

FUSELAGE STRUCTURE
crack starting midway between frames and stringers (crack A)
curvature R=1435mm
int. press. p=0.47 bar
shell thickness t=0.8 mm
$R=(\sigma_{min.}/\sigma_{max.})=0.1$
X=0.5
skin material: 2024-T3 alclad
o   left crack tip
•   right crack tip

a (mm)

70

60

50

40

30

20

10

0

0   1000   2000   3000   4000   5000

N (cycles)
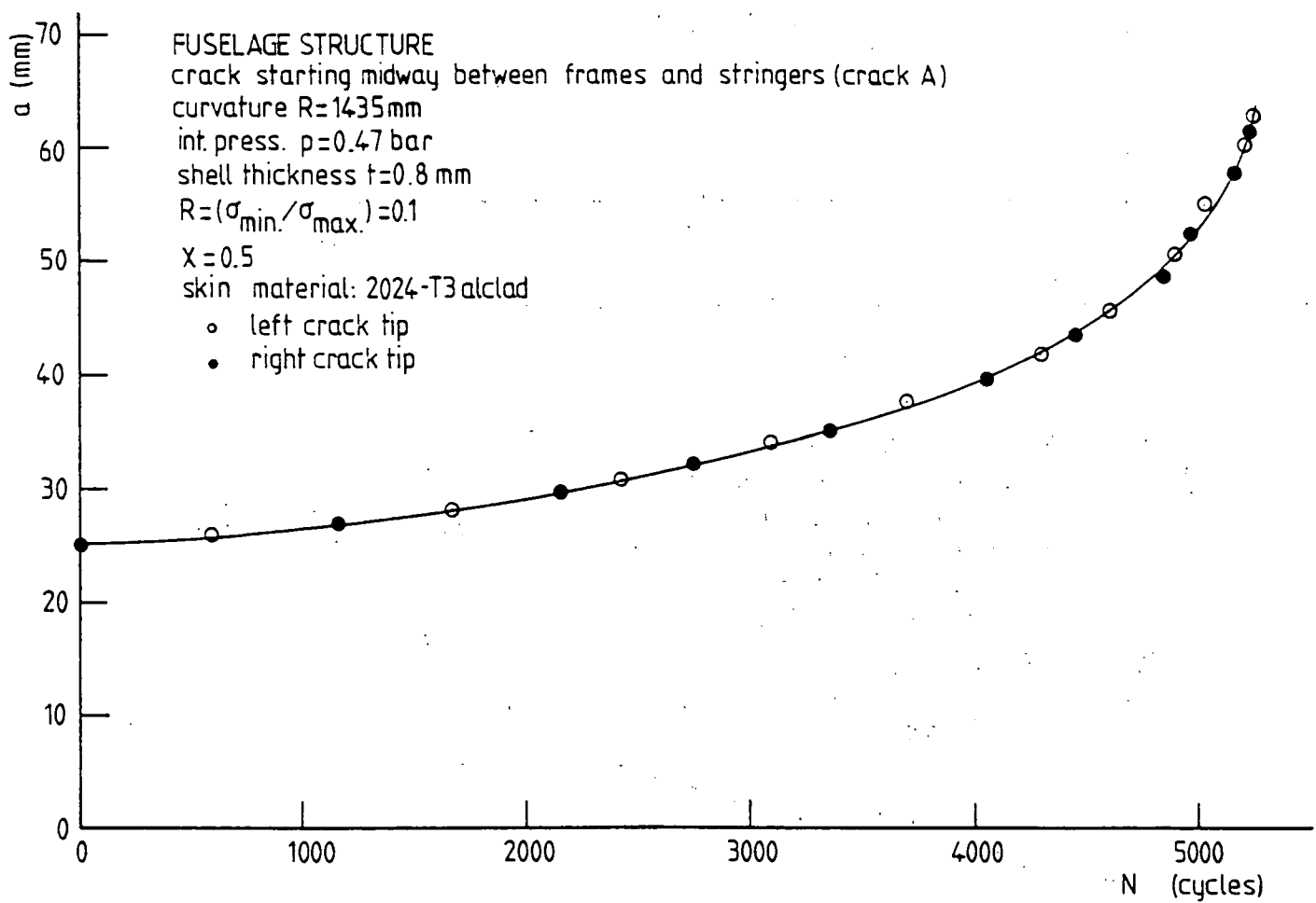
Fig.5.55 Test results of crack A *(After schwarmann[17])*

205

FUSELAGE STRUCTURE
crack starting at a frame (crack B)
curvature R=1435 mm
int. press. p=0.47 bar
skin thickness t=0.8 mm
$R=(\sigma_{min.}/\sigma_{max.})=0.1$
X=0.5
skin material: 2024-T3 alclad

left crack tip

right crack tip
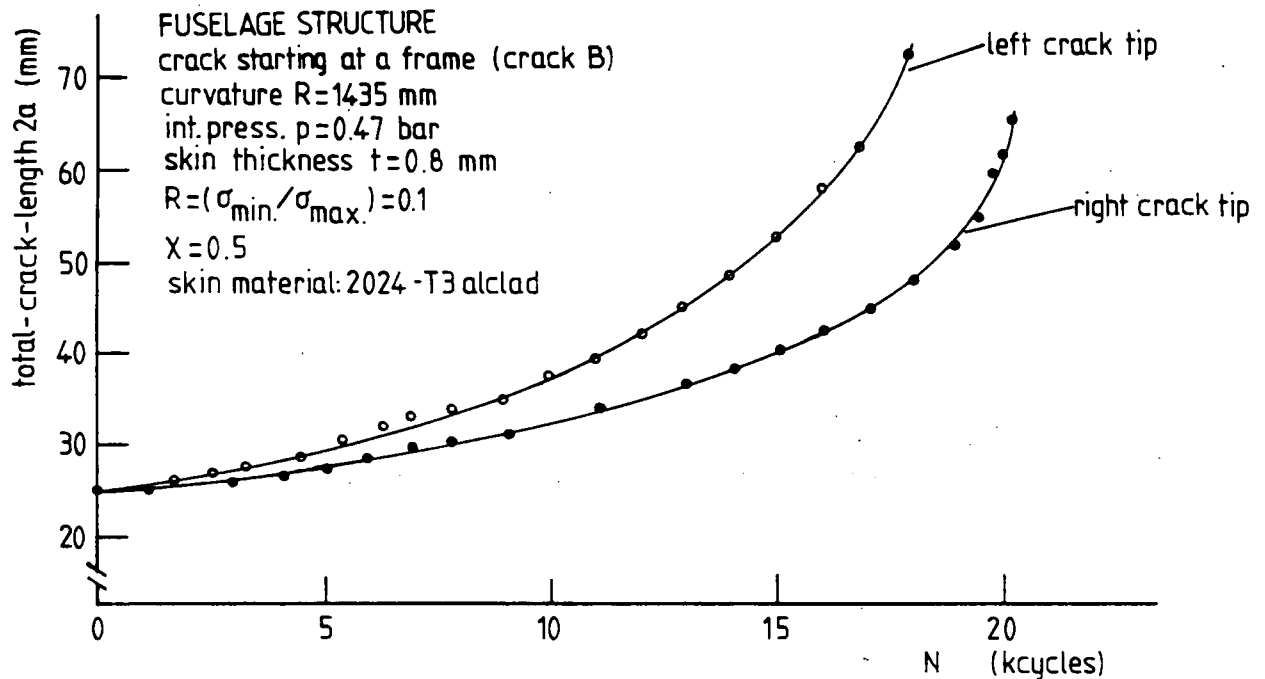
Fig.5.56 Test results of crack B *(After schwarmann[17])*

FUSELAGE STRUCTURE
crack starting between frames and
along a stringer (crack C)
curvature R=1435 mm
int. press. p=0.47 bar
skin thickness t=0.8 mm
$R=(\sigma_{min.}/\sigma_{max.})=0.1$
X=0.5
2024-T3 alclad

left crack tip

right crack tip
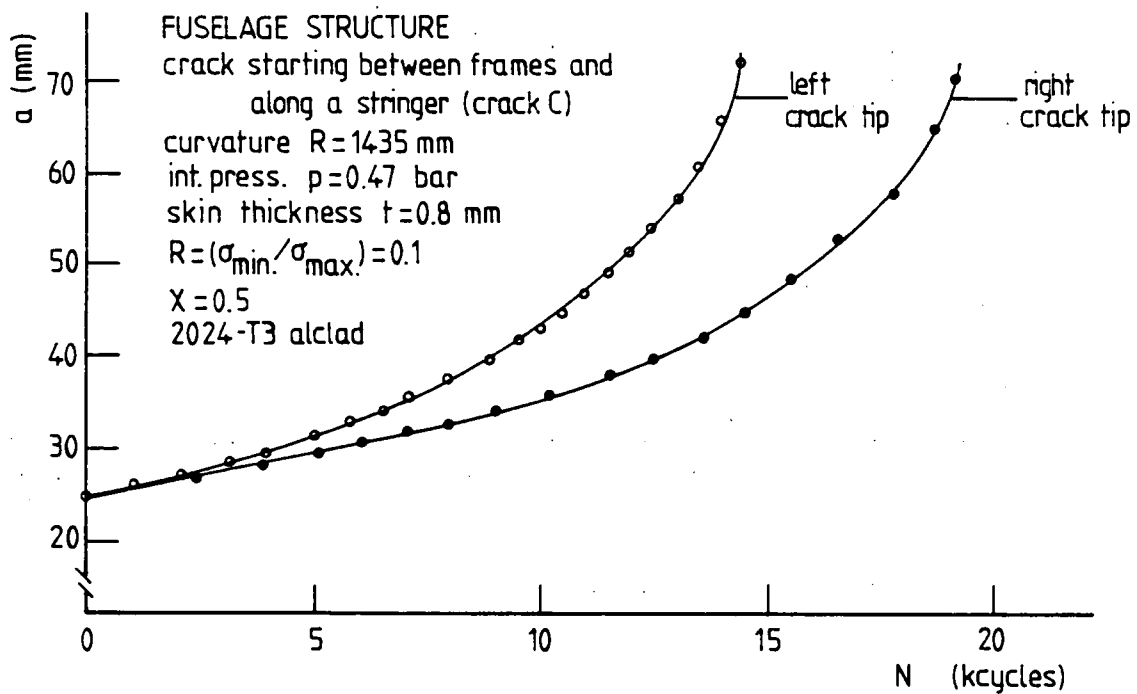
Fig.5.57 Test results of crack C *(After schwarmann[17])*
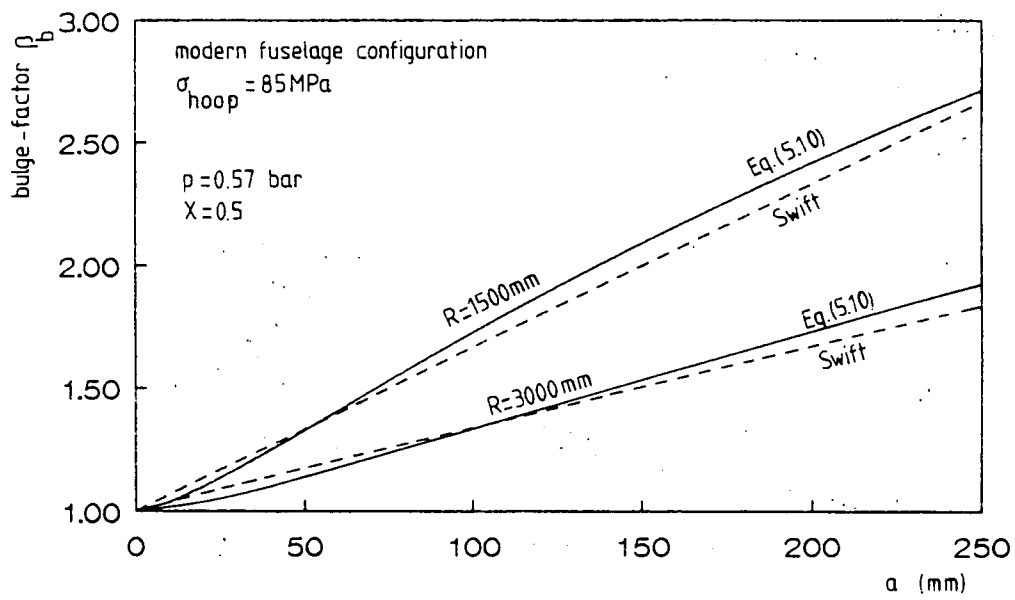
Fig.5.58 Comparison between Swift's formula and Eq.(5.10)
for modern fuselage configurations
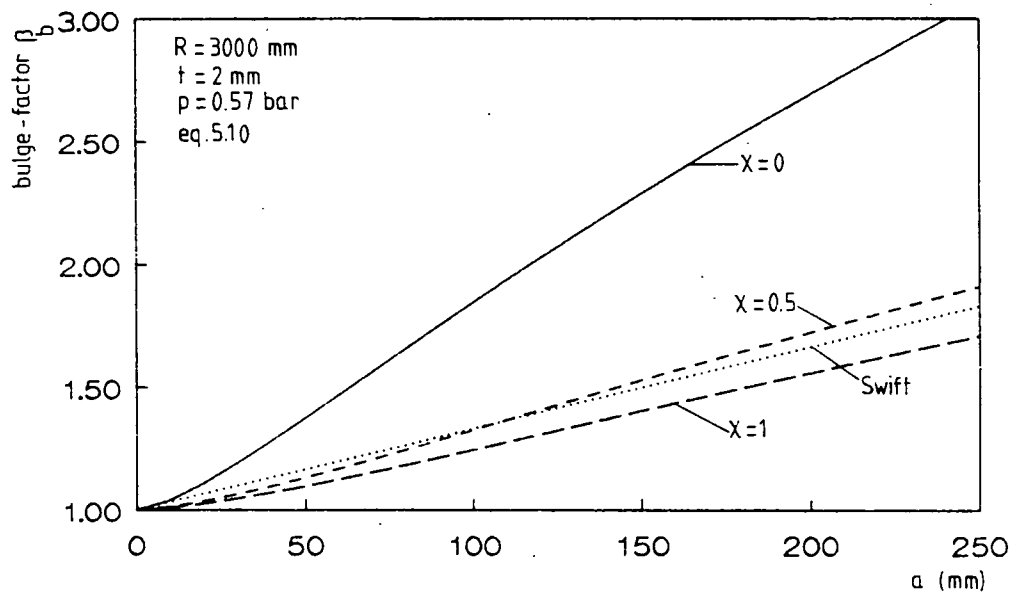
Fig.5.59 Comparison between Swift's formula and Eq.(5.10)
for various stress biaxialities
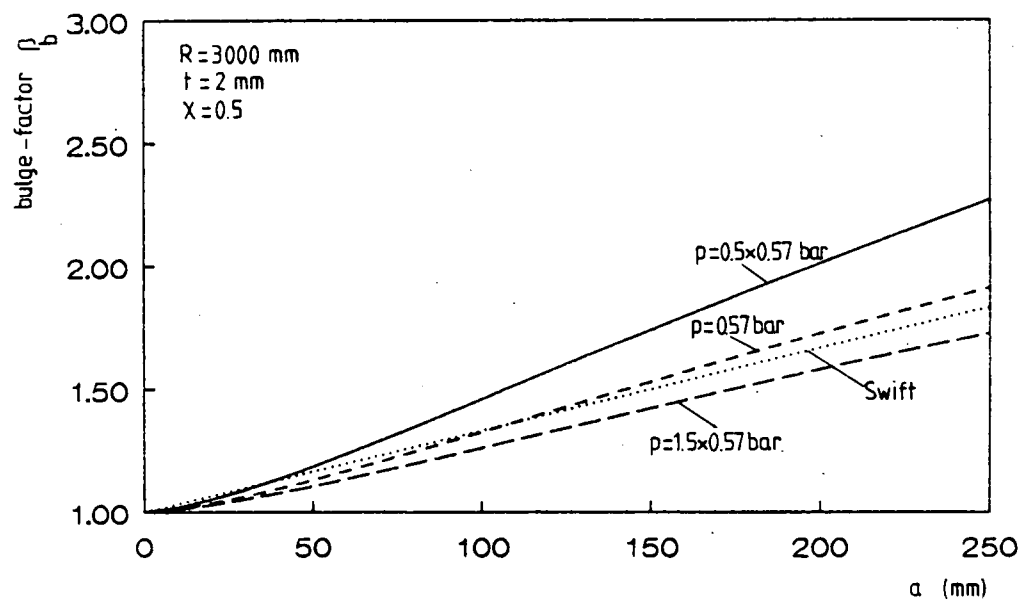
Fig.5.60 Comparison between Swift's formula and Eq.(5.10)
for various internal pressures

Nominally
1.3 mm (e.g.)

Aramid, Glass
or Carbon prepreg
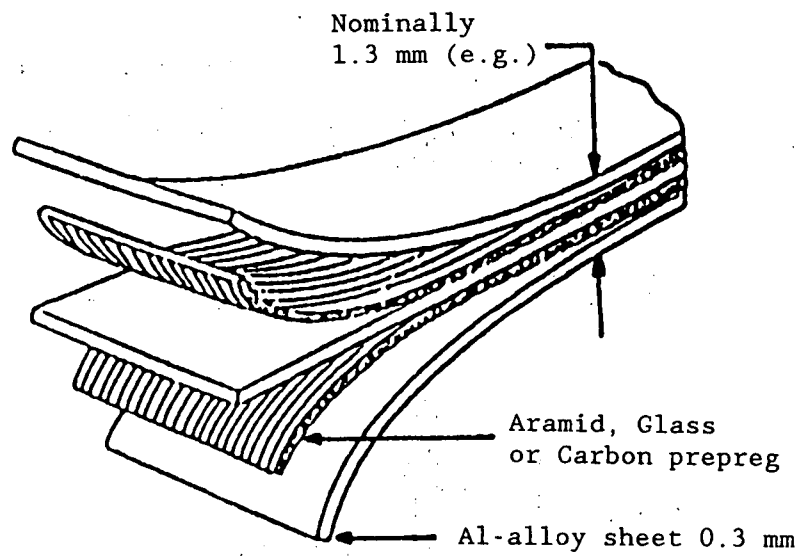
Al-alloy sheet 0.3 mm

Fig. 6.1 Principal sketch of ARALL, built up from
2 or more thin Al-alloy sheets with
intermediate fiber-prepreg layers

Al-alloy

Prepreg
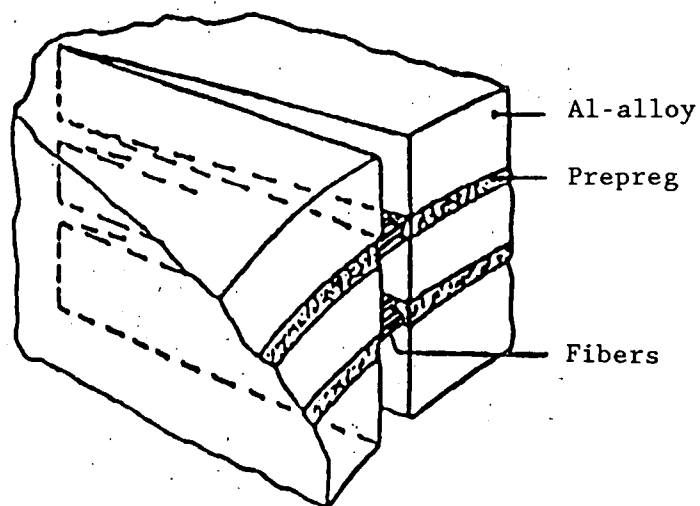
Fibers

Fig.6.2 Crack bridging of fatigue crack in ARALL

209

(a)

starter notch

boudary of delaminated area

fatigue crack in Al alloy layers

unbroken fibers
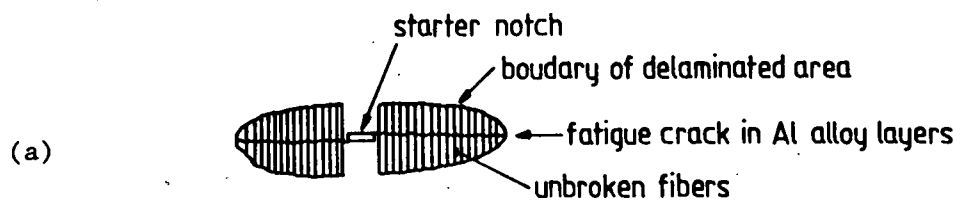
Ideal fiber bridging of a fatigue crack starting
from a central notch in a sheet specimen

(b)

delamination

adhesive-rich layer

Al   Al

prepreg layer
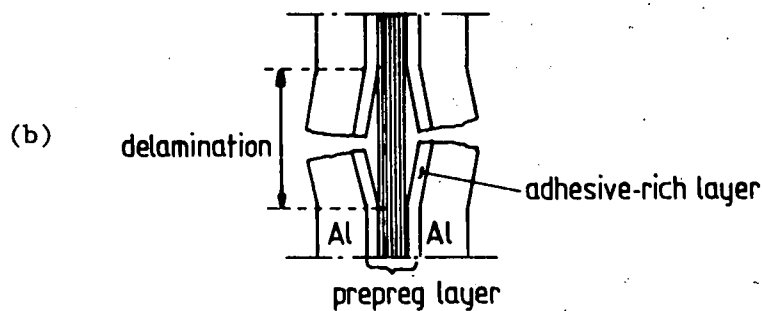
Schematic cross section in delamination area

(c)

boundary of delaminated
area if fiber failure occurs
during fatigue crack growth
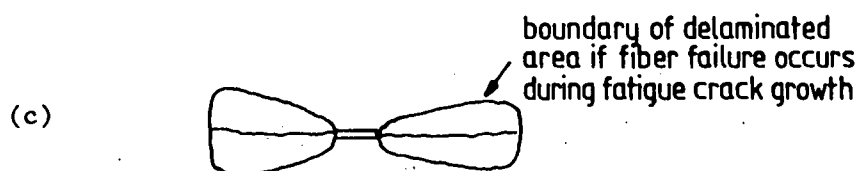
Fiber failure in delamination area

(d)

fiber splitting

delaminated area
without fiber failure

delaminated area
with fiber failure
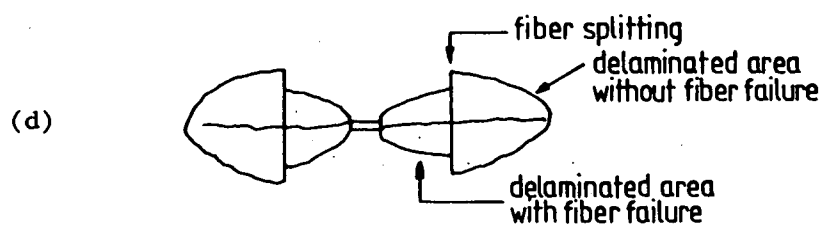
Fiber splitting

Fig.6.3 Crack growth mechanisms in ARALL

210
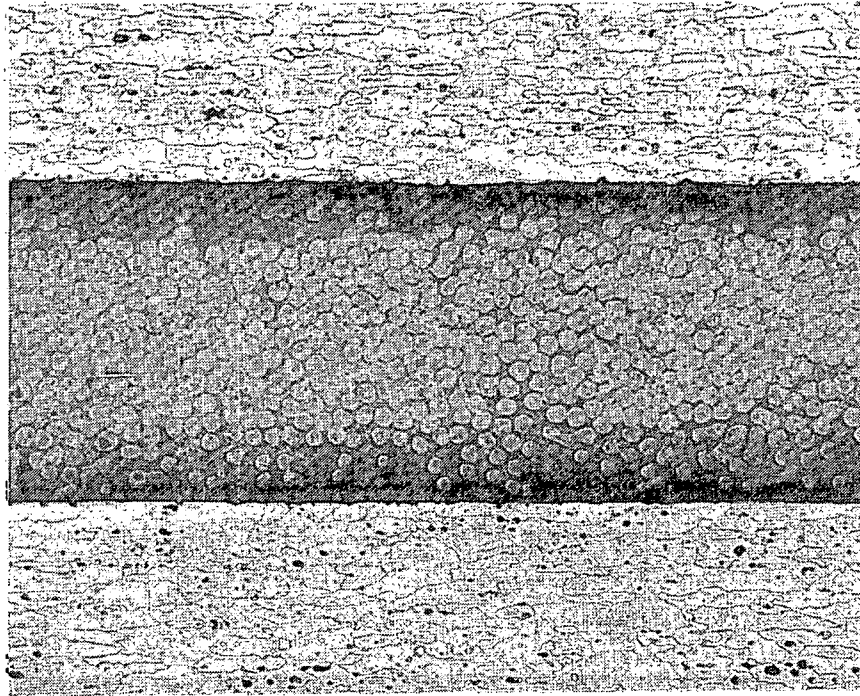
Fig.6.4   Cross section of ARALL
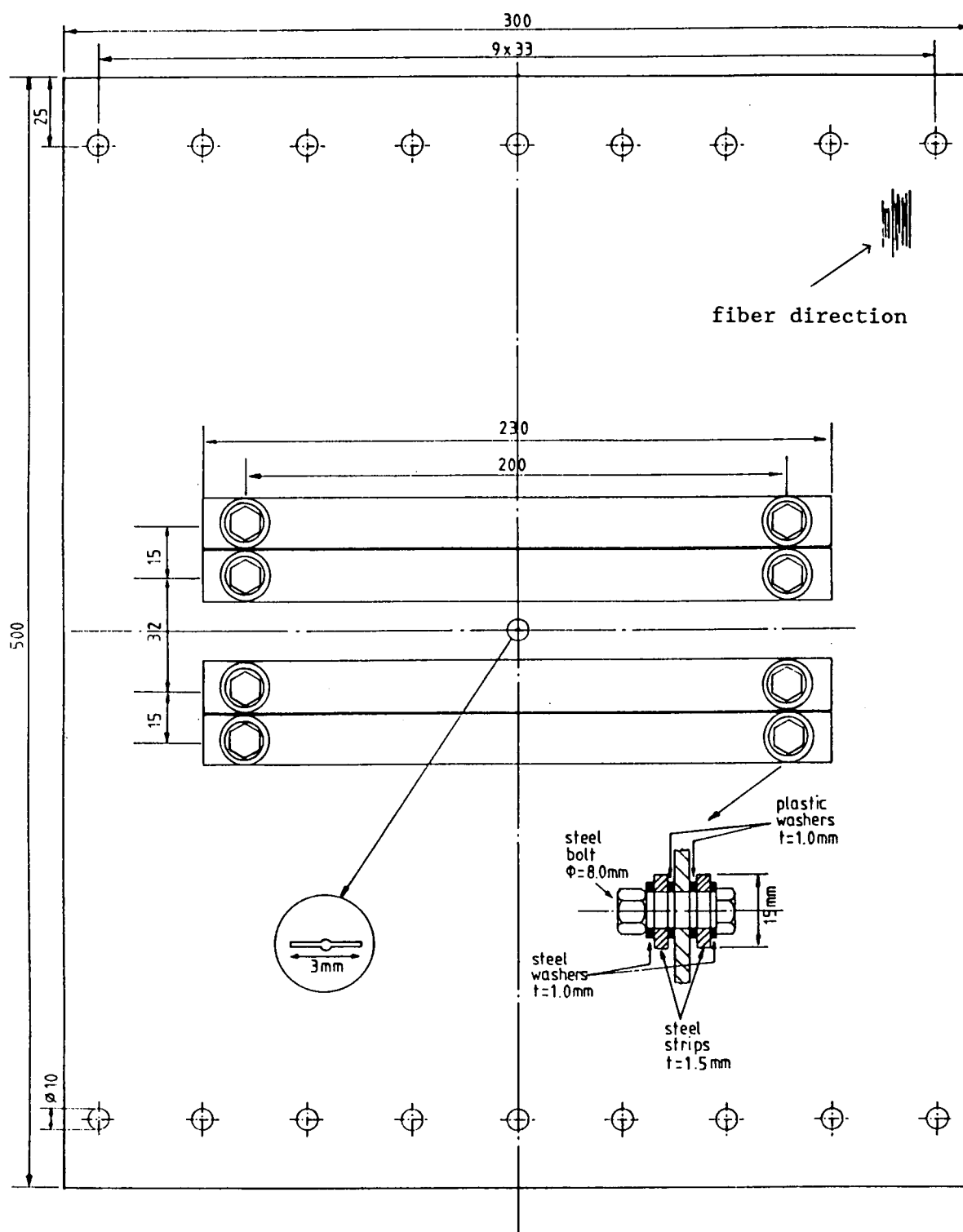
Fig.6.5 SUPERBAT specimen of ARALL

212
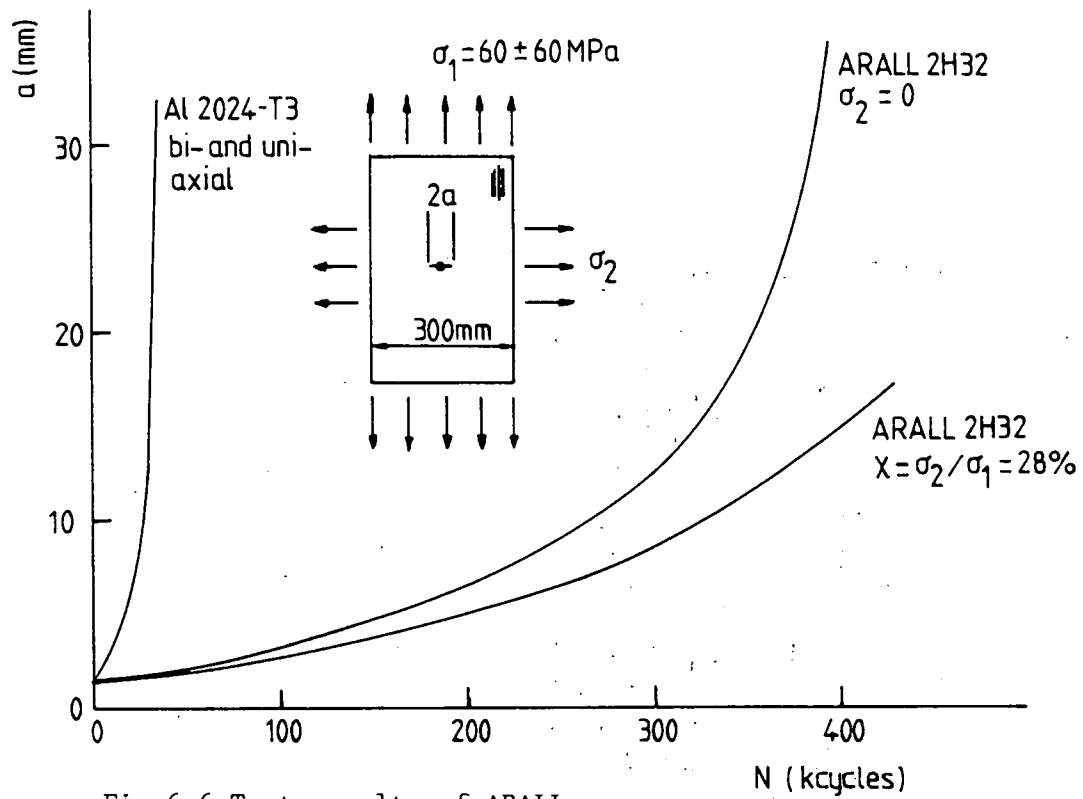
Fig.6.6 Test results of ARALL
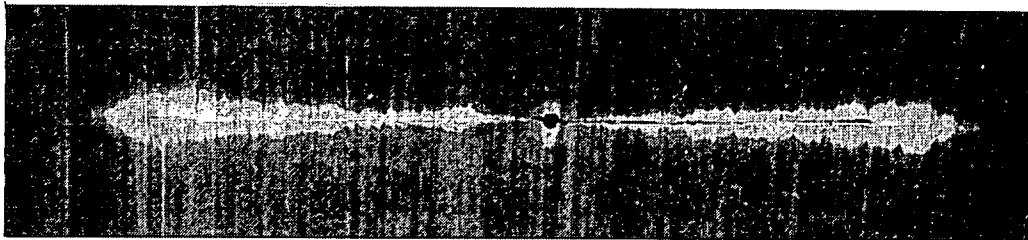
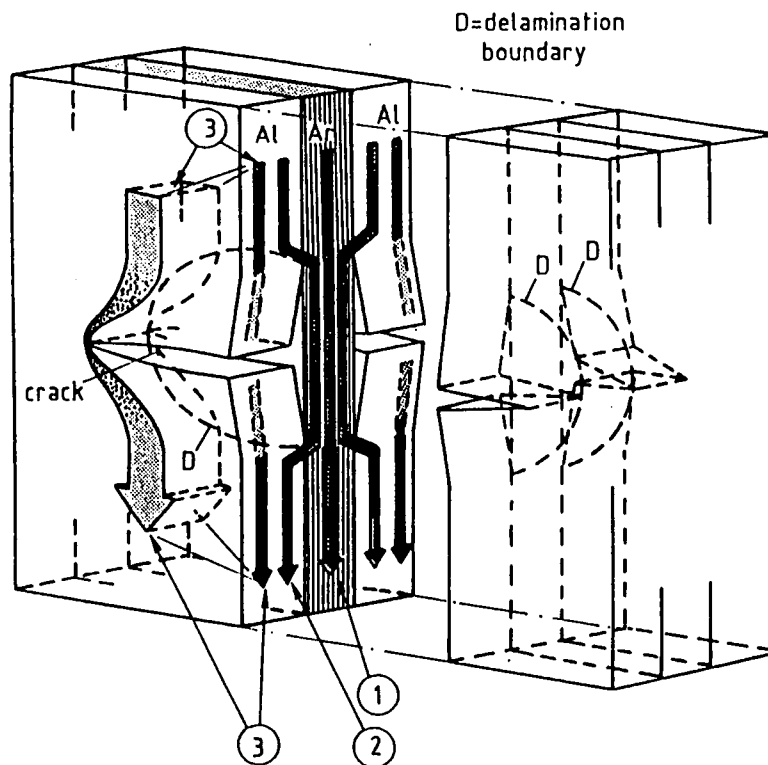Fig.6.7 Delamination area of a uniaxially
tested ARALL specimen
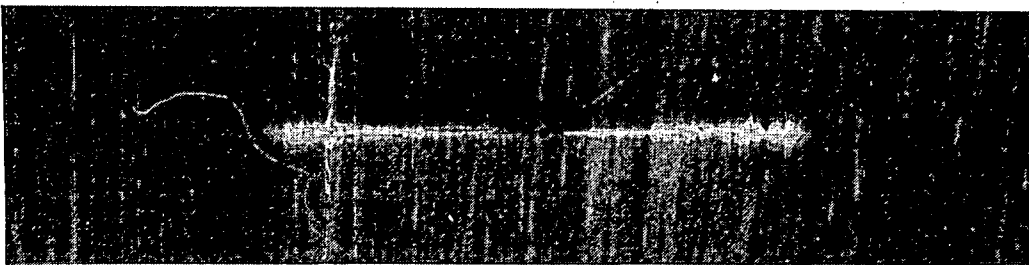
Fig.6.8 Delamination area of a biaxially
tested ARALL specimen

213

D=delamination
boundary

crack

① Part of the external load carried by the aramid fibers
② Part of the load transferred from the aluminium to the fibers, at delamination boundary
③ Part of the load, which remains in the aluminium and passes around the crack tip. This part determines the stress intensity factor
(After R. Marissen)
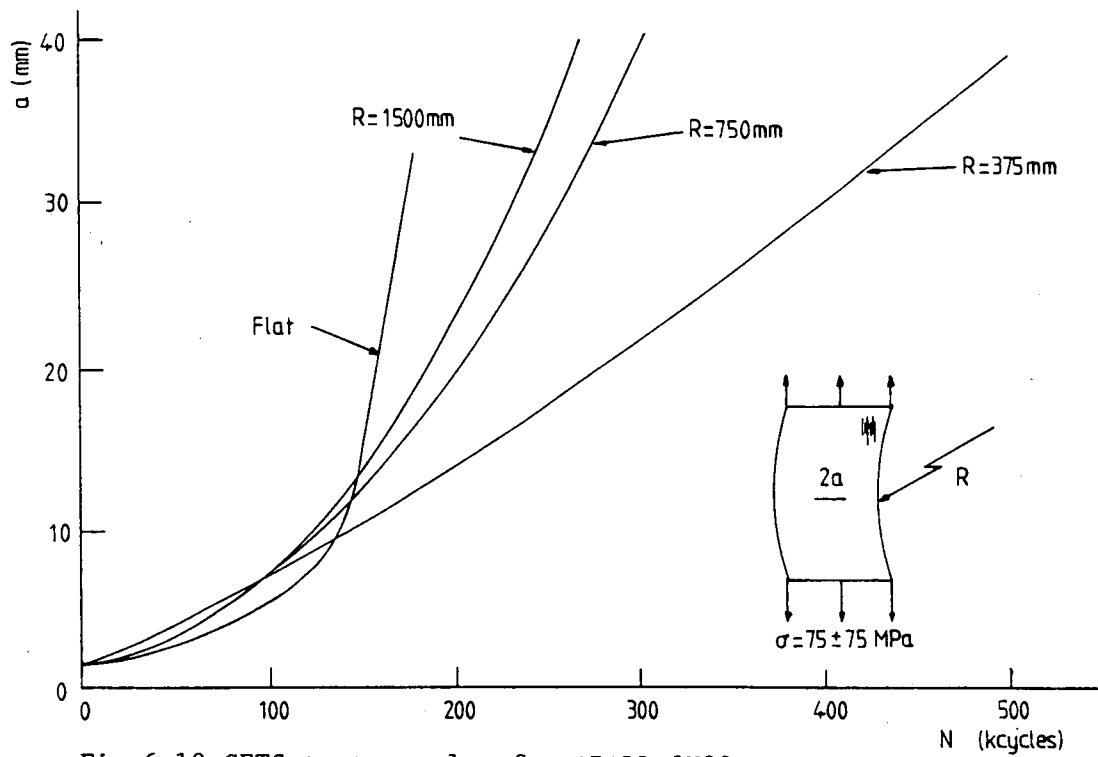
Fig. 6.9 Load distribution around a crack in ARALL
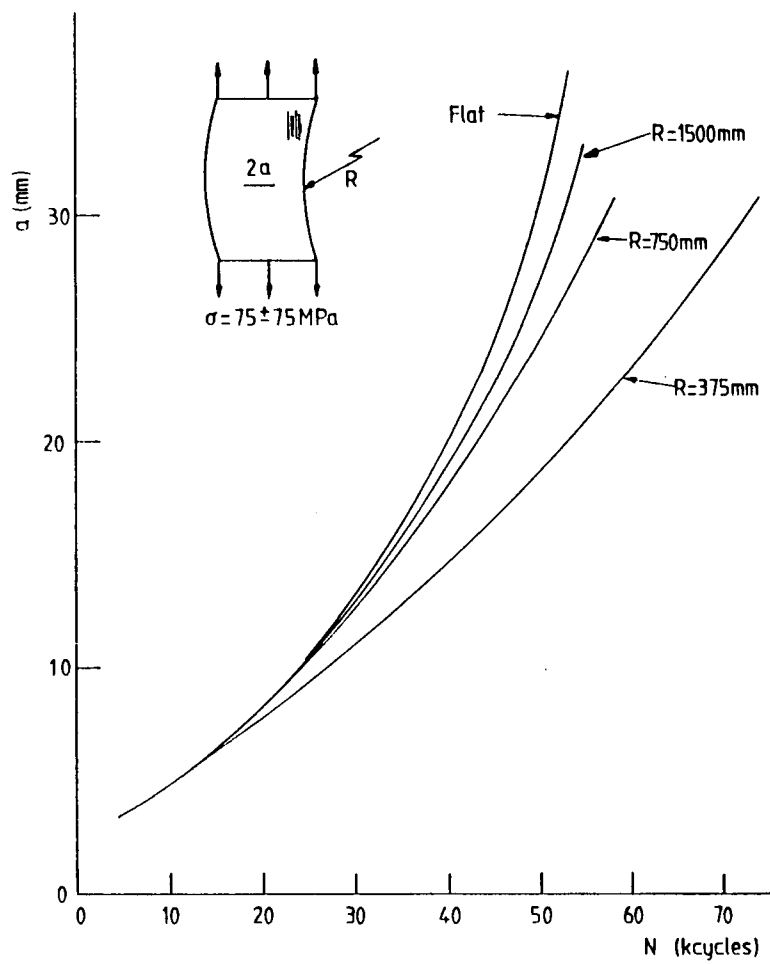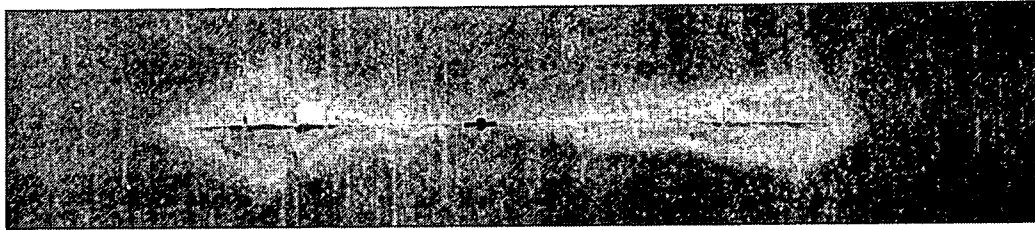
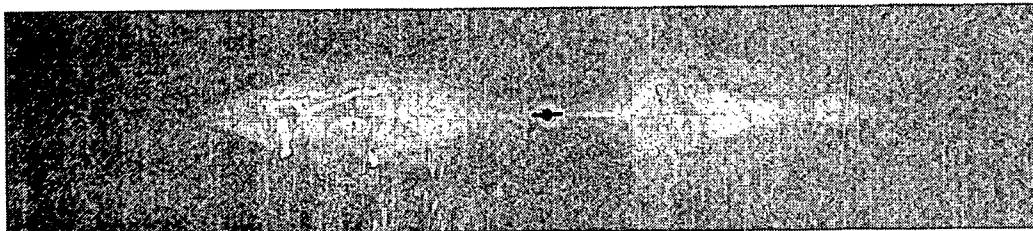Fig.6.10 CETS test results for ARALL 2H32

Fig.6.11 CETS test results for ARALL 7H32
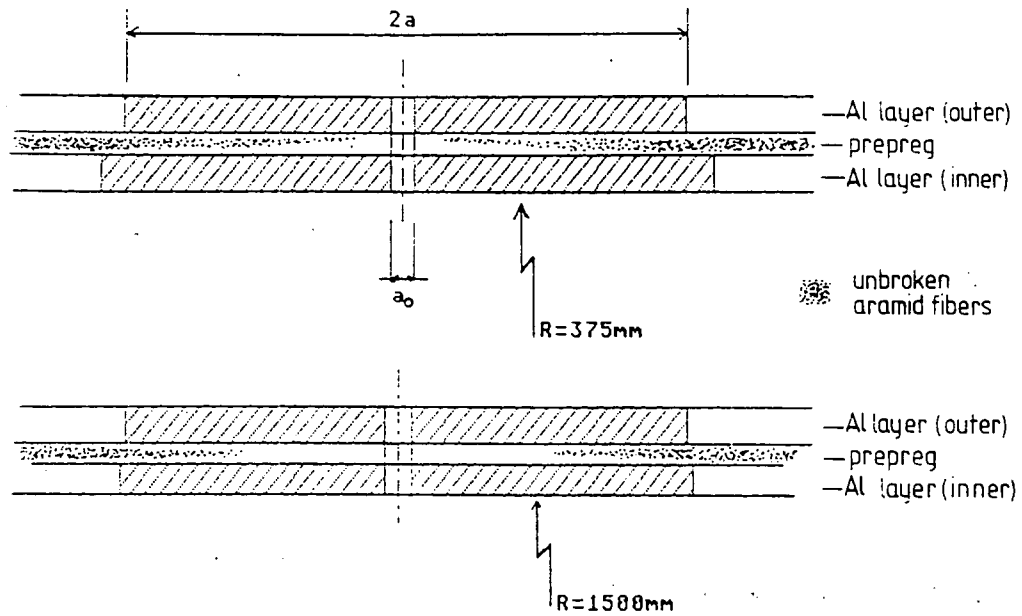
215

(a)   flat

(b)   CETS   R = 375 mm

outer side

(c)   CETS   R = 375 mm

inner side

Fig.6.12 Delamination areas of ARALL
        under flat and CETS conditions
        (2H32, $\sigma = 75 \pm 75$ MPa)

216

2a = measured crack length = crack length in the outer Al layer
a_0 = saw-cut = starter notch

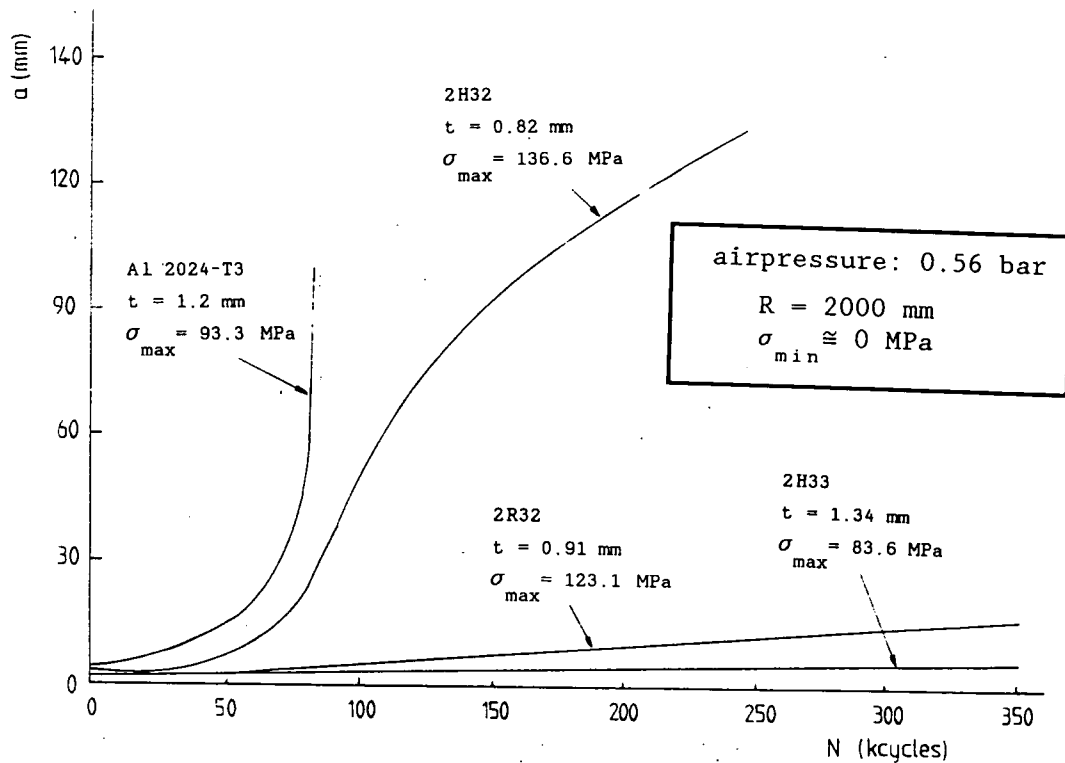Fig.6.13 Cross-section of ARALL under CETS condition

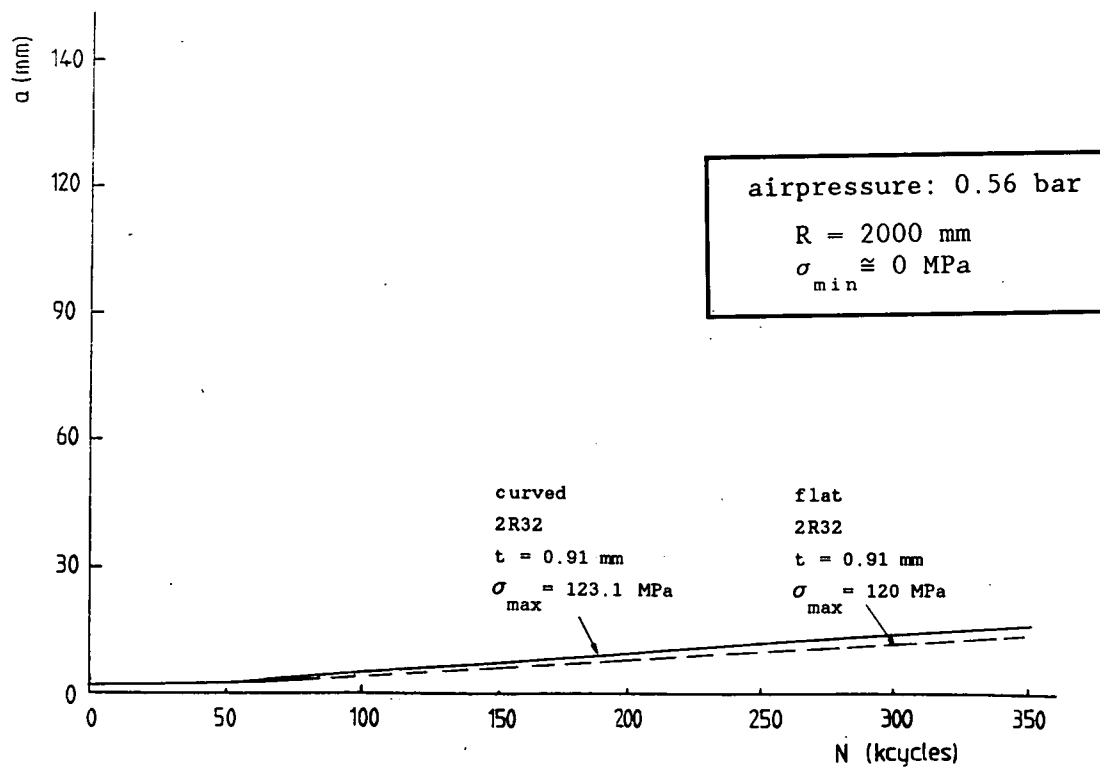Fig.6.14 Test results of ARALL under PFSTS condition

Fig.6.15 Comparison between a-N curves of GLARE 2R32
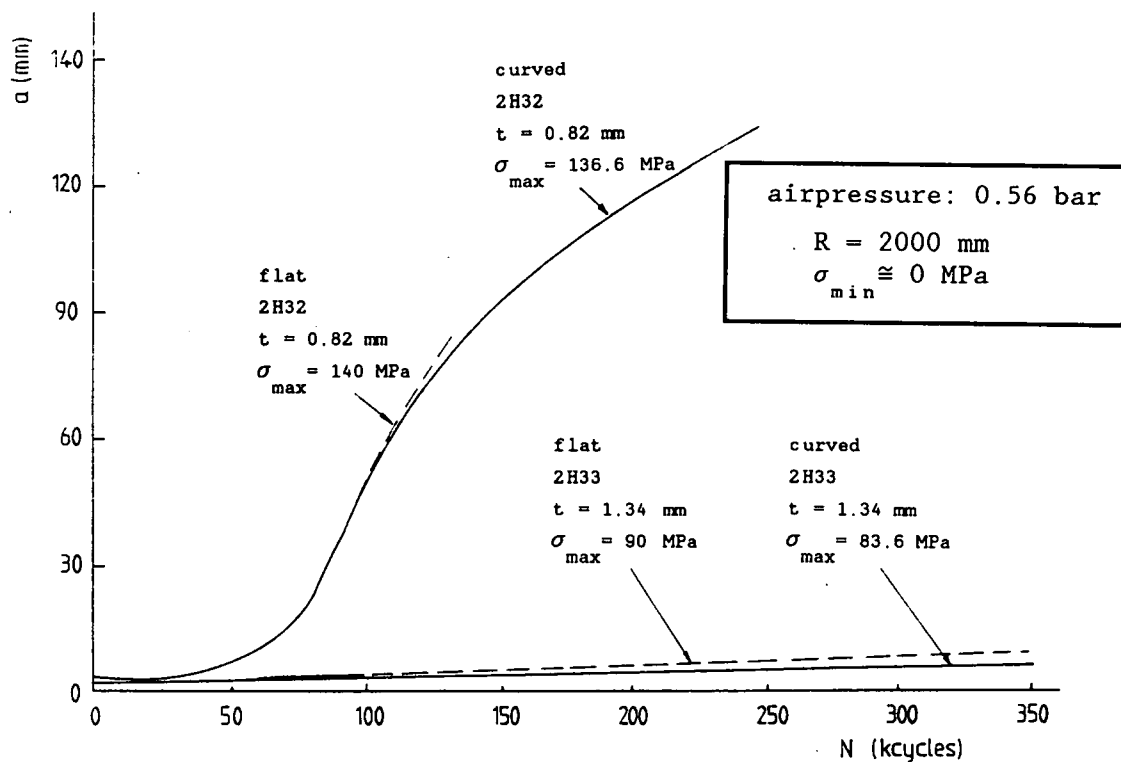under flat and PFSTS condition

Fig.6.16 Comparison between a-N curves of ARALL 2H32
and 2H33 under flat and PFSTS condition

APPENDIX A

EQUATIONS FOR DETERMINING THE INFLUENCE COEFFICIENTS IN SUPERBAT

Consider an infinite sheet of thickness t loaded by remote stress $\sigma_{appl.}$ in one direction. Steel strip pairs are symmetrically fastened with bolts in the center of the sheet (Fig.A1). The idea is to create a local biaxial stress field in the center of the sheet (SUPERBAT). The equations necessary to determine the unknown bolt reaction forces, hence the stress distribution in the biaxial stress field, can be obtained by equating the displacements at the bolt locations in the sheet and the strips. These displacements can be written in terms of the following influence coefficients: A_{ij} and B_i, which represent the displacements in the sheet at bolt no.i, because of unit values of the bolt forces P_j and the remote stress in the sheet material $\sigma_{appl.}$, respectively; and C_i, which represent the displacements in the strips at bolt no.i because of unit value of the bolt forces P_j.

Thus the displacement at bolt no.i in the sheet and strips can be written as:

$$u_i = \sum_j A_{ij} P_j + B_i \qquad\qquad (A.1)$$

$$u_i^s = C_i P_i \qquad\qquad (A.2)$$

For symmetry reasons i and j can be restricted to the bolts in one quadrant of the sheet. Equating these displacements and collecting terms gives:

$$\sum_j A_{ij} P_j - C_i P_i = -B_i \sigma_{appl.} \qquad\qquad (A.3)$$

or

$$\sum_j A_{ij} P_j - C_i P_i + B_i \sigma_{appl.} = 0 \qquad (i=1,2,3\ldots;j=1,2,3\ldots) \qquad (A.4)$$

These simultaneous equations can be solved when the influence coefficients are known. The analytical solutions for the influence coefficients are given below.

Applied uniaxial stress:

For an infinite sheet loaded in one direction (fig.A2) the displacements of any point in the X-direction can be calculated according to the following formula:

$$u = -\nu \cdot x \cdot \frac{\sigma_{appl.}}{E} \qquad (A.5)$$

For bolt no.i the displacement in the X-direction is then:

$$u_{i,remote} = -\nu \cdot x_i \cdot \frac{\sigma_{appl.}}{E} \qquad (A.6)$$

where x_i = x-coordinate of the bolt no.i;

ν = Poisson's ratio of the material;

E   = Young's modulus of the material; and

$\sigma_{appl.}$ = remote stress in the y-direction of the sheet.

The influence coefficients B_i in equation (A.1) can be determined by setting the stress σ_i equal to unity. Thus

$$B_i = -\nu \cdot \frac{x_i}{E} \qquad (A.7)$$

Bolt reaction forces:

According to Love[1], the displacement in the X-direction of an infinite plane for the single point force shown in fig.A3 can be obtained for the plane stress state from the following equation:

$$u(x,y)_{P\ at\ (0,0)} =$$

$$= -\frac{(1+\nu)}{4\pi t E}\left[\frac{1}{2}(3-\nu)\ln(x^2 + y^2)+(1+\nu)\frac{y^2}{x^2 + y^2}\right]\cdot P \qquad (A.8)$$

This equation cannot be used in this form to calculate the displacements at the location (0,0) where the point force $\dot{P}$ is acting, because of the singularity at the origin. To circumvent this problem, the point force P is assumed to be distributed uniformly over the bolt diameter d. Replacing y by $y-\bar{y}$ in the above equation and integrating with respect to $\bar{y}$ from $-d/2$ to $d/2$, the displacement becomes:

$$u(x,y)_{P \text{ at } (0,0)} =$$

$$= - \frac{(1+\nu)(3-\nu)P}{16\pi tE} \cdot \left\{ (\frac{2y}{d} + 1) \cdot \ln\left[(\frac{2y}{d} + 1)^2 + \frac{4x^2}{d^2} \right] \right.$$

$$- (\frac{2y}{d} - 1) \cdot \ln\left[(\frac{2y}{d} - 1)^2 + \frac{4x^2}{d^2} \right]$$

$$\left. + \frac{1-\nu}{3-\nu} \; \frac{8x}{d} \; \arctan\left[\frac{\frac{x}{d}}{\frac{x^2}{d^2} + \frac{y^2}{d^2} - \frac{1}{4}} \right] \right\} \qquad \text{(A.9)}$$

The origin is then moved from (0,0) to (x_j, y_j), and after adding the displacements caused by symmetric bolt forces acting at $(\pm x_j, \pm y_j)$, the displacement field can be written as:

$$u(x,y)_{P\text{'s at } (\pm x_j, \pm y_j)} = \frac{(1+\nu)(3-\nu)}{16\pi tE} \cdot P_j \cdot \Omega \qquad \text{(A.10)}$$

where

$$\Omega = (\alpha_3 + 1) \ln\left[\frac{(\alpha_3 + 1)^2 + \alpha_2^2}{(\alpha_3 + 1)^2 + \alpha_1^2} \right] - (\alpha_3 - 1) \ln\left[\frac{(\alpha_3 - 1)^2 + \alpha_2^2}{(\alpha_3 - 1)^2 + \alpha_1^2} \right]$$

$$- (\alpha_4 - 1) \ln\left[\frac{(\alpha_4 - 1)^2 + \alpha_2^2}{(\alpha_4 - 1)^2 + \alpha_1^2} \right] + (\alpha_4 + 1) \ln\left[\frac{(\alpha_4 + 1)^2 + \alpha_2^2}{(\alpha_4 + 1)^2 + \alpha_1^2} \right]$$

$$+ 4 \cdot \frac{1-\nu}{3-\nu} \cdot \left\{ \alpha_2 \left[\arctan\left(\frac{2\alpha_2}{\alpha_2^2 + \alpha_3^2 - 1} \right) + \arctan\left(\frac{2\alpha_2}{\alpha_2^2 + \alpha_4^2 - 1} \right) \right] \right\}$$

$$- \alpha_1 \left[\arctan \left(\frac{2\alpha_1}{\alpha_1^2 + \alpha_3^2 - 1} \right) + \arctan \left(\frac{2\alpha_1}{\alpha_1^2 + \alpha_4^2 - 1} \right) \right] \right] \Bigg\}$$

and

$$\alpha_1 = \frac{2(x - x_j)}{d}; \quad \alpha_2 = \frac{2(x + x_j)}{d}; \quad \alpha_3 = \frac{2(y - y_j)}{d}; \quad \alpha_4 = \frac{2(y + y_j)}{d}.$$

The coefficients $A_{i,j}$ can then be determined by setting P's equal to unity and replacing x by x_i in equation (A.10).

Forces in the strips:

The deformations, in this case, the negative elongations of the strips can easily be calculated according to Hooke's law:

$$\frac{P_i}{2B^s t^s E^s} = - \frac{u_i^s}{x_0} \tag{A.11}$$

or

$$u_i^s = - \frac{x_0}{2B^s t^s E^s} \cdot P_i \tag{A.12}$$

where

    B^s = width of strip;

    t^s = thickness of strip;

    E^s = Young's modulus of strip.

Hence, the coefficients C_i's are a constant, when P_i is set equal to unity.

Stress field and biaxial stress ratio:

Love[1] has also given the stress components in a point force stress field:

$$\sigma_{x,P \text{ at } (0,0)} =$$

$$= - \frac{P(1+\nu)}{4\pi t} \ \frac{x}{x^2+y^2} \left(\frac{3+\nu}{1+\nu} - \frac{2y}{x^2+y^2} \right) \qquad (A.13)$$

$$\sigma_{y,P \text{ at } (0,0)} =$$

$$= \frac{P(1+\nu)}{4\pi t} \ \frac{x}{x^2+y^2} \left(\frac{1-\nu}{1+\nu} - \frac{2y}{x^2+y^2} \right) \qquad (A.14)$$

By using the same procedure as for the displacements the stress field can be written as:

$$\sigma_{x,P\text{'s at } (\pm x_j, \pm y_j)} =$$

$$= \frac{P(1+\nu)}{\pi t d} \left\{ \frac{1}{2} \left(\frac{1-\nu}{1+\nu} \right) \cdot \text{Term 1} + \text{Term 2} \right\} \qquad (A.15)$$

$$\sigma_{y,P\text{'s at } (\pm x_j, \pm y_j)} =$$

$$= \frac{P(1+\nu)}{\pi t d} \left\{ \frac{1}{2} \left(\frac{1-3\nu}{1+\nu} \right) \cdot \text{Term 1} - \text{Term 2} \right\} \qquad (A.16)$$

where

$$\text{Term 1} = \frac{\alpha_2}{\alpha_3^2 + \alpha_2^2} + \frac{\alpha_2}{\alpha_4^2 + \alpha_2^2} - \frac{\alpha_1}{\alpha_3^2 + \alpha_1^2} - \frac{\alpha_1}{\alpha_4^2 + \alpha_1^2} \ ;$$

$$\text{Term 2} = \alpha_2 \cdot \left[\frac{\alpha_2}{\alpha_3^2 + \alpha_2^2} + \left(\frac{\alpha_2}{\alpha_4^2 + \alpha_2^2} \right)^2 \right]$$

$$- \alpha_1 \cdot \left[\frac{\alpha_1}{\alpha_3^2 + \alpha_1^2} + \left(\frac{\alpha_1}{\alpha_4^2 + \alpha_1^2} \right)^2 \right]$$

A5

After superposition with the uniaxial stress field, it follows:

$$\sigma_x = \sigma_{x,\text{P's at } (\pm x_j, \pm y_j)} \qquad (A.17)$$

$$\sigma_y = \sigma_{y,\text{P's at } (\pm x_j, \pm y_j)} + \sigma_{\text{appl.}} \qquad (A.18)$$

The biaxial stress ratio χ then becomes:

$$\chi = \frac{\sigma_x}{\sigma_y} = \frac{\sigma_{x,\text{P's at } (\pm x_j, \pm y_j)}}{\sigma_{y,\text{P's at } (\pm x_j, \pm y_j)} + \sigma_{\text{appl.}}} \qquad (A.19)$$

Reference

1. **Love, A.,** A treatise on the mathematical theory of elasticity. Forth ed. (First Amer. Printing), Dover Publ., 1944, p.209.
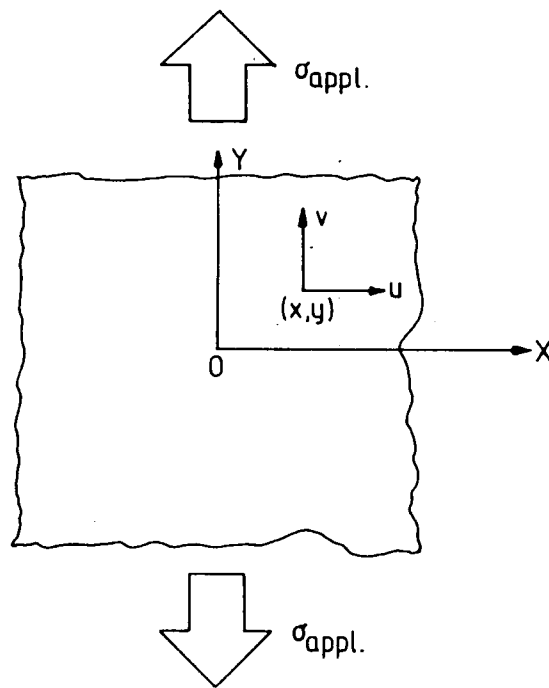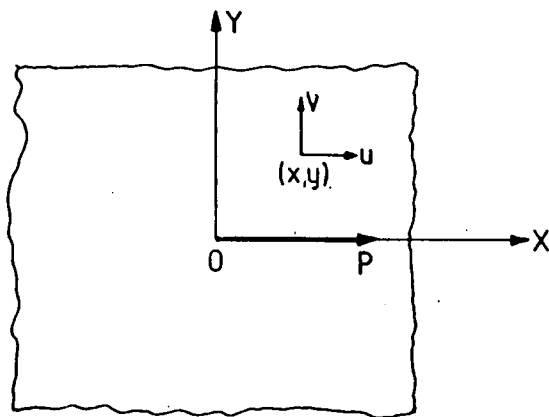
Fig.A2 Uniaxially loaded infinite sheet

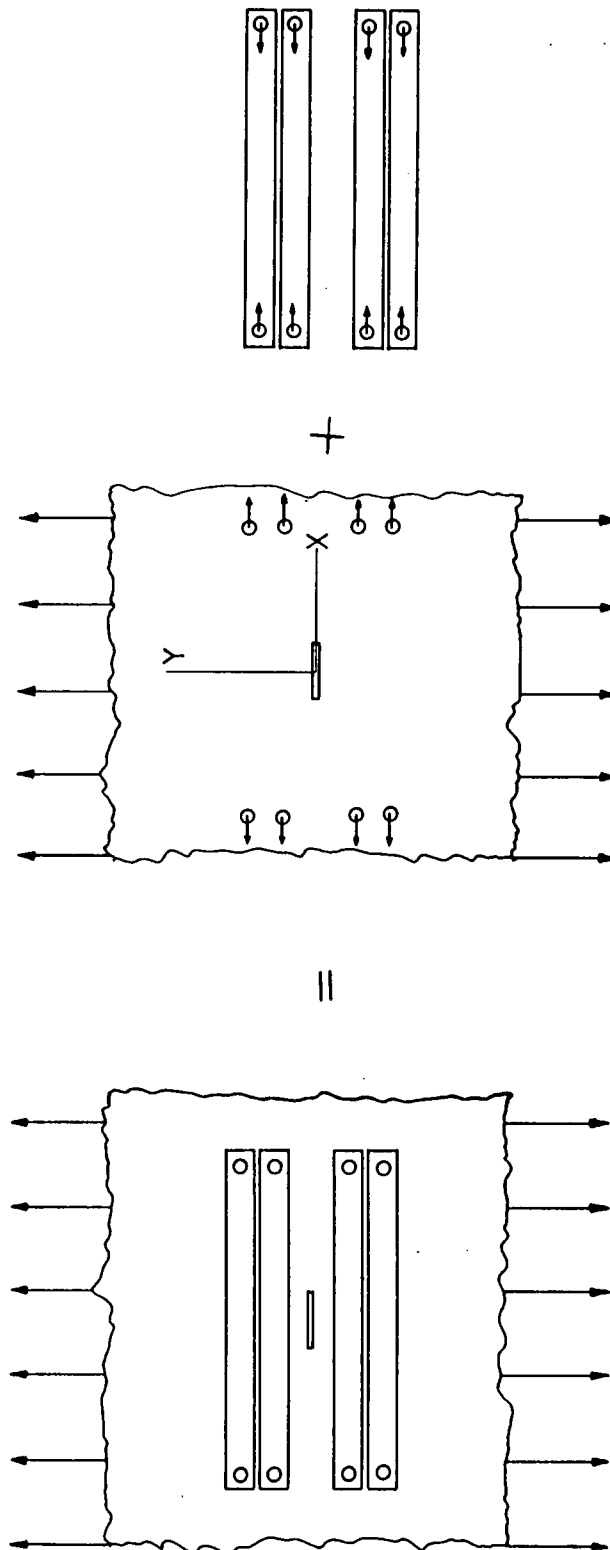
Fig.A3 Infinite sheet loaded by a single point force

A7

Fig.Al Infinite sheet with steel strips, modeled for stress analysis

SAMENVATTING

In de afgelopen 30 jaar zijn er verschillende ongelukken gebeurd met passagiersvliegtuigen als gevolg van het optreden van vermoeiingscheuren in de constructie van de romp. De katastrofale rompexplosie van twee Comet passagiersvliegtuigen in de jaren vijftig en de recente gebeurtenis met de Aloha Boeing 737 (april 1988) zijn duidelijke voorbeelden hiervan. Ondanks de vooruitgang op het gebied van de voorspellingstechnieken en de ontwerpfilosofieën kunnen vermoeiingsscheuren in de vliegtuigrompconstructie nog steeds voor grote problemen zorgen. Dit komt o.a. door dat vliegtuigen langer in dienst blijven dan oorspronkelijk bedoeld was, en door intensiever gebruik van de toestellen. Tegelijkertijd tracht men bij het ontwerpen van nieuwe vliegtuigen het spanningsniveau in vliegtuigconstructies te verhogen om gewichtsvermindering te realiseren. Om deze problemen het hoofd te kunnen bieden zijn speciale breukmechanische middelen ontwikkeld, die in vele gevallen ook met succes zijn toegepast. Echter, het gedrag van een longitudinale scheur in de romphuid van een passagiersvliegtuig vraagt om speciale aandacht. Het probleem is gecomplicieerd omdat:

a. de scheur is aanwezig in een **gekromde** dunwandige constructie;

b. er heerst vaak een **biaxiale spanningstoestand** en

c. er staat een **inwendige druk** op de rompconstructie.

Als gevolg van deze invloedsfactoren kunnen de scheurranden uitstulpen **(bulge-out)** waardoor een breukmechanische analyse moeilijk is. Uit literatuurstudie is gebleken dat een goede theorie over dit onderwerp niet bestaat en dat ook weinig experimenteel werk is verricht.

In dit proefschrift wordt getracht het probleem via een energiebeschouwing te analyseren. Voorts zijn nieuwe proefopstellingen ontwikkeld, waarmee diverse proeven zijn uitgevoerd. Het heeft geleid tot voorspellingsformules, die de relatie tussen de spanningsintensiteitsfactor van een longitudinale scheur in een rompconstructie en dezelfde factor voor een vlakke plaat vastleggen. De formules zijn semi-empirisch omdat bij het afleiden experimentele resultaten zijn gebruikt. De voorspellingen van de formules zijn vergeleken met de proefresultaten verkregen in de zelfgebouwde proefopstellingen, alsmede met resultaten van eindige elementen berekeningen en van ware-grootte proeven uit de literatuur.

Het probleem van scheurgroei in de rompconstructie kan ook opgevangen worden door nieuwe materialen met een hoge weerstand tegen scheurgroei toe te passen.

Voorbeelden hiervan zijn de nieuwe metaal/vezel laminaten ARALL en GLARE, ontwikkeld door vakgroep B2 van de Faculteit der Luchtvaart- en Ruimtevaarttechniek van de Technische Universiteit te Delft. Deze nieuwe materialen zijn dan ook beproefd met de bovengenoemde proefopstellingen. Om de toepasbaarheid van de materialen in vliegtuigrompconstruccties te onderzoeken is een analyse gemaakt op basis van de huidige ontwerpvoorschriften, **the Damage Tolerance Design Requirements**.

De belangrijkste resultaten van het onderzoek zijn:
(1) Ontwikkeling van drie nieuwe beproevingstechnieken:
   - **SUPERBAT** voor het beproeven van plaatmateriaal onder een biaxiale spanningstoestand;
   - **CETS** voor het beproeven van plaatmaterialen onder een gecombineerde buig- en trek(vermoeiings)belasting, en
   - **PFSTS** voor het beproeven van gekromde romphuidpanelen met inwendige overdruk.
(2) De biaxiale spanningen hebben geen invloed op de scheurgroeieigenschappen van monolithische Al 2024-T3 en Al 7075-T6 platen. Dit stemt overeen met conclusies uit de literatuur. Bij ARALL onder biaxiale spanningstoestand wordt wel een lagere scheurgoeisnelheid gevonden..
(3) De restterkte van monolithisch Al 2024-T3 en Al 7075-T6 platen wordt systematisch beinvloed door een aanwezige buigspanning. Een grotere buigspanning (kleinere kromtestraal) leidt tot een lagere reststerkte van de plaat.
(4) De scheurgroeieigenschappen van monolithisch Al 2024-T3 en Al 7075-T6 worden niet beinvloed door de buigspanning, mits deze buigspanning klein is (kromtestraal groter dan 350 mm). Bij een grotere buigspanning (kromtestraal kleiner dan 350 mm) is er een tendens naar een lagere scheurgroeisnelheid. Dit kan verklaard worden door de *"partiële scheursluiting ten gevolge van buiging"*. Buigspanningen leiden ook tot lagere scheurgroeisnelheid van ARALL laminaten. Dit is het gevolg van het fenomeen *"partiële vezelbreuk in aramide prepregs"*.
(5) Het uitstulpen van scheurranden (**bulge-out**) kan ook optreden onder gecombineerde buig- en trekbelastingen, zonder inwendige druk.
(6) Het uitstulpen van scheurranden verloopt niet-lineair bij toenemende inwendige druk. Het deformatieveld wordt sterk beinvloed door de biaxialiteit van de spanning.

(7)   De "bulge factor" neemt af met een toenememde inwendige druk en een
      toenemende spanningsbiaxialiteit, en neemt toe met een toenemende
      scheurlengte.

(8)   De in dit proefschrift ontwikkelde theorie komt goed overeen met de
      proefresultaten, de resultaten van eindige elementen berekeningen en
      ware-groote proeven uit de literatuur. De theorie heeft echter één
      beperking: De invloed van de verstijverafstand op de "bulge factor" kan
      niet goed voorspeld worden.

(9)   De groei van een vermoeiingsscheur in ARALL laminaten wordt niet
      beinvloed door "bulge out". Indien alle vezels worden doorgesneden, dan
      is de invloed van "bulge out" dezelfde als bij een monolithische
      aluminium plaat.

(10) Het meest kritieke "damage tolerance" ontwerpcriterium is de reststerkte
      van ARALL laminaten met een scheur met doorgesneden vezels, nagebootst
      door een zaagsnede. In vergelijking met ARALL laminaten zijn GLARE
      laminaten betere rompconstructiematerialen.

About the author

The author was born in Fujian, China, in 1963. In 1979 he started his aircraft engineering study at the Delft University of Technology, The Netherlands. He received his "ingenieurs" degree at the end of 1984. From May 1985 to December 1989 he was a scientific assistant (promovendus) of the Production and Material Section (vakgroep B2) of the Faculty of Aerospace Engineering of the same university. The subject of his research was fatigue of aircraft fuselage structures. It was carried out under the supervision of Professor Dr.Ir. J. Schijve.

The author is now working for the Royal Dutch/Shell Group of Companies in the KSLA laboratory in Amsterdam.

Rapport 647

907244